Prepared in Cooperation with University of California–Davis, Federal University of Rio de Janeiro, and the Institute for Water Education–Delft, Netherlands

South San Francisco Bay Salt Pond Restoration Project—A Synthesis of Phase-1 Mercury Studies

A8 tidal control structure

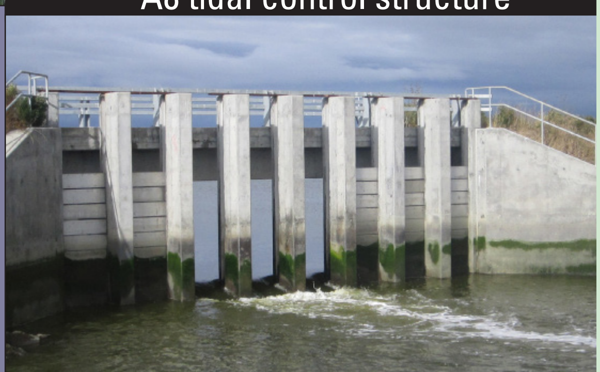

Scientific Investigations Report 2022–5113

U.S. Department of the Interior
U.S. Geological Survey

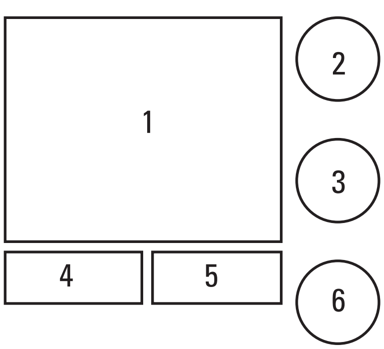

Cover Images: (1) Map of southern San Francisco Bay area depicting the A8-complex (ponds A5, A7, and A8) and the water control structures (gray boxes) around its boundary (light green line). Satellite base from Google Earth (2015). (2) Photograph of American avocet. Photograph by Josh Ackerman, U.S. Geological Survey. (3) Photograph of a three-spine stickleback. Photograph by Darrell Slotton, University of California, Davis.(4) Photograph of R/V Parke Snavely collecting high-resolution bathymetry of Alviso Slough. Photograph by Helen Gibbons, U.S. Geological Survey. (5) Photograph of the A8 Tidal control structure located on the southeast boundary of the A8-complex. Photograph by Mick van der Wegen, Institute for Water Education, Delf, Netherlands. (6) Photograph of a representative deep sediment core from the Alviso Slough. Photograph by Mark Marvin-DiPasquale, U.S. Geological Survey.

South San Francisco Bay Salt Pond Restoration Project—A Synthesis of Phase-1 Mercury Studies

By Mark Marvin-DiPasquale, Darell Slotton, Josh T. Ackerman, Maureen Downing-Kunz, Bruce E. Jaffe, Amy C. Foxgrover, Fernanda Achete, and Mick van der Wegen

Prepared in Cooperation with University of California–Davis, Federal University of Rio de Janeiro, and the Institute for Water Education–Delft, Netherlands

Scientific Investigations Report 2022–5113

U.S. Department of the Interior
U.S. Geological Survey

U.S. Geological Survey, Reston, Virginia: 2023

Suggested citation:
Marvin-DiPasquale, M., Slotton, D., Ackerman, J.T., Downing-Kunz, M., Jaffe, B.E., Foxgrover, A.C., Achete, F., and van der Wegen, M., 2022, South San Francisco Bay Salt Pond Restoration Project—A synthesis of phase-1 mercury studies: U.S. Geological Survey Scientific Investigations Report 2022-5113, 147 p., https://doi.org/10.3133/sir20225113.

Associated data for this publication:
Marvin-DiPasquale, M.C., Agee, J.L., Arias, M.R., Kakouros, E., and Kieu, L.H., 2019, Mercury speciation and other constituent data for surface sediment and water associated with the South San Francisco Bay Salt Pond Restoration, 2010–18: U.S. Geological Survey Data Release, https://doi.org/10.5066/P9MERSKP.

Marvin-DiPasquale, M.C., Arias, M.R., Agee, J.L., Kieu, L.H., Kakouros, E., Jaffe, B.E., and Wahl, D.B., 2018, Mercury speciation and other constituent data from deep sediment cores in Alviso Slough, South San Francisco Bay, California, 2012–16: U.S. Geological Survey, Data Release, https://doi.org/10.5066/F7HQ3Z3K

ISSN 2328-0328 (online)

Acknowledgments

The funding to support the writing of this synthesis report was provided by the California Coastal Conservancy. The combined research upon which this report is based was made possible by financial and logistical support through the following sources: South Bay Salt Pond Restoration Project; California State Coastal Conservancy; Santa Clara Valley Water District; U.S. Environmental Protection Agency; Resources Legacy Fund; CALFED Bay-Delta Program; U.S. Fish and Wildlife Service (Don Edwards San Francisco Bay National Wildlife Refuge and Eden Landing Ecological Reserve); U.S. Geological Survey Toxics Substances Hydrology Program, Contaminant Biology Program, Coastal/Marine Hazards and Resources Program, and Land Management Research Program; and the University of California, Davis.

The authors gratefully acknowledge the following individuals who contributed significantly to field, laboratory and (or) modeling efforts: Jennifer Agee, Evangelos Kakouros, Le Kieu, Michelle Arias, Melissa Mooradian, Francis Parcheso, Matt Toney, Alex Hartman, Mark Herzog, Sarah Peterson, Jeanne Fasan, Breanne Cooney, Kim Sawyer, Jarred Barr Paul Buchanan, Darin Einhell, Daniel Livsey, Greg Shellenbarger, Theresa Fregoso, Mike Boyle, Jackson Currie, Pete Dal Ferro, David Finlayson, Greg Gabel, Jamie Grover, Gerald Hatcher, Rachel Marcuson, Daniel Powers, Tom Reiss, Jennifer White, and Rob Wyland of the U.S. Geological Survey; Shaun Ayers, Ron Weyand, James Hobbs, Zachary Bess, and Rachel Fichman of the University of California, Davis, CA; and Carlos Rey and Johan Reyns of the IHE Delft Institute for Water Education, Netherlands.

Contents

Figures

Tables

Conversion Factors

International System of Units to U.S. customary units

Multiply	By	To obtain
	Length	
centimeter (cm)	0.3937	inch (in.)
millimeter (mm)	0.03937	inch (in.)
meter (m)	3.281	foot (ft)
kilometer (km)	0.6214	mile (mi)
kilometer (km)	0.5400	mile, nautical (nmi)
meter (m)	1.094	yard (yd)
	Area	
hectare (ha)	2.471	Acre
hectare (ha)	0.003861	square mile (mi^2)
	Volume	
cubic meter (m^3)	35.31	cubic foot (ft^3)
cubic meter (m^3)	1.308	cubic yard (yd^3)
cubic meter (m^3)	0.0008107	acre-foot (acre-ft)
liter (L)	0.03531	cubic foot (ft^3)
milliliter (mL)	0.06102	cubic inch (in^3)
	Flow rate	
cubic meter per second (m^3/s)	70.07	acre-foot per day (acre-ft/d)
cubic meter per second (m^3/s)	35.31	cubic foot per second (ft^3/s)
cubic meter per second (m^3/s)	22.83	million gallons per day (Mgal/d)
	Mass	
gram (g)	0.03527	ounce, avoirdupois (oz)
kilogram (kg)	2.205	pound avoirdupois (lb)
metric ton (t)	1.102	ton, short [2,000 lb]
metric ton (t)	0.9842	ton, long [2,240 lb]
milligram (mg)	0.00003527	ounce, avoirdupois (oz)
nanogram (ng)	3.527×10^{-8}	ounce, avoirdupois (oz)
	Density	
gram per cubic centimeter (g/cm^3)	62.4220	pound per cubic foot (lb/ft^3)

Temperature in degrees Celsius (°C) may be converted to degrees Fahrenheit (°F) as follows:

$$°F = (1.8 \times °C) + 32.$$

Temperature in degrees Fahrenheit (°F) may be converted to degrees Celsius (°C) as follows:

$$°C = (°F - 32) / 1.8.$$

Supplemental Information

Specific conductance is given either in microsiemens per centimeter at 25 degrees Celsius (µS/cm at 25 °C) or in millisiemens per centimeter at 25 degrees Celsius (mS/cm at 25 °C).

Volumetric concentrations of chemical constituents in water are given in either milligrams per liter (mg/L), micrograms per liter (µg/L), or nanograms per liter (ng/L).

Gravimetric concentrations for particle associated mercury are given in nanograms per gram (ng/g) dry weight.

Note to USGS users: Use of hectare (ha) as an alternative name for square hectometer (hm^2) is restricted to the measurement of small land or water areas. Use of liter (L) as a special name for cubic decimeter (dm3) is restricted to the measurement of liquids and gases. No prefix other than milli should be used with liter.

In this work, we employ “E notation” for scientific notation. For example, 1.0E+5 = 1×10^5.

Abbreviations

δ13C-POC	delta 13C-carbon, particulate organic carbon
δ15N-PN	delta 15N-nitrogen, particulate nitrogen
µg/g	microgram per gram
µg/L	microgram per liter
µS/cm	microsiemens per centimeter
2D	two dimensional
3D	three dimensional
ANCOVA	analysis of covariance
ANOVA	analysis of variance
CDFW	California Department of Fish and Wildlife
Chl.a	chlorophyll_a
CVAAS	cold vapor atomic absorption spectrophotometry
DOC	dissolved organic carbon
DO	dissolved oxygen
DOM	dissolved organic matter (includes carbon)
dw	dry weight
EDI	equal discharge increment
E_h	redox potential
f.DOM	fluorescent dissolved organic matter
FIMS	flow injection mercury system
FNU	formazin nephelometric units
fww	fresh wet weight
GUASL	model term indicating the sampling site in Guadalupe Slough
Kv	volume coefficient
L/(mg-C·m)	liter per milligram carbon * meter
LOI	loss on ignition
low.ALSL	model term indicating the lower Alviso Slough region
LSM	least squares mean
MALSL	model term indicating the sampling site in Mallard Slough
mg/m2	milligram per square meter

MLLW	mean low lower water
mmol/L	millimoles per liter
mS/cm	millisiemens per centimeter
mv	millivolts
ng/g	nanogram per gram
ng/L	nanogram per liter
ng/cm3	nanogram per cubic centimeter
ng/m2	nanogram per square meter
NMFS	National Marine Fisheries Service
PN	particulate nitrogen
POC	particulate organic carbon
psu	practical salinity units
Q	water discharge
QA	quality assurance
QALSL	water flux at Alviso Slough site ALSL-3
QC	quality control
QGR	water flux at Guadalupe River station
Qs	suspended-sediment flux
QSU	quinine sulfate units
RMSE	relative mean standard error
SBSPRP	South Bay Salt Pond Restoration Project
SpC	specific conductance
SRR	sulfate reduction rate (microbial)
SS	suspended sediment
SSC	suspended-sediment concentration
SUVA254	specific ultra-violet absorbance @ 254nm
TCS	tidal control structure
TEMP	temperature
TSS	total suspended solids
TURB	turbidity
up.ALSL	model term indicating the upper Alviso Slough region
USGS	U.S. Geological Survey
USWFS	U.S. Wildlife and Fisheries Service
WERC	Western Ecological Research Center
ww	wet weight

Chemical Notation

δ13C	delta 13C-carbon isotope
δ15N	delta 15N-nitrogen isotope
Cl–	chloride anion
Eh	electrochemical oxidation-reduction potential
$Fe(II)_{AE}$	acid extractable ferrous iron
$Fe(III)_a$	amorphous (poorly crystalline) ferric iron
$Fe(III)_c$	crystalline ferric iron
FeT	total measured iron ($Fe(II)_{AE}$ + $Fe(III)_a$ + $Fe(III)_c$)
f.MeHg	filter-passing methylmercury (monomethyl mercury)
f.THg	filter-passing total mercury
Hg	mercury
Hg(II)	(divalent) mercuric ion
Kd[MeHg]	distribution coefficient for methylmercury
Kd[THg]	distribution coefficient for total mercury
Kmeth	Mercury methylation rate constant
MeHg	methylmercury (monomethylmercury)
N	nitrogen
N_2	dinitrogen gas
NO_{2-}	nitrite anion
NO_{3-}	nitrate anion
O_2	molecular oxygen (gas)
P	phosphorous
p.MeHg	particulate methylmercury (surface water)
p.RHg	particulate inorganic reactive mercury (surface water)
p.THg	particulate total mercury (surface water)
PO_4^{3-}	(ortho)phosphate anion
RHg	inorganic reactive mercury
SO_4^{2-}	sulfate anion
THg	total mercury
uf.MeHg	unfiltered methylmercury (surface water)
uf.THg	unfiltered total mercury (surface water)

South San Francisco Bay Salt Pond Restoration Project—A Synthesis of Phase-1 Mercury Studies

By Mark Marvin-DiPasquale,[1] Darell Slotton,[2] Josh T. Ackerman,[1] Maureen Downing-Kunz,[1] Bruce E. Jaffe,[1] Amy C. Foxgrover,[1] Fernanda Achete,[3] and Mick van der Wegen[4]

Abstract

The South Bay Salt Pond Restoration Project (SBSPRP) encompasses over 6,000 hectares of former salt production ponds along the south edge of the San Francisco Bay and represents the largest wetland restoration effort on the west coast of North America. A series of studies associated with Phase 1 (2010–2018) restoration activities that are focused on a historically mercury contaminated slough and series of ponds within the restoration area have recently been completed. This report brings together the key findings of these loosely coordinated studies and integrates the results into a more comprehensive and holistic product that informs future restoration activities associated with the SBSPRP and elsewhere.

The focus of the Phase 1 studies was organized around two primary restoration management actions associated with Alviso Slough and its adjacent former salt ponds. The first action was a levee breach associated with pond A6 along the lower reach of Alviso Slough. The second action was associated with an adjustable tidal control structure at pond A8 (A8-TCS) that was constructed to reintroduce muted tidal connectivity between the upper portion of Alviso Slough and an area that comprises three hydrologically interconnected former salt ponds (ponds A5, A7 and A8, referred to as the A8-complex). During a 6-year period (2011–2017), the A8-TCS was gradually opened from one gate (1-gate condition, 1.5-meters wide opening) to eight gates (8-gate condition, 12.2-meters wide opening). This report focuses on addressing the extent to which these two management actions resulted in demonstrable changes in mercury concentrations associated with biota, surface water or bed sediment, and with mercury transport and flux associated with Alviso Slough bed sediment erosion caused by an increase in tidal prism.

This report documents key findings associated with the breach of pond A6: (1) a short-term spike in slough fish (Mississippi silverside) total mercury concentration in lower Alviso Slough; (2) a short-term spike in surface-water particulate total mercury in lower Alviso Slough; (3) significant sediment scour in Alviso Slough adjacent to and downstream of the breach points; (4) a decrease in surface-sediment methylmercury (as a percentage of total mercury) in lower Alviso Slough; (5) the transport of 70 kilograms per year of sediment-associated total mercury into pond A6 during the first 2 years following the breach but with much of this coming from outside of Alviso Slough, presumably from the nearby shallows, Guadalupe Slough, and the larger southern San Francisco Bay area; and (6) a slowing of bed sediment erosion in lower Alviso Slough 3–5 years after the breaching of pond A6.

Other key findings associated with the construction and gradual opening of the A8-TCS are documented in this report: (1) a short-term total mercury spike in prey fish (*Gillichthys mirabilis* [longjaw mudsucker] and *Gasterosteus aculeatus* [three-spined stickleback]) and tern eggs within the Alviso pond complex, and in Alviso Slough Mississippi silverside, all of which were attributable to construction activities within and immediately adjacent to the Alviso pond complex prior to the initial gate opening of the A8-TCS; (2) multiple lines of evidence that indicate the transition from three gates (3-gate condition, 15 feet [4.6 meters]) to five gates (5-gate condition, 25 feet [7.6 meters]) open at the A8-TCS may represent a critical tipping point beyond which the sudden increase in tidal prism resulted in increased bed sediment erosion, and the reversal of suspended sediment flux direction, towards the bay, for a prolonged period (1.6 years); (3) this period concluded with a substantial spike in surface-water methylmercury in Alviso Slough, which preceded (by 6 months) a significant spike in silverside total mercury concentrations in Alviso Slough that we ultimately attribute to the opening of five gates initiated two years prior; (4) a steady year-over-year decrease in Alviso Slough surface-water total mercury and methylmercury concentrations on a volumetric basis that is due to dilution driven by the increased tidal prism linked to the increased number of A8-TCS open gates; (5) a steady year-over-year increase in wintertime (December—February) particulate total mercury concentration on a gravimetric basis in Alviso Slough that is linked to increasing bed sediment erosion of long-buried sediment horizons containing elevated

[1]U.S. Geological Survey.

[2]University of California, Davis.

[3]Federal University of Rio de Janeiro, Brazil.

[4]Institute for Water Education, Delf, Netherlands.

concentrations of legacy mercury (derived from historic mining activities in the watershed); (6) the mass flux of suspended sediment, particulate total mercury, and particulate methylmercury past the A8-TCS was into the A8-complex during the full period of high-resolution water quality monitoring (February 2016—February 2018), which included the transition from five to eight gates open at the A8-TCS; and (7) the opening of eight gates resulted in a decrease of water flux into the A8-complex and a reversal in model-predicted filter-passing total mercury and filter-passing methylmercury flux from the A8-complex being a sink for these two species during a 5-gate condition to being a source to Alviso Slough during an 8-gate condition.

Although this report is not intended to be prescriptive in terms of the next steps the SBSPRP should or should not take, the totality of the findings presented provide critical process-level information regarding the extent and the duration of spikes in mercury levels in water, sediment, fish, and birds, which appeared to result from the two management actions under study. Thus, these results can be used to anticipate similar ecosystem responses associated with similar management actions that may be considered in the future. We also conclude this report by highlighting unanswered questions associated with mercury dynamics as it relates to the restoration project, and possible future directions for research.

Introduction

This report compiles and integrates the key findings from a series of adaptive management mercury-related studies conducted as part of the Phase 1 South Bay Salt Pond Restoration Project (SBSPRP). The focus of this report is on mercury concentrations and speciation in sediment and water, and mercury exposure to biota, primarily in response to the controlled breach project performed in upper Alviso Slough at pond A8, beginning in 2010 and continuing through at least 2018. Although extensive additional mercury research was conducted prior to this period and throughout the wider SBSPRP restoration area (Marvin-DiPasquale and Cox, 2007; Grenier and others, 2010; Miles and Ricca, 2010; Ackerman and others, 2014c); this report focuses on the Phase 1 restoration activities. Because mercury contamination within Alviso Slough and several of the Alviso ponds slated to be restored was a recognized concern, there were regulatory-driven decision points around mercury designed to inform future restoration actions as part of Phase 1. As such, the studies described herein were conducted to provide feedback and guidance to the SBSPRP management team regarding if, and to what extent, restoration activities affect mercury mobility, concentrations, speciation and biotic exposure, for this and other planned management activities in the restoration area. This report is not intended to be prescriptive in terms of what management actions should or should not be taken in the future.

The multi-investigator and multiagency research conducted during the Phase 1 restoration effort consisted of several individual research projects, loosely coordinated, to answer several specific questions related to whether management actions (that is, breaching of pond A6 levees and connecting the A8-complex to Alviso Slough through the controlled opening and closing of A8-TCS gates) affected sediment remobilization and (or) transport and mercury speciation and bioaccumulation. Some of these individual research efforts focused on mercury specifically (that is, in biota, water, and sediment). Other efforts focused on related aspects associated with restoration activities, such as sediment scour and (or) remobilization and the calculation of suspended sediment loads. This report is intended to integrate the key findings of these individual studies, as they relate to the mercury contamination issues associated with the restoration project. It is not intended to be a comprehensive report on the findings of any one study.

This synthesis is structured around four organizing questions (see the “Mercury Synthesis—Organizing Questions” section). A brief summary of results for each of the individual research efforts is first provided and includes details relevant to these questions as appropriate. We answer these questions using evidence drawn from the totality of data presented from the individual studies and (or) from new data analyses generated from combining data results from multiple individual research efforts. Some of the lines of evidence used to answer the questions are quantitative and (or) statistically based, whereas others are qualitative observations. The totality of evidence available from this synthesis of results is used to provide a qualitative degree of certainty (medium or high) for the conclusions reached.

Primary management questions relating to mercury pertained to whether biological mercury exposure and bioaccumulation were exacerbated by restoring tidal connectivity to formerly isolated salt ponds? If so, how (by what mechanisms) and to what extent? And, if so, can the findings of this research inform management of this and future restoration efforts?

Background

Historical Salt Ponds Period, 1857–1977

Salt has naturally crystallized at the margins of San Francisco Bay for millennia. It was routinely collected in small amounts for cooking and other uses by indigenous tribal people and then by Spanish and Mexican Californians in the 16th—19th centuries. The influx of American immigrants during the California Gold Rush (1848–1855) increased the demand for salt greatly, which led to the startup of numerous small salt harvesting operations in the South Bay (Booker and others, 2010). The first commercial salt evaporation ponds were constructed in 1857 by dike impoundment of bay water, and much of the South Bay perimeter ultimately was diked for salt production by 1900. In the early 1900s, Leslie Salt consolidated the many small holdings and created an underwater plumbing system in support of a salt processing plant near Newark, California (Booker and others, 2010). The southern San Francisco Bay area was under active salt production throughout most of the 1900s. In 1978, ownership of the properties was transferred to Cargill, Inc. The gradual process of salt pond acquisition by the U.S. Federal Government and the State of California began in the 1970s for the purpose of restoring natural habitats and was accelerated in the 1990s (San Francisco Bay Conservation and Development Commission, 2005). Because of the historical use as salt evaporation ponds, these restoration sites had extensive mineral accumulations in their bottom sediments and shore areas.

Historical Watershed Mercury Sources

Similar to the spike in the demand for salt created by the California Gold Rush, a major demand developed for refined liquid quicksilver (mercury). Mercury was referred to as “the magical element” that could sweep up small particles of gold that were otherwise unavailable to miners. The mercury could then be distilled and (or) boiled off, leaving consolidated gold. A part of the Coast Ranges of central California was found to be one of the world’s major mercury-enriched zones (Rytuba, 2003). An influx of American immigrants to the coast range regions consequently mirrored the Gold Rush of the Sierras to the east. The upstream watershed that drains directly to the study area contains the largest and richest historical mercury mine complex in North America, the New Almaden mining district. Approximately 1.16 million flasks of elemental mercury (40 million kilograms [kg]) were extracted over the life of the operation (Bailey and Everhart, 1964), and peak production levels were over a million kilograms per year in the 1860s. An estimated 6 million kg of mercury was lost to the watershed. The mine complex is located approximately 25 miles (40 kilometers [km]) upstream of the SBSPRP study area. Presently, the complex is connected hydrologically to Alviso Slough and the San Francisco Bay by the Guadalupe River, which also flows through the City of San Jose. Historically, the Guadalupe River flowed into Guadalupe Slough (San Francisco Estuary Institute-Aquatic Science Center, 2018). However, in the 1870’s the course of the river was diverted into the straighter Alviso Slough, 1.6 km to the north, to allow boats to more easily access the port of Alviso and to improve the conveyance of floodwater (Oakland Museum of California, undated). Thus, mercury transport from the New Almaden mining district to the San Francisco Bay transitioned from the land-to-bay connection via Guadalupe Slough to Alviso Slough in the 1870s as a direct result of this early watershed management action.

Two reservoirs were built directly downstream from the mining zone in 1935: Guadalupe Reservoir and Almaden Reservoir (Austin, 2006). Although these reservoirs undoubtedly trap some variable amount of mine-derived sediment and associated mercury annually, prior to their construction, there was little or no barrier to mine-derived mercury transport to the downstream valley and bay. A 1964 U.S. Geological Survey (USGS) study of the region stated that “Since 1890 the production [of quicksilver ore] from the district has been small as compared with its earlier output” (Bailey and Everhart, 1964, p. 2). In the pre-regulatory era of heavy mercury mining activity, substantial volumes of mercury-enriched sediments moved down the drainage, with much of it depositing upon confluence with the Bay. Although the primary source of mining related sediments has been largely blocked by the reservoirs since the 1930s, substantial amounts of mercury remain in the beds and margins of the downstream channels and have been available for erosion during high flow events. Additionally, the reservoirs, although trapping much of the mining-associated erosion after the 1930s, have generated and exported toxic methylmercury (MeHg) to downstream areas (Austin, 2006). In 1975, Santa Clara County purchased the historical mining region to create a 4,000-acre Almaden Quicksilver County Park. In 1987, the associated mercury contamination was acknowledged in a Santa Clara County fish consumption advisory and in a state order for a Superfund cleanup of the mining property; extensive cleanup began in 1990 (Austin, 2006).

Salt Pond Restoration Process, 2003–2018

In 2003, more than 15,000 acres of salt ponds in southern San Francisco Bay area were transferred from Cargill Inc., through donation and purchase, to the California Department of Fish and Wildlife and the U.S. Wildlife and Fisheries Service. An Initial Stewardship Plan was developed by the agencies to establish and maintain open-water ponds and engineer enough water circulation to stop ongoing salt crystallization and provide some wildlife habitat (Life Science! Inc., 2004). This Initial Stewardship Plan was intended as a short-term course of action. Concurrent to the development of the Initial Stewardship Plan, a long-term (50 year) restoration plan was developed to guide eventual transition of the former salt ponds (EDAW and others, 2007; Trulio and others, 2007). This work defined overall goals and objectives for the restoration process.

The salt pond restorations were planned to occur in phases, and Phase 1 projects began in 2010. Phase 1 included the breaching of targeted ponds to create approximately 3,000 acres of new fully tidal or muted tidal habitat, including the subject ponds of this report. A suite of adaptive management scientific monitoring and research efforts were key components of the restoration work (Trulio and others, 2007). Other Phase 1 projects included the creation of experimental habitat islands in some ponds, levee improvements, and the construction of new walking and (or) biking trails and other public access features. Planning for Phase 2 began in 2010 and was initiated in 2020, utilizing results of the various Phase 1 adaptive management studies (Wood and others, 2019).

Previous Mercury Studies

Sediment and Water Mercury Studies

The Guadalupe River watershed has been monitored since mine site cleanup of the upstream New Almaden, Calif., region began in the 1990s. More recently, pilot tests have been done on reservoir water column manipulations to reduce anoxia-related production of MeHg (Seelos, 2017). Mercury loading studies in the tributary streams and downstream Guadalupe River have shown ongoing, storm-discharge loading in the range of kilograms to hundreds of kilograms of Hg annually (McKee and others, 2017; McKee and others, 2018).

Deep sediment cores collected during 2001–2002 from a salt marsh site located approximately 3 km north from Alviso Slough (Conaway and others, 2004), and during 2006 along Alviso Slough and its fringing emergent marsh (Marvin-DiPasquale and Cox, 2007), showed elevated concentrations of mercury (part per million levels) in buried sediment horizons that were associated with legacy mercury associated with historical watershed mercury sources (hereafter called legacy Hg) derived from the upstream watershed. The first systematic study of total mercury (THg) and MeHg concentrations in surface sediment (0–5 centimeter [cm] interval) within various southern San Francisco Bay salt ponds was conducted during 2003–2007 by Miles and Ricca (2010) to establish mercury baseline conditions prior to initial restoration activities. That study indicated that THg and MeHg concentrations associated with salt ponds adjacent to Alviso Slough (geometric means = 0.63 microgram per gram [µg/g] and 1.94 nanogram per gram [ng/g], respectively) were significantly higher than concentrations in ponds adjacent to the Eden Landing Ecological Reserve, approximately 10 miles to the north on the east side of the San Francisco Bay (geometric means = 0.09 µg/g and 0.98 ng/g, respectively). Isolated salt pond environments, often associated with eutrophication (enrichment of nutrients) and seasonal anoxia (depletion of dissolved oxygen [DO]), are known to be prime habitats for enhanced MeHg production (Grenier and others, 2010; Miles and Ricca, 2010). The historical deposition of mining-derived mercury in the ponds near Alviso Slough, in conjunction with conditions conducive for enhanced phytoplankton production, provides for additional MeHg production.

Prior to Phase 1 management actions, estimates of bed sediment and associated THg remobilization were made on the basis of the deep core THg profile data collected from Alviso Slough during 2006 and previously modeled changes in slough cross-sectional area associated with the planned breaching of pond A8 (Marvin-DiPasquale and Cox, 2007). These estimates indicated that approximately 217,000±46,000 cubic meters (m^3) of bed sediment and 125±30 kg of THg would be mobilized, based on a 40-foot-wide levee breach scenario between pond A8 and Alviso Slough. Laboratory experiments conducted as part of this same study also indicated that previously buried inorganic Hg(II) would become relatively more available for microbial conversion to toxic MeHg once remobilized into oxygenated surface water.

Biota Mercury Studies

Often, wetland perturbations, such as reservoir creation, can alter mercury cycling and increase MeHg concentrations in water and biota. One of the best examples of the long-term consequences of altering wetland hydrology and its effects on mercury cycling comes from the Experimental Lakes Area Reservoir Project in northwestern Ontario, Canada, where a wetland was experimentally flooded to create a larger wetland-type reservoir. A series of studies documented that this experimental reservoir creation significantly increased MeHg concentrations in surface water, zooplankton, fish, and birds more than pre-flood conditions (Kelly and others, 1997; Gerrard and St. Louis, 2001; St. Louis and others, 2004). Importantly, after the reservoir was created, there were no signs that MeHg concentrations were returning to normal preflood levels, and elevated MeHg concentrations in biota remained high for at least 6 to 9 consecutive years after the reservoir was created. The bird study was ended after 6 years and the zooplankton and fish study were ended after 9 years, so it is unknown whether MeHg concentrations in birds, zooplankton, or fish would have ever returned to normal, pre-flood levels or if these elevated MeHg concentrations were the new status quo. Similarly, synthesized data on reservoirs in the western United States and Canada found that fish Hg concentrations rapidly increased after reservoir creation, peaked in 3-year-old reservoirs, and then rapidly declined in 4 to 12-year-old reservoirs (Willacker and others, 2016). Although the reservoir studies are vastly different from the current restoration project, which is restoring a former salt evaporation pond into tidal marsh, there are only a limited number of studies that have examined mercury cycling in response to large-scale wetland habitat manipulations. The limited available data indicate that large-scale wetland perturbations, such as the current restoration project, can have long-term (sometimes as long as a decade) consequences to mercury cycling and generally increase biotic mercury exposure.

Aquatic habitats of the SBSPRP area, which are associated with historical or ongoing mercury deposition originating from the Guadalupe River watershed, have been identified as elevated in mercury bioaccumulation since at least the 1990s (Schwarzbach and others, 2006). Investigations of mercury accumulation in target bird and small fish populations, done prior to the current Phase 1 studies, identified highly elevated levels of mercury bioaccumulation in the Alviso Slough area and especially in the A8-complex (Ackerman and others, 2007; Ackerman and others, 2008b; Eagles-Smith and Ackerman, 2009; Ackerman and others, 2014a; Eagles-Smith and Ackerman, 2014). Those studies found the region to contain the highest levels of mercury bioaccumulation seen throughout the estuarine portion of the San Francisco Bay.

Extensive, long-term research by the USGS has demonstrated that fish and bird mercury concentrations within San Francisco Bay, in general, are elevated (Ackerman and others, 2014a) and the estuary is a hotspot for mercury contamination of birds in western North America (Ackerman and others, 2016b). In particular, *Sterna forsteri* (Forster's tern) breeding in San Francisco Bay have the highest average blood mercury concentrations of any birds sampled in western North America (Ackerman and others, 2016b). Overall, 82 percent of birds sampled in the San Francisco Bay estuary watershed exceeded a blood-equivalent mercury concentration of 0.2 µg/g wet weight (ww; the lowest-observed effect level), 46 percent exceeded 1.0 µg/g ww (moderate risk), 14 percent exceeded 3.0 µg/g ww (high risk), and 8 percent exceeded 4.0 µg/g ww (severe risk) (Ackerman and others, 2014a). Birds that breed locally within the watershed are among the most at-risk species because they are exposed to higher levels of mercury at the critical time period during breeding (Ackerman and others, 2008b; Ackerman and Eagles-Smith, 2009; Eagles-Smith and Ackerman, 2009), and bird reproduction is thought to be among the most sensitive endpoints of mercury toxicity. On the basis of the proportion of mercury concentrations in bird eggs that exceed a general bird toxicity benchmark of 1.0 µg/g fresh wet weight (fww) (Scheuhammer and others, 2007), 79 percent of Forster's tern eggs in the estuary are at high risk to potential mercury-induced impairment (Ackerman and others, 2014a). All of the corresponding risk percentages for the Alviso Slough area, are higher than these San Francisco Bay-wide averages.

Several studies indicate that mercury contamination may be impairing reproduction and overall health of birds breeding in the San Francisco Bay estuary. Evidence for these conclusions include, elevated mercury in failed-to-hatch Forster's tern eggs relative to controls (Ackerman and others, 2014a); elevated mercury in malpositioned Forster's tern embryos, which was linked to impaired hatchability (Herring and others, 2010; Ackerman and others, 2014a); elevated mercury in *Himantopus mexicanus* (black-necked stilt) post-hatching juveniles found dead, relative to healthy controls (Ackerman and others, 2008c); a negative correlation between mercury concentration and adult bird body condition of endangered *Rallus obsoletus* (Ridgway's rail) (Ackerman and others, 2012); elevated mercury levels activating physiological demethylation (detoxification) pathways (Eagles-Smith and others, 2009); and cellular oxidative stress in various critical body organs of Forster's tern chicks and adults of both Forster's tern and *Hydroprogne caspia* (Caspian tern) (Hoffman and others, 2011).

Additional biota sampling occurred during 2007–2008 in the Alviso Slough and the larger southern San Francisco Bay area as part of a joint San Francisco Estuary Institute and USGS study (Grenier and others, 2010), in which brine flies and fish (*Gasterosteus aculeatus* [three-spined stickleback] and *Gillichthys mirabilis* [longjaw mudsucker]) were sampled from pond A8 and along the main channel and fringing marsh of Alviso Slough (main channel and fringing marsh), and song sparrows were sampled from several habitats. Consistent with USGS research, results indicated that pond A8 exhibited the highest mercury concentrations in both fish species, compared to all other managed southern San Francisco Bay ponds sampled. Additionally, song sparrows inhabiting tidal marsh and slough habitats across the southern San Francisco Bay area had elevated mercury levels, and blood mercury concentrations showed a positive correlation with corresponding MeHg percent in sediment.

Between 2008 and 2010, the Regional Monitoring Program, in conjunction with University of California, Davis, randomly sampled small fish at 99 sites distributed around greater San Francisco Bay. This program, after statistically accounting for standard ecological factors, such as fish species and season, found the spatial factor of nearness to Alviso Slough to be strongly correlated with elevated fish mercury (Greenfield and others, 2013).

Together, these studies indicate that legacy mercury contamination is likely causing significant impairment to multiple bird species breeding within the southern San Francisco Bay area salt ponds. Those exposures were the primary impetus for the current studies and highlight the importance of monitoring bird populations, bird mercury exposure, and prey fish mercury during the large-scale habitat manipulations associated with the SBSPRP.

Overview of Phase 1 Management Actions and Related Studies

Phase 1 Management Actions

Two Phase 1 management actions are relevant to the design and focus of the mercury studies summarized in this report. The first involved a levee breach (detailed below), whereas the second involved an adjustable tidal control structure (TCS) that allowed for the controlled return of tidal connectivity to a contiguous grouping of three hydrologically interconnected ponds. This latter approach drove the majority of the research described in this report and is detailed first. From September 2010 through January 2011, the adjustable TCS between the east edge of pond A8 and upper Alviso Slough was constructed (henceforth called the A8-TCS). The concrete structure contains eight removable gates, each with a width of 5 feet (1.5 m), for a maximum potential opening of 40 feet (12.2 m). Internal levees separating Alviso Slough ponds A5, A7, A8, and A8S were breached in April 2011, which led to the creation of a larger ponded area referred to herein as the A8-complex.

The initial opening between the A8-complex and upper Alviso Slough was made on June 1, 2011, by lifting a single 5-foot gate to preclude potential entrainment hazards to migrating juvenile salmonids. This opening was maintained through December of 2011, when it was closed in coordination with the National Marine Fisheries Service (NMFS). A similar action was implemented in 2012 and 2013; however, three gates (15 feet, 4.6 m) were opened between June and December. In 2014, three gates were again opened, although earlier in the year (March 3), with NMFS approval. Partly on the basis of apparently stable Alviso Slough fish mercury concentrations during the 2011–2013 period, the SBSPRP management team increased the A8-TCS opening to five gates (25 feet, 7.6 m) on September 29, 2014.

NMFS approval was also given to then leave the five gates open continuously. The 5-gate condition was maintained through June 2017. At that time, the remaining three gates were raised, which created the maximum opening of 40 feet (12.2 m, 8-gate condition) that has continued through 2018. This chronology of gate openings (table 1, fig. 1) forms the backdrop for many figures in this report.

The other management action that has bearing on the Phase 1 mercury studies was the breaching of the pond A6 levee in four locations. Pond A6 is located downstream from the main study area, near the confluence of Alviso Slough with Coyote Creek and the San Francisco Bay. The A6 breaching involved levee removal (via backhoe) between the pond and the adjacent sloughs (Alviso and Guadalupe), and this action was not intended to be reversible. Pond A6 was fully breached to both lower Alviso and lower Guadalupe Sloughs (two breach points associated with each slough, each breach between 20 m and 30 m wide) in December 2010, six months prior to initial openings of the A8-TCS. The potentially confounding effects of this downstream restoration must be considered when assessing the effect of A8-TCS operation on mercury dynamics in the study area.

Table 1. Chronology of management actions associated with the South Bay Salt Pond Restoration Project Phase 1.

[A8-TCS refers to pond A8 tidal control structure]

Location	Management Action	Start date (mm/dd/yyyy)	End date (mm/dd/yyyy)	Total Days per Event
A8-TCS	Construction period	09/15/2010	01/15/2011	150 approximately
Pond A6	Levee breach	12/06/2010	12/06/2010	1
A8-complex	Internal levees breached	04/22/2011	04/22/2011	1
A8-TCS	1 gate opened	06/01/2011	12/01/2011	183
A8-TCS	All gates closed	12/01/2011	06/01/2012	183
A8-TCS	3 gates opened	06/01/2012	12/01/2012	183
A8-TCS	All gates closed	12/01/2012	06/06/2013	187
A8-TCS	3 gates opened	06/06/2013	12/06/2013	183
A8-TCS	All gates closed	12/06/2013	03/06/2014	90
A8-TCS	3 gates opened	03/06/2014	9/29/2014	207
A8-TCS	5 gates opened	9/29/2014	6/2/2017	977
A8-TCS	8 gates opened	6/2/2017	Present	Ongoing

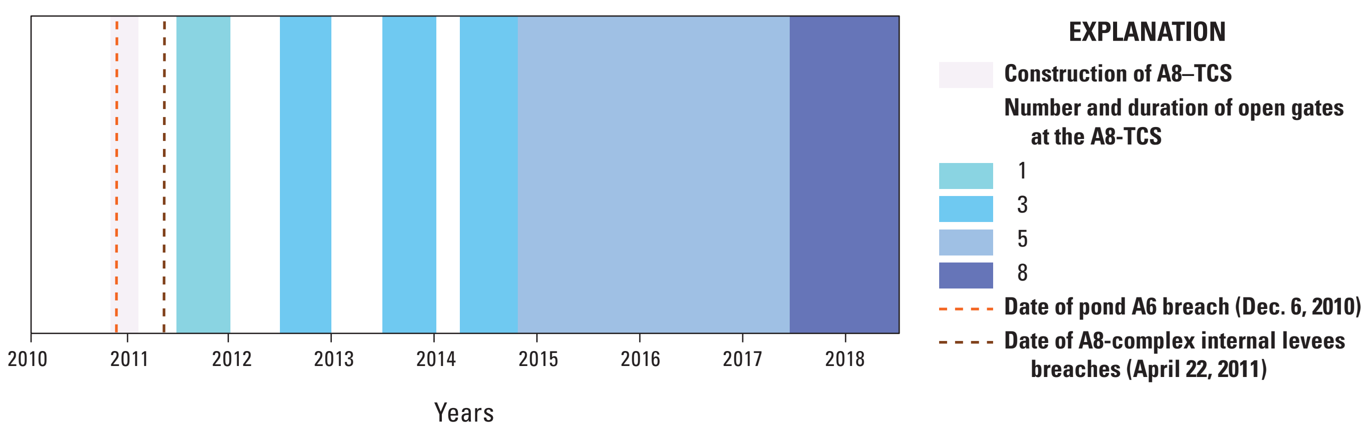

Figure 1. Graph showing the chronology of pond A8 tidal control structure (A8-TCS) gate openings, 2010–2018 associated with South Bay Salt Pond Restoration Project Phase I. Each gate is 5 feet (1.5 meters) wide, and A8-TCS has eight gates, for a maximum opening of 40 feet (12.2 meters). Year labels are centered on January 1 of each year. Nonshaded background represents duration when all gates are closed.

Phase 1 Mercury, Sediment, and Modeling Studies

Phase 1 mercury studies linked to the Alviso Slough restorations started in April 2010, a year before the first A8-TCS gate was opened in June 2011. These studies were designed primarily to investigate, in a controlled way, the potential effects of opening a representative salt pond with elevated mercury to tidal connectivity. Baseline mercury levels of pond birds and fish, slough fish, and corresponding water and sediment were studied within the A8-complex (multiple sites), Alviso Slough (multiple sites), two reference ponds (ponds A3N and A16 [sites A3N and A16, respectively]), and a reference slough (Mallard Slough [site MALSL]). The same sites continued to be monitored through 2011. After 2011, fish and sediment monitoring inside the ponds was discontinued owing to funding constraints. Pond bird eggs, slough fish, and corresponding water in both habitats continued to be monitored throughout much of the 2010–2018 Phase 1 study period. Beginning in 2013, an additional reference slough (Guadalupe Slough [site GUASL]) was added. Further details regarding the timing of these specific study components are given in the “Methods” section.

Three of the Phase 1 studies compiled in this report were directly focused on mercury: the pond biota (bird eggs and fish) work led by Josh Ackerman (USGS), slough fish work led by Darell Slotton (University of California, Davis), and the surface water and sediment work in both ponds and sloughs led by Mark Marvin-DiPasquale (USGS). Three additional Phase 1 USGS studies were peripheral to the mercury work, which consisted of other primary objectives, but provided critical supporting information for this mercury synthesis. These include the bed sediment scour and remobilization studies led by Bruce Jaffe and Amy Foxgrover (USGS), the fixed station suspended-sediment continuous monitoring work led by Maureen Downing-Kunz (USGS), and the hydrodynamic and sediment transport and geomorphic change modeling led by Mick van der Wegen and Fernanda Achete (IHE Delft Institute) in collaboration with Bruce Jaffe. The methods used for each of the individual studies are detailed in the “Methods” section, and the key findings of each study, as they relate to this overall synthesis report, are provided separately in the “Individual Study Results” section. These individual findings are then synthesized in the “Synthesis of the Independent Studies” section to assess the stated organizing questions laid out in “Mercury Synthesis—Organizing Questions” section. We conclude with “Unanswered Questions and Future Directions” section, which briefly highlights current unknowns and issues not fully addressed in the Phase 1 studies, and points to potential future research directions.

Mercury Synthesis—Organizing Questions

The four questions detailed below represent those assessed as part of this synthesis report. They transcend individual research projects and are best answered using the results of the totality of studies (or a subset), rather than the results of a single study conducted as part of the Phase 1 SBSPRP.

Question 1 (Q.1): To what extent did the pond A6 levee breach result in directly measurable changes in mercury concentrations in Alviso Slough biota, surface water, and (or) bed sediment?

Question 2 (Q.2): To what extent did the construction and gradual increased opening of the A8-TCS result in measurable changes in mercury concentrations in biota, surface water, and (or) bed sediment within the A8-complex?

Question 3 (Q.3): To what extent did the construction and gradual increased opening of the A8-TCS result in measurable changes in mercury concentrations in Alviso Slough biota, surface water, and (or) bed sediment?

Question 4 (Q.4): To what extent is the Alviso pond A8-complex a source or sink for THg and (or) MeHg?

These questions provide the framework for technical assessments of mercury in the study area to date and are intended to guide research used to inform management decisions for the SBSPRP, which include a review of the positive or negative effects future breaches or operational and structural changes may have on biota.

Methods

Overview of Field Sampling Efforts

The degree of temporal and spatial coordination of field collection efforts associated with biota, surface water, and bed sediment varied over the 2010–18 period that defined the multiple Phase 1 studies summarized in this report. An overview of the chronology of all the different study components described herein is summarized in tabular form in appendix 1, and further details are provided in the individual methods subsections below. The specific locations within the study area for the different matrices sampled are depicted on the following maps: pond and slough bird eggs (fig. 2), fish (fig. 3), surface water (fig. 4), and bed sediment (fig. 5). For a more regional view of the location of the Alviso Slough ponds study area, as well as the other SBSPRP areas (Eden Landing Ecological Reserve and Ravenswood complex—a complex of former salt ponds on the East Palo Alto peninsula) within the southern San Francisco Bay area, please see the interactive maps provided on the SBSPRP website (www.southbayrestoration.org/page/maps).

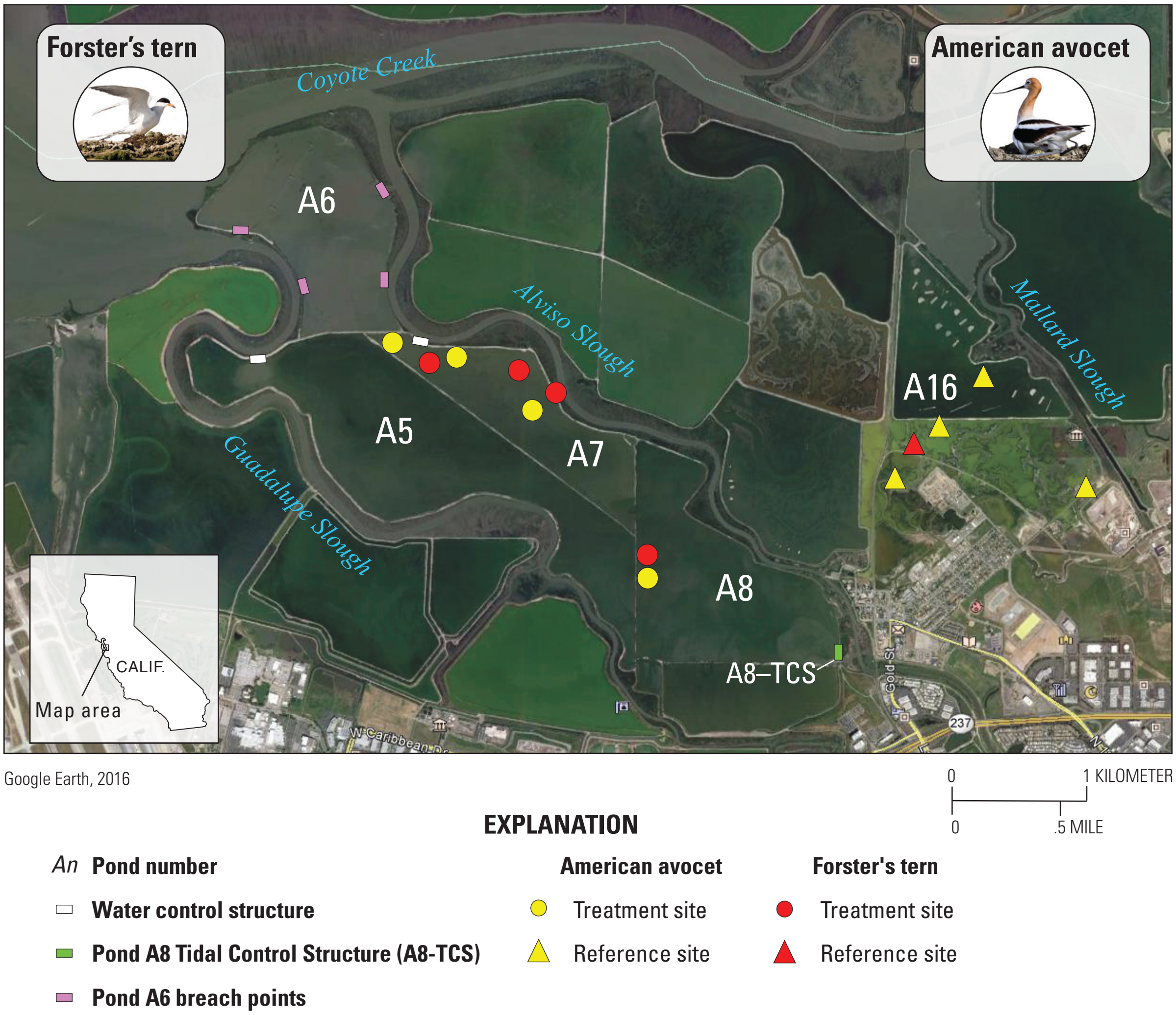

Figure 2. Map of the southern San Francisco Bay area depicting locations of bird egg sampling conducted as part of the South Bay Salt Pond Restoration Project Phase 1 studies. Bird egg sampling was conducted by the U.S. Geological Survey (J. Ackerman, lead investigator) and targeted the sampling of Forster's tern and American avocet eggs. Extensive additional Phase 1 bird egg sampling occurred at additional sites around the southern San Francisco Bay area but outside of the immediate Alviso Slough study area (not shown).

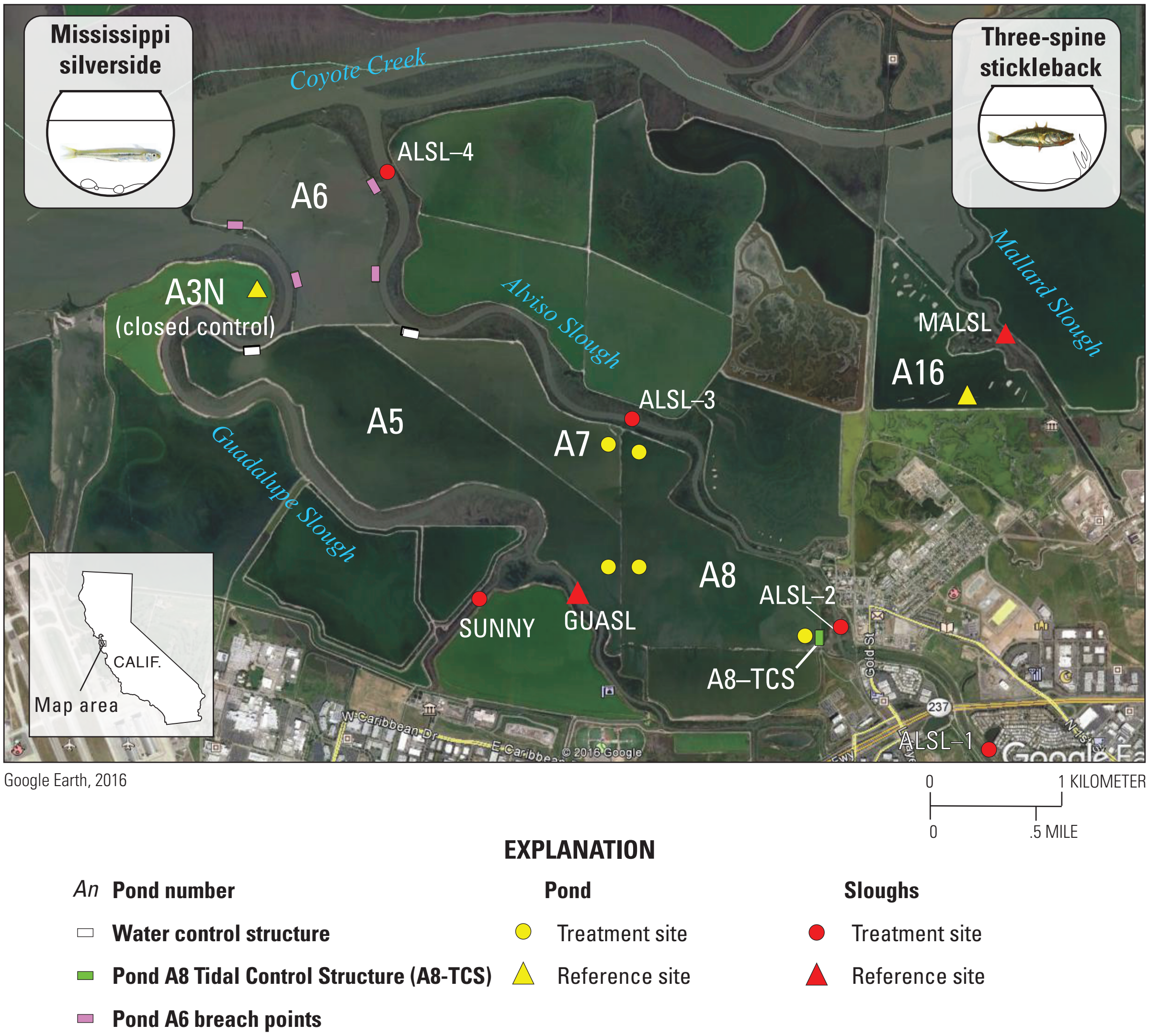

Figure 3. Map of the southern San Francisco Bay area depicting locations of small fish sampling conducted as part of the South Bay Salt Pond Restoration Project Phase 1 studies. Fish sampling within the ponds was conducted by the U.S. Geological Survey (J. Ackerman, lead investigator) and targeted longjaw mudsucker and three-spine stickleback. Fish sampling within the sloughs was conducted by University of California, Davis (D. Slotton, lead investigator) and targeted Mississippi silverside and three-spine stickleback. Pond fish were only sampled during the 2010–11 period, whereas slough fish were sampled during the full 2010–18 Phase 1 study period. Extensive additional Phase 1 small fish sampling by U.S. Geological Survey occurred at additional sites around the southern San Francisco Bay area but outside of the immediate Alviso Slough study area (not shown.)

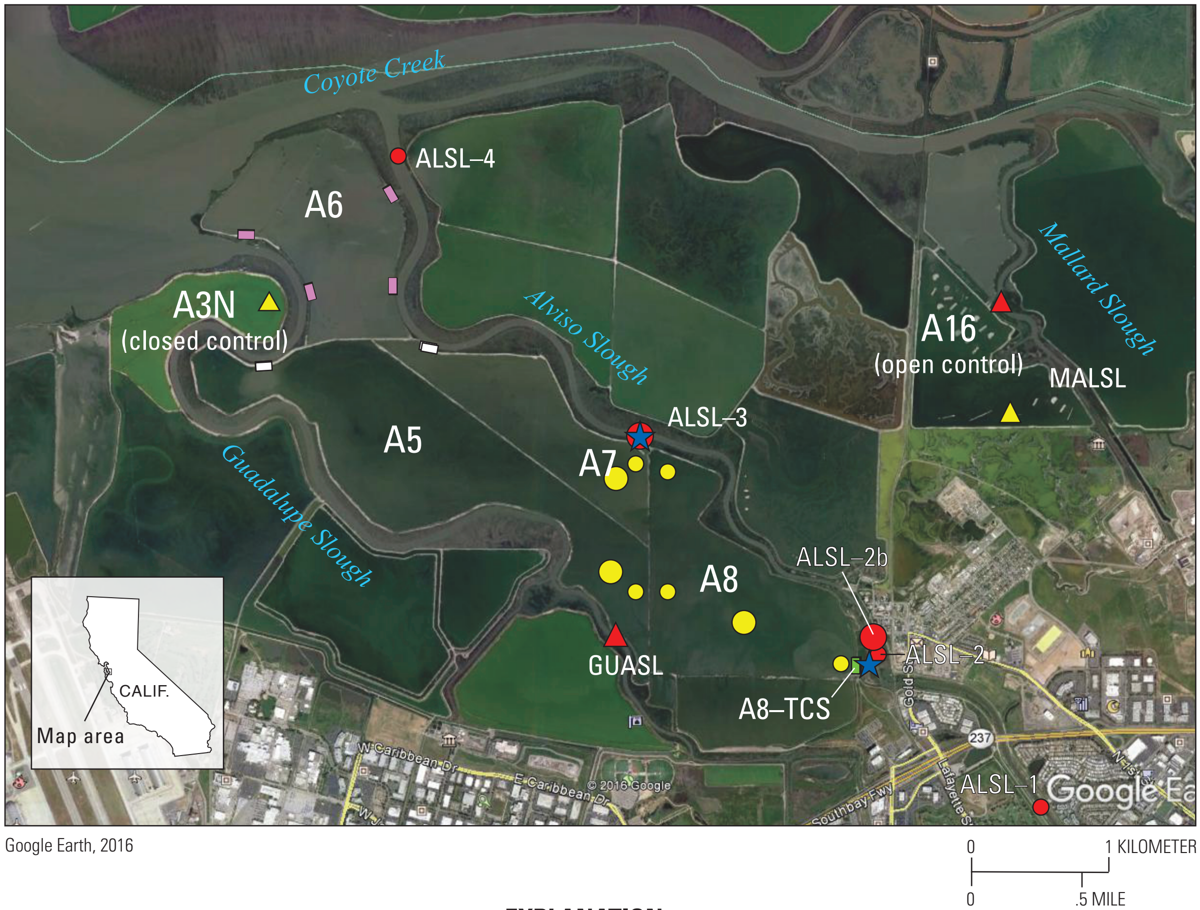

EXPLANATION

An **Pond number**

Water control structure

Pond A8 Tidal Control Structure (A8-TCS)

Pond A6 breach points

Water-quality monitoring site

Pond

- Treatment site sampled 2010–18 or 2014–18
- Treatment site sampled 2010–11
- Reference site

Slough

- Treatment site sampled 2010–18 or 2014–18
- Treatment site sampled 2010–11
- Reference site

Figure 4. Map of the southern San Francisco Bay area depicting locations of surface-water sampling conducted as part of the South Bay Salt Pond Restoration Project Phase 1 studies. Surface-water sampling was conducted by the U.S. Geological Survey (M. Marvin-DiPasquale, lead investigator). The fixed-station, high-resolution, water-quality monitoring sites, located in the middle reach of the Alviso Slough (site ALSL-3) and adjacent to the A8 tidal control structure (A8-TCS) were operated by the U.S. Geological Survey (M. Downing-Kunz, lead investigator).

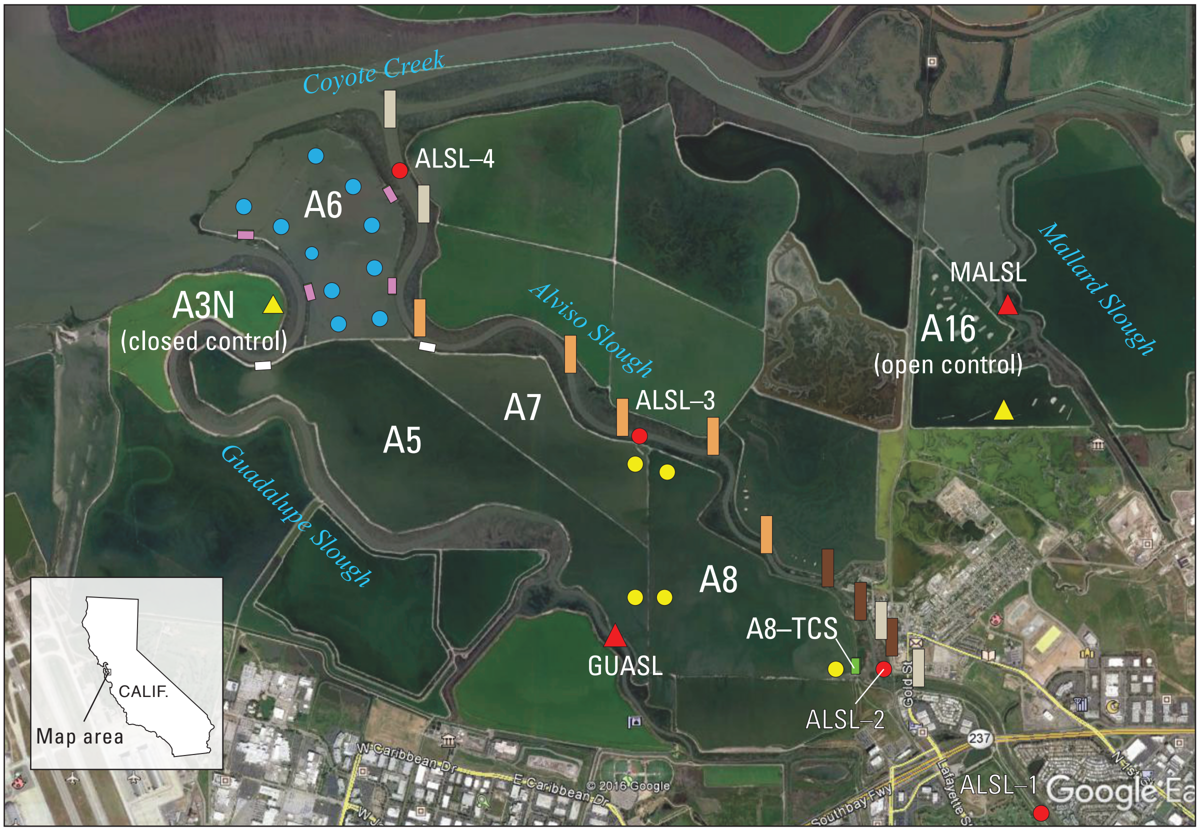

Google Earth, 2016

0 1 KILOMETER
0 .5 MILE

EXPLANATION

An **Pond number**	**Pond**	**Slough**	**Deep core**
Pond A6 sediment sample	Treatment site	Treatment site	September 2006
Water control structure	Reference site	Reference site	May 2012
Pond A8 Tidal Control Structure (A8-TCS)			January 2016
Pond A6 breach points			

Figure 5. Map of the southern San Francisco Bay area depicting locations of bed sediment sampling conducted as part of the South Bay Salt Pond Restoration Project Phase 1 studies. The primary surface sediment (top 0–2 cm) sampling was limited to 2010–11. Deep cores (as much as 2 meters) sampled within the Alviso Slough main channel were collected over three sampling events: September 2006, May 2012, and January 2016. The locations of the pond A8 tidal control structure (A8-TCS) and the four breach points in pond A6 are identified. Additional shallow samples were collected by the University of San Francisco, in pond A6 for a separate study of sediment deposition in that pond, and analyzed for mercury species by the U.S. Geological Survey (M. Marvin-DiPasquale, lead investigator) for this study.

Biota Methods: Bird Eggs

Bird egg sampling and analysis were conducted by USGS (J. Ackerman, lead investigator). The primary avian species used to detect changes in biotic mercury concentrations within the project area described in Ackerman and others (2013b; 2014a) and included sampling of American avocet, black-necked stilts, and Forster's terns. New data and analyses are presented herein for bird egg mercury concentrations that detail the methods for determining THg concentrations in bird eggs.

Bird eggs are an ideal and preferred sampling tissue for environmental mercury monitoring (Ackerman and others, 2016b; Chételat and others, 2020) because (1) 96 percent of the mercury in eggs is in the more toxic and bioaccumulative form of mercury, MeHg (Ackerman and others, 2013a); (2) mercury in eggs relates directly to mercury in the female parent (Ackerman and others, 2020a), and for Forster's terns, to the male parent as well (Ackerman and others, 2016a); (3) mercury in eggs represents recent (weeks) dietary exposure (Heinz and others, 2009) of females from locations very near the nest site (578 m for American avocets and 900 m for Forster's terns) (Bluso-Demers and others, 2008; Demers and others, 2008); and (4) mercury in eggs relates directly to MeHg toxicity benchmarks for policy decisions and management implementation (Ackerman and others, 2016b).

Bird Egg Sampling, Dissection, and Processing

Since 2005, the USGS has monitored the nesting ecology of American avocets, black-necked stilts, and Forster's terns in the southern San Francisco Bay area and have collected eggs for various mercury studies (Ackerman and others, 2013b; Ackerman and others, 2014a; Ackerman and others, 2014c). Starting in 2010, we began sampling eggs with a specific design to monitor the response of mercury bioaccumulation to the restoration of pond A8, and data summary reports are available for the years 2010–11 (Ackerman and others, 2013b), 2013 (Ackerman and others, 2014c), 2014 (Ackerman and others, 2014b), 2015 (Ackerman and others, 2015), 2016 (Ackerman and others, 2016d), and 2017 (Ackerman and others, 2017). Pond A8 was known to have the highest mercury concentrations in fish and birds among any of the >30 wetland sites sampled in the entire San Francisco Bay area (Ackerman and others, 2014a; Eagles-Smith and Ackerman, 2014). Each year since 2010 (except 2012 owing to lack of funding), about 180 eggs per year were sampled to monitor trends in bird egg mercury concentrations in the SBSPRP area (fig. 2). Ideally, a minimum of 14 eggs per colony should be sampled to accurately represent the mean mercury concentration in a small bird colony (Ackerman and others, 2016c). Since 2014, water management in the A8-complex has kept water levels extremely high throughout the bird nesting season and completely flooded most of the former nesting islands, which made them unavailable to nesting birds. Additionally, American avocet, black-necked stilt, and Forster's tern nesting population sizes and colony numbers in the southern San Francisco Bay area have declined in recent years (Hartman and others, 2021). Therefore, we used as many nesting colonies as possible to look at trends in egg mercury concentrations, and these nesting colonies' locations often changed among years. Each year, field crews searched for nesting colony locations, estimated nest numbers during weekly nest monitoring to determine appropriate egg collection sample sizes, and monitored colony development to collect eggs at the appropriate incubation stage (generally <12 days in incubation) and nest status. Once specific nests were identified for sampling, one egg was randomly collected from each nest. After collection, eggs were stored in the refrigerator at 4 °C until egg dissection.

During egg dissection, refrigerated eggs were allowed to warm to room temperature (approximately 26 °C) and then measured for length and width to the nearest 0.01 mm using digital calipers and total weight (with eggshell) to the nearest 0.01 g on an analytical balance. Using clean, stainless-steel instruments, an approximate 15 mm diameter hole was cut in the wide end of each egg and the entire egg contents were transferred into a tared, sterile 30 mL or 60 mL jar for the Forster's tern and black-necked stilt and American avocet eggs, respectively. Egg content weight (without eggshell) was then measured with an analytical balance to the nearest 0.01 g, and stored egg contents at −18° C until processing.

Total mercury concentrations were determined on a dry weight (dw) basis; therefore, eggs were first dried and homogenized. Egg contents were thawed at room temperature and then dried to completion at 50 °C for >120 hrs. To determine moisture content, the dried egg contents were reweighed with an analytical balance to the nearest 0.01 g. The dried egg contents were ground to a powder using a spice grinder with stainless steel blades, and sometimes followed by further grinding in a mortar and pestle if needed. Homogenized egg contents were stored in a desiccator until mercury determination. To account for respiration and moisture loss from the egg during embryo development (Stickel and others, 1973), the dry weight THg concentrations for egg contents were converted to a fresh wet weight THg concentration for each individual egg's contents, following the methods of Ackerman and others (2020b) and accounting for the thickness of the eggshell following Herzog and others (2016). For these calculations, an egg volume coefficient (Kv) of 0.483 for American avocets, 0.490 for black-necked stilts, and 0.506 for Forster's terns, and an egg density coefficient of 1.025 for American avocets, 1.023 for black-necked stilts, and 1.025 for Forster's terns (Herzog and others, 2016), was used.

Mercury Determination in Bird Eggs

Because 96 percent of THg in bird eggs is in the more toxic MeHg form (Ackerman and others, 2013a), THg concentrations were used as an index of MeHg concentrations. Total mercury content was determined using either a Nippon MA-3000 Direct Mercury Analyzer (data after and including 2014; Nippon Instruments North America, College Station, Texas, USA) or Milestone DMA-80 Direct Mercury Analyzer (data prior to 2014; Milestone Inc., Monroe, Connecticut, USA) following Environmental Protection Agency Method 7473 (U.S. Environmental Protection Agency, 2000) at the U.S. Geological Survey, Dixon Field Station Environmental Mercury Laboratory (Dixon, Calif.). An aliquot of 30 mg (black-necked stilts and Forster's terns) or 50 mg (American avocets) of homogenized and dried egg content was weighed to the nearest 0.00001 g, and this weight was used to calculate THg concentration. Quality assurance measures included analysis of a certified reference material (either dogfish muscle [DORM], lobster hepatopancreas [TORT], or dogfish liver [DOLT] tissues certified by the National Research Council of Canada, Ottawa, Canada), system blank, method blank, continuing calibration verification, and duplicate with each set of approximately 10 samples, and 2 spiked duplicates with each batch of about 70 samples. Recoveries (mean±SD) for all 7 years of egg data averaged 100.4±4.0 percent (n=308) for certified reference materials, 99.6±3.9 percent (n=344) for calibration verifications, and 100.3± 3.4 percent (n=204) for matrix spikes. The relative percent difference between duplicates averaged 2.6±2.5 percent (n=261) and averaged 2.3±2.4 percent (n=101) between matrix spike duplicates.

Biota Methods: Pond Fish

The primary fish species used to detect changes in biotic mercury concentrations within the project area overall are described in Ackerman and others (2013b; 2014a) and include three-spine stickleback, longjaw mudsucker, and Mississippi silverside. Pond fish were collected and analyzed by the USGS. The two targeted pond species were the longjaw mudsucker and three-spine stickleback. Field collection and laboratory analytical methods, statistical analysis, and results for fish data produced by the USGS have been previously detailed in the following publications:

- Baseline mercury concentrations for more than 3,000 individual fish (10 species from 32 sites) throughout the San Francisco Bay Estuary, including the current SBSPRP study area and other southern San Francisco Bay wetlands, sloughs, and bay habitats (Ackerman and others, 2014a; Eagles-Smith and Ackerman, 2014),
- rapid changes in fish mercury concentrations as a function of sampling date, including pond A8, that demonstrated sample timing is an important study design component (Eagles-Smith and Ackerman, 2009; Ackerman and others, 2014a),
- a comprehensive report for mercury concentrations in 2,670 fish within the SBSPRP ponds, sloughs, and mudflats collected during 2010–11 and a statistical analysis detailing the initial response to the pond A8 restoration activities associated with the initial construction and opening of the A8 TCS (Ackerman and others, 2013b),
- an update on pond A8 fish mercury concentrations with limited sampling of fish conducted by University of California, Davis in 2014 (Ackerman and others, 2014d), and
- response of pond fish mercury concentrations to experimentally manipulated water levels within ponds A11, A12, and A13 to expose submerged islands for waterbird nesting habitat in pond A12 (Ackerman and others, 2010).

On the basis of these earlier detailed reports that include fish sampled for mercury in pond A8 (and the A8-complex) during 2005–08, 2010–11, and 2014 (fig. 3), we do not repeat those methods and statistical results here. Instead, the previous publications were used to recreate the most pertinent figures for the current synthesis document. Briefly, pond fish were sampled using minnow traps and seines (nets) during spring, and fish were collected within a specified size range (see Eagles-Smith and Ackerman, 2009; Ackerman and others, 2010; Ackerman and others, 2013c; Ackerman and others, 2014a; Ackerman and others, 2014d; and Eagles-Smith and Ackerman, 2014, for more detailed methods).

Biota Methods: Slough Fish

Sampling Design

Slough fish were sampled and analyzed by University of California, Davis (Darell Slotton, Lead Investigator). Two small fish species were targeted for assessing mercury impacts in Alviso Slough directly resulting from Phase 1 management actions. The first, Mississippi silverside, is a rapidly growing, schooling, midwater species that has been used extensively as a mercury biosentinel in work throughout the San Francisco Bay watershed (Greenfield and Jahn, 2010). The second species, three-spine stickleback, is also found within the salt ponds and has been extensively studied there by the USGS (see Eagles-Smith and Ackerman (2009). The sampling of this species provided some degree of overlap between the independently conducted pond and slough fish studies. Both species were collected in the sloughs from 2010 to 2015. After 2015, three-spine stickleback became too scarce to provide statistically useful collections. Their scarcity after 2015 was suggested to be in response to successive drought years and associated changes in salinity (Hobbs, 2018). Mississippi silverside remained relatively prevalent through 2015–18 and were collected in good numbers throughout Phase 1.

The sampling design was species specific. Three-spine stickleback were analyzed individually, and as many as 15 individuals (as available) were analyzed independently for each sample. This was done to match the sampling approach conducted inside the ponds by the USGS. Also consistent with the ponds sampling, three-spine stickleback for analysis were targeted in the size range of 30–50 mm standard length, or approximately 35–55 mm total length. Mississippi silverside, in contrast, were analyzed with multiple composite samples, each containing multiple individuals. This was done to lower project costs and to roughly correspond to small fish sampling protocols conducted throughout San Francisco Bay by the Regional Monitoring Program (Greenfield and others, 2013). That program uses four composites of five Mississippi silverside each, with each composite composed of fish within a 10 mm size window, from a set of smallest fish of 40–50 mm to a largest set within the 70–80 mm size window. The SBSPRP Phase 1 study includes a compromise between this composite analysis and the typical individual fish analyses. This compromise expanded the number of composites per sample to 6, increased the number of fish per composite to 8 (48 individual Mississippi silverside per sample), and narrowed the sequential size windows to 5 mm increments, which spanned a narrower overall range of 45–75 mm.

Field Collections

Three slough sites were sampled nearly continuously across the 2010–18 Phase 1 study period (fig. 3). One site was located in upper Alviso Slough (ALSL-2) directly downstream (approximately 0.2 km) from the A8-TCS. A second Alviso Slough site was situated midway between the A8-TCS and the Alviso Slough downstream confluence with Coyote Creek (ALSL-3). The MALSL reference site is approximately 3.0 km north of ALSL-2 and is located within Mallard Slough. A second reference site within Guadalupe Slough (site GUASL) was approximately 1.6 km south of ALSL-3 and was added in 2013. Relative to the upstream mining history, GUASL functioned as a relatively high mercury reference site similar to Alviso Slough, whereas site MALSL is a relatively lower mercury reference site located in a different drainage. Other sites that were studied during 2010–11 and then discontinued include Alviso Slough sites ALSL-1, located upstream from the A8-TCS and site ALSL-4, adjacent to pond A6 near the Alviso Slough and Coyote Creek confluence, and the Sunnyvale wastewater treatment plant discharge channel to Guadalupe Slough (SUNNY) (fig. 3).

The sloughs and tidal channels of the southern San Francisco Bay salt ponds area are a challenging habitat for collecting the target small fish. This is mainly because of the dramatic tidal range of as much as 13 feet or more between low and high tides, and the mud that is exposed during all but high tides being too soft to wade upon. A wide variety of netting, seining, and trapping techniques were initially employed along Alviso Slough and in the two reference sloughs (Mallard and Guadalupe Sloughs at sites MALSL and GUASL, fig. 3). The most effective of these were boat-assisted seining and passive tidal seining, which were subsequently employed throughout the Phase 1 studies. Both utilized seines constructed with approximately 5 mm mesh size, a central box-like structure to corral fish, weighted bottom lines, and floating top lines. Seines ranged from 10 to 30 m in length and 1 to 3 m in height, which were attached at each end to 2-m-long stout wooden dowels. In boat-assisted seining, one dowel of the seine was clipped to the front of the boat and was bottom-weighted to stay vertical. A 12-m-long rope with a terminal grip bar was tied to the dowel at the other end of the seine. This shore end of the net could then be dragged by a researcher on relatively firm footing above the mudline, while the boat operator slowly matched speed, motoring in reverse. In passive tidal seining, seines were placed perpendicular to the tidal current (always on descending tides), using the seine dowel to secure the shore end and a heavy 3–5-m-long dowel to secure the deep end. Both dowels were driven deeply into the bottom sediment, at an angle toward the oncoming current. Passive seines were set adjacent to the shore for as long as an hour before retrieving. During seine retrievals of all types, target fish were transferred to temporary containers containing site water and non-target fish were quickly released. Target fish were individually measured and sorted into size class holding containers with site water. When the needed numbers of fish were accumulated, they were placed by size class into doubled zip-close bags with site water, sealed removing all bubbles, and field euthanized and preserved by gradual cooling to torpor and freezing on dry ice in a chest using a protocol approved by the UC Davis Wildlife Veterinary Oversight group. Freezing with water surrounding the samples maintains natural moisture content and subsequent analytical accuracy (Slotton and others, 2002). Samples were kept frozen during transport and in laboratory freezers before preparation and analysis.

Pre-analytical Sample Preparation

The processing of each fish sample prior to analysis began by thawing the frozen fish and determining the fresh weight. Care was taken to preserve fresh consistency for the initial weighing process and avoiding sample desiccation or excess surface moisture. Fish samples were subsequently dried to constant weight for 2–4 days (as needed) at 55 °C, and the final weight was recorded for calculation of percentage solids and used for the conversion of dry weight analytical data to corresponding fresh weight concentrations. Dried samples were each ground to a fine powder with a modified coffee grinder for analytical consistency. Samples were analyzed as homogeneous and dry powders.

Mercury Analysis

Whole-body mercury was assessed as THg. Samples were analyzed for THg by standard cold vapor atomic absorption spectrophotometry (CVAAS), using a dedicated Perkin Elmer Flow Injection Mercury System (FIMS) with an AS-90 autosampler, following a two-stage digestion at 90 °C in a mixture of concentrated nitric and sulfuric acids with potassium permanganate (Slotton and others, 2004). The method is a variant of U.S. Environmental Protection Agency Standard Method 245.6 (U.S. Environmental Protection Agency, 1991). Routine analytical Quality Assurance and Quality Control

(QA and QC) included 13 QA and QC samples for every 20 analytical samples, plus an 8-point set of aqueous mercury standards for each full run. All aqueous standards and QA and QC samples were subjected to the same acid digestion, physical and chemical treatment, and detection as analytical samples and included, for each 20 field samples, 3 method blanks, 3 standard reference materials with certified levels of THg, 3 continuing calibration samples, a laboratory duplicate, a spiked field sample, a spike duplicate, and an aqueous calibration sample. Performance was tracked with control charts and sample material was archived in case of the need to re-analyze based on QA and QC samples exceeding control limits.

Data Analysis

Several Least Squares Mean (LSM) statistical models were developed to examine slough fish data. LSM models are powerful multivariable models that allow us to test the significance of each model term (for example, temporal and spatial explanatory variables), while simultaneously controlling for the effects of the other model terms. Such models can include a combination of main effects (individual spatial and temporal model terms), interaction effects (between main effects) and random effects. The LSM values resulting from each model term differ from simple arithmetic means, which do not simultaneously consider the variability in the overall data due to multiple other factors. Thus, LSM results can isolate the effect of individual factors, while simultaneously controlling for other factors. JMP statistical software (version 14.3.0, SAS Institute, Inc.) was used for developing LSM models, as well as for generating simple summary statistics. For all statistical assessments, statistical significance was based on the traditional criteria of a probability (p) level less than 5 percent ($p < 0.05$) for Type II error. Many of the models used natural logarithm (ln) transformations of the dependent variable. Results were back-transformed into normal space for the final tabular or graphical presentation using the delta method for calculating the associated standard error (Williams and others, 2002).

Variability of the slough fish dataset resulted from multiple factors, including the temporal discontinuity in sampling during the 2010–18 Phase 1 period, the multiple sampling locations (sites and sloughs), the targeted sampling of two distinct fish species, and the natural size variability of the fish sampled. To minimize this overall variability, the length versus THg concentration relationship was developed to size-standardize fish THg concentration data for each of the two fish species. The approach followed that described in Eagles-Smith and Ackerman (2009), which used the natural logarithm (ln) transformed THg concentration data and a LSM model to control for sampling site (ALSL-2, ALSL-3, MALSL, and GUASL). The general form of this model (Model SL.FISH.1) is shown in equation 1:

$$\ln[\mathrm{THg}]_{[\mathrm{species}]} = \mathrm{SITE} + \mathrm{LENGTH} + [\mathrm{SITE} \times \mathrm{LENGTH}] \quad (1)$$

where

$\ln[\mathrm{THg}]_{[\mathrm{species}]}$ is the species-specific, natural logarithm (ln) transformed, fish THg concentration (µg/g dw);

SITE is the categorical variable for sampling site (with sites ALSL-2, ALSL-3, MALSL, and GUASL as factors);

LENGTH is the continuous variable for fish length (mm); and

[SITE x LENGTH] is the interaction term.

On the basis of the median total length values for each species and using the species-specific Model SL.FISH 1 (equation 1) prediction equations, Mississippi silverside and three-spine stickleback THg concentration data was standardized to fish lengths of 60 mm and 40 mm, respectively.

Subsequently, a LSM model (Model SL.FISH.2) was applied to the size-standardized slough fish datasets that focused on sampling site and year, and was of the general form shown in equation 2:

$$\ln[\mathrm{THg}]_{[\mathrm{s.species}]} = \mathrm{SITE} + \mathrm{YEAR} + [\mathrm{SITE} \times \mathrm{YEAR}] \quad (2)$$

where

$\ln[\mathrm{THg}]_{[\mathrm{s.species}]}$ is the species-specific, natural logarithm (ln) transformed, size-standardized fish THg concentration (µg/g dw);

SITE is the categorical variable for sampling site (with sites ALSL-2, ALSL-3, and MALSL as factors);

YEAR is the categorical variable for sampling year (with years 2010, 2011, 2013 as factors); and

[SITE x YEAR] is the interaction term.

To avoid non-convergent (non-viable) model results, Model SL.FISH.2 did not include GUASL as a factor of the variable SITE, since the sampling of fish at this site did not begin until 2013.

Although Model SL.FISH.2 was useful in describing three-spine stickleback data, it was of limited usefulness in describing Mississippi silverside data because of significant interaction effects and seasonally specific spikes in THg concentration (see “Individual Study Results” section). Thus, a more temporally discriminating model, based upon season, was necessary. Analysis of the annual slough fish data distribution led to the categorization of the small fish data into two seasonal groupings, an early annual period for samples collected from April through July (model factor used is [APR–JUL]) and a later annual period for samples collected from August through February (model factor used is [AUG–FEB]). A subsequent model (Model SL.FISH.3) used to examine seasonal differences by site was of the form shown in equation 3:

$$\ln[THg]_{[s.species]} = SITE + SEASON + [SITE \times SEASON] \quad (3)$$

where

SITE is as defined in equation 2;

SEASON is the categorical variable for season (with [APR–JUL] and [AUG–FEB] as factors); and

[SITE x SEASON] is the interaction term.

A final temporal model (Model SL.FISH.4) used to examine the small fish data involved categorizing the data by season and year (for example, [APR–JULY], 2010, and [AUG–FEB], 2011) to determine if there were annual differences in fish THg within the context of each of the two defined seasons. The form of this model is shown in equation 4:

$$\ln[THg]_{[s.species]} = SITE + YEAR.SEASON + [SITE \times YEAR.SEASON] \quad (4)$$

where

SITE is as defined in equation 2

YEAR.SEASON is the categorical variable for season and year combined (as per above example); and

[SITE x YEAR.SEASON] is the interaction term.

Separate model runs were independently conducted on the data grouped either by early season [APR–JUL] or late season [AUG–FEB] to address questions associated with differences among years, by season. In instances of model nonconvergence, owing to missing data, Model SL.FISH.4 was simplified to include only the YEAR.SEASON term, and model runs were conducted on each sampling site independently according to Model SL.FISH.5, which was of the form shown in equation 5:

$$\ln[THg]_{[s.species]} = YEAR.SEASON \quad (5)$$

Where all model terms are as previously described, and the model was applied to data subset on a site-by-site basis.

Surface-Water Methods

Surface-Water Sampling Overview

The sampling of surface water in sloughs and ponds as part of the Phase 1 studies can be grouped into three categories: (1) 2010–18 Primary mercury time series in ponds and sloughs; (2) 2012–13 middle Alviso Slough (site ALSL-3) Diel (25 hour) mercury studies; and (3) high-resolution fixed station monitoring of (nonmercury) water quality. Although the primary mercury time-series and diel studies also included a wide suite of nonmercury parameters (table 2), the temporal density of these two data collection efforts are temporally considered low-resolution (primary time series) and moderate resolution (diel studies) in nature. However, when modeled in conjunction with the high-resolution fixed-station water quality data, we were able to develop several high-resolution temporal analyses for THg and MeHg, which were primary accomplishments of this synthesis effort. The methods associated with these three components are first described independently and followed by a description of how high-resolution time-series analysis of surface-water mercury species was done.

Pond and slough surface-water parameters sampled and directly measured by the USGS laboratory in Menlo Park, Calif., for this 2010–18 dataset are listed in terms of their respective parameters measured in table 2. The numeric results, quality assurance results, sampling site coordinates, and methods citations have been previously published (Marvin-DiPasquale and others, 2019)

Ponds and Sloughs: 2010–18 Primary Mercury Time Series

The majority of the surface-water data collected for both mercury and nonmercury parameters were conducted during two main sampling periods (2010–11 and 2014–18) at a series of fixed pond and slough locations (fig. 4). The data gap between the two periods (2012–13) was associated with the availability of funding, and the difference between the two periods reflected a shift in program focus.

The first sampling period (2010–11) and the specific sampling locations generally coincided with the collection of shallow sediment samples described below, and included four sampling events (April, May, June, and August) in each year over the 2-year period. This timeframe encompassed the periods immediately preceding and immediately after the breaching of pond A6 (December 2010) and the initial opening of the A8-TCS (June 1, 2011). The focus of this data collection was to examine if any notable changes in mercury or nonmercury surface-water parameters were directly attributable to these two specific management actions, either within Alviso Slough or within the A8-complex. The surface water of two reference ponds (A16 and A3N) and a reference slough (Mallard Slough; site MALSL) were also sampled during the 2010–11 period. Owing to potential variations in constituent concentrations throughout a typical tidal cycle, water sampling from slough sites was targeted for the ebb portion of the tidal cycle, within 2 hours of peak high tide for consistency.

Routine surface-water sampling of the previously established pond and slough sites resumed in 2014 and continued through early 2018, with the following modifications: (1) in the A8-complex, sites A8-1 and A8-3 were removed, and site A8-4 was established; site A5-1 was removed, and site A5-2 was established (beginning in 2015); site A7-1 was removed after 2014, and site A7-2 was established (beginning in 2015); (2) in the Alviso Slough, sites ALSL-1 (farthest upstream site) and ALSL-4 (farthest downstream site) were removed; site ALSL-2 was moved approximately 0.5 km further downstream from the A8-TCS connector channel (site ALSL-2b established); and (3) a second reference slough site was established in Guadalupe Slough (site GUASL; fig. 4).

Table 2. List of directly measured pond and slough surface-water parameters for the 2010–18 and (or) 2012–13 datasets.

[For each parameter, the name, notation, and units measured in is given. Also noted (with 'X') is if a given parameter was associated with the primary 2010–18 time-series data (low-resolution, monthly sampling), the 2012–13 middle Alviso Slough (site ALSL-3) Diel sampling (moderate-resolution, hourly sampling), or both. Calculated parameters, derived from direct measurements (for example, percent methylmercury) are not listed, but are noted in the text and data tables as necessary. Ng/L, nanogram per liter; %, percent; ng/g, nanogram per gram; °C, degree Celsius; µS/cm, microsiemens per centimeter; mg/L, milligram per liter; mV, millivolt; QSU, quinine sulfate units; L/(mg-C*m), liter per milligram carbon per meter; dw, dry weight; per mil, parts per thousand; µg/L, microgram per liter; P, phosphorous; N, nitrogen; mmol/L, millimole per liter; FNU, formazin nephelometric units]

Parameter name	Parameter notation	Units	2010–18 time series	2012–13 Diel studies
Mercury parameters				
Filter-passing methylmercury[1]	f.MeHg	(ng/L), (% of f.THg)	X	
Filter-passing total mercury[1]	f.THg	(ng/L)	X	X
Particulate methylmercury	p.MeHg	(ng/L), (ng/g), (% of p.THg)	X	X
Particulate total mercury	p.THg	(ng/L), (ng/g)	X	X
Particulate inorganic reactive mercury	p.RHg	(ng/L), (ng/g), (% of p.THg)	X	X
Nonmercury parameters				
Temperature	TEMP	(°C)	X	X
Specific conductance	SpC	(µS/cm)	X	X
pH	pH	Unitless	X	X
Dissolved oxygen	DO	(mg/L), (%)	X	X
Redox potential	E_h	(mV)	X	X
Fluorescent dissolved organic matter	f.DOM	(QSU)	X	
Dissolved organic carbon	DOC	(mg/L)	X	
Specific UV absorbance at 254 nm	$SUVA_{254}$	(L/(mg-C*m)	X	
Particulate organic carbon	POC	(% dw)	X	X
Delta carbon-13 of particulate organic carbon	δ13C-POC	(per mil)	X	X
Particulate nitrogen	PN	(% dw)	X	X
Delta nitrogen-15 of particulate nitrogen	δ15N-PN	(per mil)	X	X
Chlorophyll a	Chl.a	(µg/L)	X	X
Phosphate	PO_4^{3-}	(mg/L as P)	X	
Nitrite + Nitrate	$NO_2^-+NO_3^-$	(mg/L as N)	X	
Sulfate	SO_4^{2-}	(mmol/L)	X	
Chloride	Cl^-	(mmol/L)	X	
Turbidity	TURB	(FNU)	X	
Total suspended solids	TSS	(mg/L)	X	X

[1] Measurement used 0.3 or 0.7 micrometer glass fiber filters.

Middle Alviso Slough Diel (25 hour) Mercury Studies

A series of hourly surface-water sampling events were conducted at a single site within Alviso Slough (ALSL-3; fig. 4), co-located with the fixed-buoy monitoring station established to collect 15-minute water quality data and suspended-sediment flux (see the "Continuous Water Quality Monitoring Stations" section). The purpose of these sampling events was to better understand how various mercury and nonmercury constituent concentrations varied over the full tidal cycle, and how this may differ seasonally. There were five sampling events of this kind, which included the four seasons: spring (May 2012), summer (July 2012), fall (November 2012) winter (February 2013), and the first high-flow event of the 2012–13 water year (December 2012). During all events, surface-water samples were collected from the top 0.5 m of the water column every hour over a 25-hour sampling period (allowing a one hour overlap between the successive start and end days to account for the approximately 25-hour tidal cycle to fully complete). All water constituents were either measured immediately upon collection (for example, electrochemical probe measurements of pH, DO, and salinity) or sub-sampled (for example, filtered) and preserved (for example, chilled or frozen) immediately after collection.

Surface Water: Statistics

For the purposes of statistical modeling, surface-water data were spatially categorized into 7 sampling regions (the categorical model term used is, REGION): 3 ponds (A8-complex, A3N, and A16) and 4 sloughs (upper Alviso Slough [the model factor used is, up.ALSL], lower Alviso Slough [the model factor used is, low.ALSL], Mallard Slough [as site MALSL], and Guadalupe Slough [as site GUASL]). Each sampling region consisted of one or more (pooled) sampling locations (discrete sites), depending on sampling period and sampling region, as noted below.

The specific statistical models employed to examine surface-water data are summarized below relative to the specific questions they are associated with (from the "Mercury Synthesis—Organizing Questions" section).

QUESTION 1: To what extent did the pond A6 levee breach result in directly measurable changes in mercury concentrations in Alviso Slough biota, surface water, and (or) bed sediment?

This question focuses on whether, and to what extent, the breaching of pond A6 resulted in any measurable changes in surface-water mercury (and nonmercury) parameters. The breaching of this pond is expected to have had the most direct effect on surface water chemistry in the lower Alviso Slough sampling region during the period immediately after the breach. Thus, the model focused on surface-water data collected from the lower Alviso Slough sampling region (model factor low.ALSL) and the reference slough site MALSL for comparison during 2010–11, which encompassed the periods immediately prior to (2010 data) and following (2011 data) the pond A6 breach event. In this instance, the LSM model was used to spatially and temporally analyze the surface-water data collected during the 2010–11 time period. The form of the LSM model (Model SW.1) used to address Q.1 is shown in equation 6:

$$Y = YEAR + REGION + [YEAR \text{ x } REGION] \tag{6}$$

where

- Y is any surface water parameter;
- YEAR is the categorical variable for sampling year (with years 2010 and 2011 as factors);
- REGION is the categorical variable for sampling regions (with lower Alviso Slough [low.ALSL] and Mallard Slough [site MALSL] as factors) ; and
- [YEAR x REGION] is the interaction term.

No random effect was included in this model.

QUESTION 2: To what extent did the construction and gradual increased opening of the A8-TCS result in measurable changes in mercury concentrations in biota, surface water, and (or) bed sediment within the A8-complex?

This question focuses on whether the gradual opening of the A8-TCS resulted in measurable changes in surface water mercury (and nonmercury) parameters within the A8-complex as a result of gate operations. To address this question the surface-water data was subset to include only sites within the A8-complex. The one-way analysis of variance (ANOVA) model used (Model SW.2) was of the form shown in equation 7:

$$Y_{[COMPLEX]} = GATE \tag{7}$$

where

- $Y_{[COMPLEX]}$ is any surface water parameter, limited to sites within the A8-complex; and
- GATE is the categorical variable for the number of A8-TCS gates open (with factors of PRE, 1, 3, 5, and 8), which included the 'PRE' condition defined as the April 2010—May 2011 period before the initial gate opening event.

The number of open gates at the A8-TCS are herein referred to as gate conditions (for example, 3 would refer to the 3-gate condition). Because there was only a single sampling event (February 2014) with no gates open (0-gate condition) after the initial opening of the A8-TCS, this event was dropped from the analysis.

QUESTION 3: To what extent did the construction and gradually increased opening of the A8-TCS result in measurable changes in mercury concentrations in Alviso Slough biota, surface water, and (or) bed sediment?

This question focuses on whether the gradual opening of the A8-TCS resulted in any measurable changes in Alviso Slough surface water mercury (and nonmercury) parameters. To address this question, the surface-water data was first subset to include only sites ALSL-2, ALSL-2b, and ALSL-3. Data from sites ALSL-1 (upstream from the A8-TCS) and ALSL-4 (near the mouth of the Alviso Slough) were excluded from the analysis because they were only sampled during the 2010–11 period, and thus only included the 0- and 1-gate conditions. In contrast, the three Alviso Slough sites that were included in the analysis represented all five A8-TCS operation conditions (0, 1, 3, 5 and 8 gates open) over the 2010–18 study period. In addition, these three sampling locations are representative of the two defined sampling regions within Alviso Slough: upper Alviso Slough (sites ALSL-2 and ALSL-2b, just downstream from the A8-TCS; model factor used is up.ALSL) and lower Alviso Slough (site ALSL-3; model factor used is low.ALSL). The LMS model (Model SW.3) initially used to assess Q.2 was of the form shown in equation 8:

$$Y_{[ALSL]} = GATE + REGION + [GATE \text{ x } REGION] \tag{8}$$

where

- $Y_{[ALSL]}$ is any surface water parameter measured in Alviso Slough (at sites ALSL-2, ALSL-2b and ALSL-3 only);
- GATE is the categorical variable for the number of A8-TCS gates open (with factors 0, 1, 3, 5, or 8);

REGION is the categorical variable for sampling regions within Alviso Slough (with factors up.ALSL and low.ALSL); and

[GATE x REGION] is the interaction term.

Note that for Model SW.3, sites ALSL-1 and ALSL-4 were not included in the sites that defined REGION factors up.ALSL and low.ALSL, respectively, because the sampling of these two sites was not continued after 2011.

In instances for which the interaction term was statistically significant ($p < 0.05$), indicating that the GATE effect (statistically significant differences found among the GATE factors) differed between the model factors up.ALSL and low.ALSL regional groupings, the water quality parameter was rerun using Model SW.4 shown in equation 9, which assessed the GATE effect for the two regions independently.

$$Y_{[\text{up.ALSL, low.ALSL}]} = \text{GATE} \tag{9}$$

where

$Y_{[\text{up.ALSL, low.ALSL}]}$ is any surface-water parameter measured in sampling regions factor up.ALSL or factor low.ALSL, analyzed independently, and

GATE as defined in equation 8.

In addition, Model SW.4 was also used where Model SW.3 did not converge owing to missing Y-parameter data for a given GATE condition (number of open gates at A8-TCS) at one of the two Alviso Slough regions.

Continuous Water Quality Monitoring Stations

An instrument package was deployed from October 14, 2010, through February 27, 2018, in the thalweg of Alviso Slough (USGS station 11169750 [Alviso Slough near Alviso, Calif.], study site ALSL-3, fig. 4) approximately 4.4 km from the confluence with Coyote Creek (6 km to San Francisco Bay). The package consisted of two instruments: a near-bottom (0.46 m above bottom) water quality sonde (model YSI 6920), which measured conductivity, temperature, depth, turbidity and dissolved oxygen, and an upward-looking acoustic Doppler current profiler (ADCP, 1000 kHz Nortek Aquadopp model), which profiled velocity throughout the water column. All instruments collected data on a 15-minute interval and were serviced every 4 to 6 weeks for data download, instrument cleaning, and calibration checks following standard USGS procedures (Wagner and others, 2006). Values of salinity were reported using the practical salinity units (psu) scale (unitless). Data gaps in the time series data were the result of biofouling of the sensors, instrument malfunction, or servicing.

An identical instrument package was deployed in the connector channel between the A8-TCS and Alviso Slough (USGS station 372525121584701 [Alviso Slough feeder channel at Alviso, Calif.]) between September 23, 2015, and February 27, 2018. Instruments were situated 0.4 m above the benthos in the connector channel thalweg.

Suspended-sediment flux (Qs) was calculated as the product of water discharge (Q) and suspended-sediment concentration (SSC). Water discharge was computed by calibrating an index velocity and stage measured at the instrument package to channel-averaged velocity and cross-sectional area, on the basis of periodic boat-mounted ADCP velocity and depth measurements (Ruhl and Simpson, 2005; Levesque and Oberg, 2012).

Point turbidity measurements were calibrated to depth-integrated, cross sectionally averaged, equal discharge increment (EDI) suspended-sediment samples to compute a time series of cross sectionally averaged SSC collected during boat-based discharge measurements (Edwards and Glysson, 1999). This method accounts for vertical variability in SSC by collecting depth-integrated EDI samples over the range of conditions experienced at the site. The turbidity to SSC calibration was conducted following the methods described by Rasmussen and others (2009).

Q Ratio

To examine if there was a measurable change in discharge (Q) in tidally affected Alviso Slough in response to changes in A8-TCS manipulations (Q.3 of the “Mercury Synthesis—Organizing Questions” section), discharge from USGS streamgage station 11169025 (Guadalupe River above Highway 101 at San Jose, Calif.) located approximately 8 km upstream from the A8-TCS in the Guadalupe River and upstream of tidal influence) was used as a reference. Guadalupe River is the only freshwater inflow into Alviso Slough. The A8-TCS is located downstream from streamgage station 1169025 and upstream from the continuously monitored station 11169750 (co-located with study site ALSL-3, fig. 4). Thus, the comparison of Q between these two monitoring stations can be used as a metric to examine the effect of management actions that occurred between the two, specifically the varying A8-TCS gate operations. Daily averaged Q for Guadalupe River (Q_{GR}) was computed from the upstream USGS streamgage station 11169025 by averaging the 15-minute discharge data over each day. Computation of daily mean Q at the tidally affected study site ALSL-3 at station 1169750 (Q_{ALSL}) required first computing the tidally filtered 15-minute discharge to remove aliasing introduced by tidal periodicity; this was accomplished using a low-pass Butterworth filter with a 30-hour stop period and a 40-hour pass period (Downing-Kunz and Schoellhamer, 2015) to retain subtidal variations in discharge. Q_{ALSL} is the resulting mean of the tidally filtered 15-minute data from each day. The Q ratio was computed as the ratio of daily averaged discharge for Alviso Slough to that for Guadalupe River (Q_{ALSL}/Q_{GR}), which provides a daily comparison of inflow from the watershed to outflow to the estuary. For a Q ratio of about 1, daily inflow and outflow are balanced. Q ratio < 1 indicates less outflow than inflow, whereas Q ratio > 1 indicates more outflow than inflow.

High-Resolution Time Series Modeling of Mercury Species at Site ALSL-3

To further address Q.3, high-resolution time series predictions of 15-minute and cumulative flux for particulate total mercury (p.THg) and particulate methylmercury (p.MeHg) were developed for the ALSL-3 site. The predictive models created for this purpose were developed from the low temporal resolution sampling (monthly to seasonally during 2010–11 and 2014–18) of surface-water p.THg and p.MeHg concentration data (volumetric basis), plus the higher resolution diel sampling (five discrete sampling events between May 2012 and February 2013, each with hourly sampling over 25 hours). The models were applied to the high-resolution (15-minute) fixed station monitoring data (SSC, tidal stage, and Q) at site ALSL-3.

The final models developed to predict both p.THg and p.MeHg concentration at site ALSL-3 included the following explanatory variables, filter-derived total suspended solids (TSS) concentration; Julian Day (JD, day of year); and tidal stage (ST). The resulting predictive equations for both models are given in appendix 2. The models produced some unrealistic (negative) values of concentration: 17 percent of the predicted p.THg values were negative, and 1 percent of the predicted p.MeHg values were negative. To calculate fluxes from these models, negative concentration values were substituted with concentrations of 1 nanogram per liter (ng/L) for p.THg and 0.1 ng/L for p.MeHg.

To apply the p.THg and p.MeHg predictive models to the high-resolution data collected at site ALSL-3, SSC (estimated from an optical turbidity sensor at fixed station) data were used in place of TSS (filter-derived data from periodic sampling, which were used to develop the predictive models). This was done in lieu of developing a site-specific relationship between SSC and TSS, because the correlation between these parameters was poor ($r < 0.3$). This weak relationship is likely due to three main factors: (1) temporally paired TSS and SSC data were not determined from the same water sample and were not necessarily concurrent samples (that is, they were not collected within 15-minutes of each other); (2) the samples for TSS and mercury analysis were collected just below the water–air interface (top 0–20 cm of water column), whereas the optical turbidity data were measured near the channel bottom (40 cm above the bed); and (3) the TSS data were directly measured in the laboratory (based on 0.7-micrometer [µm] filtered particulate mass), whereas the SSC data were estimated from a regression between optical turbidity versus cross sectionally averaged SSC, as described above. Had TSS and SSC laboratory measurements been made on splits from the same water samples, we would anticipate a higher correlation between these two variables. Considering this, and for the purposes of developing the high-resolution time series datasets for mercury species, the simplifying assumption was made that SSC is equal to TSS. This assumption can be problematic when sediment is course or SSC exceeds 1,000 mg/L (Gray and others, 2000). However, the vast majority (>95 %) of bottom sediment at site ALSL-3 is silt and (or) clay (< 63 µm size fraction), and suspended sediment is expected to be finer than the bottom sediment. In addition, none of the TSS samples from site ALSL-3 and fewer than 1 percent of optical turbidity-derived SSC samples exceeded this 1,000 mg/L threshold. Thus, the assumption that SSC is equal to TSS was deemed reasonable for the purposes of generating high-resolution time series data at site ALSL-3 for surface-water particulate mercury species.

The high-resolution model-predicted p.THg and p.MeHg concentration dataset generated for site ALSL-3 was also assessed temporally to examine both seasonal and inter-annual differences that may have been affected by the management actions under study. The following LSM (Model SW.5) was applied to the complete 15-minute model-predicted dataset for site ALSL-3 and is shown in equation 10:

$$Y = \text{SEASON} + \text{YEAR} + [\text{SEASON x YEAR}] \tag{10}$$

where

Y is the p.THg or p.MeHg concentration (either volumetric or gravimetric);

SEASON is the categorical variable for season with factors coded as follows: [winter] for December–February, [spring] for March–May, summer for June–August, and [fall] for September–November;

YEAR is the categorical variable for year with individual sampling years 2012–2017 as factors; and

[SEASON x YEAR] is the interaction term.

Since the winter grouping includes months that overlap two consecutive years, for the purposes of this model, the YEAR coding represents the year the winter seasonal grouping began (for example, January and February of 2018 would be coded as *YEAR* 2017 since the winter seasonal grouping began in December 2017).

Modeling Mercury Flux at the A8-TCS

To address Q.4 (“Mercury Synthesis—Organizing Questions” section), the flux of mercury species (filtered and particulate) into and out of the A8-complex was modeled at the A8-TCS fixed monitoring site using a high temporal resolution approach similar to that described above for site ALSL-3, with a few key differences. First, because of the existence of the A8-TCS and the separation of water on either side of it, two predictive models were needed for each mercury species; one model is associated with flood tides derived from surface-water data collected within the Alviso Slough at sites ALSL-2 and ALSL-2b (located less than 0.4 km downstream from the A8-TCS fixed monitoring station) and the other associated with ebb tides derived from surface-water data collected within the A8-complex. Second, in addition to particulate THg and MeHg flux as assessed for site ALSL-3, dissolved THg and MeHg flux were also assessed at the A8-TCS site. Third, stepwise regression was used to derive the best predictive model from a suite of likely independent variables.

For the flood tide mercury species concentration models, independent variables considered included, Julian Day (JD, day of year), specific conductance (SpC), TSS, Q_{GR}, tidal stage (ST, water depth at the A8-TCS monitoring site) and water temperature. Owing to the limited number of observations at sites ALSL-2 and ALSL-2b (n=19 combined), the number of variables in the final models were limited to two (excluding potential interaction terms). For the ebb tide mercury species concentration models, the same variables were included, with the exception of tidal stage at the A8-TCS fixed monitoring site, which was excluded. To assess whether the individual mercury species concentrations differed between the three ponds that make up the A8-complex (A5, A7, A8), a LSM statistical analysis of mercury species concentrations was performed to test for spatial differences among the three ponds, while controlling for sampling event. There were differences among the ponds for all mercury species with the exception of p.MeHg (on a volumetric (ng/L) basis). Thus, for this sole mercury parameter, the ebb tide predictive model was constructed to leverage data from all three A8-complex ponds, whereas all other mercury models relied only on data from pond A8 (closest to the A8-TCS). The resulting predictive models for all mercury species concentrations used to calculate high-resolution mercury flux at the A8-TCS fixed monitoring site are given in appendix 2.

Bed Sediment Methods

Bed Sediment Sampling Overview

Sediment sampling conducted as part of the Phase 1 Mercury studies can be grouped into three categories: (1) ponds and sloughs: shallow sediment routine sampling, 2010–11; (2) pond A6: intensive sampling of shallow sediment, 2010–12; and (3) Alviso Slough deep cores, 2012 and 2016. The focus of the 2010–11 shallow sediment sampling efforts was to determine if there were any notable changes in surface-sediment mercury concentrations in the A8-complex or in Alviso Slough that were directly attributable to, or affected in the months immediately after, the initial breach of pond A6 or the initial opening of the A8-TCS. The sampling of pond A6 shallow sediment was limited and designed to assess how much mercury was transported into this pond following its breaching. The collection of deep cores during 2012 and 2016 was to augment the bathymetry mapping work being done along Alviso Slough (Foxgrover and others, 2018) and to model the mobilization of sediment-associated mercury as a function of these two management actions (Foxgrover and others, 2019). The complete list of directly measured parameters for each of these three sediment sampling efforts is provided in table 3.

Table 3. List of directly measured bed sediment and porewater parameters.

[For each parameter, the chemical notation, units, and full name description is given. Also noted (with 'X') is if a given parameter was associated with one or more of the three primary sediment studies. Calculated parameters, derived from direct measurements (for example, percent methylmercury) are not listed, but are noted in the text, data tables, graphs, and appendices as necessary. Ng/g, nanogram per gram; dw, dry weight; 1/d, fraction per day; pg/g dry sed/d, picogram per gram dry sediment per day; °C, degree Celsius; mV, millivolts; %, percent; ww, wet weight; g/cm^3, gram per cubic centimeter; ml pw/cm^3 wet sed, milliliters of porewater per cubic centimeter wet sediment; µm, micrometer; µmol/g, micromole per gram; ng/g dry sed/d, nanogram per gram dry sediment per day; nmol/g, nanomole per gram; mmol/L, millimole per liter; mg/L, milligram per liter; µmol/L, micromole per liter]

Parameter name	Parameter notation	Units	2010–11 ponds and sloughs	2010–12 pond A6	2012 and 2016 deep cores
Mercury parameters [whole sediment]					
Total mercury	THg	(ng/g) dw	X	X	X
Methylmercury	MeHg	(ng/g) dw	X	X	X
Inorganic reactive mercury	RHg	(ng/g) dw	X	X	X
Mercury methylation rate constant	K_{meth}	(1/d)	X		
Methylmercury production potential	MPP	(pg/g dry sed/d)	X		
Nonmercury parameters [whole sediment]					
Temperature	TEMP	(°C)	X		
pH	pH	unitless	X		
Redox potential corrected for standard hydrogen electrode	E_h	(mV)	X		
Dry weight	DW	(% of ww)	X	X	X
Loss on ignition	LOI	(% of dw)	X	X	X

Table 3. List of directly measured bed sediment and porewater parameters.—Continued

Parameter name	Parameter notation	Units	2010–11 ponds and sloughs	2010–12 pond A6	2012 and 2016 deep cores
Nonmercury parameters [whole sediment]—Continued					
Bulk density	BD	(g/cm^3)	X	X	X
Porosity	POR	$(ml\ pw/cm^3$ wet sed)	X	X	X
Grain size	GS	(% < 64 µm)	X	X	X[1]
Ferrous iron, acid extractable	$Fe(II)_{AE}$	(mg/g) dw	X		
Ferric iron, crystalline	$Fe(III)_c$	(mg/g) dw	X		
Ferric iron, amorphous [poorly crystalline]	$Fe(III)_a$	(mg/g) dw	X		
Total reduced sulfur	TRS	(µmol/g) dw	X		
Sulfate reduction rate	SRR	(nmol/g dry sed/d)	X		
Nonmercury parameters [porewater]					
Sulfate anion	SO_4^{2-}	(mmol/L)	X		
Chloride anion	Cl^-	(mmol/L)	X		
Ferrous iron	Fe(II)	(mg/L)	X		
Dissolved organic carbon	DOC	(mg/L)	X		
Sulfide	H_2S	(µmol/L)	X		
Acetate	Ac	(µmol/L)	X		

[1]Grain size data associated with 2012 deep cores only.

Ponds and Sloughs: Shallow Sediment Routine Sampling, 2010–11

The collection of surface sediment (0–2 cm interval) from 12 fixed sites occurred on 6 occasions (May, June, and August in both 2010 and 2011), covering the period immediately before and after the breaching of pond A6 (December 2010) and the initial opening of the A8-TCS on June 1, 2011. Sediment sampling sites (fig. 5) were the same as those sampled for surface water during the same 2010–11 period (fig. 4) and included 7 pond and 5 slough sites. Five pond sites were within the A8-complex. One site was in pond A16, a positive control reference pond (representing the post-breach condition) that is tidally connected to Mallard Slough. One site was in pond A3N, a negative control reference pond (representing the pre-breach condition) that has minimal connection with bay water through a small and poorly functioning water control structure. The 5 slough sites included 2 in upper Alviso Slough (sites ALSL-1 and ALSL-2), 2 in lower Alviso Slough (sites ALSL-3 and ALSL-4) and 1 in Mallard Slough (site MALSL, reference slough). Site specific coordinate are published on-line (Marvin-DiPasquale and others, 2019). Sediment from these locations was co-collected with surface water samples and more roughly coordinated with the collection of biota samples.

Sediment was initially sampled from a boat with a stainless steel Eckman style box core. The 0–2 cm surface layer was immediately subsampled into acid-cleaned mason jars, which were filled to exclude all atmospheric O_2 and were subsequently stored chilled in a dark cooler until further subsampling. Within 24 hours of field collection, sediment was further subsampled in the laboratory in a N_2 flushed glove bag under anaerobic conditions for a wide suite of mercury and nonmercury parameters (table 3), and each was appropriately preserved until final constituent specific analysis. Sediment pore water was collected under anaerobic conditions via centrifugation, and all porewater samples were filtered through a 0.45 µm (nylon) filter prior to further preservation (except dissolved organic carbon [DOC], which was filtered through a 0.7-µm glass fiber filter). Methods citations for each sediment parameter are published online (Marvin-DiPasquale and others, 2019).

Pond A6: Intensive Sampling of Shallow Sediment, 2010–12

As part of a separate but related effort focused on sediment deposition within pond A6, and in collaboration with Dr. J. Callaway (University of San Francisco), surface sediment was collected from 10 locations within pond A6 prior to (August 2010) and after (June 2011, December 2011, July 2012, and November 2012) the December 2010 breach event. Sediment was collected by hand, using acid-cleaned 0–2 cm polycarbonate core rings (Lutz and others, 2008). Sample transfer to mason jars, chilled preservation during transport, and subsequent sub-sampling steps in the laboratory are the same as those described above. The focus of this sampling was to determine how much mercury was deposited within pond A6 on the basis of measured concentrations and Dr. Callaway's sediment deposition estimates (Callaway and others, 2013). As such, the suite of shallow sediment parameters assayed on the pond A6 samples was limited when compared to the primary pond and slough samples collected during the 2010–11 period, and included: THg, MeHg, inorganic reactive mercury (RHg), percent dry weight (DW), bulk density (BD), porosity (POR), percent loss on ignition (LOI) and grain size (GS) (table 3).

Alviso Slough Deep Cores, 2012 and 2016

Four deep cores (79–214 cm maximum depth) and three deep cores (188–200 cm maximum depth) were collected from the thalweg of Alviso Slough (fig. 5) during May 2012 and January 2016, respectively. These 7 core profiles are in addition to 15 deep cores collected from the fringing marsh (10 total; not shown in fig. 5) and thalweg (5 total; shown in fig. 5) of Alviso Slough during September 2006. The sampling of the 2012 and 2016 cores used the same approach as previously reported for the 2006 cores (Marvin-DiPasquale and Cox, 2007). The seven cores collected during 2012 and 2016, as part of the Phase 1 studies, were designed to supplement the 2006 effort by providing more detailed mapping of buried horizons of elevated mercury concentrations within Alviso Slough. The mercury profile data garnered from all three of these collection efforts was then used in conjunction with the bed sediment bathymetry change data to calculate the amount of mercury remobilized during the Phase 1 period (Foxgrover and others, 2019). The full suite of analyses associated with the 2012 and 2016 deep cores in included: THg, MeHg, RHg, DW, BD, POR, LOI, and GS (2012 only) (table 3), in addition to non-destructive multi-sensor core logger scans of magnetic susceptibility and gamma bulk density and split core photography, the images of which are available on-line (Marvin-DiPasquale and others, 2018).

Shallow Sediment Data: Statistics, 2010–11

For the purposes of statistical analysis, shallow sediment samples (0–2 cm interval) collected from the multiple slough and pond locations during 2010–11 (not including pond A6 data) were initially grouped into two spatial categories. The primary spatial grouping, model term TYPE (pond, slough), distinguishes between pond and slough sites. At a more refined spatial scale, the model term REGION for Model.SED.1, refers to the grouping of six general sediment and water sampling regions: three pond sampling regions (A8-complex [5], reference pond A16 [1], reference pond A3N [1]); and three slough sampling regions (upper Alviso Slough [2], lower Alviso Slough [2], and the single reference slough, Mallard Slough [1]), where [n] equals the number of unique sites per subgrouping (during 2010–11).

The number of sampling events prior to and after the pond A6 breach event (December 2010) was balanced (n=3) for the study years 2010 and 2011 (May, June, and August each year). However, relative to the initial opening of the A8-TCS in June 2011, there were 4 events prior to that date and only 2 afterwards. Not including the data separately collected for the pond A6 study, the pond and slough sediment data included 72 observations for each parameter.

Two general types of LSM models were used to analyze the sediment data. The first (Model SED.1) assessed differences at both spatial levels (model terms TYPE and REGION) and differences by year, and is of the form shown in equation 11:

$$Y = \text{TYPE} + \text{REGION[TYPE]} + \text{YEAR} + [\text{REGION x YEAR}] \quad (11)$$

where

Y is any surface-sediment parameter;
TYPE is the categorical variable for two primary spatial groupings (pond and slough as factors);
REGION is the categorical variable that includes as factors the six sediment and water sampling regions as defined above and that is nested within TYPE;
YEAR is the categorical variable for year (with factors: 2010 and 2011); and
[REGION x YEAR] is the interaction term.

This global model (using all of the sediment data) allows us to address the following questions simultaneously:

- Is there a difference between pond and slough sites overall?
- Is there a difference among the six sediment and water sampling regions?
- Is there a difference between years 2010 and 2011?
- Is there an interaction between REGION and YEAR?

When Model SED.1 was expanded to also include the [TYPE x YEAR] interaction term, degrees of freedom (the number of independent values that have the freedom to vary) were lost, and viable results were not obtained. In instances where the [REGION x YEAR] interaction term was significant and there was a desire to understand this interaction in more detail, Model SED.2 was run, where differences by YEAR were assessed for each individual REGION grouping:

$$Y_{[\text{REGION}]} = \text{YEAR} \quad (12)$$

A second level of spatial and temporal analysis was conducted using Model SED.3, which considers the temporal component at the level of individual sampling event. Owing to the limited number of observations in the overall dataset, the use of Model SED.3 was restricted to considering differences among the 3 pond REGION groupings separately from the differences among the 3 slough REGION groupings. The general form of the model is shown in equation 13:

$$Y_{[\text{TYPE}]} = \text{REGION} + \text{EVENT} + [\text{REGION x EVENT}] \quad (13)$$

where

$Y_{[TYPE]}$ is any surface-sediment parameter, subset either by pond or slough (TYPE grouping);

REGION is the categorical spatial grouping as defined above;

EVENT is the categorical variable for sampling event (with each of the six individual sampling events, designated by month and year, as factors); and

[REGION x EVENT] is the interaction term.

Sediment Scour and THg Remobilization

High-resolution bathymetric surveys were used to quantify volumes of sediment erosion and deposition within Alviso Slough on a biannual basis since restoration began in 2010. Measurements of sediment scour were used in combination with THg measurements from deep sediment cores to estimate the amount of THg remobilized from subsurface sediments within the slough during 2010 through March 2017. A brief description of this work is presented here; for greater detail, see Foxgrover and others (2019). The bathymetry of Alviso Slough was mapped in 2010 to document baseline conditions prior to initiation of the restoration project. Biannual surveys were then collected every spring (either March or April) and fall (either October or November) from October 2011 through March 2017, with the exception of spring 2014, to document change as restoration progressed (data available from Foxgrover and others, 2018). An interferometric swath bathymetry system optimized for collecting data in shallow conditions was able to map the entire slough in two passes, outputting a continuous, 1-meter (m) horizontal resolution surface with an average density of 20 soundings per square meter and a mean vertical precision of 2 cm. Discrete measurements of bathymetric change were generated by differencing pairs of bathymetric surveys and volumetric changes calculated on a cell-by-cell basis.

Data from 12 sediment cores (Marvin-DiPasquale and Cox, 2007; Marvin-DiPasquale and others, 2018) were used to represent the variability of THg concentrations in the subsurface sediments of Alviso Slough. The cores were collected from the center of the channel, ranged in length from 79 to 231 cm (mean = 189 cm, median = 198), and spanned a length from the mouth of the slough to upstream from the A8-TCS (fig. 5). Although subsampling intervals varied on the basis of the characteristics of the individual cores, for this study, THg concentrations were interpolated to regularly spaced, 10-cm-thick horizons to a depth of 2 m below the surface. Each 10-cm-thick horizon was then linearly interpolated between each core location and extrapolated to the channel margins to generate a continuous two-dimensional (2D) surface of THg variation with both depth below the surface and distance along the length of the slough (see fig. 6B in Foxgrover and others, 2019).

To determine THg remobilization, the entire time series of 13 bathymetric surveys was compared on a cell-by-cell basis. The maximum depth of scour, and corresponding time period in which it occurred, was recorded for each 1x1 m cell. The volume of sediment eroded was then multiplied by the corresponding THg concentration for that specific location, which varied with depth below the surface. The volume of THg remobilized was summed by seasonal time step, and also by slough reach (lower, middle, and upper slough), to help elucidate the influence of restoration actions (for example, A6 breaches and A8-TCS gate operations) on THg remobilization.

Hydrodynamic and Geomorphic Models

Both 2D and three-dimensional (3D) process-based models were employed to explore the effect of tidal restoration to ponds on sediment scour in Alviso Slough and the associated mercury remobilization and transport. The first models did not update hydrodynamics with changes in bathymetry, so they were only applicable to short (several months or shorter) simulations where sediment depth change was small enough that it did not substantially change the hydrodynamics (Rey, 2015). These initial models (both 2D and 3D) quantified changes in hydrodynamic and sediment transport resulting from the breaching of pond A6 and the management (opening and [or] closing) of the A8-TCS, and for simulation of hypothetical levee breach scenarios. Particle tracking was subsequently added to investigate the fate of mercury associated with the remobilization of Alviso Slough bed sediment, resulting from an increase in tidal prism (Achete, 2016). The most recent model iteration (van der Wegen and others, 2018) was 2D and updated hydrodynamics when sediment scour or deposition occurred. This model was called a “fully geomorphic” model because it allowed for multiyear simulations of hydrodynamics and sediment transport as the slough deepened or shoaled. This model is also able to simulate geomorphic change and to include long-term processes such as sea level rise.

The hydrodynamics for all model approaches were simulated using the Delft3D Flexible Mesh (Delft3D FM) model (Deltare, 2014). To calculate SSC and sediment transport, Deflt3D FM was coupled with a water-quality model, Delft-WAQ DELWAQ (Achete and others, 2015). Sediment transport was calculated using standard formulations, with the exception of the inclusion of a sediment floc layer formulation in the fully geomorphic model to account for unconsolidated sediment that is easily suspended at low flow speeds. The study area was modeled using a mesh with cell size ranging from 15x30 m in channels to 120x120 m in the ponds (fig. 6). The base bathymetry and topography from 2010 (Foxgrover and others, 2018) were augmented with 2004 pond bathymetry (Athearn and others, 2010), and both were collected prior to the opening of the ponds to tidal exchange. Model inputs were tides and SSC at the mesh boundary in South San Francisco Bay, and river discharges and SSC at the mesh boundary in Coyote Creek and Guadalupe River. All models were validated using field-based observations. The Rey (2015) model was calibrated

Google Earth January 2021

Figure 6. Satellite image of the southern San Francisco Bay area showing the Delft3D Flexible Mesh model framework used to model suspended-sediment dynamics in the South Bay Salt Pond Restoration Project study region. White arrows indicate boundary locations of model inputs.

and validated against measured water levels, velocities, and SSC. The fully geomorphic model (van der Wegen and others, 2018) was calibrated and validated against geomorphic change (measured via seasonally repeated side-scan sonar) and SSC.

For the purposes of modeling the redistribution of Alviso Slough bed sediment and associated THg, and in response to various management actions (pond A6 levee breaches and A8-TCS operations), THg concentration fractions were assigned to the sediment in the lower, middle, and upper reaches of Alviso Slough. Vertically averaged THg concentration values were calculated from sediment cores collected from the thalweg of Alviso Slough during 2006 (Marvin-DiPasquale and Cox, 2007) and 2012 (Marvin-DiPasquale and others, 2018). The three fractions (fr##) used for the model were subsequently defined as follows: (1) fr05, low THg (168 nanogram per cubic centimeter [ng/ cm^3]), which represents lower Alviso Slough bed sediment; (2) fr03, moderate THg [370 ng/cm^3], which represents upper Alviso Slough bed sediment; and (3) fr04, high THg [757 ng/cm^3], which represents middle Alviso Slough bed sediment. A 3-month model simulation was run to examine where and how much of each bed sediment THg fraction was remobilized on the basis of various scenarios of pond A6 being breached (or not) and the number of A8-TCS gates being opened. Further details regarding this model can be found in Achete (2016).

Individual Study Results

This section summarizes the results of the independent studies focused on (1) mercury in bird eggs, (2) mercury in pond and slough fish, (3) mercury in surface water, (4) high-resolution fixed-monitoring station surface-water data, (5) mercury in sediment, (6) slough bed sediment mobilization, and (7) hydrodynamic and geomorphic models. The emphasis here is to highlight key results in each study that most directly address the four primary questions detailed in "Mercury Synthesis—Organizing Questions" section.

At the time of publication, data were not publicly available from the South Bay Salt Pond Restoration Project and Resources Legacy Fund. Data from reports prepared for the SBSPRP are available upon request.

Biota: Mercury in Bird Eggs

For all eggs sampled between 2005 and 2017, mercury concentrations in 80 percent of Forster's tern and 18 percent of American avocet eggs exceeded their toxicity benchmarks of 0.75 µg/g fww and 0.44 µg/g fww, respectively (Eagles-Smith and others, 2009; Ackerman and others, 2016a). Historically, mercury concentrations in eggs were substantially higher in ponds A8 and A7 than at any other nesting ponds (Ackerman and others, 2014a). Mercury concentrations in bird eggs remained high throughout the Phase 1 restoration (Ackerman and others, 2017) (figs. 7, 8), particularly with respect to Forster's tern eggs collected from pond A7 within the A8-complex (fig. 7) where a majority of the nests occurred (fig. 2). THg concentrations in Forster's tern eggs far exceeded their toxicity benchmark (80 % were >0.75 µg/g fww) in both the A8-complex and southern San Francisco Bay reference sites during Phase 1 (fig. 7). In contrast, THg concentrations in American avocet eggs were generally below their toxicity benchmark (18% were >0.44 µg/g fww) in both the A8-complex and southern San Francisco Bay reference sites during Phase 1 (fig. 8). This contrast in avian toxicity risk reflects differences in foraging strategies between fish-eating terns and invertebrate-feeding American avocets.

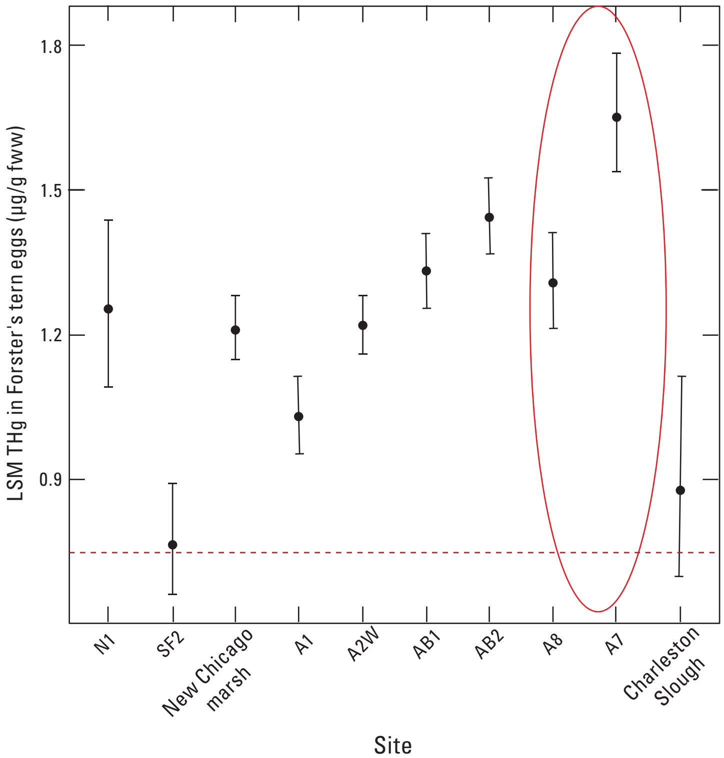

Figure 7. Graph showing model-averaged geometric least squares mean (LSM) total mercury (THg) concentrations in Forster's terns eggs (n = 522) averaged across all years: 2010–11 and 2013–17. The red dashed line indicates the avian toxicity benchmark for Forster's terns (0.75 microgram per gram in fresh wet weight [µg/g fww; Eagles-Smith and others, 2009, Ackerman and others, 2016a]). The response variable was log-transformed egg total mercury concentration. Year, site, and nest initiation date were included as covariates. Error bars represent the standard error. Red oval denotes ponds sampled within the A8-complex.

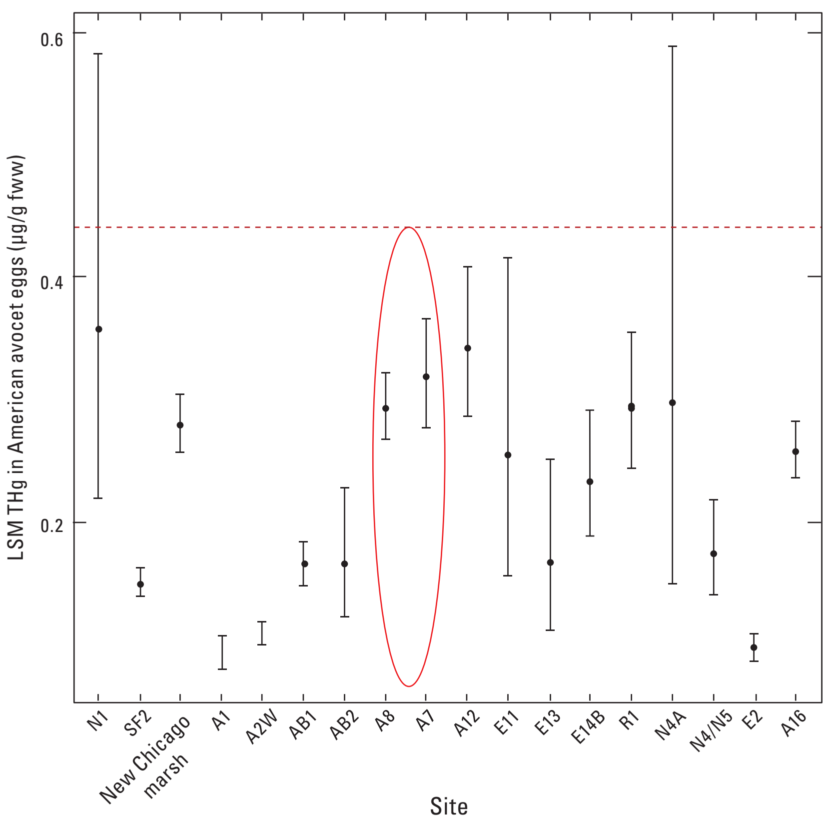

Figure 8. Graph showing model-averaged geometric least squares mean (LSM) total mercury (THg) concentrations in American avocet eggs (n = 610) averaged across all years: 2010–11 and 2013–17. The red dashed line indicates the avian toxicity benchmark for American avocets (0.44 microgram per gram in fresh wet weight [µg/g fww; Eagles-Smith and others, 2009, Ackerman and others, 2016a]). The response variable was log-transformed egg total mercury concentration. Year, site, and nest initiation date were included as covariates. Error bars represent the standard error. Red oval denotes ponds sampled within the A8-complex.

We tested the effect of the A8-complex restoration by specifically examining the change in mercury concentrations in biosentinel fish and bird eggs between 2010 and 2011, when most of the actual restoration activities (earth moving and A8-TCS construction) occurred between yearly sampling events, as well as before and after the A8-TCS opening on June 1, 2011. The actual opening of the A8-TCS on June 1, 2011, was not the sole restoration activity, because internal levee breaches conducted prior to the opening of the A8-TCS significantly altered the interior hydrology of the A8-complex between 2010 and 2011. We accounted for any ambient changes in mercury concentrations not related to restoration activities (construction, levee breaches, and staged opening of the A8-TCS) by using reference ponds (depending on year and bird species; reference ponds included A1, A2W, Charleston Slough, A12, AB1, AB2, New Chicago marsh, A16, E2, E11, E13, E14B, N1, N4A, N4/5, R1, SF2) that were outside of the restoration area.

The results show a rapid and substantial response of mercury contamination in Forster's tern eggs following the restoration of the A8-complex (fig. 9). Mercury concentrations in Forster's tern eggs increased by 63 percent (+0.90 µg/g fww) between 2010 and 2011 within the A8-complex but were similar between years at reference ponds outside of the restoration area (−9% or −0.12 µg/g fww). This increase of mercury concentrations in Forster's tern eggs to 2.34 µg/g fww was substantial and should not be understated; the increase in mercury contamination resulted in mercury concentrations in eggs being more than three-fold higher than the calculated toxicity benchmark of 0.75 µg/g fww developed for Forster's terns in San Francisco Bay (Eagles-Smith and others, 2009; Ackerman and others, 2016a). In contrast, the change in mercury concentrations in American avocet eggs between years in the A8-complex (−1% or −0.00 µg/g fww), relative to reference ponds (+1% or +0.00 µg/g fww), was negligible (fig. 10).

The increased mercury concentrations in Forster's tern eggs occurred during 2011, the year after the majority of the earth moving associated with the construction of the A8-TCS and internal levee breaches within the A8-complex. By the next sampling event in 2013 (no funding available for 2012 egg sampling), mercury concentrations in Forster's tern eggs declined substantially. By 2013, mercury concentrations had decreased from 2010 at both within the A8-complex and at the reference ponds by 33–35 percent in Forster's tern eggs (fig. 9) and 24–29 percent for American avocet eggs (fig. 10). Nonetheless, in 2013, most Forster's tern (70 %) and American avocet (50 %) egg mercury concentrations within the A8-complex still remained higher than concentrations associated with reproductive impairment.

Continued monitoring of mercury concentrations in bird eggs after 2013 showed that mercury concentrations in American avocet eggs increased by 54 percent from 2010 to 2015 within the A8-complex, similar to the 45 percent

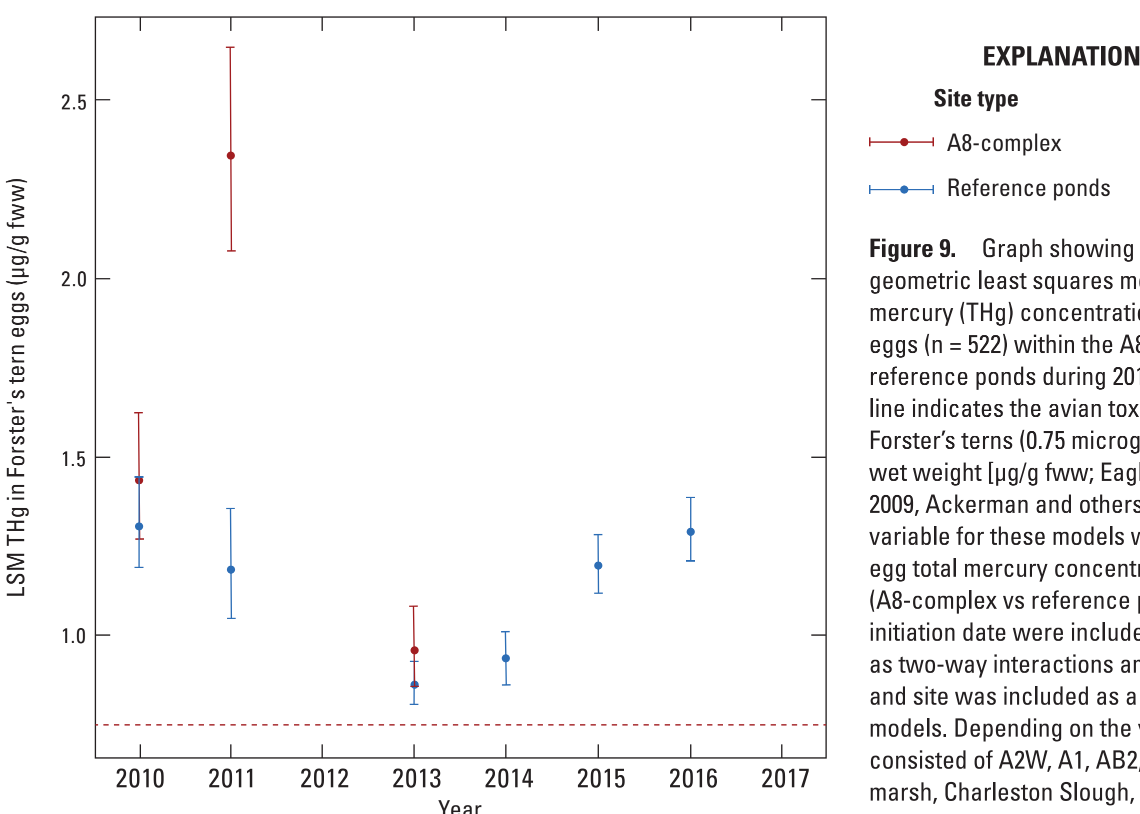

Figure 9. Graph showing model-averaged geometric least squares mean (LSM) total mercury (THg) concentrations in Forster's tern eggs (n = 522) within the A8-complex and at reference ponds during 2010–17. The red dashed line indicates the avian toxicity benchmark for Forster's terns (0.75 microgram per gram in fresh wet weight [µg/g fww; Eagles-Smith and others, 2009, Ackerman and others, 2016a]). The response variable for these models was log-transformed egg total mercury concentration. Year, treatment (A8-complex vs reference pond), and nest initiation date were included as covariates as well as two-way interactions among the variables, and site was included as a random effect in all models. Depending on the year, reference ponds consisted of A2W, A1, AB2, AB1, New Chicago marsh, Charleston Slough, N1, and (or) SF2. Error bars represent the standard error.

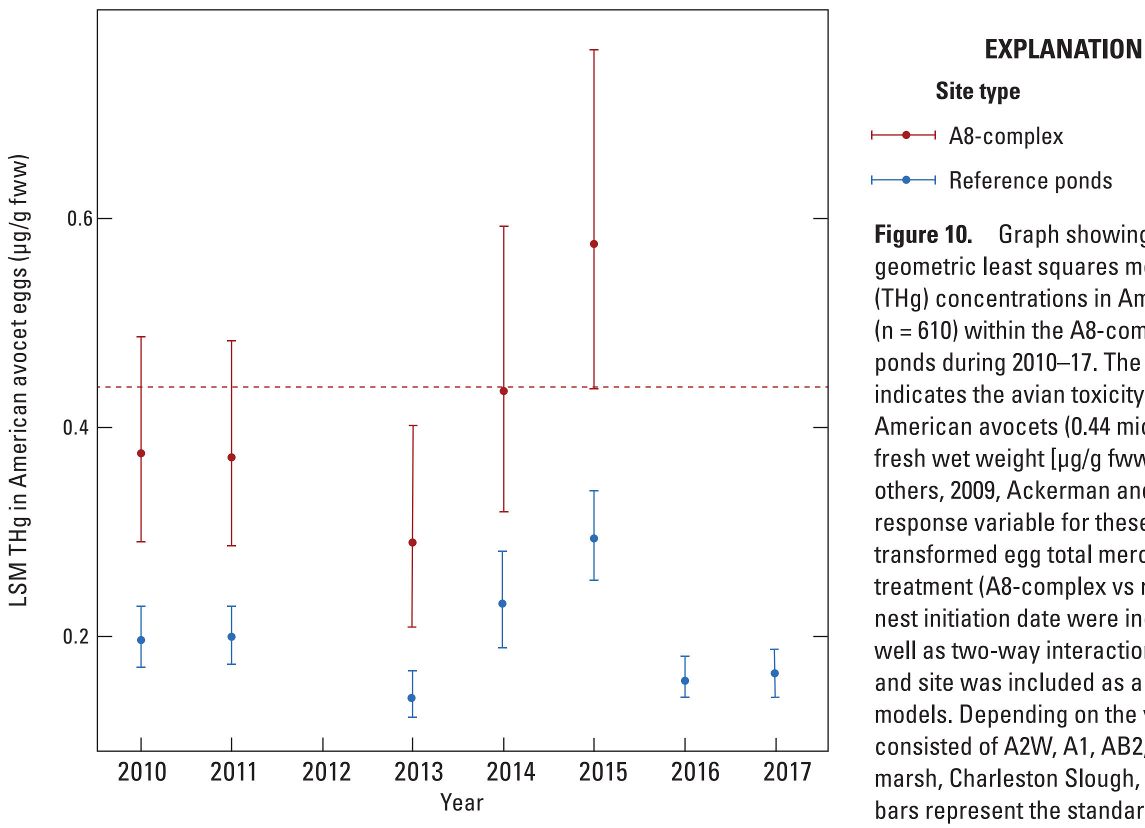

Figure 10. Graph showing model-averaged geometric least squares mean (LSM) total mercury (THg) concentrations in American avocet eggs (n = 610) within the A8-complex and at reference ponds during 2010–17. The red dashed line indicates the avian toxicity benchmark for American avocets (0.44 microgram per gram in fresh wet weight [µg/g fww; Eagles-Smith and others, 2009, Ackerman and others, 2016]). The response variable for these models was log-transformed egg total mercury concentration. Year, treatment (A8-complex vs reference pond), and nest initiation date were included as covariates as well as two-way interactions among the variables, and site was included as a random effect in all models. Depending on the year, reference ponds consisted of A2W, A1, AB2, AB1, New Chicago marsh, Charleston Slough, N1, and (or) SF2. Error bars represent the standard error.

increase from 2010 to 2015 in reference ponds, indicating that although mercury concentrations in eggs collected from the A8-complex are still among the highest in the San Francisco Bay and have increased recently, their trajectory after the initial spike in 2011 has generally followed those of ambient mercury conditions within the larger southern San Francisco Bay (fig. 10). In general, American avocets have lower egg mercury concentrations than many of the other locally breeding birds using the area, including black-necked stilts, Forster's terns, Caspian terns, *Phalacrocorax uratus* (double-crested cormorants), *Rynchops niger* (black skimmers), Ridgway's rails, and *Charadrius nivosus* (western snowy plovers) (Ackerman and others, 2012, 2014a). The differences in mercury concentrations between American avocet and Forster's tern eggs reflect their differences in microhabitat use (Ackerman and others, 2007; Ackerman and others, 2008a) and diet (Ackerman and others, 2020b; McNicholl and others, 2020); American avocets eat mostly aquatic invertebrates (lower trophic level and lower mercury concentrations) and terns eat mostly fish (higher trophic level and higher mercury concentrations).

Long-Term Trends of Mercury in Bird Eggs

At a broader scale, we have used all of our available egg mercury data to track the trends in Forster's tern (fig. 11) and American avocet (fig. 12) egg mercury concentrations in the southern San Francisco Bay since our initial studies in 2005. Mixed models were used and performed separately for Forster's terns and American avocets. Two models were developed for comparison: (1) a model where year was used as a factor and site was included as a random effect or (2) a null model where year was not a factor and site was included as a random effect. The response variable was natural log-transformed total mercury concentrations in Forster's tern and American avocet eggs. These data overwhelmingly supported the model with a year effect (table 4); the model with year included as a factor was 10^{115} and 10^{30} times more likely than the model without year for Forster's terns and American avocets, respectively. There are a number of pronounced and short-lived peaks evident in the long-term THg data for eggs of both species in the southern San Francisco Bay. The first peak occurred during 2006 (figs. 11,12), which was prior to

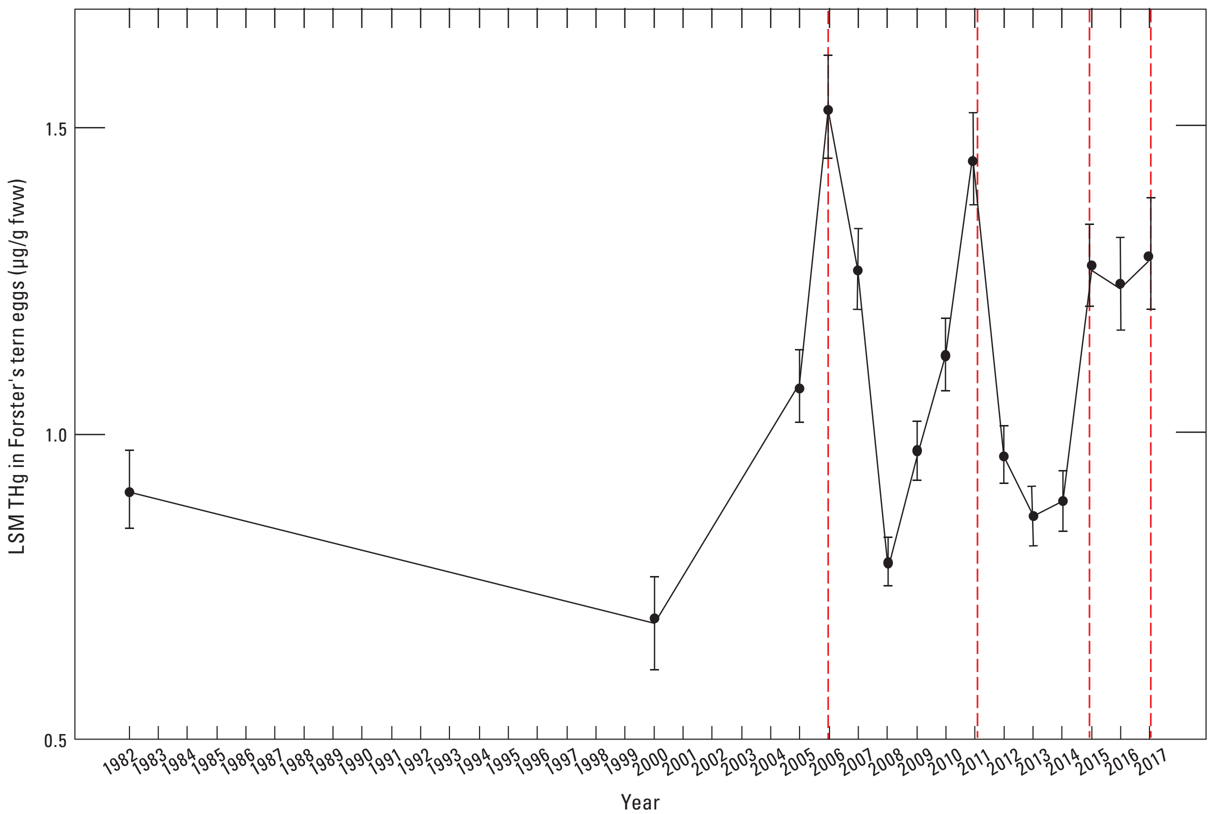

Figure 11. Graph showing long-term trend in total mercury (THg) concentrations in Forster's tern eggs collected from southern San Francisco Bay during 1982–2017. The time series also includes historical reference values in 1982 for Bair Island (n=10 eggs) by Ohlendorf and others (1988) and in 2000 for 4 sites (n=21 eggs) by Schwarzbach and Adelsbach (2003). Values from 2005–2017 are least squares means (LSM) in micrograms per gram in fresh wet weight [µg/g fww] accounting for site as a random effect (model results in table 1). Error bars represent the standard error. The red dashed lines highlight peaks in years prior to (2006) and during (2011 and 2015–17) the South Bay Salt Pond Restoration Project Phase 1 period of study (2010–2017).

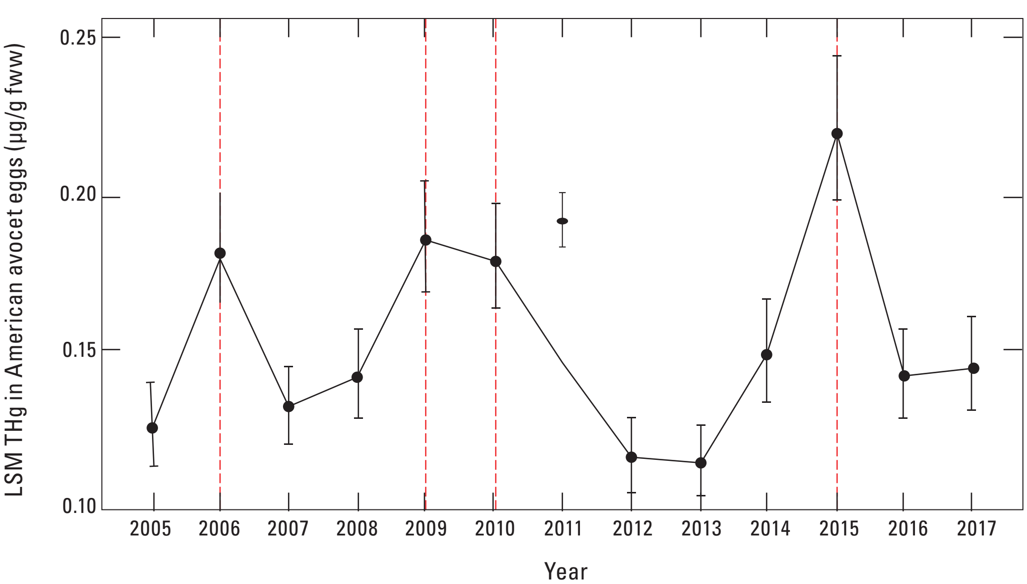

Figure 12. Long-term trend in total mercury (THg) concentrations in American avocet eggs collected from southern San Francisco Bay during 2005–2017. Values are least squares means (LSM) in micrograms per gram in fresh wet weight [µg/g fww] accounting for site as a random effect (model results in table 1). Error bars represent the standard error. The red dashed lines highlight peaks in years prior to (2006 and 2009) and during (2010 and 2015) the South Bay Salt Pond Restoration Project Phase 1 period of study (2010–17).

Table 4. Model diagnostics for statistical analyses of total mercury concentrations in Forster's tern and American avocet eggs in southern San Francisco Bay during 2005–2017.

[The Akaike information criterion (AIC) modeling approach was used. The response variable was log-transformed total mercury concentration in Forster's tern and American avocet eggs, year was as a factor (year), and site was included as a random effect in all models. Model inference was conducted separately for each species. k, the number of parameters; AICc, Akaike Information Criterion for small sample sizes]

Model	K	AICc	Delta AICc	Model weight	Evidence ratio
Forster's tern					
Year	15	4,217.82	0.00	1.00	1.00
Intercept only	3	4,749.53	531.71	0.00	4.12×10^{115}
American avocet					
Year	15	5,532.69	0.00	1.00	1.00
Intercept only	3	5,672.00	139.30	0.00	1.77×10^{30}

the Phase 1 management actions but coincident with some of the initial restoration actions at the island ponds (ponds A19–21). The second peak observed in the American avocet data (fig. 12) occurred during 2009–2010, which initiated prior to the breaching of pond A6 (December 2010) and was not coincident with any known SBSPRP management action. The second peak observed in the Forster's tern egg data (fig. 11) was during 2011, after the breaching of pond A6 and the construction and initial opening of the A8-TCS. The third peak in THg concentrations in Forster's tern eggs was observed during the 2015–17 period (fig. 11), which followed the 3-gate condition to 5-gate condition transition in the operation of the A8-TCS (September 2014) and encompassed the extreme flow event during January–February 2017. We similarly observed a third spike in THg concentration in American avocet eggs during 2015 (fig. 12). This A8-TCS transition to the 5-gate condition is believed to represent an important tipping point in the remobilization of historically buried legacy mercury in bed sediment of Alviso Slough for a prolonged period afterwards. Although we note this sequence of events and potential associations with observed peaks in THg concentrations in bird eggs for the southern San Francisco Bay area, we cannot conclusively assign a direct cause and effect relationship between them on the basis of the current data. However, the above noted correspondence in timing between regional peaks of mercury concentrations in bird egg (figs. 11, 12) and known management actions associated with the SBSPRP indicates that a link is possible. The sequence of events that could lead to such a regional response would likely include management actions that abruptly mobilize large quantities of sediment that contain previously buried legacy mercury, followed by an initial spike in microbial Hg(II)-methylation, a resulting increase in surface-water MeHg concentrations, uptake of MeHg into the base of the food web (phytoplankton and zooplankton) and small prey fish, and ultimately an accumulation in nesting birds, which manifests itself in observed and short-lived spikes in bird egg THg concentration data from the southern San Francisco Bay.

The long-term pattern of high mercury concentrations in eggs at all Forster's tern colonies (figs. 7, 9, 11) is important to recognize, especially at a time when effort is being made by managers and stakeholders to increase and bolster tern populations in the SBSPRP area using social attraction techniques (calls and decoys) in ponds that have had islands recently constructed for nesting birds (Hartman and others, 2017). Mercury concentrations in Forster's tern eggs still remain at high levels that exceed the tern toxicity benchmark, placing the species at high risk for reduced reproductive success and other behavioral and physiological impairment (Ackerman and others, 2014a). Therefore, current mercury concentrations in bird eggs indicate that several species foraging within the SBSPRP area remain at risk to potential reproductive impairment due to current mercury exposure (Ackerman and others, 2014a).

Importantly, the nesting populations and numbers of breeding colonies of American avocets, Forster's terns, and black-necked stilts in the southern San Francisco Bay seem to have declined (Hartman and others, 2021). In recent years, some of the largest waterbird nesting populations at ponds A7 and A8, as well as A1, A2W, and A16, have been reduced significantly or disappeared entirely. This is likely attributable to recent changes in water management and restoration activities, especially at ponds A7 and A8, and erosion of nesting habitat, especially at pond A1. At the same time, waterbirds have not consistently utilized newly created nesting islands at ponds A16 and SF2. This period of uncertainty in nesting colonies for American avocets, Forster's terns, and black-necked stilts comes at the beginning of Phase 2 of the SBSPRP, which may ultimately change the landscape within this area even more. The combination of factors indicates that a regional approach to monitoring changes in mercury concentrations in bird eggs within the SBSPRP area is warranted. This long-term approach in documenting mercury trends in bird eggs is illustrated in fig. 11. In response to substantial changes in bird egg mercury concentrations, this approach would allow for informed scientific feedback under the Adaptive Management Framework (Trulio and others, 2007) and would provide actionable data to alter management actions, such as the management decision to temporarily suspend opening further A8-TCS gates after observing the dramatic spike in tern egg mercury concentrations in 2011.

Biota: Mercury in Pond Fish

Pond fish were used to assess fine-scale temporal changes (for example, days) in biotic mercury concentrations immediately before and after the initial opening of the A8-TCS to Alviso Slough. Figure 13 shows the baseline total mercury concentrations in small prey fish within the San Francisco Bay, including the highest mercury concentrations in fish occurring in pond A8, during 2005–2008 before the

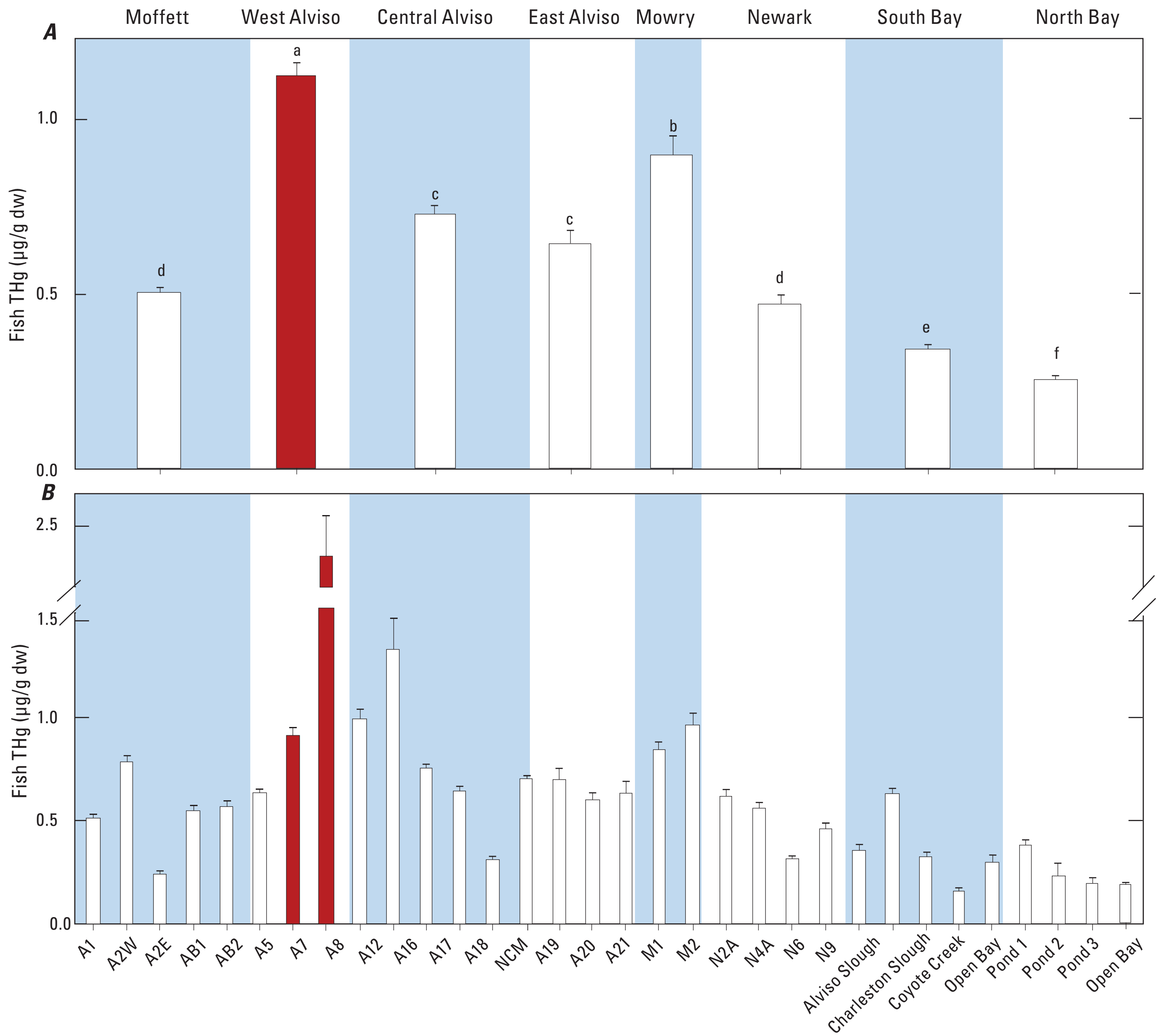

Figure 13. Graphs showing least squares mean (LSM) baseline total mercury (THg) concentrations in size-standardized prey fish from San Francisco Bay wetlands during 2005–08. LSM values (± standard error) accounted for global model effects: species, region, wetland (nested within region), day of year^2, and year. *A*, Bar graph showing how THg concentrations in fish differed among regions, with different letters indicating significant differences (α<0.05, Tukey's post-hoc pairwise comparisons). *B*, Bar graph showing how THg concentrations in fish differed among wetlands nested within regions. Figure is modified from Eagles-Smith and Ackerman (2014). Error bars represent the standard error. The red bars highlight the A8-complex (west Alviso region in 13*A*) and ponds sampled within the complex (13*B*). THg concentrations are given in micrograms per gram dry weight (µg/g dw).

pond A8 restoration actions occurred. Mercury concentrations in longjaw mudsucker and three-spined stickleback were substantially higher within the A8-complex than in reference ponds (Ackerman and others, 2013b), a result in concurrence with our earlier baseline study of fish mercury concentrations in the South Bay (Ackerman and others, 2014a; Eagles-Smith and Ackerman, 2014). Mercury concentrations generally decreased between 2010 and 2011 in both longjaw mudsucker and three-spined stickleback (fig. 14). However, mercury concentrations decreased in fish between years (2010 and 2011) much more in the reference ponds than in the A8-complex during the early April and mid-May sampling periods, prior to the initial opening of the A8-TCS. This result indicated that the restoration activities between 2010 and 2011 initially increased mercury concentrations in fish within the A8-complex relative to ambient mercury levels in reference ponds. However, once the A8-TCS was opened on June 1, 2011, mercury concentrations in fish dramatically decreased in the A8-complex but not in the reference ponds (fig. 14). The mercury patterns in pond fish are consistent with mercury patterns in bird eggs, because both document a substantial short-term increase in biotic mercury concentrations in the A8-complex during 2011 after the restoration actions (and associated construction activity). Additionally, mercury concentrations in pond fish and bird eggs decreased in the months (fish) to years (bird eggs) after the opening of the A8-TCS. Pond fish have not been sampled since 2011, so no further interpretation is possible.

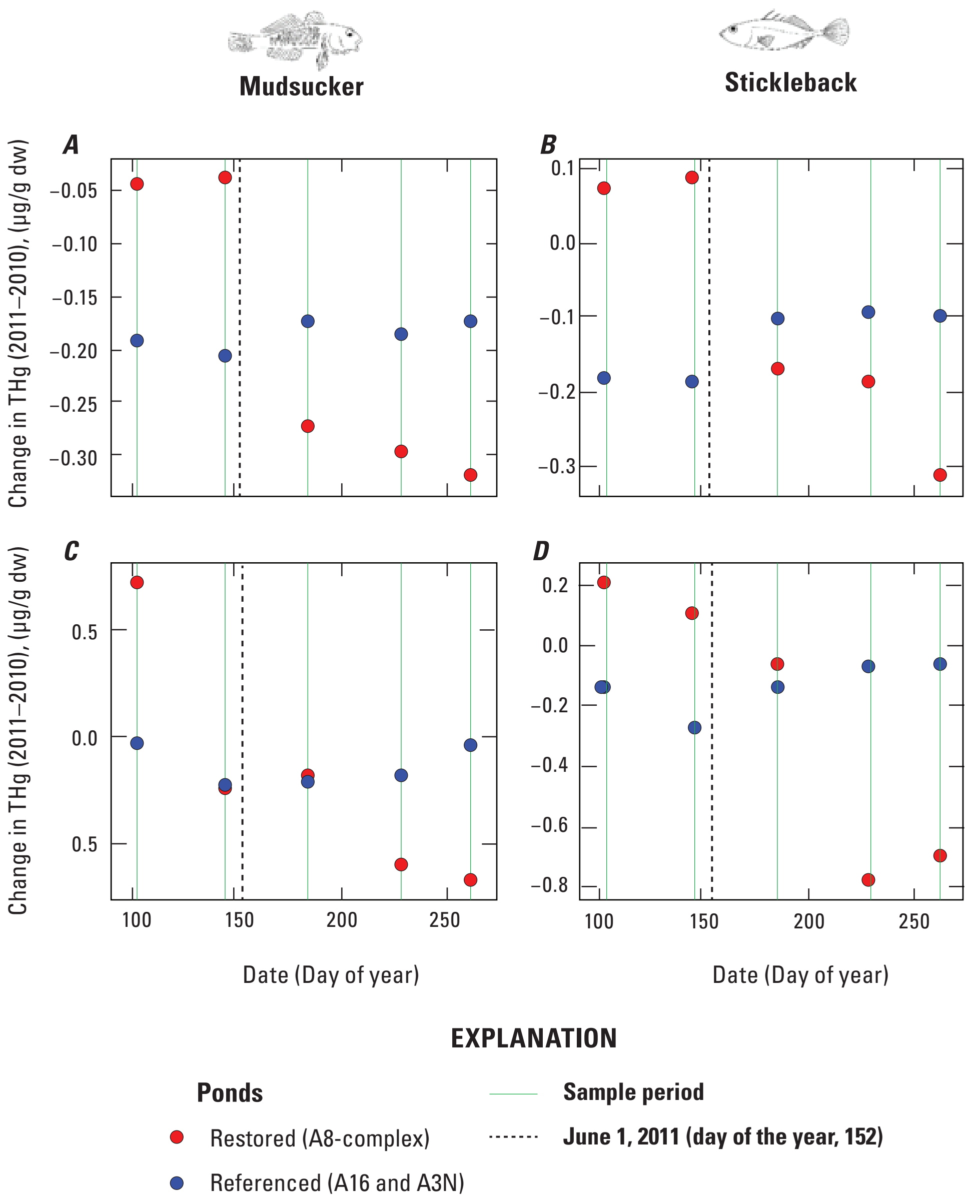

Figure 14. Graphs showing the difference between post-restoration (2011) and pre-restoration (2010) total mercury (THg) concentrations in fish versus sampling period, for reference ponds and the A8-complex. The 2011–2010 difference (change) in fish THg concentration, in micrograms per gram dry weight (µg/g dw), is given on the y-axis for each sampling period. The five annual sampling periods, done similarly during both 2010 and 2011, are indicated as the mean day of year (green vertical lines) on the x-axis. The pond A8-TCS was initially opened to tidal influence on June 1, 2011 (day of year = 152; black dotted vertical line). Longjaw mudsucker and three-spine stickleback data are presented as both model-predicted data (14*A*, 14*B*, respectively) and raw data (14*C*, 14*D*, respectively). Modeled data accounts for other variables that influenced fish THg concentrations. Figure modified from, and statistical analysis available in, Ackerman and others (2013b).

Biota: Mercury in Slough Fish

Small and wild biosentinel fish (Mississippi silverside and three-spine stickleback) collected from sloughs within the project area were used to monitor mercury exposure and bioaccumulation within Alviso Slough throughout the SBSPRP Phase 1 studies (2010–18), particularly in relation to operations of the A8-TCS. This portion of the synthesis is particularly focused on addressing whether measurable temporal and (or) spatial variations in slough fish THg levels throughout Phase 1 can be directly linked to A8-TCS operations or the potential export of MeHg from the A8-complex (through the A8-TCS) and subsequent variations in surface-water MeHg concentrations in Alviso Slough.

General Long-Term Trend throughout Phase 1

The complete time series of Mississippi silverside THg concentration data, collected throughout the Phase 1 sampling period (2010–18), is depicted in fig. 15*A* for the two primary Alviso Slough locations (sites ALSL-2 and ALSL-3), the low mercury reference slough (site MALSL), and the high mercury reference slough (GUASL). Similarly, the complete time series of three-spine stickleback THg data is depicted in fig. 15*B*. For context, the regulatory targets for small-fish mercury levels in San Francisco Bay and upstream in the Guadalupe River watershed are also shown in fig. 15. These regulatory targets are specified on a whole fish (wet weight) basis, and are 0.030 µg/g fww for San Francisco Bay fish between 30

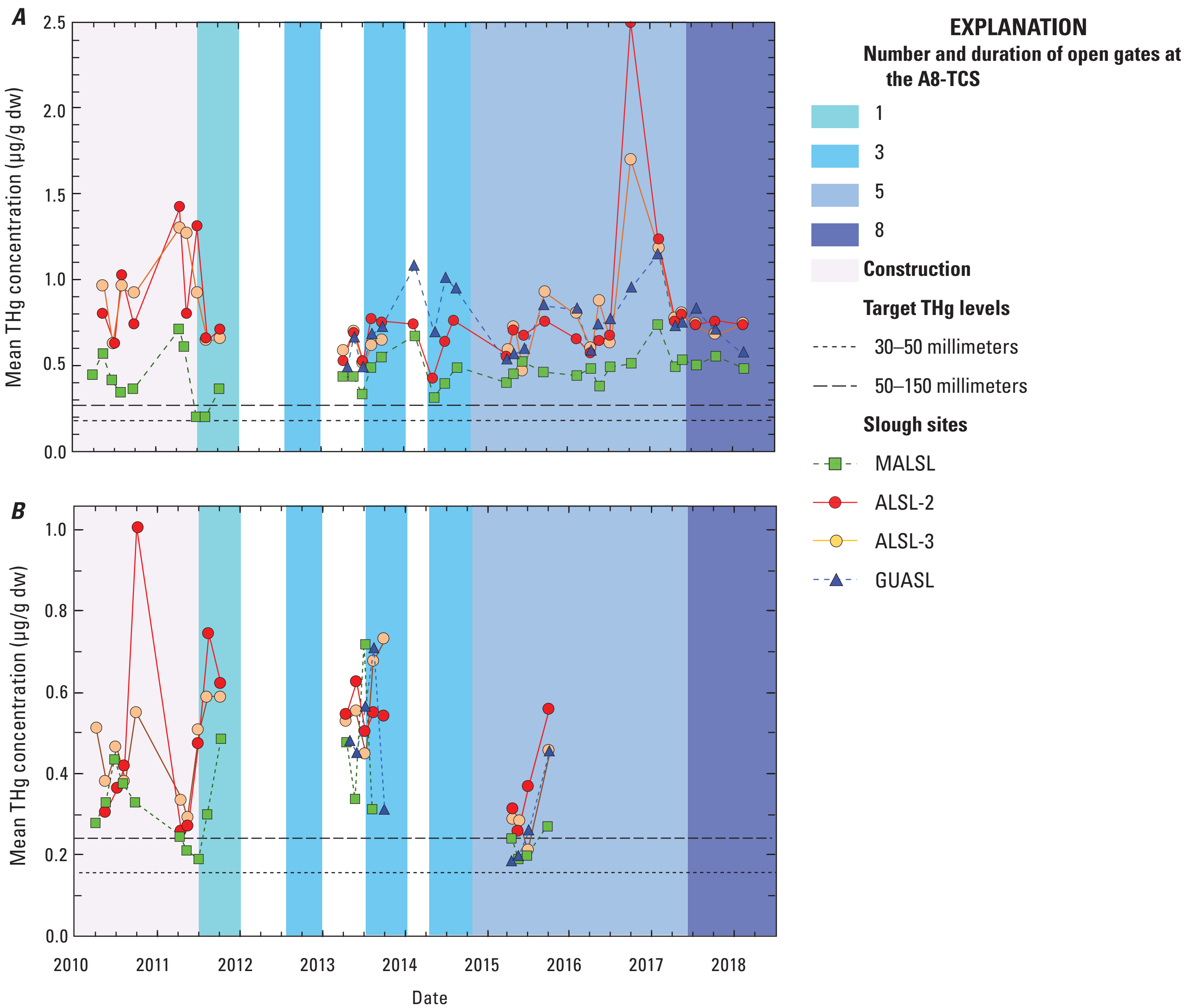

Figure 15. Graphs showing mean total mercury (THg) concentrations of Mississippi silverside (*A*) and three-spine stickleback (*B*), by slough site, for the years 2010–18 and 2010–16, respectively. Each Mississippi silverside data point (*A*) represents the mean of 6 composite samples of 8 fish each; 48 fish total, whereas each three-spine stickleback data point (*B*) represents the mean of 10–15 individually analyzed fish (homogenized whole body). Target THg levels (horizontal dashed lines) for 30–50 millimeters and 50–150 millimeters fish are in dry weight equivalents of 0.03 and 0.05 microgram per gram (µg/g) wet weight regulatory targets, respectively. Year labels are centered on January 1 of each year. THg concentrations are given in micrograms per gram dry weight (µg/g dw). Locations of samples shown on figure 3. Nonshaded background represents duration when all gates are closed.

and 50 millimeters (mm; total length), and 0.050 µg/g fww for Guadalupe watershed fish between 50 and 150 mm (California Water Boards, 2019). Using the mean percent solids value of all fish collected (20.5%), these wet weight target concentrations were converted into dry weight equivalents (0.146 µg/g dw and 0.244 µg/g dw, respectively) to correspond with the dry weight mercury concentrations reported for this project. Virtually all of the slough fish samples were at or above these targets (fig. 15), consistent with the elevated historical mercury legacy of the study region.

An initial ANOVA analysis of the slough fish dataset (no data transformations) indicated that THg concentrations in Mississippi silverside sampled in the Alviso Slough (sites ALSL-2 and ALSL-3 data combined) were significantly ($F[1, 351]$ 15.01, $p = 0.0001$) higher (mean±standard error, 0.97±0.04 µg/g) in the 13-month period (April 2010–May 2011) prior to the initial opening of the A8-TCS (June 1, 2011) compared to the 6.5-year period (July 2011–February 2018) afterwards (0.78±0.02 µg/g), which included extended periods of 0, 1, 3, 5, and 8 gates open. In contrast, Mississippi silverside THg concentrations in the MALSL reference site were not statistically different ($F[1, 197]$ 1.73, $p = 0.19$) prior to the initial A8-TCS opening (0.49±0.03 µg/g) compared to the period afterwards (0.45±0.01 µg/g). A similar analysis of the three-spine stickleback data indicated that for Alviso Slough, THg concentrations were slightly, but significantly ($F[1, 379]$ 9.39, $p = 0.0023$), lower (0.42±0.02 µg/g) in the period prior to the initial opening of the A8-TCS compared to the 4-year period (July 2011–September 2015) afterwards (0.49±0.01 µg/g). However, a similar temporal trend was found for the MALSL reference site where three-spine stickleback THg concentrations were also significantly ($F[1, 174]$ 4.21, $p = 0.0415$) lower (0.31±0.02 µg/g) prior to the initial A8-TCS opening compared to the 4-year period afterwards (0.37±0.02 µg/g). Simple summary statistics for the slough fish dataset, relative to the initial opening of the A8-TCS, are given in table 5.

There were two notable spikes in THg concentration of Mississippi silverside during the 2010–18 time series (fig. 15). The first was during 2011, about the time of the initial single A8-TCS gate opening, when mean Mississippi silverside THg concentrations rose to 1.20–1.50 µg/g for several months. The second spike was five years later, in the late 2016 to early 2017 time period, when mean concentrations spiked as high as 2.5 µg/g. The drivers of these two spikes in Mississippi silverside THg concentration are explored in more detail under the “Fish Mercury Spike Event During 2011” and “Fish Mercury Spike Event During Late 2016 to Early 2017” subsections.

After the initial 2010–11 study period, A8-TCS gate openings gradually increased in magnitude and duration between 2012 and 2018 (fig. 15), a period that coincided with lower mean THg concentrations in Alviso Slough Mississippi silverside (table 5), notwithstanding the late 2016 to early

Table 5. Summary statistics for total mercury concentrations in slough fish relative to the initial opening of tidal control structure (A8-TCS).

[Simple summary statistics for total mercury (THg) in both Mississippi silverside and three-spine stickleback include minimum (Min), maximum (Max), median, mean, standard deviation (Std. dev.) and the number of observations (N). All numeric data, with the exception of N, reflects whole body THg concentrations (micrograms per gram dry weight). Data are categorized by sample site and time period before (Pre) and after (Post) the initial opening of the tidal control structure A8-TCS (June 1, 2011)]

Sample site	Period	Min	Max	Median	Mean	Std. dev.	N
Mississippi silverside							
ALSL-2	Pre	0.23	1.93	0.88	0.91	0.38	36
ALSL-2	Post	0.33	2.88	0.70	0.79	0.42	152
ALSL-3	Pre	0.48	1.72	1.05	1.02	0.30	36
ALSL-3	Post	0.34	2.14	0.70	0.77	0.30	129
MALSL	Pre	0.22	1.00	0.47	0.49	0.20	41
MALSL	Post	0.16	0.97	0.44	0.45	0.16	158
GUASL	Post	0.31	1.39	0.69	0.75	0.23	136
Three-spine stickleback							
ALSL-2	Pre	0.14	1.61	0.33	0.44	0.32	70
ALSL-2	Post	0.15	0.97	0.48	0.49	0.19	117
ALSL-3	Pre	0.17	0.77	0.39	0.40	0.13	73
ALSL-3	Post	0.15	1.28	0.43	0.50	0.25	121
MALSL	Pre	0.13	0.58	0.30	0.31	0.11	80
MALSL	Post	0.09	0.91	0.31	0.37	0.22	96
GUASL	Post	0.08	0.95	0.33	0.38	0.22	91

2017 short-term spike. An ANOVA analysis confirmed that Mississippi silverside THg concentrations in Alviso Slough (ALSL-2 and ALSL-3 data combined) were significantly lower (mean±standard error, 0.78±0.02 µg/g dw) during the 6.5-year period (July 2011–February 2018) after the initial opening of the A8-TCS, compared to the 13-month period (April 2010–May 2011) preceding it (0.97±0.04 µg/g dw).

THg concentrations were generally lower in three-spine stickleback, compared to Mississippi silverside, for each individual sampling site (table 5). Similar to the Mississippi silverside data, some of the highest three-spine stickleback THg concentrations were seen in Alviso Slough during 2010 and 2011, prior to and immediately following the initial opening of the A8-TCS (fig. 15*B*). Three-spine stickleback also exhibited an apparent seasonal increase in THg concentrations in the later part of each year analyzed (fig. 15*B*). During the period following the initial opening of the A8-TCS (July 2011 through August 2015), three-spine stickleback mean THg concentrations were highest at the two primary Alviso Slough sites (ALSL-2 and ALSL-3), followed by site GUASL, and lowest at site MALSL (table 5).

The fish length versus THg concentration relationships used to derive the size-standardized fish THg concentration datasets for 60-mm Mississippi silverside and 40-mm three-spine stickleback shown in fig. 16. For Mississippi silverside, the positive relationship between fish length and THg concentration was the same for all four sampling sites (parallel slopes), although the intercept was lower for site MALSL compared to the other three sites (fig. 16*A*). In contrast, the relation between three-spine stickleback length and THg differed greatly among sites (fig. 16*B*, nonparallel slopes), and was significant and negative at the upper Alviso

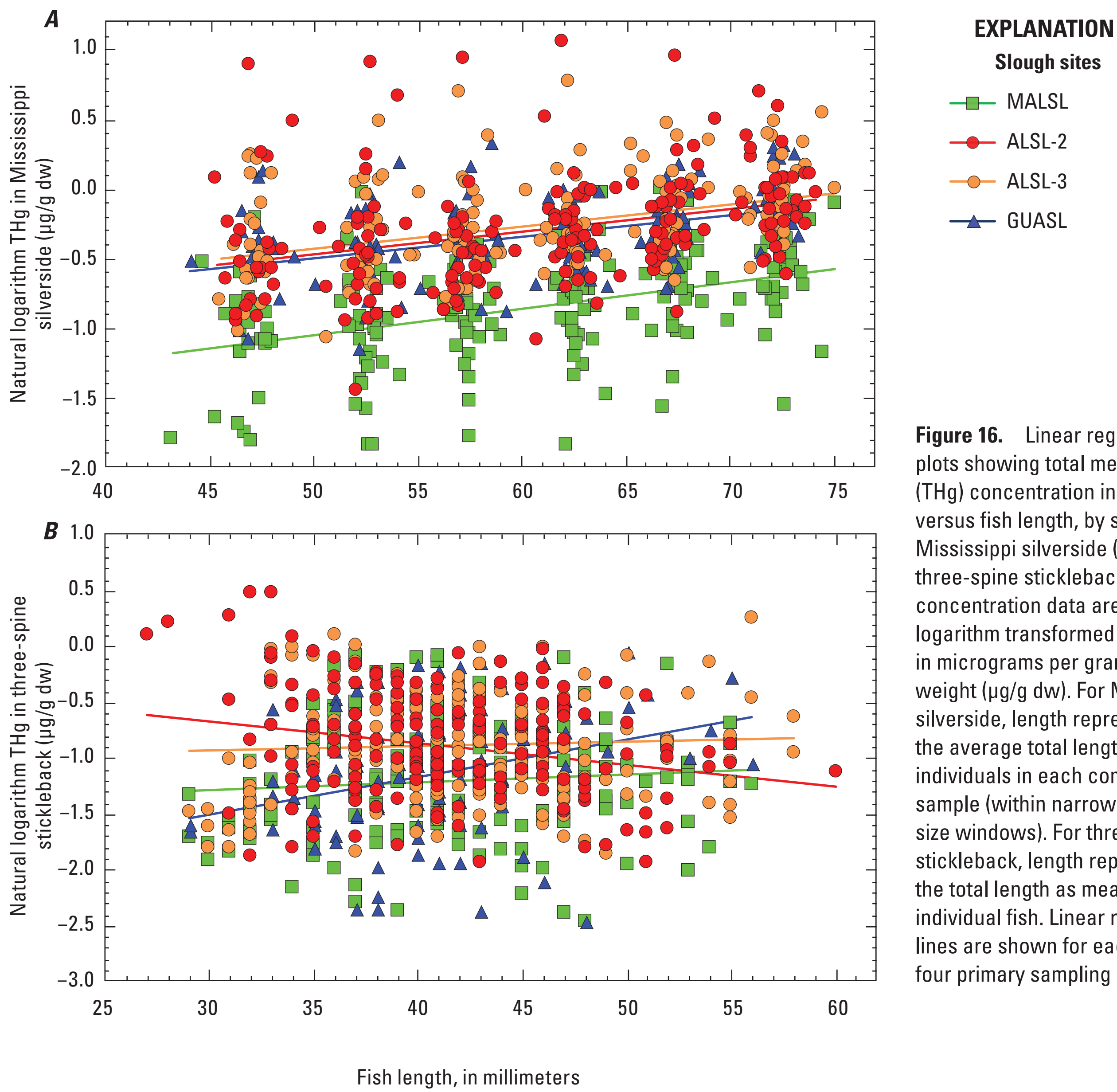

Figure 16. Linear regression plots showing total mercury (THg) concentration in fish versus fish length, by site, for Mississippi silverside (*A*) and three-spine stickleback (*B*). THg concentration data are natural logarithm transformed and are in micrograms per gram dry weight (µg/g dw). For Mississippi silverside, length represents the average total length of all individuals in each composite sample (within narrow 5 mm size windows). For three-spine stickleback, length represents the total length as measured on individual fish. Linear regression lines are shown for each of the four primary sampling sites.

Slough site (ALSL-2), nonsignificant for both the lower Alviso Slough (ALSL-3) and MALSL sites, and significant and positive at site GUASL. The observed differences between the two species, with respect to the length to THg relation, could reflect differences in diet specificity, growth kinetics, site fidelity, or cohort (population born in the same spawning season) variability or some combination of these factors. Unraveling the underlying causes of the differences between these two species, as it relates to the length:THg relationship, is beyond the scope of the research conducted.

Although the sampling of three-spine stickleback was temporally more limited than that for Mississippi silverside, the size-standardized fish THg dataset for 40-mm three-spine stickleback was suited for analysis by Model SL.FISH.2 (equation 2), which consisted of two main terms (SITE and YEAR) and an interaction term [SITE x YEAR]. Both model terms SITE and YEAR were statistically significant (SITE = (F[2, 545] 19.6, $p < 0.001$); YEAR = (F[3, 545] 30.3, $p < 0.001$)), whereas the interaction term was not (F[6, 545] 1.17, $p = 0.32$). Data from the GUASL reference site was not included in the initial run of this model since sampling of GUASL did not begin until 2013. The LSM model results are graphically depicted in figure 17, along with the Tukey's post-hoc pairwise ranking, which shows that among sites, three-spine stickleback from site MALSL had significantly lower THg concentrations, compared with three-spine stickleback from both Alviso Slough sites (ALSL-2 and ALSL-3), while controlling for sampling year (fig. 17*A*). Further, THg concentrations in three-spine stickleback were higher in sampling year 2013 (across all sites, while controlling for the model term SITE), when compared to sampling years 2010 and 2011, whereas the lowest THg concentrations occurred during sampling year 2015 (fig. 17*B*). The most relevant finding was that the interaction term was not significant, which implies that these interannual variations occurred across both Alviso Slough sites and at the reference site (MALSL) and that these variations in three-spine stickleback THg concentrations were not associated with the management actions associated with pond A6 and the A8-complex, but instead were more regional in nature.

Model SL.FISH.2 was reapplied to the 40-mm three-spine stickleback size-standardized fish THg data (ln-transformed) after excluding years 2010 and 2011 and including data from site GUASL. The back-transformed LSM model results indicate that THg concentrations were significantly (F[3, 309] 9.18, $p < 0.0001$) lower at sites GUASL (0.30±0.01 ng/g dw) and MALSL (0.29±0.02 ng/g dw) compared to both ALSL-2 (0.39±0.02 ng/g dw) and ALSL-2 (0.38±0.02 ng/g dw), for sampling years 2013 and 2015, while controlling for the model term YEAR.

To better understand and explore the fish THg time series data for both species (fig. 15), an analysis of seasonal differences (while controlling for site) was first conducted using size-standardized fish THg concentration data (Model SL.FISH.3). The results indicated that fish THg concentrations were significantly lower during the April through July (early season), compared to August through February (late season) (fig. 18). This seasonal differentiation allowed us to more precisely examine the two previously noted dominant spikes in fish THg concentrations observed during 2011 (seasonally confined to the April–July period) and 2016–17 (seasonally confined to the August–February period), as further detailed in the "Fish Mercury Spike Event During 2011" and "Fish Mercury Spike Event During Late 2016 to Early 2017" sections.

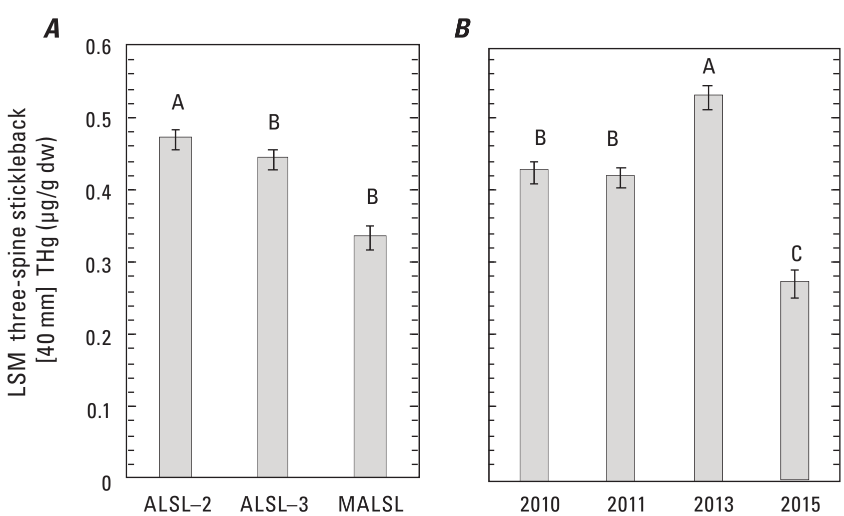

Figure 17. Bar graphs showing least squares mean model (LSM) results of size-standardized fish total mercury (THg) concentration for 40-millimeter three-spine stickleback, by site (*A*) and year (*B*). Data reflect the statistical LSM results from Model SL.FISH.2, which included model terms SITE and YEAR. The interaction term [SITE x YEAR] was not statistically significant. The letters above each bar reflect the post-hoc Tukey's pairwise ranking, with 'A' being the highest, and with bars sharing the same letter not being significantly different. Error bars reflect standard errors. Total mercury concentration is given in micrograms per gram dry weight (µg/g dw).

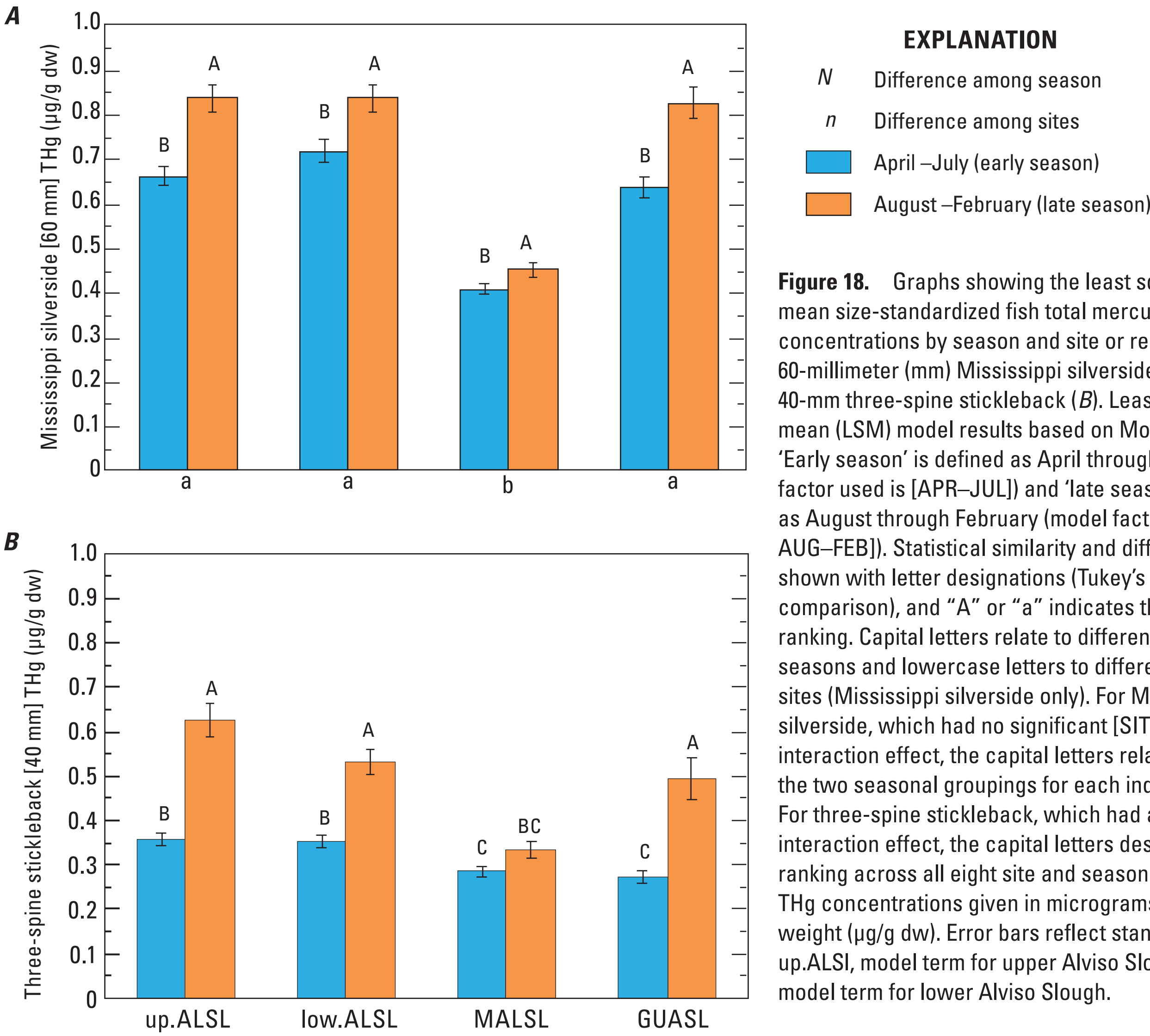

Figure 18. Graphs showing the least squares mean size-standardized fish total mercury (THg) concentrations by season and site or region, for 60-millimeter (mm) Mississippi silverside (*A*) and 40-mm three-spine stickleback (*B*). Least squares mean (LSM) model results based on Model SL.FISH.3. 'Early season' is defined as April through July (model factor used is [APR–JUL]) and 'late season' is defined as August through February (model factor used is AUG–FEB]). Statistical similarity and differences are shown with letter designations (Tukey's pairwise comparison), and "A" or "a" indicates the highest ranking. Capital letters relate to differences between seasons and lowercase letters to differences among sites (Mississippi silverside only). For Mississippi silverside, which had no significant [SITE x SEASON] interaction effect, the capital letters relate only to the two seasonal groupings for each individual site. For three-spine stickleback, which had a significant interaction effect, the capital letters designate the ranking across all eight site and season combinations. THg concentrations given in micrograms per gram dry weight (µg/g dw). Error bars reflect standard errors. up.ALSl, model term for upper Alviso Slough; low.ALSL, model term for lower Alviso Slough.

Fish Mercury Spike Event During 2011

Total mercury concentrations of Mississippi silverside in the Alviso Slough (sites ALSL-2 and ALSL-3) increased approximately 50 percent during April through July 2011, relative to 2010 prebreach concentrations (fig. 15) and commenced prior to the initial opening of the A8-TCS (June 1, 2011). The April through May 2011 time period coincided with A8-TCS construction activities and occurred after the breaching of pond A6 (December 2010) (table 1). Construction activities associated with the A8-complex during the late 2010 through early 2011 period were concluded to be a key driver of the observed short-term spike in bird egg and fish THg concentrations sampled within the A8-complex, as noted in the "General Long-Term Trend throughout Phase 1" section. Thus, it is likely that these same A8-TCS construction activities also contributed to the observed elevation in THg concentrations of Alviso Slough fish, particularly at the upper slough site (ALSL-2), because these activities resulted in the disturbance of large amounts of mercury-contaminated sediment around the A8-TCS and the engineered channel connecting Alviso Slough to pond A8. Previous laboratory studies have shown that mixing previously buried mercury-contaminated sediment from this same region with slough surface water resulted in an increase in RHg over a very short time scale (Marvin-DiPasquale and Cox, 2007). This rapid increase in RHg could potentially lead to a subsequent spike in new MeHg production through the microbial Hg(II)-methylation process.

Apart from the A8-TCS construction activities, the full tidal breaching of pond A6 in December of 2010 may have been a much larger sediment disruption event in the Alviso Slough that preceded the observed spike in THg concentrations of fish sampled in 2011. Pond A6 is located downstream from the two primary Alviso Slough fish sites

(ALSL-2 and ALSL-3), near the confluence with Coyote Creek, and adjacent to ALSL-4 (sampled during 2010–11 only). Appendix 3 (three-spine stickleback) and appendix 4 (Mississippi silverside) present detailed 2011 and 2010 data for the MALSL reference site, ALSL-2, ALSL-3, and ALSL-4. By subtracting the month and site specific 2010 data from the 2011 data, these results highlight the trends of THg concentration in fish around the various early Phase 1 management actions that likely affected Alviso Slough.

At sites ALSL-2 and ALSL-3, Mississippi silverside showed year-over-year increases in THg concentrations in July 2011, relative to July 2010. These increases were particularly relevant in relation to the corresponding July year-over-year trend at the MALSL reference site, which was declining (appendix 4). The elevated THg concentrations in Mississippi silverside sampled during July 2011 could be linked to either (1) A8-TCS construction activities (as previously discussed), (2) the December 2010 breaches at A6, (3) the initial one gate opening of the A8-TCS on June 1, 2011, or (4) some combination of these. It is unlikely however that this spike was associated with the initial one-gate (5 ft) opening of the A8-TCS, because the timing between this management action and the collection of the 2011 fish do not coincide with the weeks to months needed for newly produced MeHg from the sediment or in surface-water to bioaccumulate through the food web to the levels that would result in the observed 2011 versus 2010 differences. Further, the 2011 peak in mean THg concentrations in Mississippi silverside collected from the Alviso Slough, which is apparent in the time-series (fig. 15, prior to the A8-TCS opening), indicate that the other perturbations played a role. At all three Alviso Slough sites, the highest THg concentrations occurred during April 2011. The very highest mean THg concentration (2.18 µg/g) of any single collection between 2010 and 2015 was observed during April 2011 at the downstream ALSL-4 site, adjacent to pond A6. At both ALSL-3 and ALSL-4, near and adjacent to the pond A6 breaches, respectively, Mississippi silverside THg concentrations remained elevated in May of 2011, compared to May 2010, while the year-over-year change for the May sampling event was not significant at the MALSL reference site (appendix 4). Following this early 2011 THg concentration spike in Mississippi silverside collected from the Alviso Slough, by mid-August of 2011, these concentrations returned to baseline or lower levels, where they remained until late 2016 (fig. 15).

Since this apparent 2011 spike in Mississippi silverside THg concentrations was confined to the early season (April–July) a more focused statistical analysis of interannual variability was conducted using only April–July data (factor APR–JUL under categorical variable SEASON in Model SL.FISH.3 and combined with year for categorical variable YEAR.SEASON in Model SL.FISH.4). Because of missing data in some locations (for example, no 2014 data for ALSL-2), and associated issues of model nonconvergence, the model was rerun for each sampling site (ALSL-2, ALSL-3, MALSL, GUASL) independently, with the model term YEAR. SEASON as the sole independent categorical variable (Model SL.FISH.5). The results indicate that for the early season, size-standardized fish THg concentrations for 60-mm Mississippi silverside were significantly elevated during 2011, compared to all other years, at both Alviso Slough sites (ALSL-2 and ALSL-3) (fig. 19). This contrasted with the MALSL reference site, in which THg concentrations of Mississippi silverside collected during the early season remained constant across all years. Results for the GUASL reference site, for this same early season period, were not directly comparable with respect to the 2011 spike observed in Alviso Slough, because no data for GUASL existed prior to 2013.

A parallel statistical analysis was conducted on three-spine stickleback data, which focused on the early season (April–July) time period and ran the SEASON.YEAR model on the individual sites independently (see appendix 3 table 3.1). Early season THg concentrations in three-spine stickleback were significantly higher during 2013 (compared to 2011) at sites ALSL-2, MALSL, and GUASL. At ALSL-2, concentrations during 2013 were not significantly different from 2010. These interannual differences for three-spine stickleback are akin to the more general interannual analysis that used Model SL.FISH.1 (fig. 16) and contrast to the temporal results observed for Mississippi silverside during the early season, when 2011 spikes in THg concentration were observed at both ALSL-2 and ALSL-3, but not at the MALSL reference site (fig. 19). The three-spine stickleback results indicate that the interannual variations for this species were more regional in nature and not directly due to Phase 1 management actions.

In an independent statistical analysis designed to examine among-year differences in THg concentrations of Mississippi silverside in the two Alviso Slough sites (ALSL-2 and ALSL-3), while correcting for regional changes at the MALSL reference site, a new dataset was created by subtracting the mean size-standardized fish THg concentration of 60-mm Mississippi silverside data collected at site MALSL from the same data collected at ALSL-2 and ALSL-3 (individual observations) for each sampling event. The resulting dataset reflected the reference site corrected mean size-standardized fish THg concentration data for 60-mm Mississippi silverside for sites ALSL-2 and ALSL-3. Model SL.FISH.5 was applied to this dataset, for each Alviso site individually, to verify if the interannual differences described above persisted. Indeed, for the early season, the 2011 reference site corrected mean size-standardized fish THg concentration data for 60-mm Mississippi silverside was significantly greater than all other years sampled for both ALSL-2 and ALSL-3 (see appendix 4 table 4.1). This simply reaffirms that the 2011 THg concentration spike observed in the Mississippi silverside was unique to Alviso Slough, linked to Phase 1 management actions, and not simply a regional phenomenon.

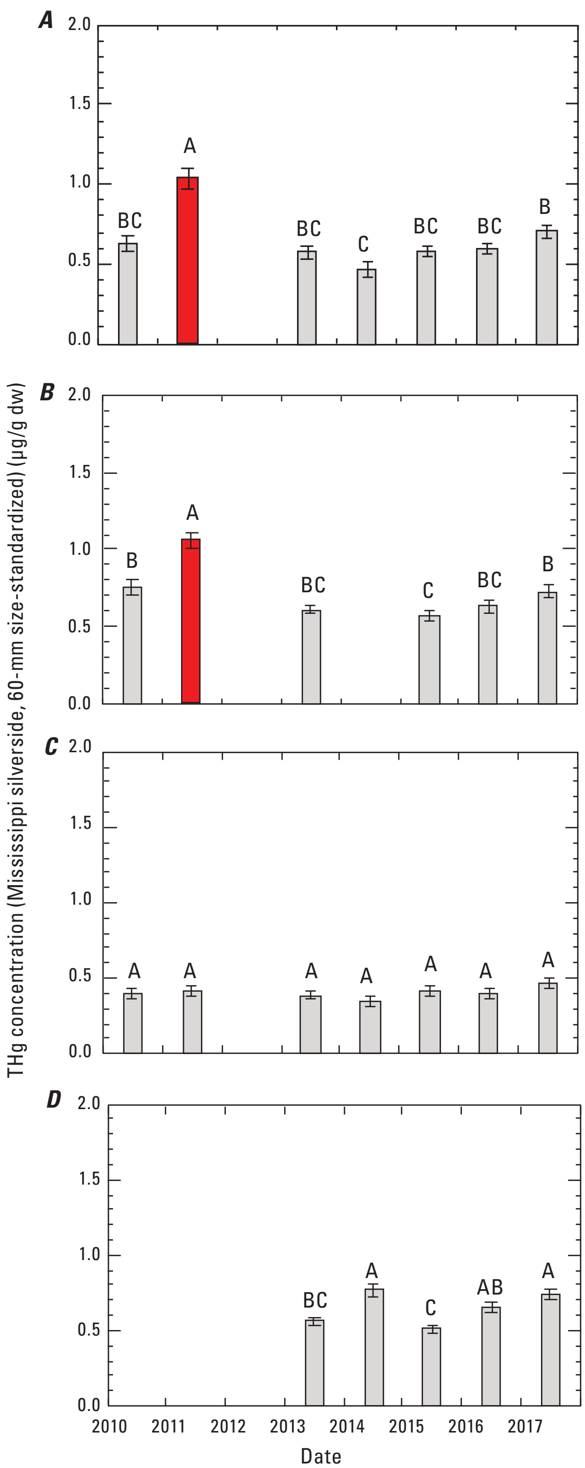

Figure 19. Bar graphs showing the size-standardized fish mean total mercury (THg) in 60-millimeter (mm) Mississippi silverside sampled during the early season (April–July) for slough sites ALSL-2 (*A*), ALSL-3 (*B*), MALSL (*C*), and GUASL (*D*). Results of Model SL.FISH.5, with among-year differences within each site is identified with letter designations (Tukey's pairwise comparison), with 'A' being the highest ranking. Years sharing the same letter are not significantly different. THg concentrations given in micrograms per gram dry weight [µg/g dw]. Error bars represent standard errors. Red highlighted bars emphasize maximum THg concentrations at sites ALS-2 and ALSL-3 during 2011.

Fish Mercury Spike Event During Late 2016 to Early 2017

Three-spine stickleback became too sparse to sample effectively after 2015, but the Mississippi silverside record continued without interruption. The largest increase of the entire 8-year study for THg concentration in Mississippi silverside occurred in the Alviso Slough between July 2016 and April 2017 (fig. 15), when concentrations increased over 300 percent, to a mean (± standard error) of 2.47±0.12 µg/g dw in October 2016 at site ALSL-2 and to 1.67±0.13 µg/g dw at site ALSL-3. The higher concentrations at ALSL-2 indicate exposure was greater in the upper reaches of Alviso Slough and closer to the A8-TCS. Four months later, during February 2017, THg concentrations in Mississippi silverside at both Alviso Slough stations were down to approximately 1.20 µg/g, a substantial decline, although still elevated well above baseline levels (approximately 0.68 µg/g dw). By April 2017, mean THg concentrations were back below 0.80 µg/g dw at both sites, where they remained until the end of the study (February 2018).

Because this dominant 2016–17 spike in THg concentration in Mississippi silverside was confined to the late season (August–February), a more focused statistical analysis was made of interannual variability using only August–February data (Model SL.FISH.4). Owing to missing data in some locations (for example, no 2014 data for ALSL-2) and associated issues of model nonconvergence, the model was rerun as a single-term (YEAR.SEASON) ANOVA on the four primary sampling sites (ALSL-2, ALSL-3, MALSL, and GUASL) independently (Model SL.FISH.5). The results indicate that late season size-standardized fish THg concentrations for 60-mm Mississippi silverside were significantly elevated during 2016, compared to all other years, at both Alviso Slough sites (ALSL-2 and ALSL-3; fig. 20). In contrast, the late season interannual trend showed no significant 2016 spike in Mississippi silverside THg concentration at either the MALSL or the GUASL reference sites.

Because of the unusual and unexpected nature of this 2016–2017 late season spike in Mississippi silverside THg concentrations in Alviso Slough, a more detailed examination of the data in this relevant time period was warranted. Figure 21 depicts the THg concentration of Mississippi silverside, by fish length, from April 2016 through February 2017 at the upper Alviso Slough sampling site (ALSL-2). The fish length data represent the mean of multiple individuals composited into narrowly defined size ranges. The very high THg concentrations seen during October 2016 were consistent across all 6 composite samples, each composed of 8 individual fish (48 Mississippi silverside total for the overall mean). Similarly, the declining, but still elevated, concentrations seen during February 2017 were consistent across all samples. This consistency is clear evidence that the 2016–17 mercury spike event was a significant phenomenon in the Alviso Slough. Additionally, this pattern of THg concentrations in fish plotted against fish size indicates that the peak exposure levels may have already passed at the time of the early

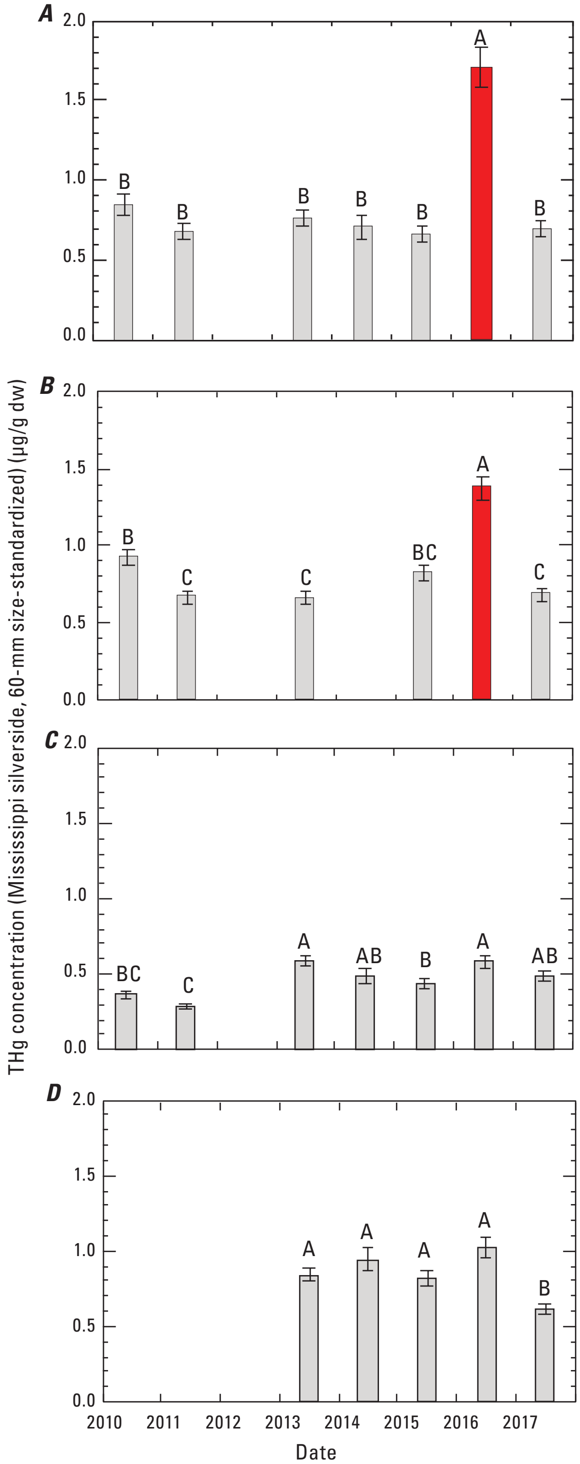

Figure 20. Bar graphs showing the modeled mean size-standardized fish total mercury (THg) concentrations for 60-millimeter (mm) Mississippi silverside sampled during the late season (August–February) for slough sites ALSL-2 (*A*), ALSL-3 (*B*), MALSL (*C*), and GUASL (*D*). Results of Model SL.FISH.5, with among-year differences within each site are identified with letter designations (Tukey's pairwise comparison), with 'A' being the highest ranking. Years sharing the same letter are not significantly different. Error bars represent standard errors. Red highlighted bars emphasize maximum THg concentrations at sites ALS-2 and ALSL-3 during 2016. THg concentrations given in micrograms per gram dry weight (µm/g dw).

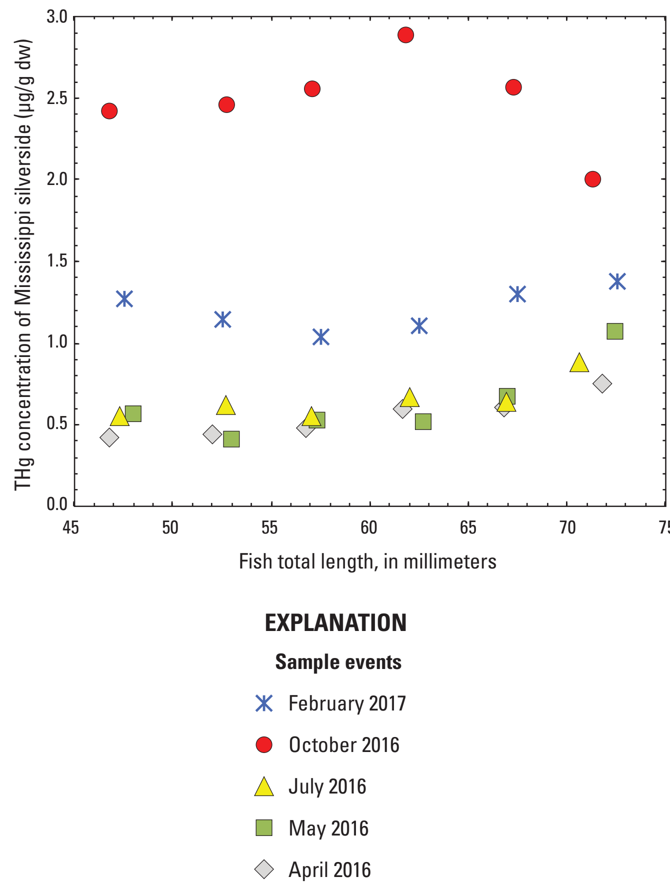

Figure 21. Graph showing total mercury (THg) concentration of Mississippi silverside versus fish total length at site ALSL-2 between April 2016 and February 2017, by sampling event. Each data point represents one composite analytical sample, composed of eight closely sized whole fish. The x-axis reflects mean fish size of the individuals comprising each composite (within the 5-millimeter target size range). THg concentrations given in micrograms per gram dry weight (µm/g dw).

October 2016 sampling event. Since size generally tracks age in these rapidly growing, short-lived fish, under relatively steady-state exposure conditions we would expect to see THg concentration increase with size (Grieb and others, 1990; Greenfield and others, 2013), as was the case for the samples collected during the April through July 2016 period. However, under rapidly changing exposure conditions, the immediate effect of the new exposure (and uptake) condition is typically most pronounced in the smallest size classes (Eagles-Smith and Ackerman, 2009). This is because, for these smallest and (or) youngest fish, recent exposure conditions constitute a larger proportion of their entire short lives, whereas, for the larger and (or) older fish, exposures of the recent few weeks integrate with previous bioaccumulation from a much longer period. Therefore, under rapidly increasing mercury exposure, the smallest and (or) youngest fish often demonstrate the very highest levels, counter to the normal distribution. During rapidly declining exposure, the smallest and (or) youngest fish typically reflect the drop more rapidly as well. The October

2016 distribution indicates that peak exposure levels for the 2016 spike event likely occurred earlier in the summer and, although still very high in early October, levels may have been declining. The abiotic factors that may have led up to this late season spike in THg concentrations in Mississippi silverside during 2016 are further discussed in the "Synthesis of the Independent Studies" section.

Akin to analysis of early season data, an independent statistical analysis of among-year differences in late season THg concentrations of Mississippi silverside in the two Alviso Slough sites (ALSL-2 and ALSL-3) was done. The mean size-standardized fish THg concentration data for 60-mm Mississippi silverside were adjusted for sites ALSL-2 and ALSL-3 by subtracting the MALSL concentration data to account for regional changes for each sampling event. Model SL.FISH.5 was applied for each Alviso Slough site individually. A similar interannual trend in THg concentrations was observed for ALSL-2, where late season THg concentrations of Mississippi silverside collected in 2016 were significantly ($p < 0.05$) greater than all other years sampled, paralleling the interannual trend obtained when ALSL-2 data were analyzed without subtracting the reference site (fig. 20*A*). However, although having the greatest difference from the MALSL reference site, the reference site adjusted late-season 2016 THg concentrations at ALSL-3 were not significantly different ($p > 0.05$) from the 2010 or 2015 values. Thus, these reference site adjusted results differed in the degree of statistical detectability, but not in interannual trend, from the less ambiguous results presented in fig. 20*B* (ALSL-3) and fig. 20*C* (site MALSL).

Surface Water

2010–18 Time-Series of Mercury Parameters

The temporal and spatial trends for all mercury parameters, directly measured or calculated, are graphically presented as time series plots for both ponds (figs. 22–28) and sloughs (figs. 29–35). The mercury-specific species associated with the time-series plots for the three pond regions

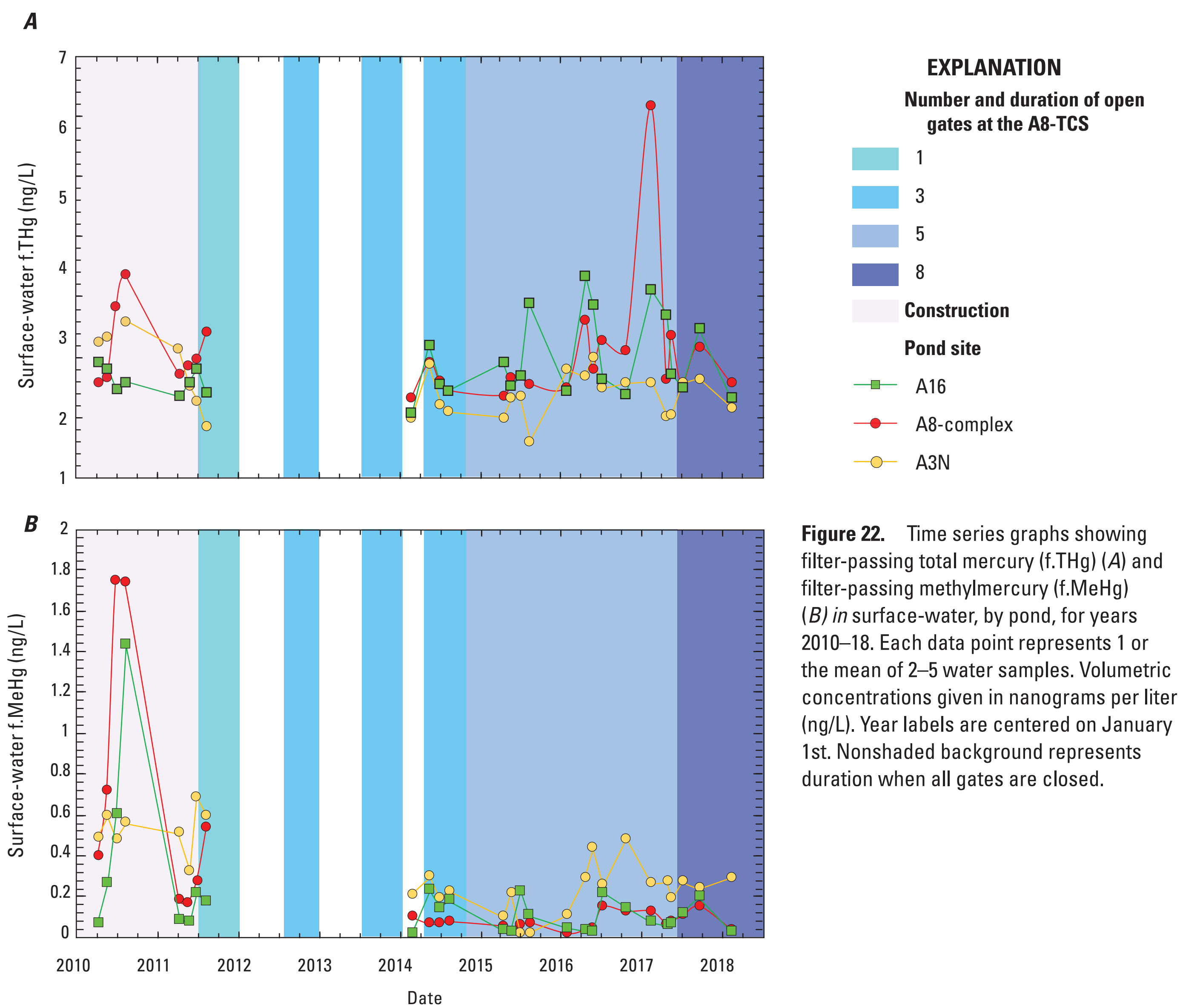

Figure 22. Time series graphs showing filter-passing total mercury (f.THg) (*A*) and filter-passing methylmercury (f.MeHg) (*B*) *in* surface-water, by pond, for years 2010–18. Each data point represents 1 or the mean of 2–5 water samples. Volumetric concentrations given in nanograms per liter (ng/L). Year labels are centered on January 1st. Nonshaded background represents duration when all gates are closed.

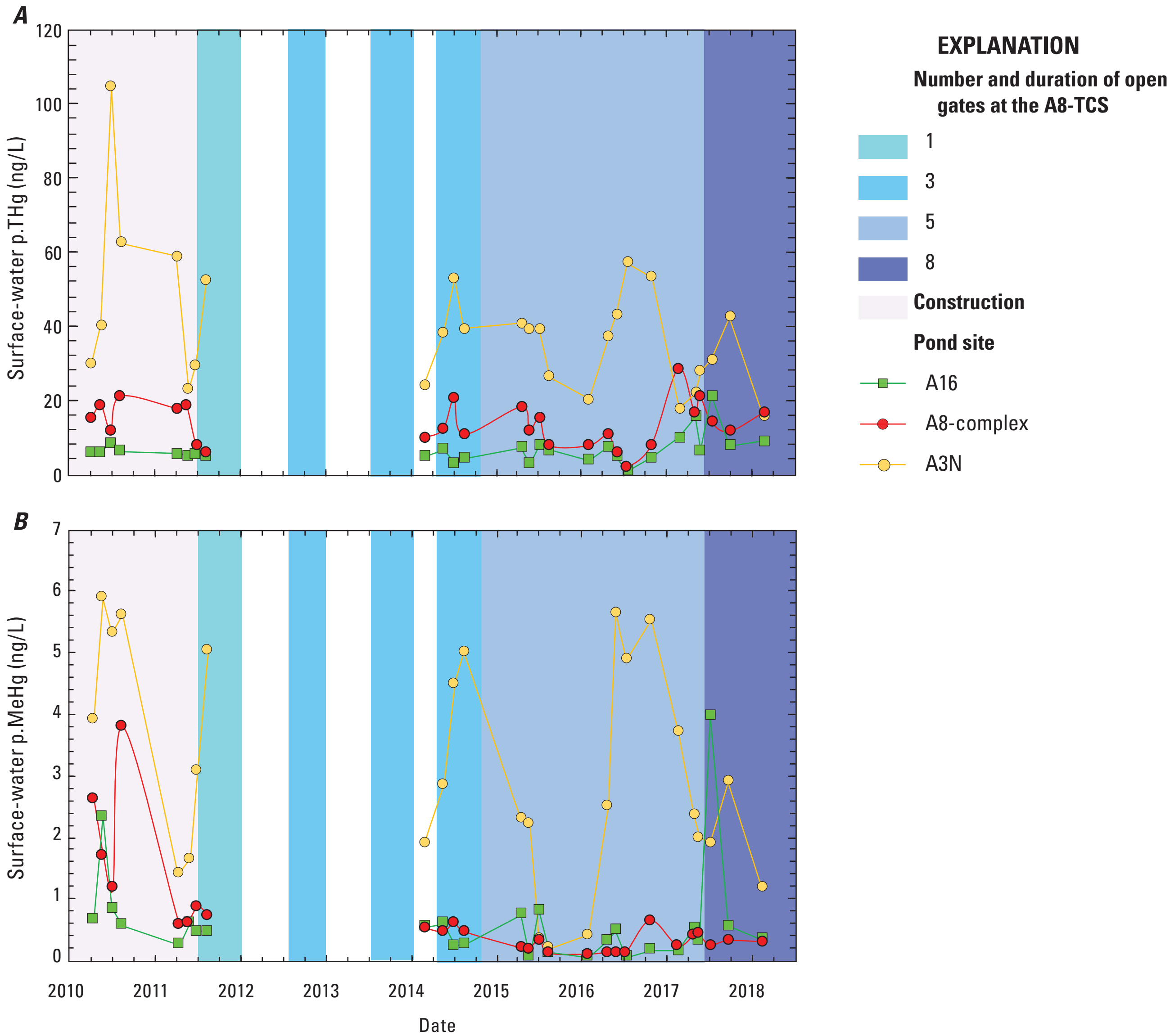

Figure 23. Time series graphs showing particulate total mercury (p.THg) (*A*) and particulate methylmercury (p.MeHg) (*B*) on a volumetric basis in surface-water, by pond, for years 2010–18. Each data point represents 1 or the mean of 2–5 water samples. Volumetric concentrations given in nanograms per liter (ng/L). See figure 22 for additional information on graphic attributes.

(A8-complex, pond A3N, and pond A16) are as follows: (1) filter-passing total mercury (f.THg) and filter-passing MeHg (f.MeHg) (fig. 22); (2) particulate (surface-water) THg (p.THg) and particulate MeHg (p.MeHg) (volumetric basis, fig. 23); (3) p.THg and p.MeHg (gravimetric basis, fig. 24); (4) unfiltered THg (uf.THg) and unfiltered MeHg (uf.MeHg) (fig. 25); (5) particulate inorganic reactive mercury (p.RHg), gravimetric and as a percentage of THg (fig. 26); (6) f.MeHg as a percentage of f.THg and p.MeHg as a percentage of p.THg (fig. 27); and (7) the distribution coefficients for THg and MeHg, Kd(THg) and Kd(MeHg), respectively (fig. 28).

Several observations are apparent from these time series plots and are noteworthy with respect to Q.2 ("Mercury Synthesis—Organizing Questions" section), which focuses on

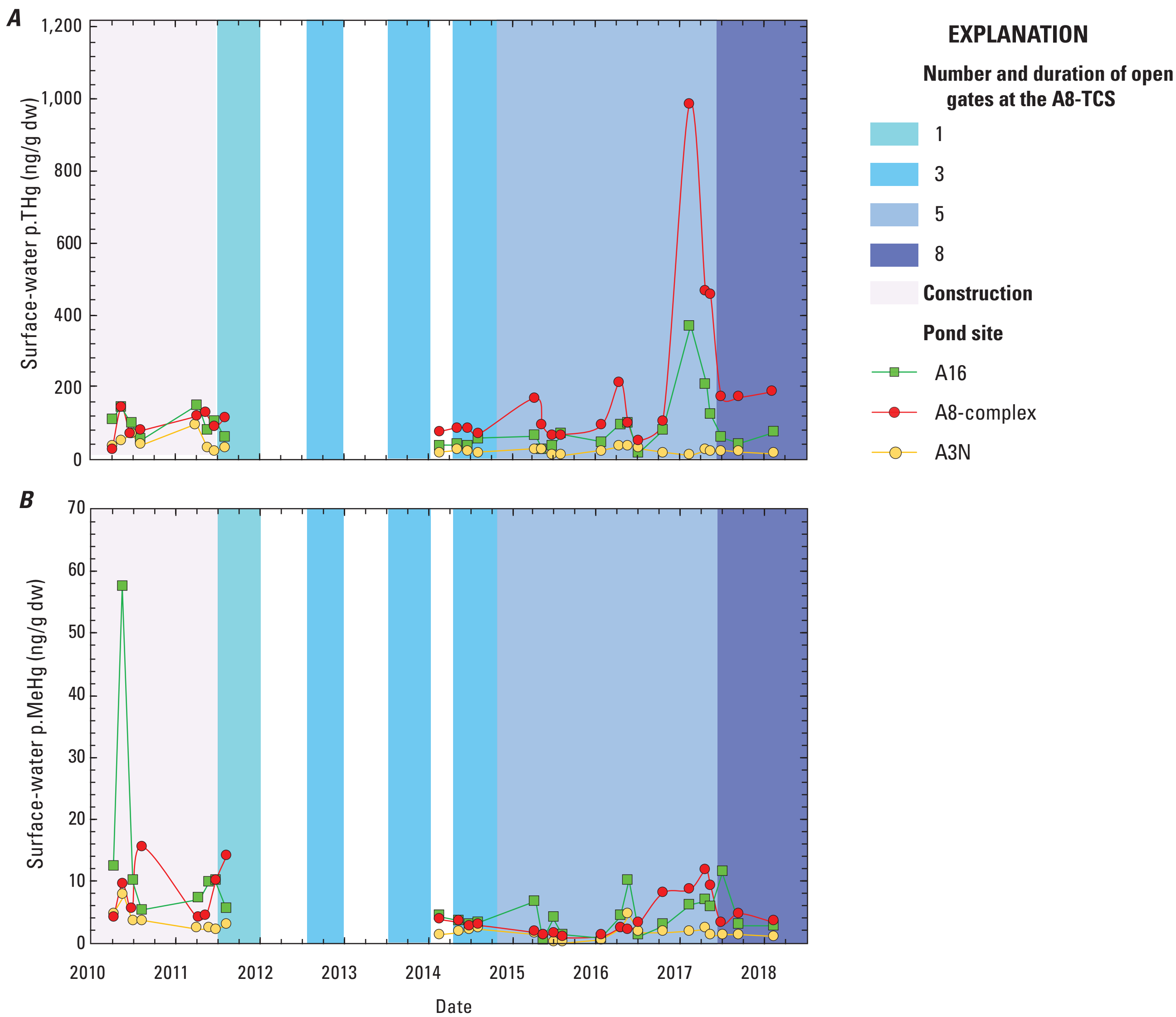

Figure 24. Time series graphs showing particulate total mercury (p.THg) (*A*) and particulate methylmercury (p.MeHg) (*B*) on a gravimetric basis in surface-water, by pond, for years 2010–18. Each data point represents 1 or the mean of 2–5 water samples. Gravimetric concentrations given in nanograms per gram dry weight (ng/g dw). See figure 22 for additional information on graphic attributes.

the construction period within and around the A8-complex, the initial and gradual opening of the A8-TCS, and if any surface-water mercury parameters measured within the A8-complex were directly affected by these management actions. The strongest evidence for this would be a dramatic change in a specific mercury species observed within the A8-complex, but not similarly occurring in reference ponds A3N or A16. To this end, uf.MeHg concentrations (fig. 25*B*) are appreciably elevated within the A8-complex prior to the initial opening of the A8-TCS, but much lower in the period after that. A similar trend is seen for f.MeHg as a percentage of THg, within the A8-complex, in the periods before and after the opening of the A8-TCS (fig. 27*A*). In contrast, the hydrologically isolated reference pond A3N (limited circulation with bay water) was

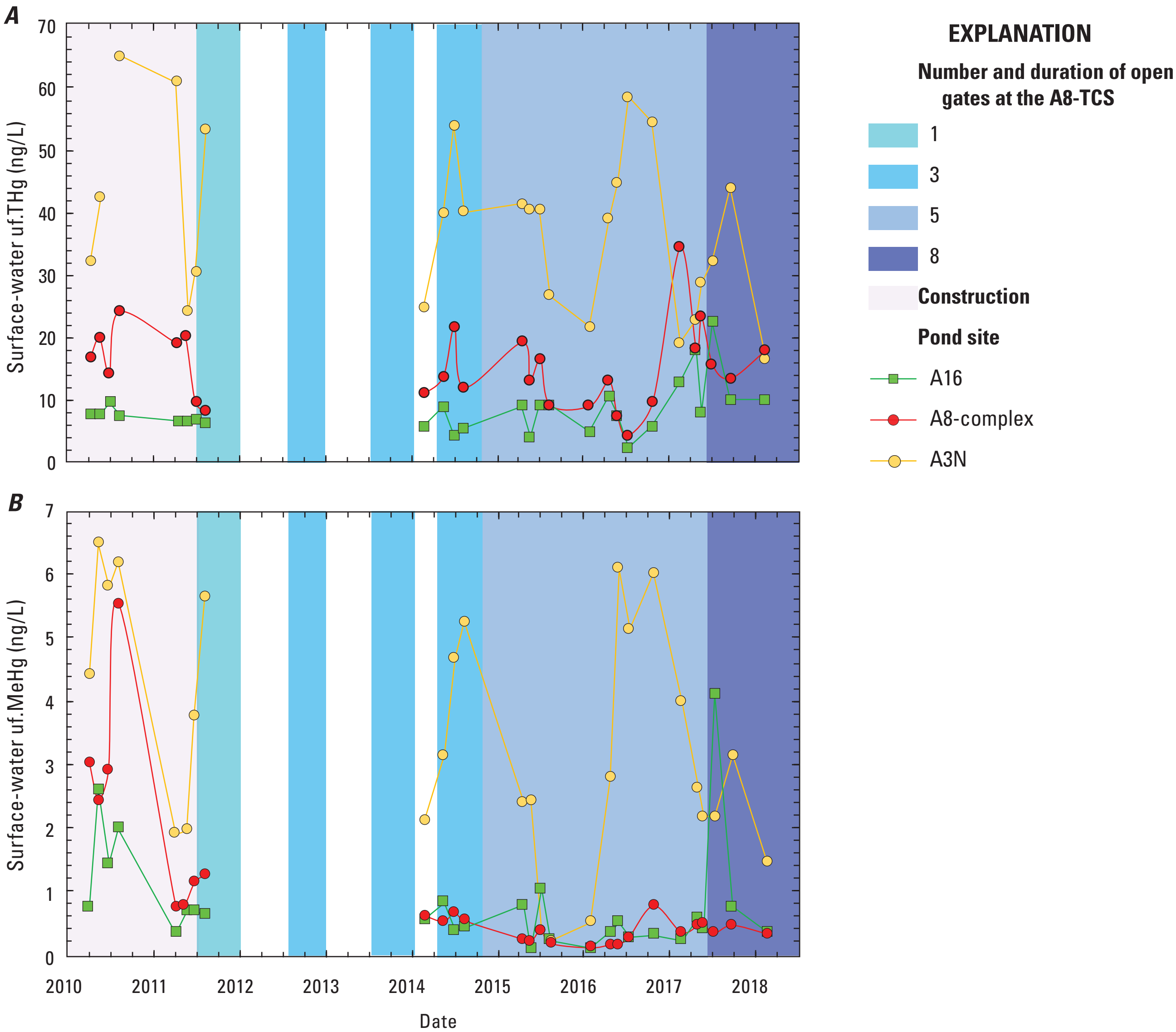

Figure 25. Time series graphs showing unfiltered (particulate + filtered) total mercury (uf.THg) *(A)* and unfiltered methylmercury (uf.MeHg) *(B)* in surface-water, by pond, for years 2010–18. Each data point represents 1 or the mean of 2–5 water samples. Volumetric concentrations given in nanograms per liter (ng/L). See figure 22 for additional information on graphic attributes.

seasonally elevated in uf.MeHg both before and after the period following the opening of the A8-TCS (fig. 25*B*).

The mercury-specific species associated with the time-series plots for the four slough sampling regions (upper Alviso Slough, lower Alviso Slough, Mallard Slough, Guadalupe Slough) are as follows: (1) f.THg and f.MeHg (fig. 29); (2) p.THg and p.MeHg (plotted on a volumetric basis, fig. 30); (3) p.THg and p.MeHg (plotted on a gravimetric basis, fig. 31); (4) uf.THg and uf.MeHg (fig. 32); (5) p.RHg, plotted on a gravimetric basis and as a percentage of p.THg (fig. 33); (6) f.MeHg as a percentage of f.THg and p.MeHg as a percentage of p.THg (fig. 34); and (7) Kd(THg) and Kd(MeHg) (fig. 35). The slough-specific time series graphs visually inform both Q.1 and Q.3, but it is important to note that the sampling of

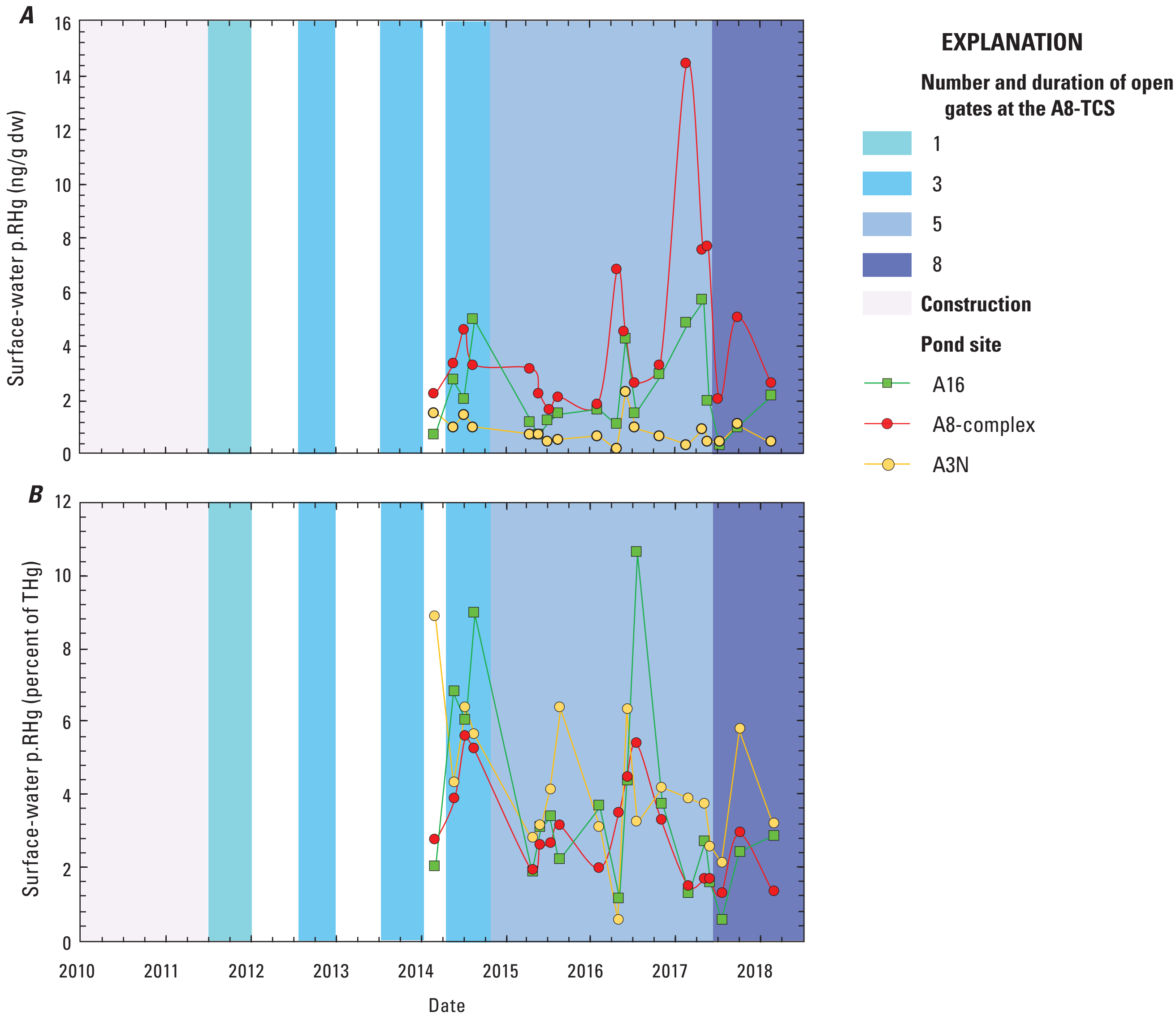

Figure 26. Time series graphs showing particulate reactive inorganic mercury (p.RHg) on a gravimetric basis (*A*) and as a percentage of total mercury (THg) (*B*) in surface-water, by pond, for years 2014–18. Each data point represents 1 or the mean of 2–5 water samples. Gravimetric concentrations given in nanograms per gram dry weight (ng/g dw). See figure 22 for additional information on graphic attributes.

Guadalupe Slough did not begin until 2014, and that the upper Alviso Slough and lower Alviso Slough sampling regions included sites ALSL-1 and ALSL-4, respectively, that were subsequently dropped after 2011. Question 1 focuses on the breaching of pond A6 and whether any surface-water mercury parameters were demonstrably affected by this management action. The clearest evidence of such an effect would be observed in Alviso Slough (particularly in lower Alviso Slough), but not at the MALSL reference site. A spike in both p.THg and p.MeHg (volumetric basis, fig. 30), and in uf.THg and uf.MeHg (fig. 32) was observed during June 2011 only in lower Alviso Slough.

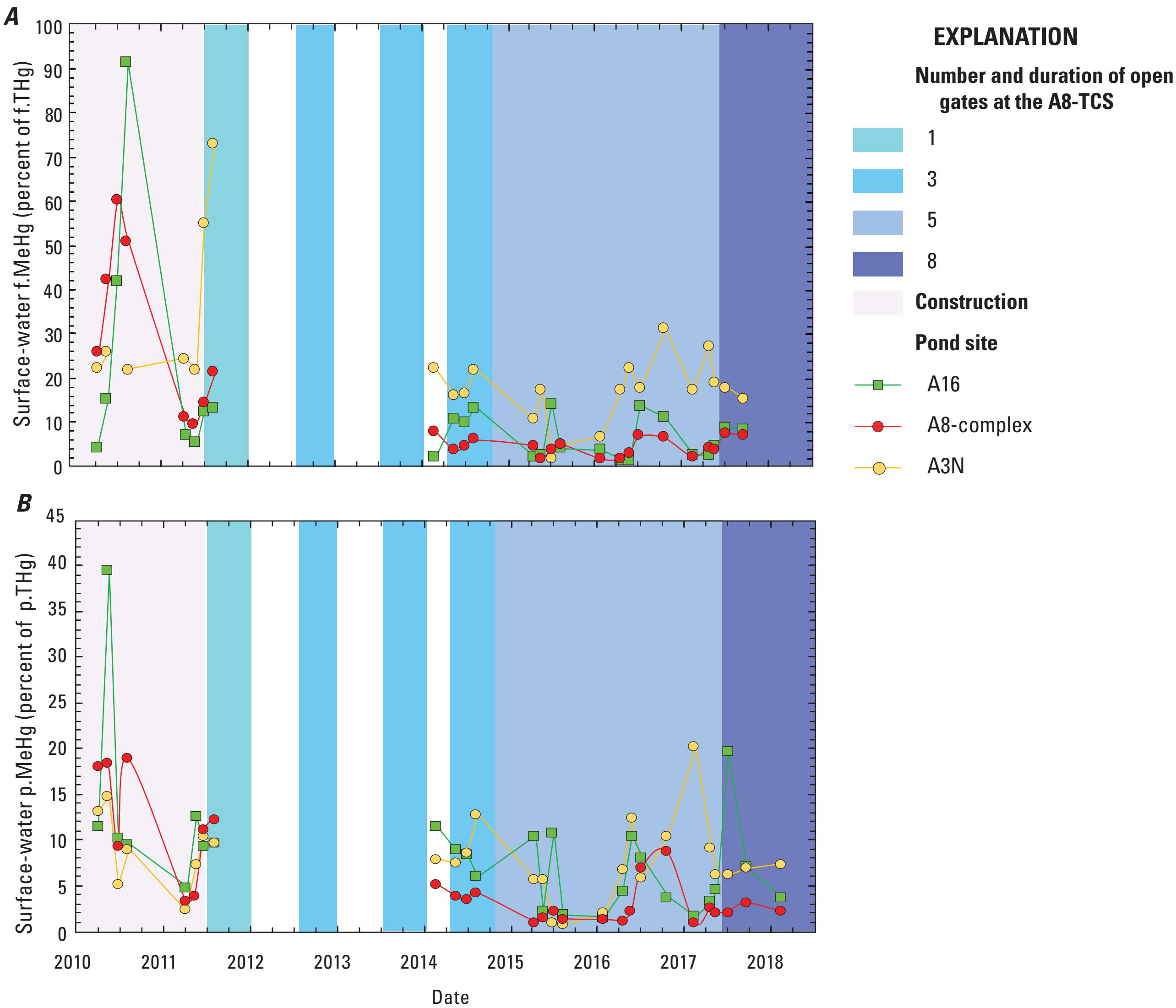

Figure 27. Time series graphs showing filter-passing methylmercury (f.MeHg) as a percentage of filter-passing total mercury (f.THg) (*A*) and particulate methylmercury (p.MeHg) as a percentage of particulate total mercury (p.THg) (*B*) in surface-water, by pond, for years 2010–18. Each data point represents 1 or the mean of 2–5 water samples. See figure 22 for additional information on graphic attributes.

Although these spikes occurred one month after the initial opening of the A8-TCS (1-gate condition or 5 ft), it is very unlikely that this action caused a spike in particulate mercury species in the lower Alviso Slough and not in the upper Alviso Slough. More likely is that the pond A6 breach in December 2010, which appeared to trigger the extended bed sediment scour event that ensued over the subsequent months, was the primary cause of these observed spikes. Also, a spike of p.THg (gravimetric basis) was observed in the upper Alviso Slough during April and May 2011 (fig. 31*A*), which was after the pond A6 breach and prior to the opening of the A8-TCS. This peak in p.THg was coincident with the highest Kd(THg) levels seen during the time series (fig. 35), indicating a very strong association with surface-water particulates. A peak in p.THg (gravimetric basis) of this magnitude was not seen again in the upper Alviso Slough until the extreme flow event of late 2016

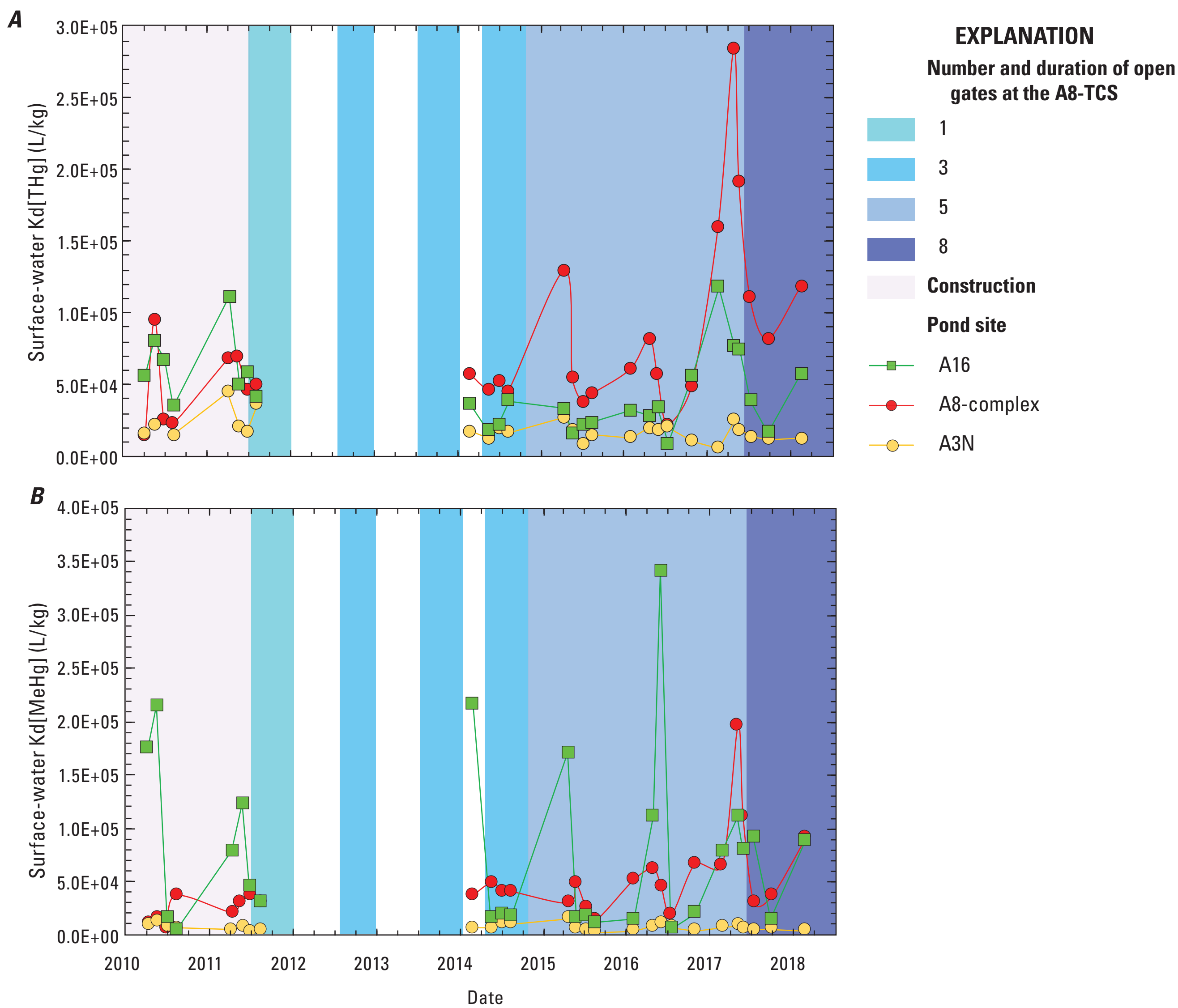

Figure 28. Time series graphs showing distribution coefficients (Kd) for total mercury (THg) (*A*) and methylmercury (MeHg) (*B*) in surface-water, by pond, for years 2010–18. Each data point represents 1 or the mean of 2–5 water samples. Distribution coefficient units given in liters per kilogram (L/kg). See figure 22 for additional information on graphic attributes.

(fig. 31*A*). Because of the timing, magnitude, and Kd signature associated with this early 2011 peak in p.THg in the upper Alviso Slough, it is also likely that it was related to the pond A6 breach, although this evidence is not conclusive.

The slough time-series plots also communicate some visual data that inform Q.3, which focuses on whether the gradual opening of the A8-TCS resulted in any demonstrable change in surface-water mercury concentrations in Alviso Slough itself. Evidence of this change in surface-water mercury concentrations would involve notable changes in Alviso Slough, but not in the MALSL reference site. However, given the gradual and evolving nature of the A8-TCS manipulations between June 2011 and June 2017 and the timing of opening all eight gates (June 2017), visual time-series evidence alone is more difficult to interpret than was the case for Q.1, which addressed the pond A6 levee breach—a

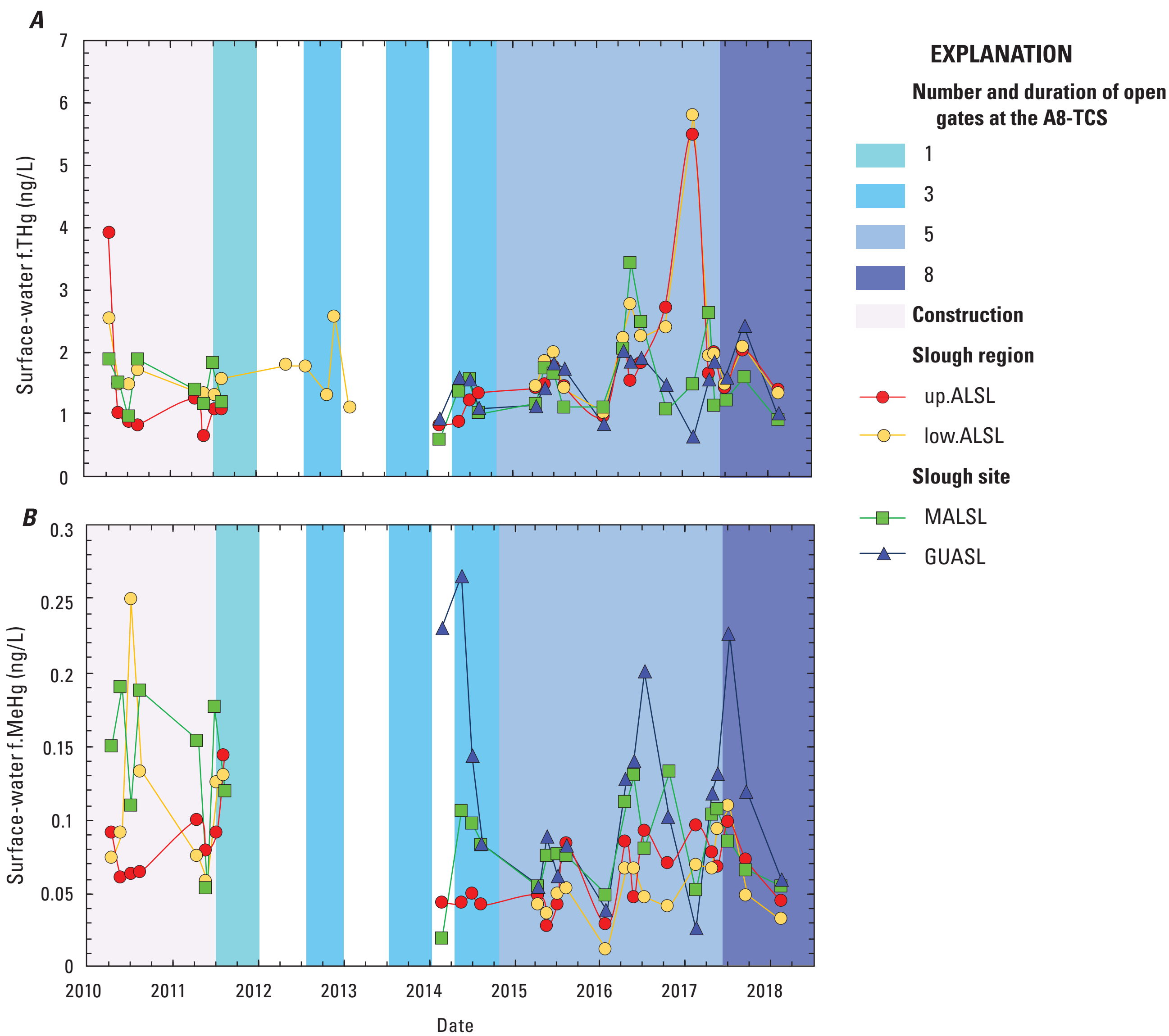

Figure 29. Time-series graphs showing filter-passing total mercury (f.THg) (*A*) and filter-passing methylmercury (f.MeHg) (*B*) in surface-water, by slough region or site, for years 2010–18. Alviso Slough sampling sites ALSL-1 and ALSL-4 were included in the calculation of the mean values for the upper Alviso Slough (up.ALSL) and lower Alviso Slough (low.ALSL) sampling regions, respectively, during the 2010-11 study period. After this period these two sites were dropped and up.ALSL and low.ALSL only reflect data collected from sites ALSL-2 and ALSL-3, respectively. Volumetric concentrations given in nanograms per liter (ng/L). See figure 22 for additional information on graphic attributes.

one-time discrete event. Potential evidence that addresses Q.3 is the overall decrease in p.THg (gravimetric basis, fig. 31) in the 2014–18 period after the initial opening of the A8-TCS. The exception to this is the dramatic spike in p.THg that was coincident with the very high flow event during January–February 2017. However, Q.3 is best addressed with more rigorous statistical analyses, as was done and discussed in the "Results of Models SW.3 and SW.4", "Fixed Monitoring Station Time series Results for Water Quality, Discharge, and Suspended-Sediment Flux", and "Ponds and Sloughs: Shallow Sediment Routine Sampling, 2010–11" sections.

To examine overall spatial differences among the different study ponds and slough sampling areas, the surface-water dataset was spatially grouped by the six sampling regions (or sites) as defined by the model term REGION for model SED.1 (see "Shallow Sediment Data: Statistics, 2010–11" section) and analyzed with simple summary statistics (mean, standard error, range, median, and percentiles [25 and 75%]) for all

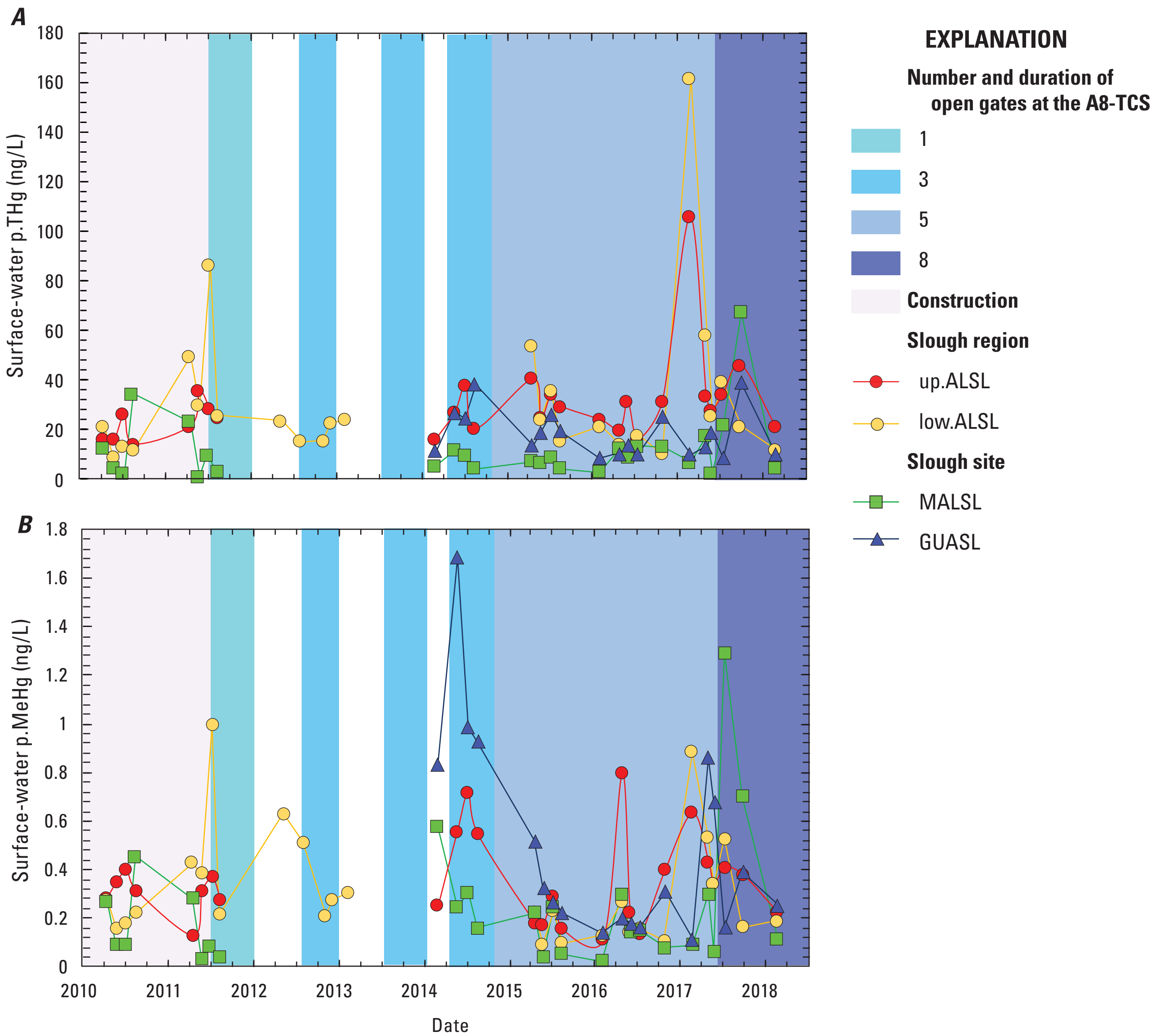

Figure 30. Time-series graphs showing particulate total mercury (p.THg) (*A*) and particulate methylmercury (p.MeHg) (*B*) in surface-water on a volumetric basis, by slough region or site, for years 2010–18. Alviso Slough sampling sites ALSL-1 and ALSL-4 were included in the calculation of the mean values for the upper Alviso Slough (up.ALSL) and lower Alviso Slough (low.ALSL) sampling regions, respectively, during the 2010–11 study period. After this period these two sites were dropped and up.ALSL and low.ALSL only reflect data collected from sites ALSL-2 and ALSL-3, respectively. Volumetric concentrations given in nanograms per liter (ng/L). See figure 22 for additional information on graphic attributes.

mercury and nonmercury surface-water parameters directly measured or calculated (appendix 5). Although this analysis sheds no light on changes in water chemistry over time, it does provide some valuable and statistically defensible insights into the large-scale spatial differences over the full study period (2010–2018), which can also be gleaned from the time series plots (figs. 22–35). However, owing to the data distribution, this spatial analysis is skewed towards the time period and conditions that existed after the pond A6 breach during December 2010 and the A8-TCS initial opening during June 2011.

A brief description of mercury specific highlights evident in appendix 5 (and the time series plots; figs. 22–28), with respect to the three pond sampling regions (A8-complex, pond A3N, pond A16) include the following (see appendix 5 for geometric mean values cited):

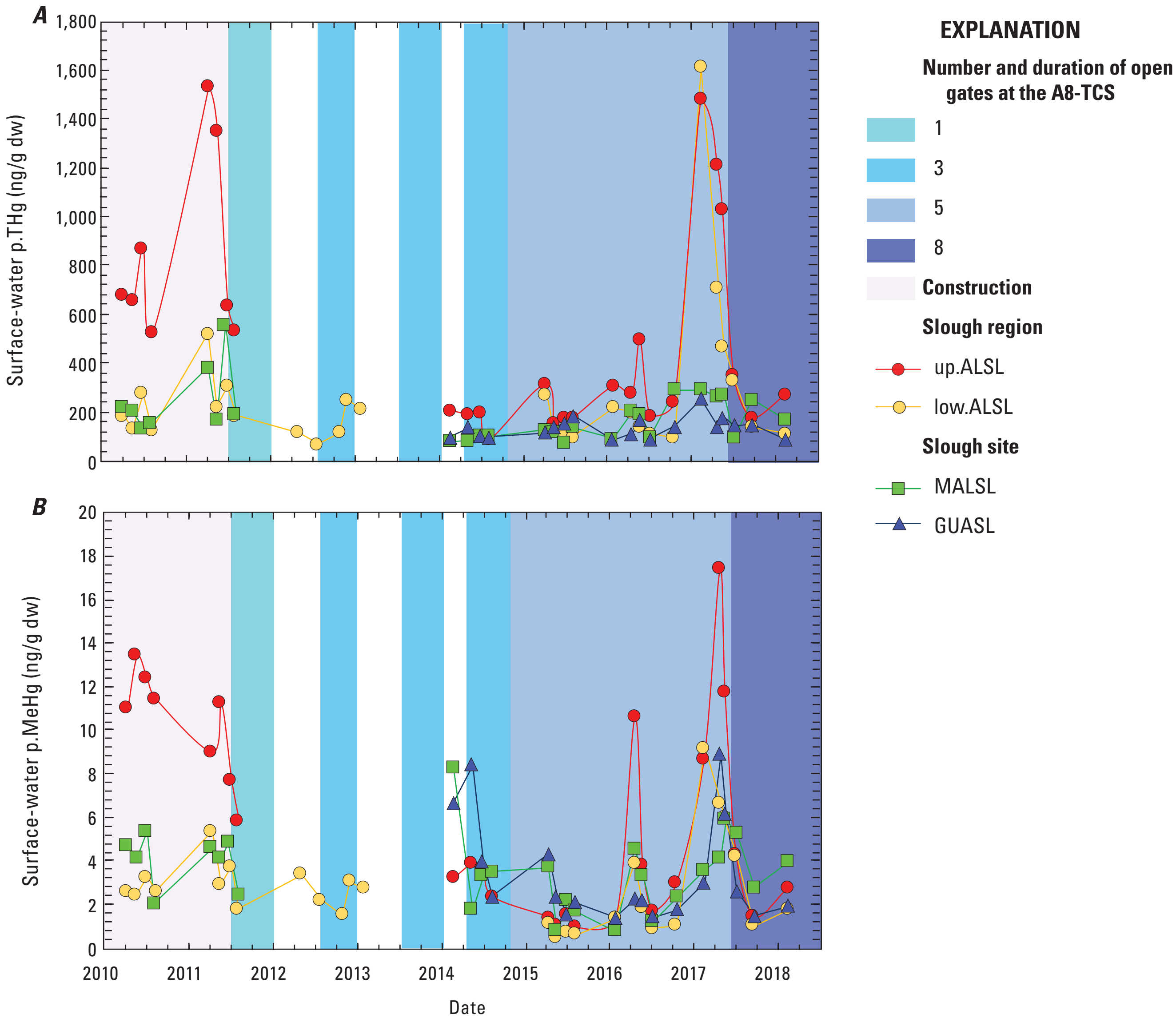

Figure 31. Time-series graphs showing particulate total mercury (p.THg) (*A*) and particulate methylmercury (p.MeHg) (*B*) in surface water on gravimetric basis, by slough region or site, for years 2010–18. Alviso Slough sampling sites ALSL-1 and ALSL-4 were included in the calculation of the mean values for the upper Alviso Slough (up.ALSL) and lower Alviso Slough (low.ALSL) sampling regions, respectively, during the 2010–11 study period. After this period these two sites were dropped and up.ALSL and low.ALSL only reflect data collected from sites ALSL-2 and ALSL-3, respectively. Gravimetric concentrations given in nanograms per gram dry weight (ng/g dw). See figure 22 for additional information on graphic attributes.

- f.THg, in ng/L, (fig. 22) fell within a narrow range among all three ponds, from 1.42 ng/L in pond A3N to 1.94 ng/L in the A8-complex;
- f.MeHg, in ng/L, (fig. 22) was highest in A3N (0.23 ng/L) and lowest in A16 (0.10 ng/L);
- f.MeHg, as a percentage of f.THg, (fig. 27) was similarly highest in A3N (15.9%) and lowest in A16 (5.7%);
- p.THg, in ng/g dw, (fig. 24) was highest in the A8-complex (115 ng/g) and lowest in A3N (24 ng/g);
- p.THg, in ng/L, (fig. 23) was highest in A3N (34.4 ng/L) and lowest in A16 (5.7 ng/L);
- p.MeHg, in ng/g dw, (fig. 24) was highest in A16 (4.78 ng/g) and lowest in A3N (1.46 ng/g);

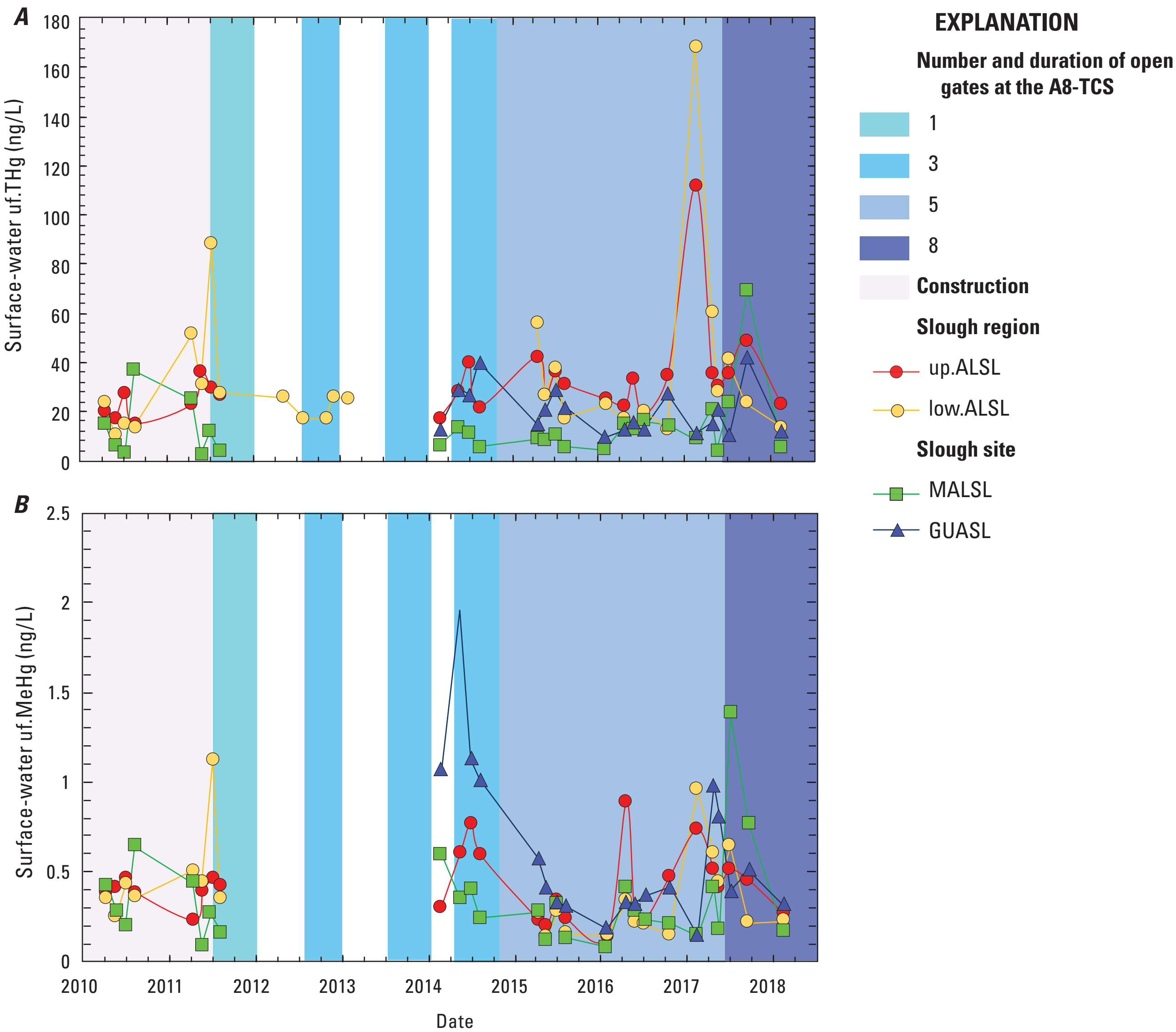

Figure 32. Time-series graphs showing surface-water unfiltered total mercury (uf.THg) (*A*) and unfiltered methylmercury (uf.MeHg) (*B*) in surface-water, by slough region or site, for years 2010–18. Alviso Slough sampling sites ALSL-1 and ALSL-4 were included in the calculation of the mean values for the upper Alviso Slough (up.ALSL) and lower Alviso Slough (low.ALSL) sampling regions, respectively, during the 2010–11 study period. After this period these two sites were dropped and up.ALSL and low.ALSL only reflect data collected from sites ALSL-2 and ALSL-3, respectively. Unfiltered total mercury is calculated from the sum of the particulate and filter-passing total mercury fractions. Volumetric concentrations given in nanograms per liter (ng/L). See figure 22 for additional information on graphic attributes.

- p.MeHg, in ng/L, (fig. 23) also was highest in A3N (2.18 ng/L) and similar in both the A8-complex and A16 (0.38 ng/L);
- p.MeHg, as a percentage of p.THg, (fig. 27) was similarly high in A3N and A16 (6.17% and 6.69%, respectively) and lower in the A8- complex (3.48%);
- p.RHg, in ng/g dw, (fig. 26) was highest in the A8-complex (3.49 ng/g) and lowest in A3N (0.68 ng/g);
- conversely, p.RHg, in ng/L, (not shown) was highest in the A3N (1.13 ng/L) and lowest in the A8-complex (0.27 ng/L);
- p.RHg, as a percentage of p.THg, (fig. 26) was similar among the three ponds, ranging from 2.55 percent (A8-complex) to 3.58 percent (A3N);
- the distribution coefficient for THg (Kd[THg]) (fig. 28) was highest for the A8-complex (58,819 L/kg) and lowest for A3N (16,033 L/kg);

- the distribution coefficient for MeHg (Kd[MeHg]) (fig. 28) was highest for the A16 (45,844 L/kg) and lowest for A3N (6,294 L/kg).

A similar descriptive summary of appendix 5 results of mercury parameters associated with the four slough sampling regions (upper Alviso Slough, lower Alviso Slough, Mallard Slough, and Guadalupe Slough) highlight the following (geometric mean values cited):

- f.THg, in ng/L, (fig. 29) fell within a narrow range among all four slough sampling regions, from 1.35 ng/L (upper Alviso Slough) to 1.70 ng/L (lower Alviso Slough);
- f.MeHg, in ng/L, (fig. 29) also fell within a narrow range, from 0.07 ng/L (both upper Alviso Slough and lower Alviso Slough) to 0.11 ng/L (Guadalupe Slough);
- f.MeHg, as a percentage of f.THg, (fig. 34) ranged from 4.0 percent (lower Alviso Slough) to 7.3 percent (Guadalupe Slough);
- p.THg, in ng/g dw (fig. 31) was highest in the upper Alviso Sough (440 ng/g) compared to the other three regions (p.THg ranged from 129 to 183 ng/g);
- p.THg, in ng/L, (fig. 30) was highest in the upper Alviso Slough and lower Alviso Slough (25.6 and 22.3 ng/L, respectively) compared to Mallard Slough (8.1 ng/L) and Guadalupe Slough (16.4 ng/L);
- p.MeHg, in ng/g dw, (fig. 31) was highest in the upper Alviso Slough (5.21 ng/g) compared to the other three regions (p.MeHg ranged from 2.16 to 3.05 ng/g);
- p.MeHg, in ng/L, (fig. 30) ranged between 0.15 ng/L (Mallard Slough) and 0.36 ng/L (Guadalupe Slough);
- p.MeHg, as a percentage of p.THg, (fig. 34) ranged between 1.19 percent (both upper and lower Alviso Slough) and 2.19 percent (Guadalupe Slough);
- p.RHg, in ng/g dw, (fig. 33) ranged narrowly between 2.94 ng/g (Guadalupe Slough) and 3.82 ng/g (lower Alviso Slough);
- p.RHg, in ng/L, (not shown) ranged between 0.21 ng/L (Mallard Slough) and 0.50 ng/L (lower Alviso Slough);
- p.RHg, as a percentage of p.THg, (fig. 33) ranged between 1.16 percent (upper Alviso Slough) and 2.41 percent (Mallard Slough);
- the distribution coefficient for THg (Kd[THg]), in L/kg, (fig. 35) was highest for upper Alviso Slough (324,959 L/kg) and lowest for Guadalupe Slough (87,895 L/kg); and
- the distribution coefficient for MeHg (Kd[MeHg]) in L/kg, (fig. 35) was similarly highest for upper Alviso Slough (77,415 L/kg) and lowest for Guadalupe Slough (26,279 L/kg).

A few nonmercury spatial trends for both pond and slough sampling regions, as summarized in appendix 5, merit mention. First, reference pond A3N stood out among the three pond regions sampled with respect to several nonmercury parameters:

- a comparatively high POC/PN molar ratio (10.35);
- a comparatively low δ15N-PN isotopic signature (5.124 per mil), potentially indicative of enhanced nitrification (Kendall and others, 2001));
- high specific conductance (71.0 mS/cm);
- very high DOC (24.15 mg/L);
- a comparatively low $SUVA_{254}$ value (1.49 liter per milligram carbon per meter);
- nearly depleted NO2- +NO3- concentrations (0.05 mg/L as nitrogen);
- elevated chlorophyll a (Chl.a; 59.1, in milligrams per cubic meter [mg/m^3], as measured on filters using the absorbance method, and very high EXO Chlorophyll (500.9 micrograms per liter [µg/L]), as measured by the EXO water quality sonde;
- extremely high TSS (1474 mg/L) and EXO turbidity (67.9, in formazin nephelometric units); and
- elevated SO_4^{2-} and Cl^- (53.3 and 929 millimole per L, respectively).

On the basis of these biogeochemical observations, the hydrologically isolated pond A3N exhibits all the characteristics of being hypersaline with high algal production and degradation (high DOC), and which is driven by intense nitrogen cycling (low nitrogen [NO_2^-+NO_3^-] coupled with an isotopic signature associated with nitrification). The high salinity and DOC likely resulted in the observed comparatively low partitioning of THg and MeHg onto particulates (respectively reflected as low Kd[THg] and Kd[MeHg] values), because both may facilitate a shift of mercury species from the particulate phase into the dissolved phase. Pond A3N was chosen as a reference pond because it represents the hydrologically isolated end-member within the wider Alviso pond sampling region and the pre-breach condition that existed prior to tidal flushing being reintroduced. Second, among the sampling sites, MALSL was particularly enriched in nitrogen (NO_2^- +NO_3^-), whereas GUASL was particularly enriched in PO_4^{3-}, and the nitrogen to (ortho)phosphate molar ratio was over sevenfold between these two sampling regions (37.3 for MALSL and 5.0 for GUASL), indicating very different nutrient regimes between Mallard Slough and Guadalupe Slough compared to the upper and lower Alviso Slough sampling regions. Ponds tended to have higher concentrations of Chl.a, higher levels of DO, high pH, and lower nitrogen (NO_2^- +NO_3^-) concentrations and nitrogen to (ortho)phosphate molar ratios, compared to sloughs, indicating that ponds were generally more conducive to primary production compared to sloughs.

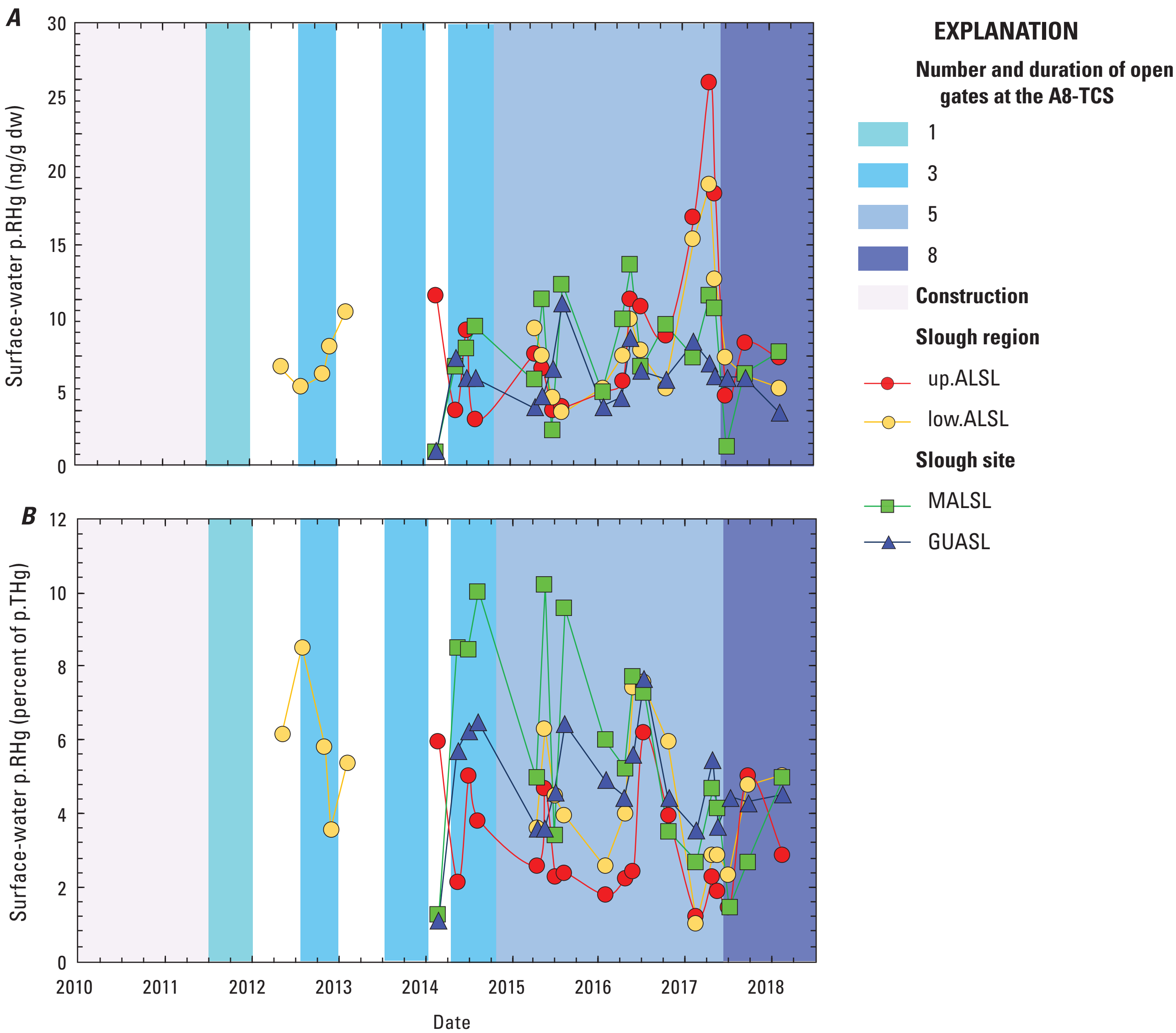

Figure 33. Time-series graphs showing particulate inorganic reactive mercury (p.RHg) on a gravimetric basis (*A*) and as a percentage of particulate total mercury (p.THg) (*B*) in surface water, by slough region or site, for years 2010–18. Alviso Slough sampling sites ALSL-1 and ALSL-4 were included in the calculation of the mean values for the upper Alviso Slough (up.ALSL) and lower Alviso Slough (low.ALSL) sampling regions, respectively, during the 2010–11 study period. After this period these two sites were dropped and up.ALSL and low.ALSL only reflect data collected from sites ALSL-2 and ALSL-3, respectively. Gravimetric concentrations in panel (*A*) given in nanograms per gram dry weight (ng/g dw). See figure 22 for additional information on graphic attributes.

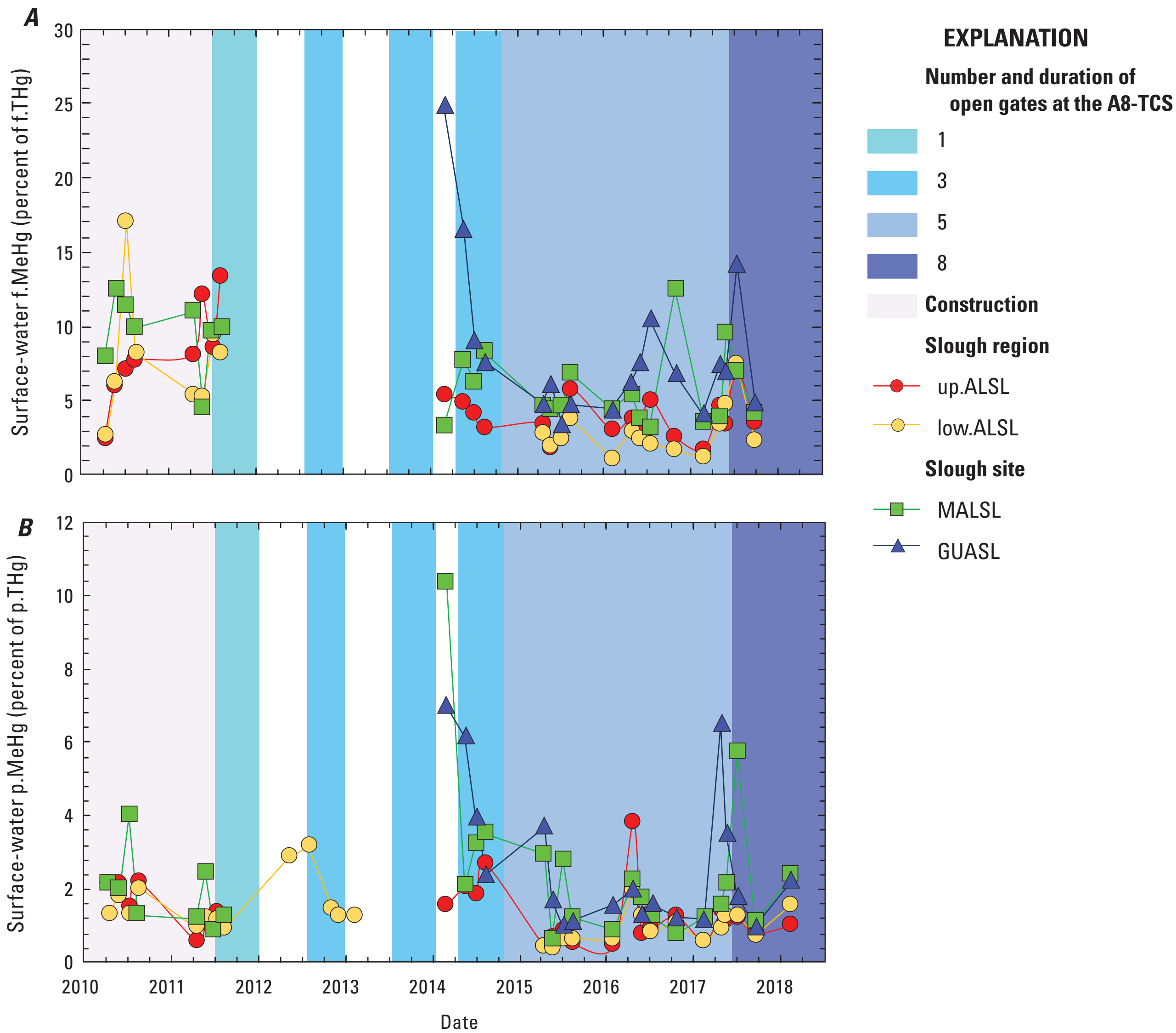

Figure 34. Time-series graphs showing percent filter-passing methylmercury (f.MeHg) as a percentage of filter-passing total mercury (f.THg) (*A*) and percent particulate methylmercury (p.MeHg) as a percentage of particulate total mercury (p.THg) (*B*) in surface water, by slough region or site, for years 2010–18. Alviso Slough sampling sites ALSL-1 and ALSL-4 were included in the calculation of the mean values for the upper Alviso Slough (up.ALSL) and lower Alviso Slough (low.ALSL) sampling regions, respectively, during the 2010–11 study period. After this period these two sites were dropped and up.ALSL and low.ALSL only reflect data collected from sites ALSL-2 and ALSL-3, respectively. See figure 22 for additional information on graphic attributes.

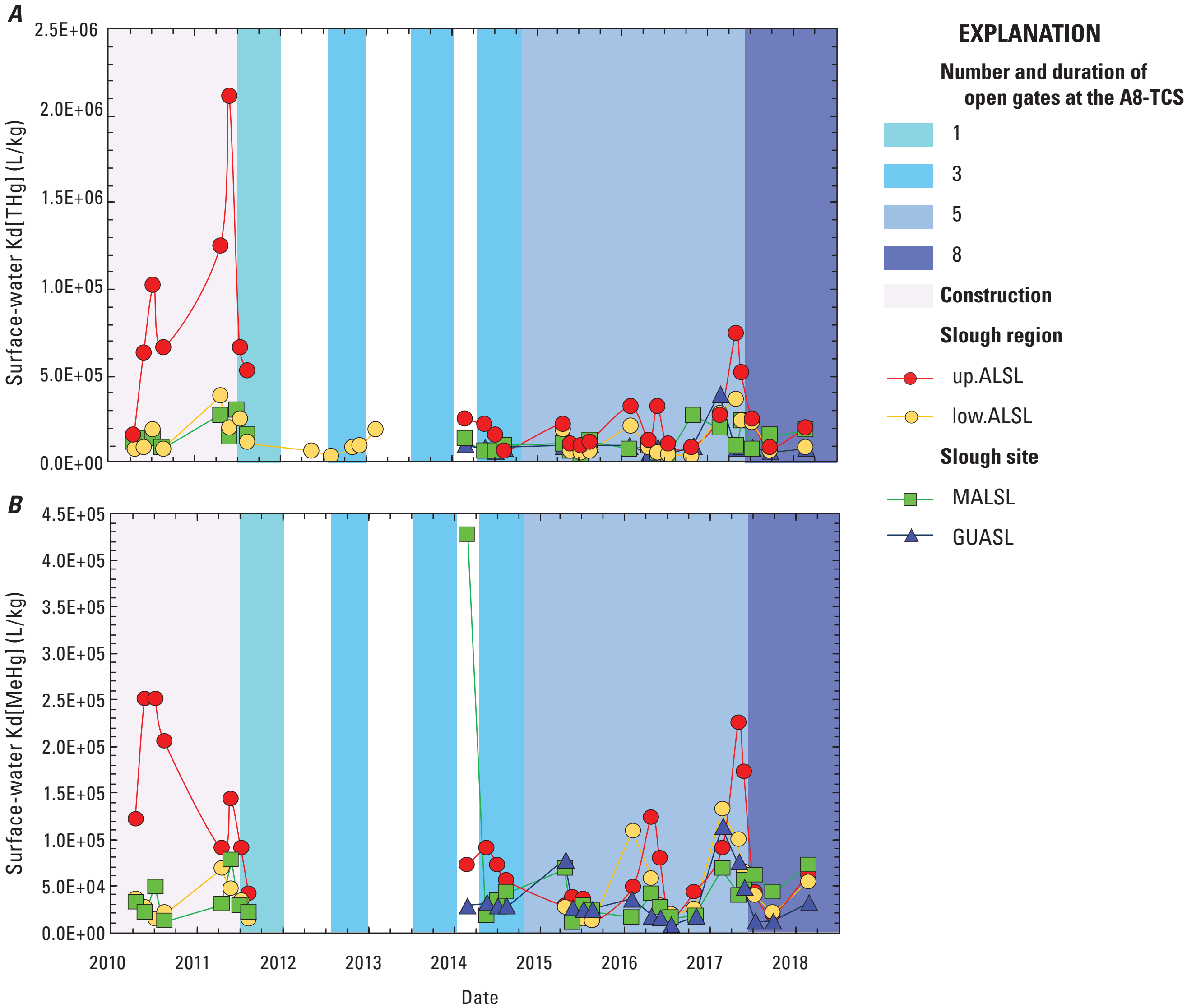

Figure 35. Time-series graphs showing distribution coefficients (Kd) for total mercury (Kd[THg]) (*A*) and methylmercury (Kd[MeHg]) (*B*), in surface water, by slough region or site, for years 2010–18. Alviso Slough sampling sites ALSL-1 and ALSL-4 were included in the calculation of the mean values for the upper Alviso Slough (up.ALSL) and lower Alviso Slough (low.ALSL) sampling regions, respectively, during the 2010–11 study period. After this period these two sites were dropped and up.ALSL and low.ALSL only reflect data collected from sites ALSL-2 and ALSL-3, respectively. Distribution coefficient units in liters per kilogram (L/kg). See figure 22 for additional information on graphic attributes.

Diel (25 Hour) Sampling Events

The 2010–18 time-series data (figs. 22–35) represent a robust examination of mercury speciation trends at the monthly, seasonal, and interannual temporal scales. However, for the purposes of most accurately modeling mercury species flux, and to better understand the role of hydrodynamics on slough mercury concentrations overall, a higher temporal resolution sampling strategy is needed. We conducted five such high-resolution sampling events at the ALSL-3 site, collocated with the fixed-station high-resolution monitoring site that was collecting 15-minute data on basic water quality parameters (see "Continuous Water Quality Monitoring Stations" section). The five sampling events represented each of the four seasons, between May 2012 and February 2013, plus one event that represented the first seasonal high-flow event ('first-flush' event, December 2012). The resulting 24-hour time-series plots are provided for the following mercury species: volumetric p.THg (fig. 36), gravimetric p.THg (fig. 37), volumetric p.MeHg (fig. 38), gravimetric p.MeHg (fig. 39). Additional mercury and nonmercury parameters also measured as part of these diel studies include: f.THg, percent p.MeHg, p.RHg, Kd(THg), POC, PN, POC:PN molar ratio, δ13C-POC, δ15N-PN, temperature, redox potential (E_h), pH, DO, spC, Chl.a, and TSS. These additional data are available in Marvin-DiPasquale and others (2019).

Several important trends are evident from these diel time-series plots. First, peak concentrations of all four mercury species depicted (figs. 36–39) generally occur during low tide. However, of the two low tides in a 24-hour cycle, the highest peak tends to occur during the lower of the two. Further, upon close inspection, the very highest peak concentrations of volumetric p.THg (fig. 36) and p.MeHg (fig. 38) tend to occur towards the end of the ebb tide cycle, but just prior to actual low tide. The same is generally not true for gravimetric p.THg (fig. 37) and p.MeHg (fig. 39), for which the peak concentration does seem to more generally coincide with the hour(s) of low tide (not prior to it). These observations indicating a few important things with respect to how mercury speciation varies within Alviso Slough surface water as a function of tides. First, the range of values observed within a given tidal cycle can be quite large (for example, more than tenfold for volumetric p.MeHg during May 2012, fig. 38). This is why for the monthly to seasonal sampling events that were done at a much lower temporal resolution, the collection of slough surface water was always targeted to be just after high tide (daylight hours) for both logistical considerations and to help minimize the effects of variability within a given tidal cycle. Second, the observed increases in volumetric p.THg (fig. 36) and p.MeHg (fig. 38) during low tide may be partially explained by the physical concentration of particulates that occurs as the water column depth shallows under low tide conditions, compared to the high tide condition when particulate concentrations may be physically diluted. However, the gravimetric p.THg (fig. 37) and p.MeHg (fig. 39) concentrations also show peak concentrations during low tide, which implies that the observed trend in volumetric concentrations is also driven in part by real changes in particulate mercury concentration on a dry weight basis (ng/g dw). Because the proportion of landward derived water, compared to bay water, is maximal at low tide, the trend in intratidal variations in gravimetric mercury concentrations in Alviso Slough is thought to reflect the inherent gradient in gravimetric p.THg and p.MeHg concentrations, which generally increase moving landward (towards the terrestrial point source) and decrease moving bayward. Finally, during the period of highest flow (first flush during December 2012), we observed very little intratidal variation in volumetric p.THg and p.MeHg species when compared to the other four time periods with much lower flow regimes. This minimal variation in particulate mercury species concentration (volumetrically) likely reflects the magnitude of outflowing water overwhelming the more typical bidirectional tidal hydrology observed during lower flow and base flow conditions.

Surface-Water Model Results

Although simple summary statistics (for example, appendix 5) provides an overall sense of mercury and nonmercury surface-water parameters spatial variation among the seven sampling locations, it does not lend itself readily to examining changes over time and within each sampling location. A more sophisticated and targeted approach is needed to examine temporal changes, particularly since both management events (the breaching of pond A6 and the incremental opening of the A8-TCS) and natural events (for example, extremes in seasonal and interannual hydrology) of interest occurred during the 2010–18 period. However, with over 30 directly measured and calculated surface-water parameters (Marvin-DiPasquale and others, 2019), a comprehensive interrogation of the complete surface-water dataset is beyond the scope of this report. Instead, the statistical approach taken here is selective with respect to (1) the individual questions this report is designed to address ("Mercury Synthesis—Organizing Questions" section), (2) the subset of the surface-water parameters examined linked to those specific questions, and (3) the spatial and temporal grouping of the data. Thus, the key results of the specific surface-water models (SW.1–SW.4) developed to address targeted questions are summarized below, with numerical results presented in appendixes 6–9. Although the emphasis for this synthesis is primarily on the mercury results, the statistical analyses were conducted for all nonmercury surface-water parameters and are reported in the abovementioned appendixes.

Results of Model SW.1

The LSM surface-water Model SW.1 (equation 6) was developed to address Q.1 of the "Mercury Synthesis—Organizing Questions" section, which asks, in part, if there were any demonstrable effects of the pond A6 breach on

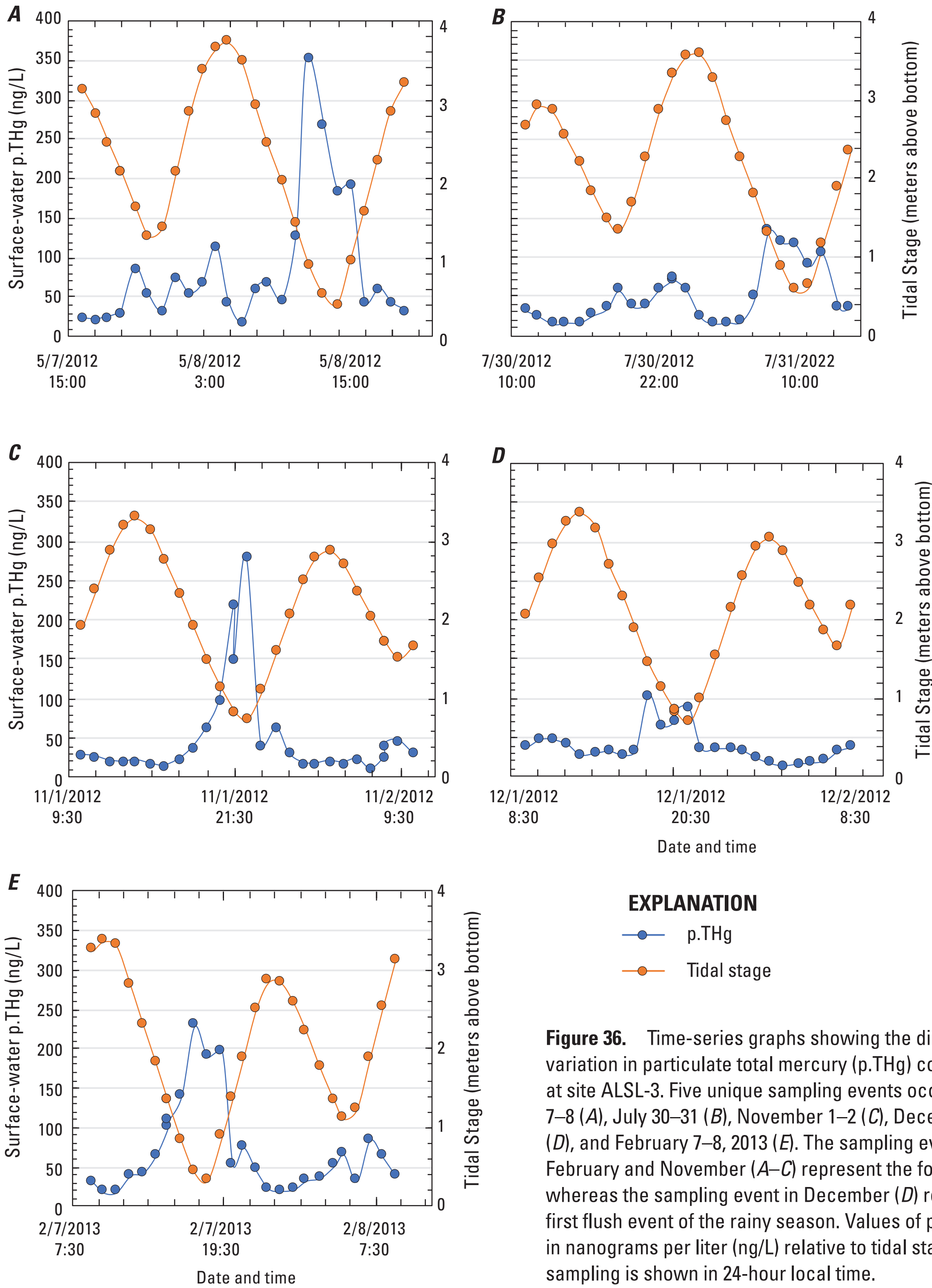

Figure 36. Time-series graphs showing the diel (25 hour) variation in particulate total mercury (p.THg) concentration at site ALSL-3. Five unique sampling events occurred on May 7–8 (*A*), July 30–31 (*B*), November 1–2 (*C*), December 1–2, 2012 (*D*), and February 7–8, 2013 (*E*). The sampling events between February and November (*A*–*C*) represent the four seasons, whereas the sampling event in December (*D*) represents the first flush event of the rainy season. Values of p.THg are given in nanograms per liter (ng/L) relative to tidal stage. Time of sampling is shown in 24-hour local time.

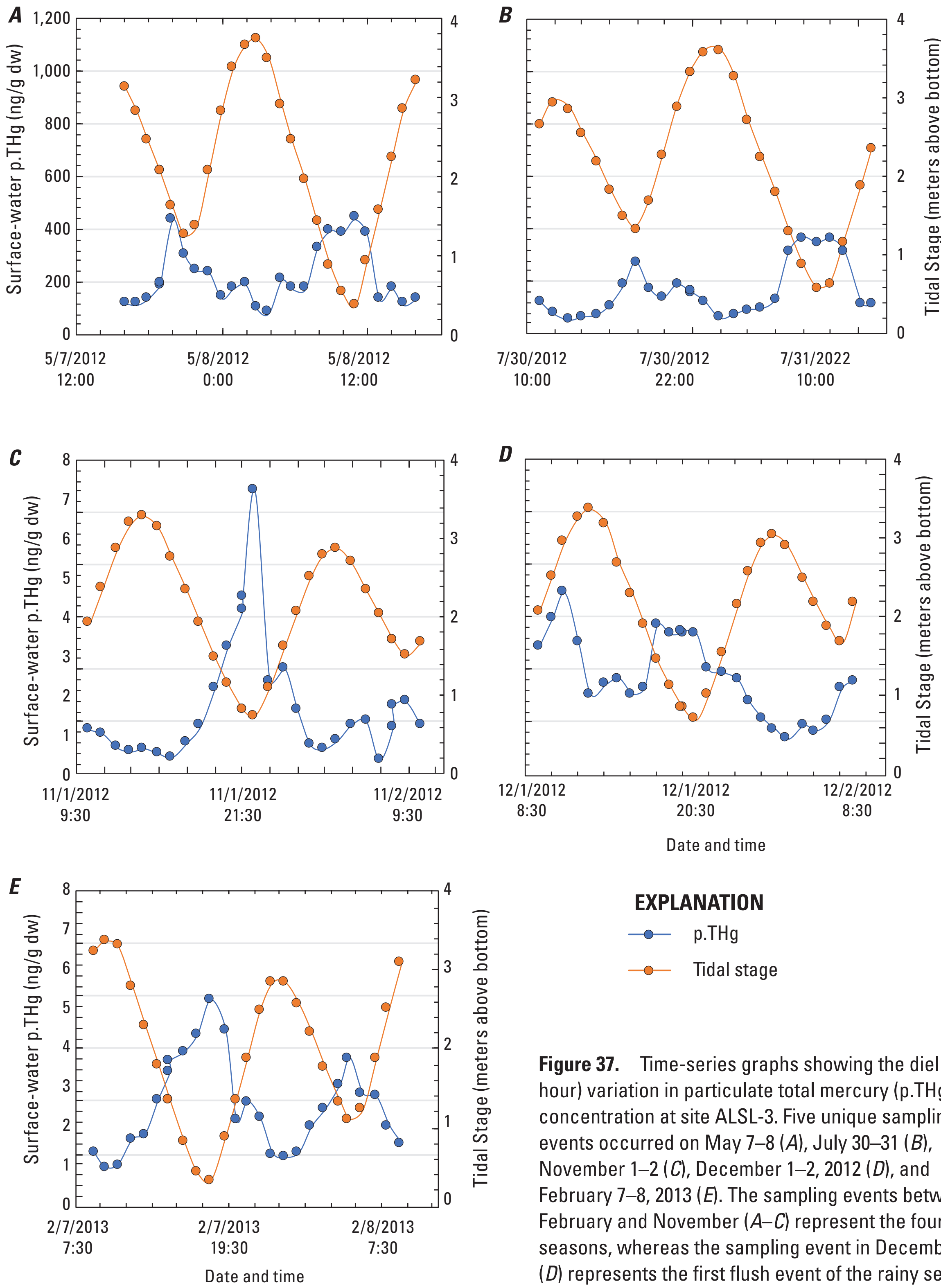

Figure 37. Time-series graphs showing the diel (25 hour) variation in particulate total mercury (p.THg) concentration at site ALSL-3. Five unique sampling events occurred on May 7–8 (*A*), July 30–31 (*B*), November 1–2 (*C*), December 1–2, 2012 (*D*), and February 7–8, 2013 (*E*). The sampling events between February and November (*A*–*C*) represent the four seasons, whereas the sampling event in December (*D*) represents the first flush event of the rainy season. Values of p.THg are given in nanograms per gram dry weight (ng/g dw) relative to tidal stage. Time of sampling is shown in 24-hour local time.

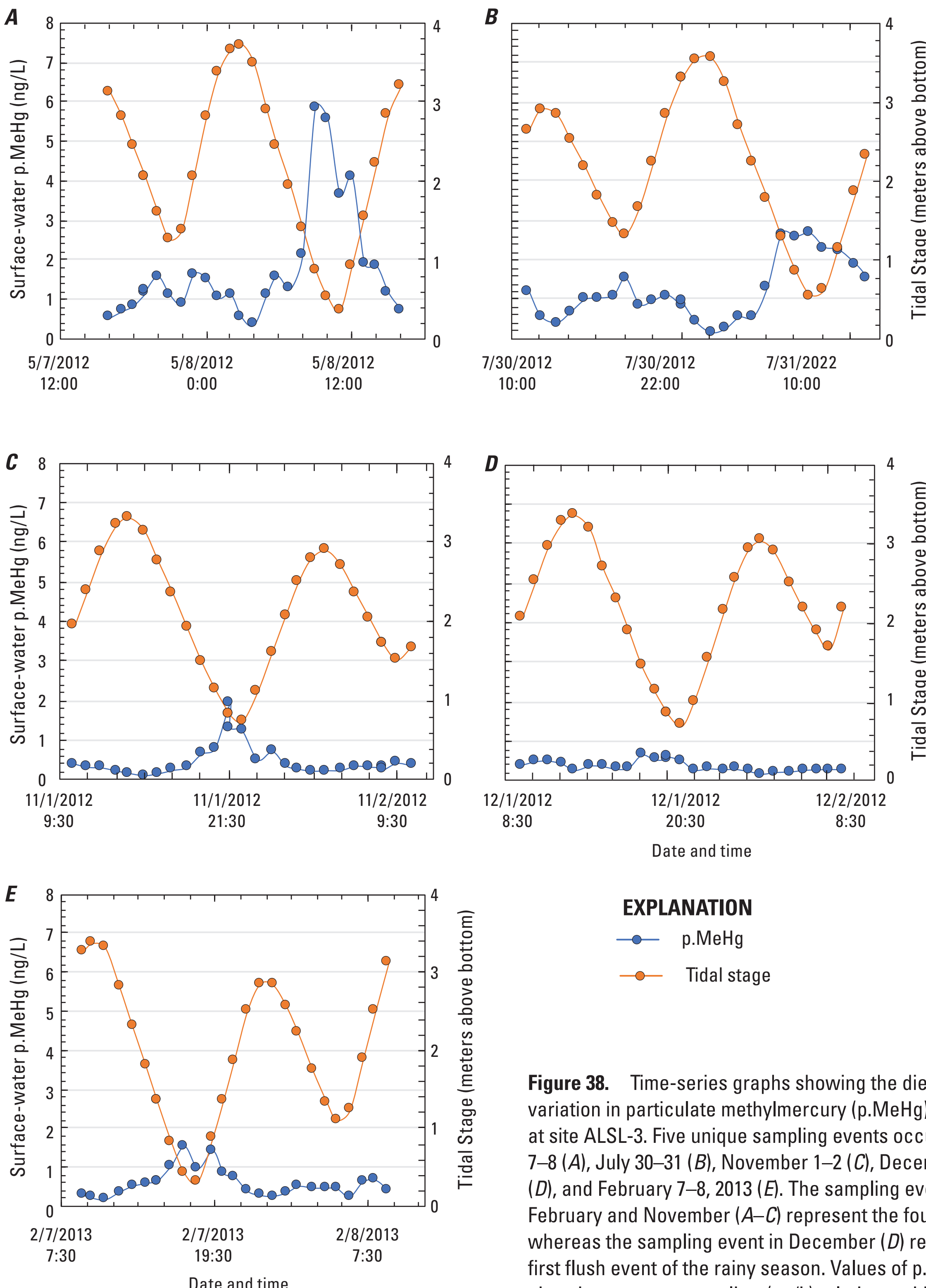

Figure 38. Time-series graphs showing the diel (25 hour) variation in particulate methylmercury (p.MeHg) concentration at site ALSL-3. Five unique sampling events occurred on May 7–8 (*A*), July 30–31 (*B*), November 1–2 (*C*), December 1–2, 2012 (*D*), and February 7–8, 2013 (*E*). The sampling events between February and November (*A*–*C*) represent the four seasons, whereas the sampling event in December (*D*) represents the first flush event of the rainy season. Values of p.MeHg are given in nanograms per liter (ng/L) relative to tidal stage. Time of sampling is shown in 24-hour local time.

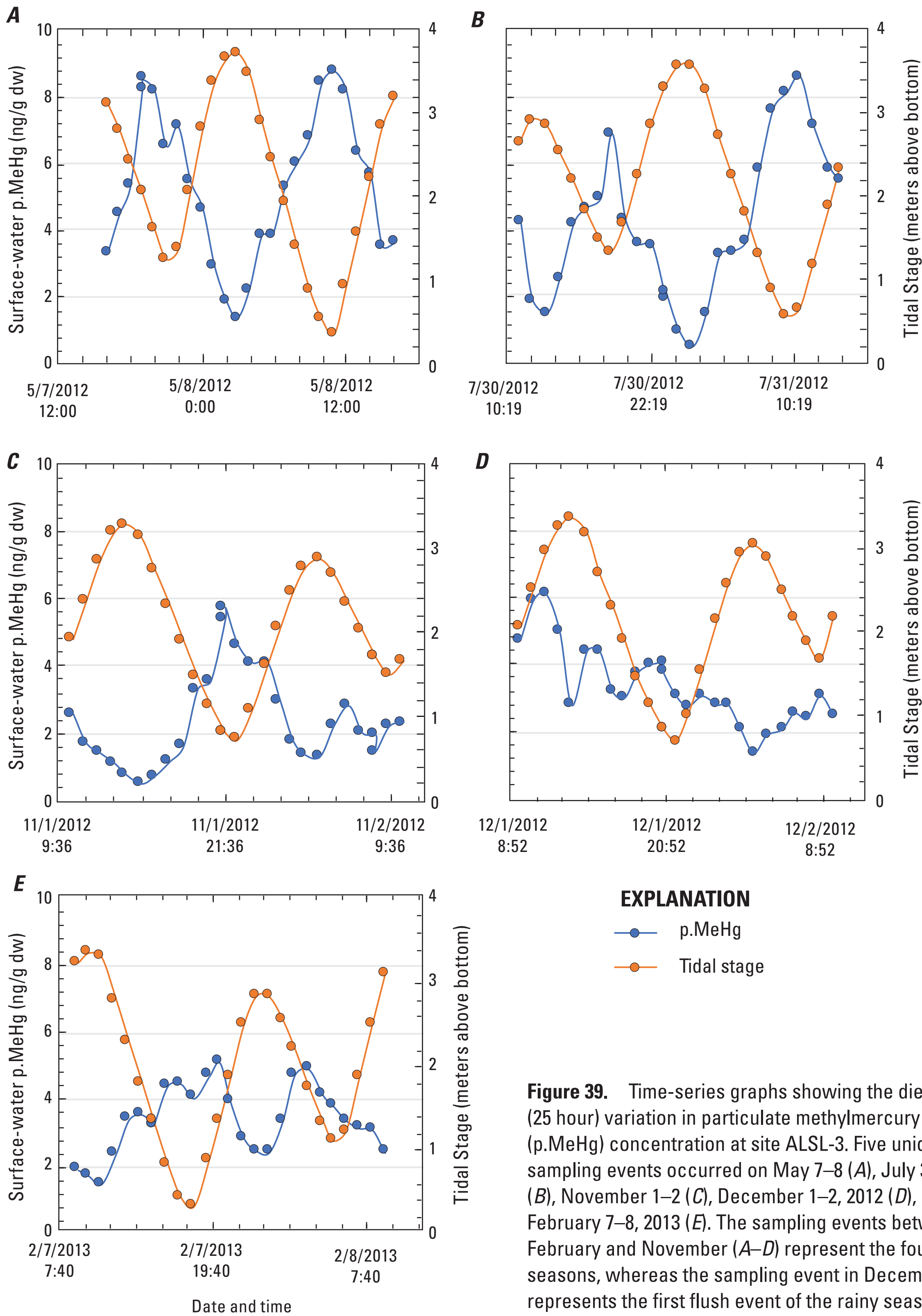

Figure 39. Time-series graphs showing the diel (25 hour) variation in particulate methylmercury (p.MeHg) concentration at site ALSL-3. Five unique sampling events occurred on May 7–8 (*A*), July 30–31 (*B*), November 1–2 (*C*), December 1–2, 2012 (*D*), and February 7–8, 2013 (*E*). The sampling events between February and November (*A–D*) represent the four seasons, whereas the sampling event in December represents the first flush event of the rainy season. Values of p.MeHg are given in nanograms per gram dry weight (ng/g dw) relative to tidal stage. Time of sampling is shown in 24-hour local time.

surface-water mercury parameters. This model has two main terms, YEAR (with factors: 2010, 2011) and REGION (with factors: low.ALSL and MALSL), and an interaction term [YEAR x REGION]. The focus here is on the lower Alviso Slough (model factor used is low.ALSL), which consists of data from sites ALSL-3 and ALSL-4 combined, compared to the Mallard Slough reference site (site MALSL), during the 2010–11 period immediately before and after the breaching of pond A6 (December 2010). The SW.1 model results for all mercury and nonmercury surface-water parameters are summarized in appendix 6 and are presented qualitatively in terms of the ranking of factors associated with statistically significant model terms only.

Mercury parameters with between-year differences, but no regional differences or significant interactions, included p.THg (ng/g dw), which was higher in 2011 compared to 2010; percent p.MeHg, which was higher in 2010 compared to 2011; and Kd(THg), which was higher in 2011 than in 2010. Higher Kd values indicate a strong association with the particulate fraction compared to lower Kd values. Percent uf.MeHg (percent of uf.THg) was both higher in 2010 compared to 2011 and higher in the Mallard Slough compared to the lower Alviso Slough, although the interaction between year and region was not significant. Mercury parameters that showed no significant difference either between regions or between years included f.THg, f.MeHg, f.MeHg (percent of f.THg), p.MeHg (ng/g dw), uf.MeHg (ng/L), and Kd(MeHg). Mercury parameters did not show a difference between regions exclusively, without a corresponding significant difference between years or a significant interaction effect.

Mercury parameters with significant interaction terms include (1) volumetric p.THg and uf.THg, which were both higher in the lower Alviso Slough during 2011 compared to 2010 and to the Mallard Slough (both years); and (2) volumetric p.MeHg, which was higher in the lower Alviso Slough compared to the Mallard Slough during 2011. These parameters likely reflect the substantial amount of sediment scour near and around the A6 breach locations that occurred after the December 2010 management action, as discussed in more detail below (see “Deep Cores and the Modeling of Bed Sediment and Total Mercury Mobilization in Alviso Slough” section).

Results of Model SW.2

Surface-water model SW.2 was developed to address Q.2 of the “Mercury Synthesis—Organizing Questions” section, which asks, in part, if there were any demonstrable effects of the initial and subsequent gradual opening of the A8-TCS, reconnecting the A8-complex to muted tidal flushing, on surface-water mercury parameters within the A8-complex itself. This model has only one explanatory term, GATE (with factors: PRE, 1, 3, 5, and 8 gates open). The model SW.2 results, for all mercury and nonmercury surface-water parameters (dependent variables), are summarized in appendix 7 and are presented both quantitatively (as model derived mean values) and qualitatively (in terms of the Tukey’s ranking associated with the reported means).

Almost every mercury parameter showed some statistically significant ($p < 0.05$) difference as a function of the number of gates open, with the exception of f.THg and gravimetric p.RHg (appendix 7). Surface-water mercury parameters, within the A8-complex, that showed a clear statistically significant decrease as the number of A8-TCS gates opened increased include volumetric f.MeHg, f.MeHg (percent of f.THg), volumetric and gravimetric p.MeHg, percent p.MeHg (percent of p.THg), uf.MeHg and percent uf.MeHg (percent of uf.THg), and volumetric and percent p.RHg (percent of p.THg). Parameters that showed a clear statistically significant increase as the number of A8-TCS gates opened increased include Kd(THg) and Kd(MeHg), both of which indicated that as tidal flushing increased, the proportion of both THg and MeHg that was associated with the particulate fraction (as opposed to the filter-passing fraction) increased within the A8-complex. Noteworthy trends in nonmercury parameters that decreased within the A8-complex, as the number of open gates increased, include salinity (as SpC), DOC, and TSS. Nonmercury parameters that increased within the A8-complex, as the number of open gates increased, include Chl.a, DO, and E_h. Most of these trends occurred rapidly after the opening of only one gate, which indicates that the return of tidal flushing to former hydrologically isolated ponds results in a rapid change in surface-water chemistry.

Results of Models SW.3 and SW.4

Surface-water Models SW.3 and SW.4 were developed to address Q.3 of the “Mercury Synthesis—Organizing Questions” section, which asks in part, if there were any demonstrable effects owing to the gradual opening of the A8-TCS on surface-water mercury parameters within Alviso Slough. Model SW.3 includes two main terms: GATE (number of A8-TCS gates open; with factors: 0, 1, 3, 5 or 8) and REGION (with factors: up.ALSL, low.ALSL), in addition to an interaction term (GATE x REGION). The SW.3 model results, for all significant (only) mercury and nonmercury surface-water parameters (dependent variables), are summarized in appendix 8 and are presented both quantitatively (as model derived LSM values) and qualitatively (in terms of the Tukey’s ranking associated with the reported LSM values). Model SW.4 was developed to address situations when the interaction term of Model SW.3 was statistically significant. Model SW.4 included only one explanatory term (GATE, as described above) but was applied independently to data from either up.ALSL or low.ALSL (the two factors for model term REGION under Model SW.3). Results from Model SW.4 are summarized in appendix 9 and are presented both quantitatively (as model derived mean values) and qualitatively (in terms of the Tukey’s ranking associated with the reported means).

The results of Model SW.3 (appendix 8) show that, of the four mercury parameters for which the model term GATE was statistically significant (gravimetric and percent p.MeHg, percent RHg, and Kd[THg]), only Kd(THg) showed a clear and decreasing trend as the number of open gates increased. This trend in Kd(THg) indicates a physical shift from particulate-associated THg to filter-passing THg with more gates open. This trend is opposite of what was seen in terms of Kd(THg) within the A8-complex, where Kd(THg) values increased as more gates opened (see the “Results of Model SW.2” section). Because DOC is a strong ligand that can compete with particulate associated THg, this contrast in Kd(THg) trends may be driven by a lowering of DOC inside of the A8-complex (from the entrainment of low-DOC slough water) and a corresponding increase in DOC in Alviso slough (exported from the A8-complex), each affecting particulate-to-dissolved partitioning of THg in the respective and interconnected regions. Evidence in support of this DOC hypothesis is both a clear decrease in DOC within the A8-complex (appendix 7) and a general increase in DOC in the upper Alviso Slough (appendix 9) as the number of A8-TCS opened gates increased.

Spatially, Model SW.3 indicates that Kd(THg), gravimetric p.MeHg, and POC were all statistically higher in upper Alviso Slough compared to lower Alviso Slough, whereas percent p.RHg was statistically higher in lower Alviso Slough compared to upper Alviso Slough (appendix 8). Surface-water parameters for which a Model SW.3 [GATE x REGION] interaction effect existed indicate a gate effect was only observed in one of the two sampling regions within Alviso Slough (appendix 9). For upper Alviso Slough, the clearest trends associated with gate management were seen for percent f.MeHg and the POC/PN ratio, both of which decreased as the number of opened gates increased. For lower Alviso Slough, volumetric and percent f.MeHg, as well as percent uf.MeHg, all decreased as the number of opened gates increased, which may reflect a simple dilution effect in lower Alviso Slough associated with an increased tidal prism.

Fixed Monitoring Station Time Series Results for Water Quality, Discharge, and Suspended-Sediment Flux

Although the primary focus of this synthesis report is on mercury in the study area, to better understand and model mercury species transport in Alviso Slough as a function of management actions (Q.1 and Q.3), and into or out of the A8-complex (Q.4), an examination of basic slough hydrology, suspended-sediment flux, and associated water quality is warranted. In this section, results are presented from three fixed monitoring stations: USGS streamgage station 11169025, which is located upstream of tidal influence in the Guadalupe River; study site ALSL-3 at USGS station 11169750, which is located in the tidally affected reach of middle Alviso Slough; and USGS station 372525121584701, which is located adjacent to the A8-TCS and on the Alviso Slough side of the tidal control structure (fig. 4).

At USGS streamgage station 11169025 in the Guadalupe River, water discharge and cumulative water volume flux during 2012–18 demonstrate that most discharge occurs during winter months, which is in response to precipitation events in the watershed (fig. 40). Steps in the cumulative water volume flux curve (fig. 40) indicate the relative amount of precipitation falling in the watershed; the largest step observed during this study occurred during January 2017 storm events.

Salinity in tidally affected Alviso Slough is generally lower during ebb tides and higher during flood tides in response to tidal action moving watershed discharge downstream and estuary waters upstream, respectively. The

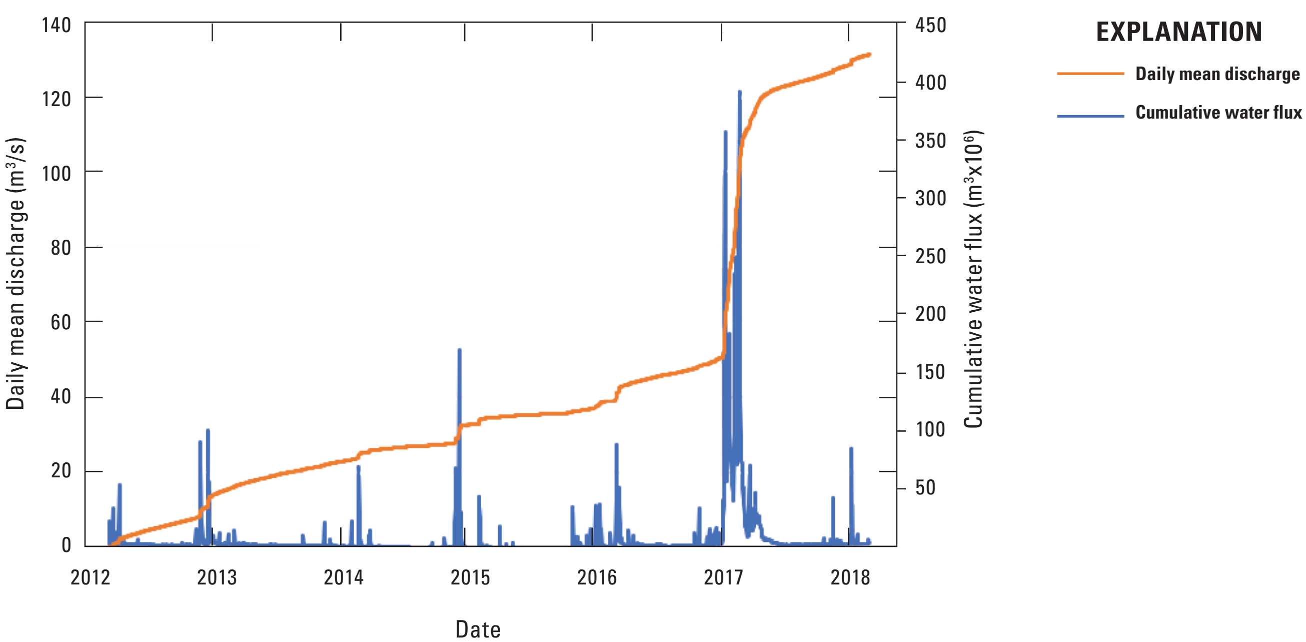

Figure 40. Time series graph showing the daily mean discharge and cumulative water volume flux for U.S. Geological Survey streamgage station 11169025 in the Guadalupe River. Daily mean discharge, in cubic meters per second (m^3/s), is shown on left y-axis and cumulative water flux, in million cubic meters ($m^3 \times 10^6$) is shown on the right axis. This site experiences unidirectional flow and is upstream of tidal influence. The time period depicted is March 13, 2012–February 27, 2018, and year labels are centered over January 1 of each respective year.

system quickly responds to storm events; when precipitation falls in the watershed, Guadalupe River discharge increases and lowers salinity in Alviso Slough. Salinity at the ALSL-3 fixed-monitoring site (USGS station 11169750) was generally lower across the range of values when A8-TCS gates were closed (fig. 41*A*), and values of almost zero indicate that Guadalupe River discharge dominated the water source composition (the relative mix of watershed and bay derived water) during most ebb tides when A8-TCS gates were closed. After A8-TCS gate openings, the minimum values of salinity increased at the ALSL-3 sensor despite continued Guadalupe River discharge, indicating mixing of watershed discharge with pond effluent upstream of the sensor. The highest values of salinity observed were during summer 2015 (maximum: 31.8 psu on September 12, 2015), at the height of the 2012–16 drought and during the period of lowest discharge from Guadalupe River (fig. 40); the variability of salinity during this time was the smallest in the record (range: 29.1–31.8 psu) outside of periods of prolonged watershed discharge (for example, January and February 2017).

Water temperature at site ALSL-3 varied seasonally and ranged from minimum values near 10 °C during the winter to maximum values near 26 °C during the summer (fig. 41*B*). Dissolved oxygen concentration at site ALSL-3 showed annual periodicity, and the highest DO values were during the winter and lowest values were during the summer (fig. 41*C*). When the A8-TCS gates were open in winter periods with little watershed discharge (for example, January 2015 and January 2016, fig. 41*C*), DO concentrations were very high, almost 20 mg/L (> 200% DO saturation).

Suspended-sediment concentration at site ALSL-3 showed slight annual periodicity, and in general, the highest concentrations of SSC occurred in the summer (fig. 41*D*). Storm events caused brief episodes of high SSC associated with sediment-laden watershed discharge, as indicated by periods of high SSC with low salinity (figs. 41*A*, *D*). After the opening of five or more A8-TCS gates, average SSC at site ALSL-3 decreased by 25 percent (average SSC for the period with three open gates or less during October 14, 2010–September 28, 2014, was 162 mg/L, n = 107,921; average SSC

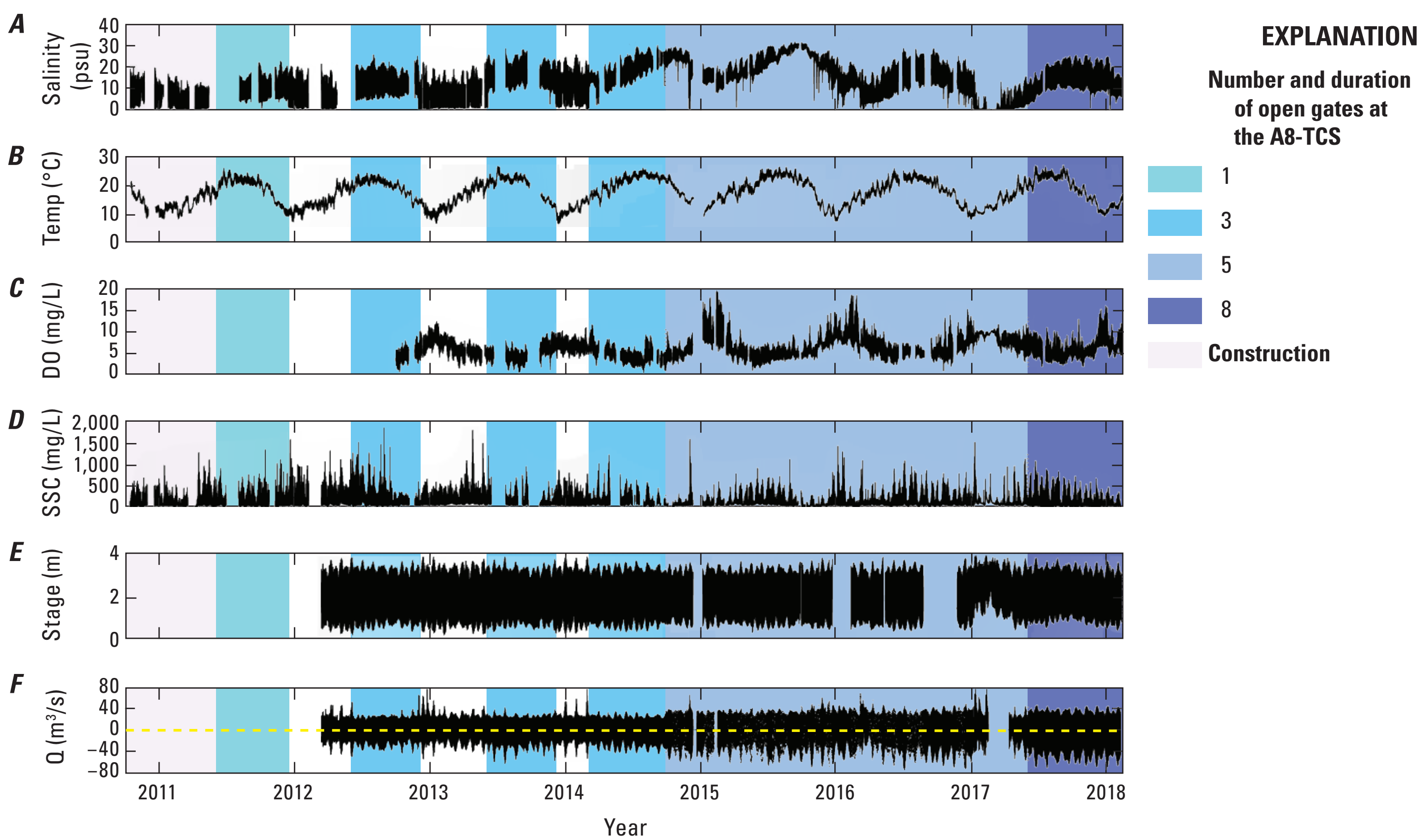

Figure 41. Time series graphs of 15-minute instantaneous data for U.S. Geological Survey station 11169750 (study site ALSL-3) surface water showing salinity (*A*), temperature (Temp) (*B*), dissolved oxygen (DO) (*C*), suspended-sediment concentration (SSC) (*D*), water depth (tidal stage) (*E*), and discharge (Q) (*F*) for the duration of October 14, 2010–February 27, 2018. Site ALSL-3 experiences bidirectional flow in the tidally influenced reach of middle Alviso Slough. Positive Q values indicate flow from the watershed to the estuary. Each tick mark on the x-axis is centered on the first day of each year (for example, the 2011 tick mark indicates January 1, 2011). Nonshaded background represents duration when all gates are closed. Missing data are due to instrument failure or biological fouling of signal. The yellow horizontal dashed line in panel *F* aligns with the zero value for Q. Units of Salinity are given in practical salinity units (psu), temperature in degrees Celsius (°C), DO in milligrams per liter (mg/L), tidal stage in meters (m), and Q in cubic meters per second (m^3/s).

for the period with five or more open gates during September 29, 2014–February 27, 2018, was 122 mg/L, n = 111,633).

Tidal stage (depth of water) and discharge at ALSL-3 varied tidally and seasonally. During flood tides, stage rises and Q is negative indicating landward-directed flow; during ebb tides, stage falls and discharge is positive indicating bayward-directed flow (figs. 41*E*, *F*). In response to watershed discharge in the winter, stage increases and is elevated during all tidal phases (for example, see February 2017, fig. 41*E*), whereas discharge increases to more positive values during all tidal phases (for example, see March 2016, fig. 41*F*). Discharge also varied in response to A8-TCS gate operations; when the A8-TCS was in the 5-gate condition, the range of discharge at site ALSL-3 increased, likely caused by more water entering the Alviso Slough from pond A8.

Cumulative water volume flux at ALSL-3 was always bayward, whereas cumulative suspended-sediment flux was generally landward with three notable exceptions identified as time periods B, E–F, and H on table 6 and figure 42. Because these periods of bayward flux may represent either sediment (and associated mercury) flux from the upper watershed or sediment (and associated mercury) erosion events within Alviso Slough, it is instructive to look more closely at these three periods and to compare the fluxes measured at site ALSL-3 with those measured for the same time frames at USGS streamgage station 11169025 (Guadalupe River monitoring site).

Period B represents the three-month period during the winter of 2012–13 immediately after all A8-TCS gates were closed. The bayward mean (± standard error) daily water flux (334,300±19,100 m^3/d) at ALSL-3 (table 6) exceeded that measured upstream at USGS streamgage station 11169025 in the Guadalupe River (242,900±41,400 m^3/d) during the same time period. However, suspended-sediment flux (40.5±4.5 metric tons per day [t/d]) at ALSL-3 (table 6) was comparable to that measured at Guadalupe River (30.5±14.8 t/d) given the associated errors. The fact that suspended-sediment flux was similar between these two locations indicates that suspended sediment was transported more or less conservatively between the Guadalupe River USGS streamgage station (11169025) and ALSL-3 for the 3-month period following the winter closing of all A8-TCS gates, before sediment flux returned to a landward trajectory (period C of fig. 42 and table 6) at a rate comparable in magnitude (−48.2±5.0 t/d) to the previous bayward flux. This overall landward trend continued throughout period D, albeit at a lower rate (−12.9±2.3 t/d), through the winter of 2013–14 and several managed 3-gate and 0-gate conditions.

The next landward-to-bayward reversal in the movement of suspended sediment past the ALSL-3 site occurred immediately after the 3-gate to 5-gate transition on September 29, 2014. Sediment bayward flux continued for an extended period, through mid-May 2016 (approximately 600 days [1.6 year]) and occurred in two phases. Period E was a prolonged record (521 days [1.4 year]) of steady bayward flux through the beginning of March 2016. This was followed by period F, which was a brief (78 day) period of enhanced water and sediment bayward flux, that occurred before sediment flux finally returned to a landward trajectory (period G of fig. 42 and table 6).

Period E is best characterized as one of low flow, during which daily mean water fluxes at ALSL-3 (181,700±13,800 m^3/d) again exceeded those measured at Guadalupe River (73,800±13,000 m^3/d) and suspended-sediment flux at ALSL-3 (9.0±2.5 t/d) was again comparable to that of Guadalupe River (14.2±4.4 t/d; excludes 6-month window [May 1, 2015–November 1,2015] of no reported SSC data), given the error estimates. This prolonged 1.4-year period of bayward suspended-sediment transport measured at site ALSL-3 is atypical and likely points to a period of sediment erosion within Alviso Slough that is upstream of the ALSL-3 monitoring site. During the period between April and October 2015 there was significant sediment deposition in lower Alviso Slough, below the ALSL-3 monitoring site, which indicates that some of this suspended-sediment flux past site ALSL-3 was deposited there (see the "Deep cores and the Modeling of Bed Sediment and Total Mercury Mobilization in Alviso Slough" section).

Period F is a short duration of time between early March and mid-May 2016, during which daily mean water flux (597,400±28,800 m^3/d) was more than threefold greater than for period E (table 6) and 2.7 times greater than Guadalupe River (216,100±43,300 m^3/d). Likewise, bayward suspended-sediment flux at ALSL-3 (60.8±5.2 t/d) was threefold higher than at Guadalupe River (19.7±8.6 t/d) for the same period. These trends indicate a comparatively brief period of enhanced sediment erosion within Alviso Slough following a much longer period of slower erosion (period E) that began immediately upon the 3-gate to 5-gate management action. Together, periods E and F resulted in an estimate 9,413±1,373 metric tons of suspended sediment moving in the bayward direction past ALSL-3, and approximately 50 percent of this mass was contributed by each time period. We suggest that periods E and F (fig. 42, table 6) reflect a tipping point in the energetics of Alviso Slough that began once the A8-TCS was opened to five gates and ended approximately 1.6 years later when suspended-sediment transport past site ALSL-3 resumed a landward trajectory under low flow conditions (period G).

The third and final landward-to-bayward reversal suspended-sediment flux was associated with the January–February 2017 extreme high flow event (period H; fig. 42, table 6), which occurred after the A8-TCS had maintained in the 5-gate condition for the previous 2.3 years. Daily mean water flux at ALSL-3 (1,851,300±50,000 m^3/d) was 56 percent the daily mean measured at the Guadalupe River site (3,283,900±314,600 m^3/d) over the same 38-day period, whereas suspended-sediment flux at ALSL-3 (532 t/d) was 45 percent of the daily mean flux at Guadalupe River (1,195±287 t/d). Thus, although a massive amount of sediment was transported past the Guadalupe River monitoring station during this extreme event, approximately half was not

Table 6. Daily mean surface-water and suspended-sediment flux at U.S. Geological Survey station 11169750 (study site ALSL-3), by time period.

[Daily mean water and suspended-sediment flux rates are calculated for each time period labeled as A-J on figure 42. The start and end date, total days, and number of A8-tidal control structure gates open are given for each time period. The directions of flux are given as Bayward (positive slopes) and Landward (negative slopes). The values in parentheses represent the standard error of the mean. Dates are given in month, day, and year format. m³/d x 1000, thousands of cubic meters per day; t/d, metric tons per day]

Time period (figure 42)	Gates open	Start date	End date	Total days	Mean water flux (m³/d x 1000)	Water net direction	Sediment flux (t/d)	Sediment net direction
A	0 and 1	03/14/2012	12/01/2012	262	72.7 (11.4)	Bayward	−18.7 (3.3)	Landward
B	0	12/01/2012	03/01/2013	90	334.0 (19)	Bayward	40.5 (4.5)	Bayward
C	0	03/01/2013	06/06/2013	97	84.5 (18.1)	Bayward	−48.2 (5.0)	Landward
D	0 and 3	06/06/2013	09/29/2014	480	61.7 (10.7)	Bayward	−12.9 (2.3)	Landward
E	5	09/29/2014	03/03/2016	521	182.0 (14)	Bayward	9.0 (2.5)	Bayward
F	5	03/03/2016	05/20/2016	78	597.0 (29)	Bayward	60.8 (5.2)	Bayward
G	5	05/20/2016	01/07/2017	232	20.2 (25.9)	Bayward	−32.0 (6.2)	Landward
H[1]	5	01/07/2017	02/14/2017	38	1,851.0 (50)	Bayward	533.0 (22)	Bayward
I[1]	5	04/11/2017	06/02/2017	52	179.0 (26)	Bayward	−2.1 (7.1)	Landward
J	8	06/02/2017	02/27/2018	270	71.7 (15.6)	Bayward	−11.0 (3.2)	Landward

[1]Data gap between periods H and I is due to equipment failure.

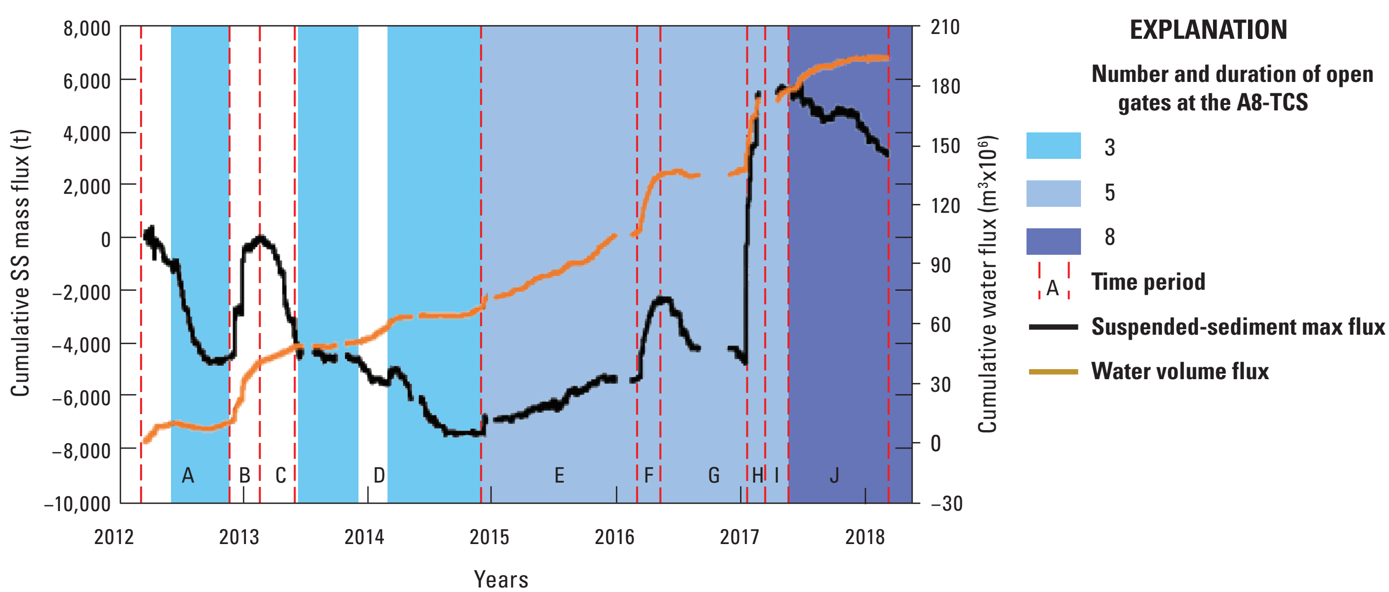

Figure 42. Time series graph showing the cumulative sum of 15-minute instantaneous surface-water suspended-sediment (SS) mass flux at U.S. Geological Survey station 11169750 (study site ALSL-3). Positive values on the y-axes indicate bayward flow from watershed towards the estuary, whereas negative values indicate landward flow from estuary towards the watershed. The time period shown is March 13, 2012–February 27, 2018. Shading indicates when and how many gates at the A8 tidal control structure were open; white shading indicates that all gates were closed. Missing data are due to instrument failure or biological fouling of signal. The letters (A–J) indicate time periods (separated by red dashed vertical lines) that are identified by an obvious change in X–Y slope or number of gates open at the A8 tidal control structure (A8-TCS). The exact date range and the calculated daily mean water and suspended-sediment flux rate for each time period is summarized in table 6. Suspended-sediment mass flux was measured in metric tons (t), and water-volume flux in million cubic meters (m³ x 10⁶).

transported past the ALSL-3 monitoring site. This is one line of evidence that indicates the A8-complex (with the A8-TCS in the 5-gate condition) was likely an important sink for both sediment and water during this period. After this extreme high-flow event, suspended-sediment flux again reverted to a landward direction (period I) and remained so, even after eight gates were open (period J).

Overall, this time series of sediment and water flux (fig. 42 and table 6) illustrates how dynamic and large the particulate sediment loads can be in Alviso Slough as a function of both natural meteorological variations in hydrology and management manipulations of the A8-TCS that can affect the tidal prism in Alviso Slough. This sequence of sediment and water flux observation is critical for understanding and integrating the interrelated observation from the independent Phase 1 investigations presented in this report (see "Synthesis of the Independent Studies" section).

Unlike the 6–year time series of high-resolution water quality data collected at the ALSL-3 fixed station (USGS station 11169750) (fig. 41), data collection at the A8-TCS fixed station (USGS station 372525121584701) (fig. 43) was limited to just under 2.5 years for most parameters (September 2015–February 2018). At the A8-TCS site, salinity varied less on the tidal time scale compared to ALSL-3 but exhibited similar seasonal variations with lower values during the winter (fig. 43*A*). Like ALSL-3, the highest values of salinity observed were during the summer of 2015 (maximum: 31.4 psu on September 29, 2015), at the height of the 2012–16 drought; the variability of salinity during this time was the smallest in the record (range: 27.2–31.4 psu) outside of periods of prolonged watershed discharge (for example, January–February 2017, fig. 43*A*).

Water temperature at A8-TCS varied seasonally, with minimum values near 8 °C in the winter months and maximum values near 30 °C in the summer (fig. 43*B*). Dissolved oxygen concentration at A8-TCS was generally higher than at ALSL-3 and had less annual periodicity (fig. 43*C*), which indicates comparatively high primary

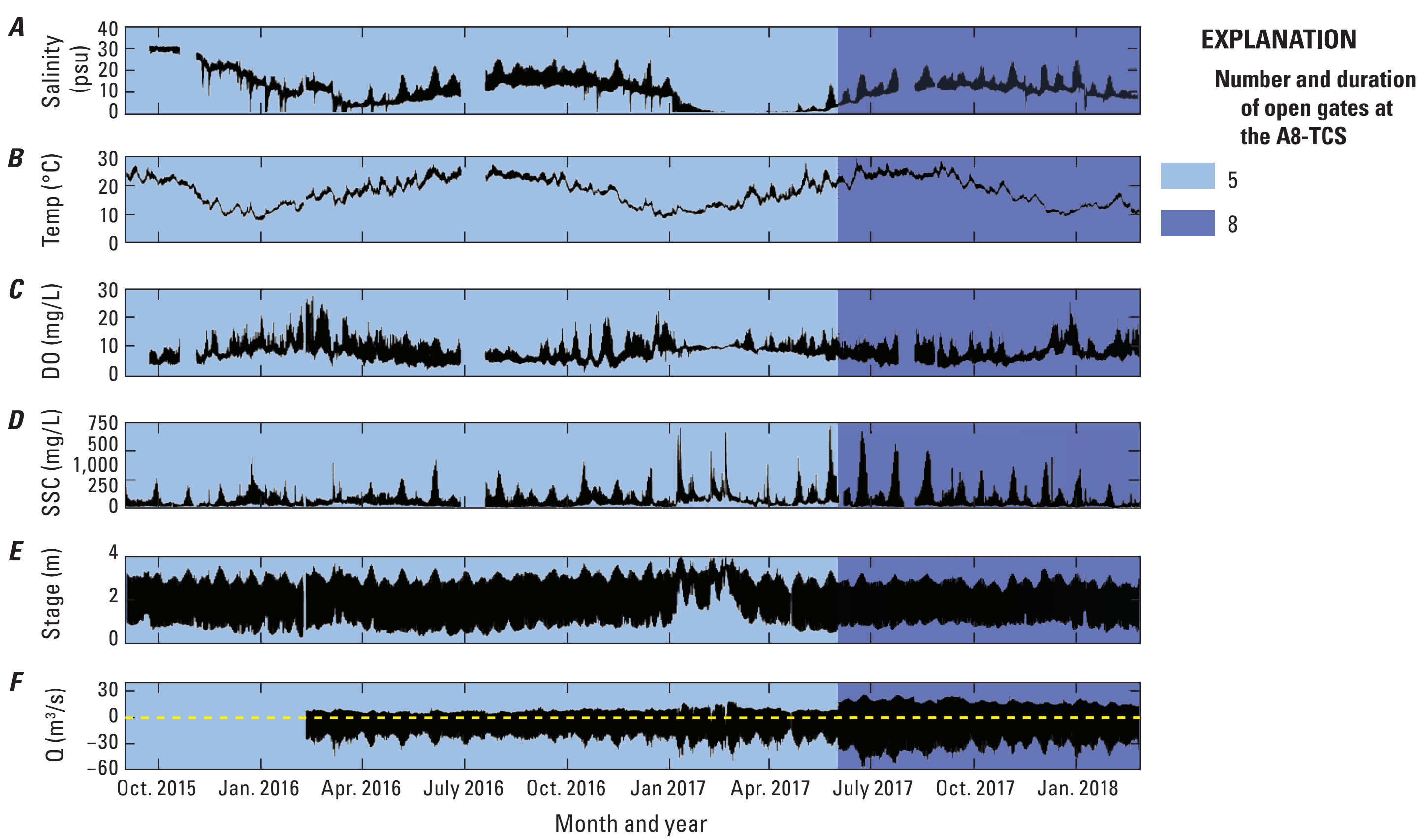

Figure 43. Time series graphs showing 15-minute instantaneous data for surface-water salinity (*A*), temperature (Temp) (*B*), dissolved oxygen (DO (*C*), suspended-sediment concentration (SSC) (*D*), water depth (stage) (*E*), and discharge (Q) (*F*) at U.S. Geological Survey station 372525121584701 (A8-TCS fixed monitoring site). Fixed monitoring site A8-TCS experiences bidirectional flow in the tidally influenced channel that connects the A8-complex to Alviso Slough. Positive Q values indicate flow from the A8-complex to the slough. Horizontal axis limits are September 1, 2015–February 27, 2018; each tick mark denotes the first day of the month indicated (for example, Oct15 indicates October 1, 2015). Missing data are due to instrument failure or biological fouling of signal. The yellow horizontal dashed line in panel *F* highlights the zero value for Q. Units of Salinity are given in practical salinity units (psu), temperature in degrees Celsius (°C), DO in milligrams per liter (mg/L), tidal stage in meters (m), and Q in cubic meters per second (m^3/s).

production within A8-complex. Maximum DO concentration at A8-TCS was observed during the relatively dry winter of 2016 (27.2 mg/L on February 16, 2016; 317 percent DO saturation). During the wetter winter of 2017, salinity at A8-TCS was about 0 psu, SSC was elevated, and DO concentration showed low variability of lower values (average DO concentration for January 15, 2017–March 15, 2017: 9.9 mg/L, n = 5,638; 94.3 percent DO saturation), which indicates comparatively less primary production during sediment-laden watershed discharge (fig. 43*C*).

Suspended-sediment concentration at A8-TCS station exhibited a 14-day periodicity related to the spring (highest high) and neap (lowest low) tidal cycle and increased during high watershed discharge in the winter of 2017 (fig. 43*D*). Following the opening of eight gates at the A8-TCS, spring-tide peak SSC magnitude increased from 300 mg/L to 600 mg/L (fig. 43*D*), which could indicate more scour in Alviso Slough, or may indicate more sediment in the system following the winter 2017 storms (see fig. 42, time period H).

Tidal stage and discharge at the A8-TCS outlet varied tidally and seasonally. During flood tides, stage increases and discharge is negative, which indicates flow into the A8-complex; on ebb tides, stage decreases and discharge is positive, which indicates bayward-directed flow (figs. 43*E*, *F*). At this location, flood-ebb asymmetry is evident in discharge, and higher peak discharge occurs during flood tides (fig. 43*F*). During the winter 2017 storms, stage increased and remained elevated during all tidal phases (fig. 43*E*), while discharge exhibited slightly higher ebb-tide values and much higher flood-tide values (fig. 43*F*). Discharge also varied in response to A8-TCS gate operations; when under the 8-gate condition, the range of outlet discharge increased owing to greater flow area and more water entering the slough from pond A8, and the pond from the slough (fig. 43*F*).

Suspended-sediment mass flux and water-volumetric flux at the A8-TCS fixed monitoring station were consistently into the A8-complex (table 7, fig. 44). Daily mean suspended-sediment flux into the A8-complex was highest (more than 100 t/d) during the high flow period that started in early January 2017 during the 5-gate condition. During low-flow conditions before and after the 2017 high flow event, sediment flux into the A8-complex ranged between 33 and 36 t/d, a rate that was not affected once the A8-TCS was opened to the 8-gate condition. Daily mean water flux into the A8-complex increased approximately 35 percent during high-flow compared to low-flow conditions during the 5-gate condition but was also substantially lower (4.2-fold compared to the 5-gate low-flow condition) during the 8-gate condition (table 7). It is important to recognize that measurements of sediment and water flux made at the A8-TCS site do not allow for a sediment or water budget for the A8-complex, because it is not a closed system in that there are two additional water control structures, one connecting pond A7 to Alviso Slough and the other connecting pond A5 to Guadalupe Slough (figs. 2–5). Water and sediment flux measurements were not made at these other two water conveyance structures, and detailed notes on their operation (that is, when they were set for one or two directional flow) are not complete. We can surmise, however, that although sediment and water flux at the A8-TCS station appeared to be flood dominated (flux into the A8-complex), water also exited the A8-complex at other two water control structures located on Alviso Slough and Guadalupe Slough or at least during periods when they were managed for bidirectional flow.

Table 7. Daily mean flux rates of water and suspended sediment at U.S. Geological Survey station 372525121584701 (A8-TCS fixed monitoring station), as a function of time period.

[Daily mean flux rates for each time period (A, B, C, and D) identified in figure 44. Date ranges are in month, day, year (mm/dd/yyyy) format. Means are calculated from all individual 15-minutetime-integrated data, converted to daily rates. Values in parentheses represent the standard error of the daily mean flux rate. Negative daily mean flux values represent flux into the A8-complex. Whether the “Flux” is in or out of the A8-complex (as measured at the A8-TCS) for a given time period and matrix is indicated. The defined time periods represent different scenarios: A, 5 gates open and low Guadalupe River flow prior to the January-February 2017 high flow event; B, 5 gates open during the 2017 high flow event; C, 5 gates open and low Guadalupe River flow after the 2017 high flow event; and D, 8 gates open. (m^3 x 1000)/d, thousand cubic meters per day; t/d, metric tons per day; SS, suspended sediment]

Matrix	Time period	Start date	End date	Total days	Daily mean flux rate	Units	Flux
Water	A	02/10/2016	01/07/2017	332	−372.0 (5.0)	(m^3 x 1000)/d	In
Water	B	01/07/2017	02/28/2017	52	−500.0 (19.0)	(m^3 x 1000)/d	In
Water	C	03/01/2017	06/01/2017	92	−332.0 (11.0)	(m^3 x 1000)/d	In
Water	D	06/01/2017	02/27/2018	271	−83.0 (10.0)	(m^3 x 1000)/d	In
SS	A	02/10/2016	01/07/2017	332	−36.2 (0.5)	t/d	In
SS	B	01/07/2017	02/28/2017	52	−122.8 (3.6)	t/d	In
SS	C	03/01/2017	06/01/2017	92	−32.6 (1.3)	t/d	In
SS	D	06/01/2017	02/27/2018	271	−35.1 (1.0)	t/d	In

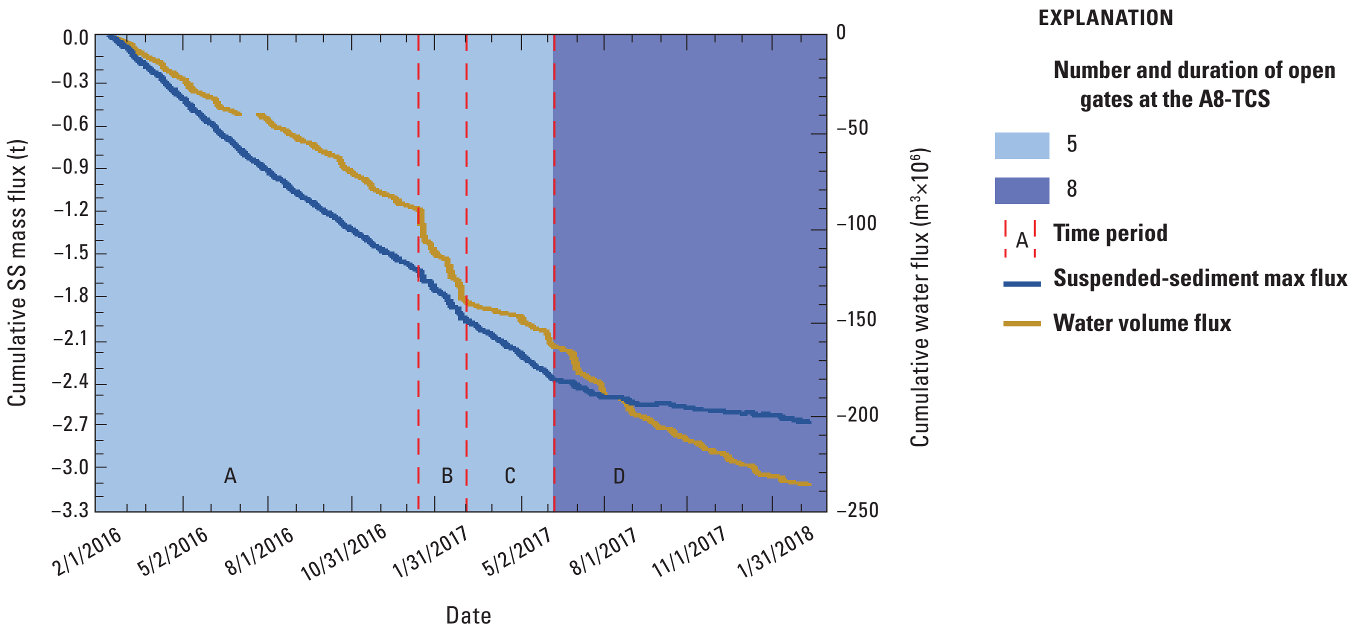

Figure 44. Time series graph showing cumulative surface-water suspended-sediment (SS) mass flux and water volume flux at U.S. Geological Survey station 372525121584701 (A8-TCS fixed monitoring station). Negative values indicate flow from Alviso Slough into the A8-complex. Time period of data shown is February 10, 2016–February 27, 2018. Missing data are due to instrument failure or biological fouling of signal. Values of cumulative SS flux are in metric tons (t), and values of cumulative water flux are in million cubic meters (m^3 x 10^6). Time periods (letters A–D separated by red dashed vertical lines) are identified by an obvious change in X-Y slope or number of gates open at the A8 tidal control structure (A8-TCS gate conditions). The exact date range and the calculated daily mean flux rate for each time period are summarized in table 7.

The Effect of A8-TCS Gate Operations on Alviso Slough Discharge—The Q Ratio

Analysis of ebb tide outflow from Alviso Slough relative to the inflow from the Guadalupe River, was assessed by the Q-ratio metric (Q_{ALSL}/Q_{GR}). For Q ratio of about 1, inflow and outflow are balanced at the daily time scale. Q ratio < 1 indicates less outflow than inflow, which can be explained by water diverted into the A8-complex or other off-channel reservoirs. Q ratio > 1 indicates more outflow than inflow, which can be explained by water leaving temporary storage reservoirs.

A one-way ANOVA analysis was performed on the calculated Q ratio as a function of the number of A8-TCS gates open (0, 3, 5, or 8; no data for the 1-gate condition) and exempted from the analysis any days when the daily averaged Q_{ALSL} was negative (that is, net landward flow), which were 496 days out of 2,178 days (23 percent of all Q_{ALSL} data). Over the entire range of observed positive discharge, a significant effect was observed for the number of gates open [$F(3,2056)=178$, $p<0.0001$)], and the 5-gate condition had a significantly higher Q ratio (6.30±0.16) compared to the other three gate condition scenarios (range: 1.34–1.72).

To investigate the Q ratio relative to watershed inflow intensity, the data were subset into low-flow and high-flow conditions on the basis of Guadalupe R discharge (Q_{GR}). The distribution of Q_{GR} was analyzed via nonparametric ranking. The 90th percentile Q_{GR} of 2.6 cubic meters per second (m^3/s) was selected as the threshold between low- and high-flow. The one-way ANOVA was rerun under both flow conditions. During the low-flow condition ($Q_{GR} < 2.6$ m^3/s), there was a significant gate effect [$F(3,1438)=208$, $p<0.0001$)] and again the 5-gate condition had a significantly higher Q ratio (8.30±0.22) compared to the other three gate condition scenarios (range: 1.48–2.02) (fig. 45). During the high-flow condition ($Q_{GR} \geq 2.6$ m^3/s), there was no significant difference among gate conditions [$F(3,135)=1.68$, $p = 0.17$)]. However, there was a general decreasing trend in the Q ratio with the more gates open, decreasing from the 0-gate or 3-gate conditions (1.02±0.13 and 1.16±0.20, respectively) to the 5-gate condition (0.88±0.07) to the 8-gate condition (0.22±0.41). The lack of a statistically significant difference for gate operations during high-flow condition may partially reflect the comparatively low sample size (n=139) compared to the low-flow condition (n=1,442), particularly for the 8-gate condition data grouping during the high-flow condition (n=6). However, the decreasing trend in the Q ratio with increasing number of gates open during high-flow conditions indicates that as the connectivity between the A8-complex and Alviso Slough is increased (that is, more gates open), the A8-complex acts increasingly as a temporary reservoir of watershed discharge. With the gates closed or slightly open (that is the 3-gate condition), the entire pulse of a storm-related flow passes through Alviso Slough en route to the estuary in approximately one day (Q ratio of about 1). As the number of gates open increases, an increasing fraction of the

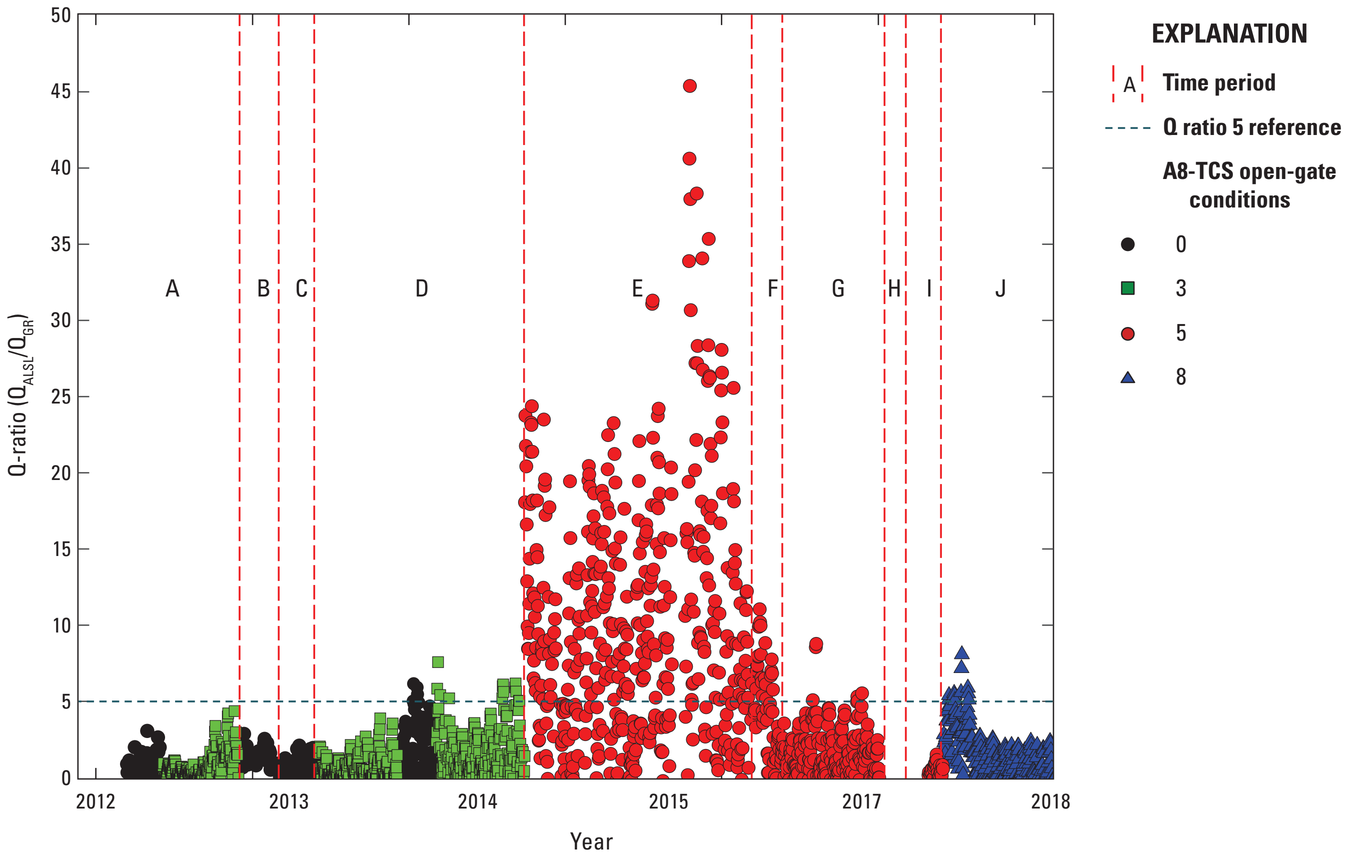

Figure 45. Time series graph showing the Q ratio (Q_{ALSL} / Q_{GR}) of U.S. Geological Survey (USGS) station 11169750 (site ALSL-3; Q_{ALS}) and USGS streamgage station 11169025 in the Guadalupe river (Q_{GR}) during low-flow and when different A8 tidal control structure gates were open (A8-TCS gate conditions). The Q ratio is Q_{ALSL}/Q_{GR}, where Q_{ALSL} is the daily mean discharge at station 11169750 and Q_{GR} is the daily mean discharge from streamgage station 11169025 in the Guadalupe River. Low-flow conditions are defined as Q_{GR} < 2.6 cubic meters per second. Horizontal axis limits are November 18, 2011–February 13, 2018; each tick mark denotes the first day of each year (for example, 2012 indicates January 1, 2012). The letters A–J represent time periods (separated by red dashed vertical lines) correspond to those in fig. 42 and table 6, which identify the notable sequence in suspended-sediment landward and bayward flux. The horizontal dashed blue line represents Q ratio equal to 5 for visual reference.

storm-related flow is diverted into the pond A8-complex and is stored temporarily (Q ratio < 1). Thus, the conveyance of storm-related watershed discharge to the estuary is affected by the level of connectivity between the A8-complex and Alviso Slough.

A demonstrable and dramatic increase in the average Q ratio started September 29, 2014, and ended mid-May 2016 (time periods E and F in fig. 45), the beginning of which coincided with the transition from the 3-gate to 5-gate condition (table 6). However, this time period also coincided with the most severe part of a multi-year drought. Median flow conditions measured at streamgage station 11169025 in the Guadalupe River decreased more than five-fold between 2012 and 2015 for the low-flow period of the annual hydrologic cycle (June 1 through September 30) as follows: 2012 = 0.89 m^3/s, 2013 = 0.66 m^3/s, 2014 = 0.23 m^3/s, and 2015 = 0.17 m^3/s. As such, we wanted to verify the extent to which the pronounced increase in the average Q ratio during the 5-gate condition period was not simply owing to decreasing flow from the Guadalupe River associated with the drought. To examine this, the net positive (bayward) daily mean discharge measured at ALSL-3 (Q_{ALSL}) was statistically modeled as a function of both gate operations (number of A8-TCS gates open) and Q_{GR}. The model also included an interaction term between these two main effects. During low-flow conditions (Q_{GR} < 2.6 m^3/s), the main effect for the number of open gates was significant [$F(3,1434) = 84.5$, $p < 0.0001$], as was the main effect of Q_{GR} [$F(1,1434) = 10.9$, $p = 0.001$], whereas the interaction term was not [$F(3,1434) = 2.32$, $p = 0.073$]. A post-hoc Tukey's test of the gate effect indicated that Q_{ALSL} was statistically lower under the 0-gate and 3-gate conditions (1.22±0.11 m^3/s and 0.98±0.09 m^3/s, respectively) compared to the 5-gate and 8-gate conditions (2.58±0.07 m^3/s and 2.23±0.18 m^3/s, respectively). Thus, discharge in the tidally affected reach of Alviso Slough was approximately two-fold greater under the 5-gate and 8-gate conditions, compared to the 0-gate and 3-gate conditions, when controlling for variations in Guadalupe River flow during low-flow conditions.

The same multivariate model described above was run for the high-flow conditions ($Q_{GR} > 2.6$ m^3/s), except data associated with the 8-gate condition were excluded owing to the very low number of observations (n=6). Significant results were found for the number of open gates [$F(2,130) = 6.65$, $p = 0.0018$], Q_{GR} [$F(1,130) = 92.5$, $p < 0.0001$], and the interaction term [$F(2,130) = 6.49$, $p = 0.021$]. The post-hoc Tukey's test of the gate effect indicated that Q_{ALSL} was statistically higher under the 0-gate condition (16.5±1.6 m^3/s) compared to the 5-gate condition (11.0±0.6 m^3/s), and the 3-gate condition (14.8±2.2 m^3/s) was not significantly different from the 1-gate condition. Thus, while controlling for Q_{GR}, there was a statistically significant decrease in Q_{ALSL} as the number of open A8-TCS gates increased during high-flow conditions.

The above statistical analysis of the low-flow Q-ratio data indicates that the increasing drought conditions during the 2012–15 period was not the cause of the large increase in the range of Q ratios observed immediately upon the 3-gate to 5-gate transition (fig. 45). Instead, we interpret this response as an indication that the initial opening the A8-TCS to the 5-gate condition represented a tipping point in the balance between the sudden increase in tidal prism and the capacity of Alviso Slough to accommodate this jump in hydrologic energy within its existing geometry. We suggest that the result of this was a prolonged period of slough instability, reflected by Q ratios exceeding values of approximately 5 for a period of 1.6 years (from late September 2014 until mid-May 2016). This timeframe coincides precisely with periods E and F of figure 42, which reflect a reversal in suspended-sediment flux from landward to bayward immediately after the 5-gate condition was initiated (period E of fig. 42) and that culminated in a 2.5-month increase in bayward sediment flux between early March and mid-May 2015 (period F of fig. 42, table 6). The highest Q ratio values (> 25) occurred towards the end of period E (between late July 2015 and the end of January 2016). This was followed by a sharp 3.5 month decrease in the Q ratio to values below 5, between February and mid-May 2016 (fig. 45), which coincides with the increased water and suspended-sediment flux of period F (fig. 42, table 6). Once suspended-sediment flux finally returned to a landward direction (period G of fig. 42, table 6), Q ratios below 5 were reestablished (fig. 45). Immediately upon the initiation of the 8-gate condition at the A8-TCS, we again see a spike in Q ratio (maximum value of about 8), but one that was short lived (2 months) before the values of ≤ 3 were consistently seen throughout the remainder of the time series (period J of fig. 45). We suggest that this short-lived spike observed after the 5-gate to 8-gate transition similarly reflects a brief period of energetic instability within Alviso Slough, which was a result of the sudden further increase in tidal prism. This short-lived spike was minor compared to the 3-gate to 5-gate transition, which represented the most substantial change in system energetics that occurred during the Phase 1 study period caused by A8-TCS management actions.

The Effect of A8-TCS Gate Operations on Suspended-Sediment Flux in Middle Alviso Slough

To better understand the extent to which SSC may have been affected by A8-TCS gate operations, a LSM fixed-effects model was constructed, the dependent variable of which was ebb tide (that is, bayward directed flow only) high-resolution (15-minute) SSC data from the ALSL-3 fixed monitoring site during the 2012–18 period of record. The independent variable model terms included the A8-TCS gate condition (0, 3, 5, or 8 gates open), the daily mean discharge at USGS streamgage station 11169025 in the Guadalupe River (Q_{GR}), and an interaction term. Model results indicate significant effects from the number of gates open (gate effect [$F(3, 850) = 74.3$, $p < 0.0001$] and Guadalupe River discharge (Q_{GR} effect [$F(1, 850) = 9.68$, $p = 0.0019$]) but not the interaction term [$F(3, 850) = 0.31$, $p = 0.82$]. A post-hoc Tukey's pair-wise comparison of the modeled SSC results attributed to the gate effect alone demonstrated that, while controlling for variation in Q_{GR}, the ebb tide SSC concentration at ALSL-3 decreased as the number of A8-TCS open gates increased (fig. 46).

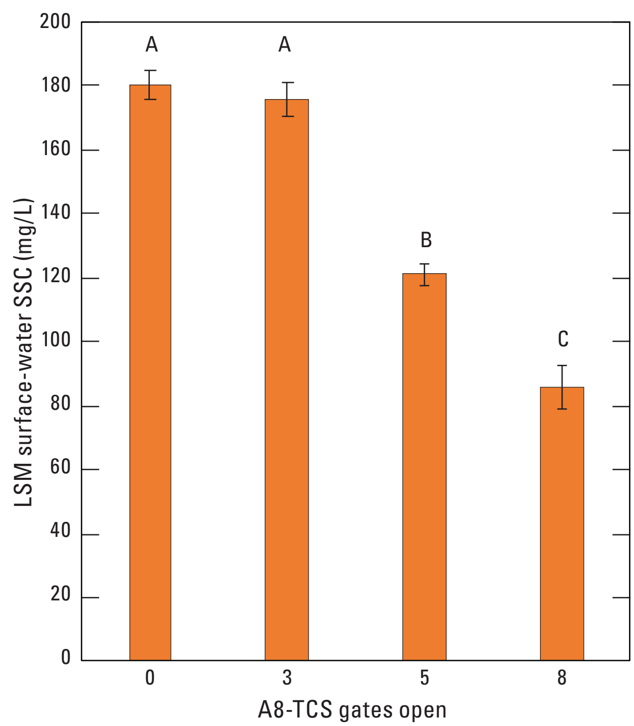

Figure 46. Bar graph showing the modeled least squares mean (LSM) values of surface-water suspended-sediment concentration (SSC) during ebb tide at U.S. Geological Survey station 11169750 (site ALSL-3), as a function of the number of A8-TCS gates open. The modeled results control for variations in Guadalupe River discharge. Error bars represent modeled standard errors. The letter above each bar indicates the post-hoc Tukey's pair-wise ranking, with letter 'A' reflecting the highest ranking. Bars sharing the same letter are not significantly different. Values of SSC are given in milligrams per liter (mg/L).

Specifically, the 0-gate and 3-gate conditions had equally high LSM model-predicted SSC concentrations (180±4 mg/L and 176±5 mg/L, respectively), which were significantly higher than the 5-gate condition (121±3 mg/L), which was significantly higher than the 8-gate condition (86±7 mg/L). Thus, there was approximately a two-fold decrease in ebb tide SSC concentrations at ALSL-3 going from the 0-gate or 3-gate condition to the 8-gate condition. This likely reflects the fact that (1) the A8-complex is a sink for suspended particulates entering during the flood tide (fig. 44), (2) this lower SSC water coming out of the A8-complex represents some portion of the total water going past the ALSL-3 monitoring site during the ebb tide, and (3) this proportion of A8-complex water increases as the number of gates open increases.

The Effect of A8-TCS Gate Operations on Surface-Water Particulate Mercury Flux at Middle Alviso Slough Site ALSL-3

A high-resolution predictive model of p.THg and p.MeHg flux was developed for the middle Alviso Slough by coupling the high-resolution (15-minute) fixed-station water-quality data collected at site ALSL-3 (figs. 41, 42) with the low-resolution (monthly to seasonal, fig. 30) and medium resolution (hourly, figs. 36, 38) surface-water volumetric p.THg and p.MeHg data collected at the same site. The first step in this process was to develop prediction relations for surface-water mercury species measured at medium to low resolution with nonmercury data measured at high-resolution. The resulting equations are provided in appendix 2, and include the explanatory model terms TSS, Julian day and tidal stage for both p.THg and p.MeHg as the dependent variable. The predictability of both relations (actual versus predicted) was high, with linear regression R^2 values of 0.80 for p.THg and 0.92 for p.MeHg (fig. 47).

Both tidal stage and SSC were measured in high-resolution at site ALSL-3. The simplifying assumption that SSC = TSS (as measured on particulate mercury filters) was made for modeling purposes, as discussed in the "Methods" section. Applying the 15-minute data for tidal stage and SSC, along with Julian day (as a cosine function), to the predictive model equations (appendix 2), high-resolution (15-minute) predictions of p.THg and p.MeHg were developed (fig. 48), and from those predictions, p.THg and p.MeHg

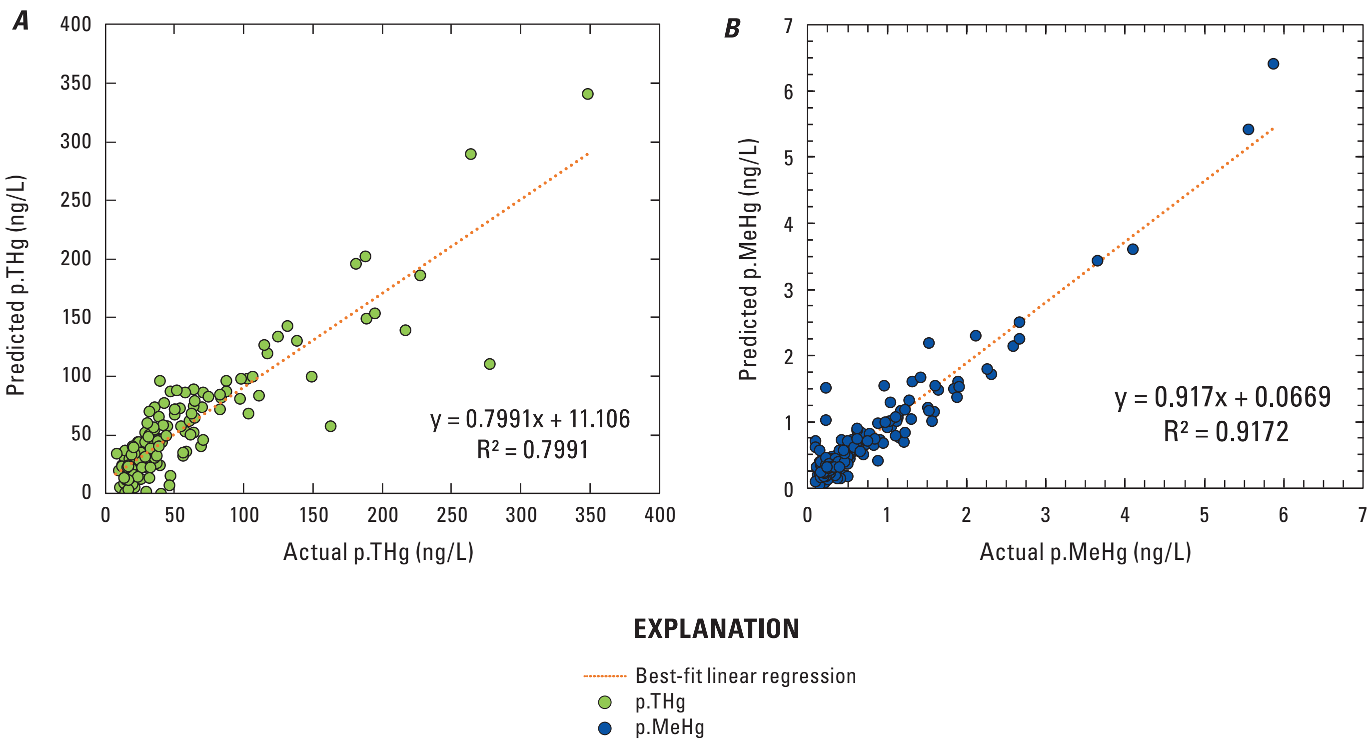

Figure 47. Line graphs showing actual versus model-predicted surface-water particulate total mercury (p.THg) (*A*) and particulate methylmercury (p.MeHg) (*B*) at U.S. Geological Survey station 11169750 (site ALSL-3). Values of p.THg and p.MeHg are given in nanograms per liter (ng/L).

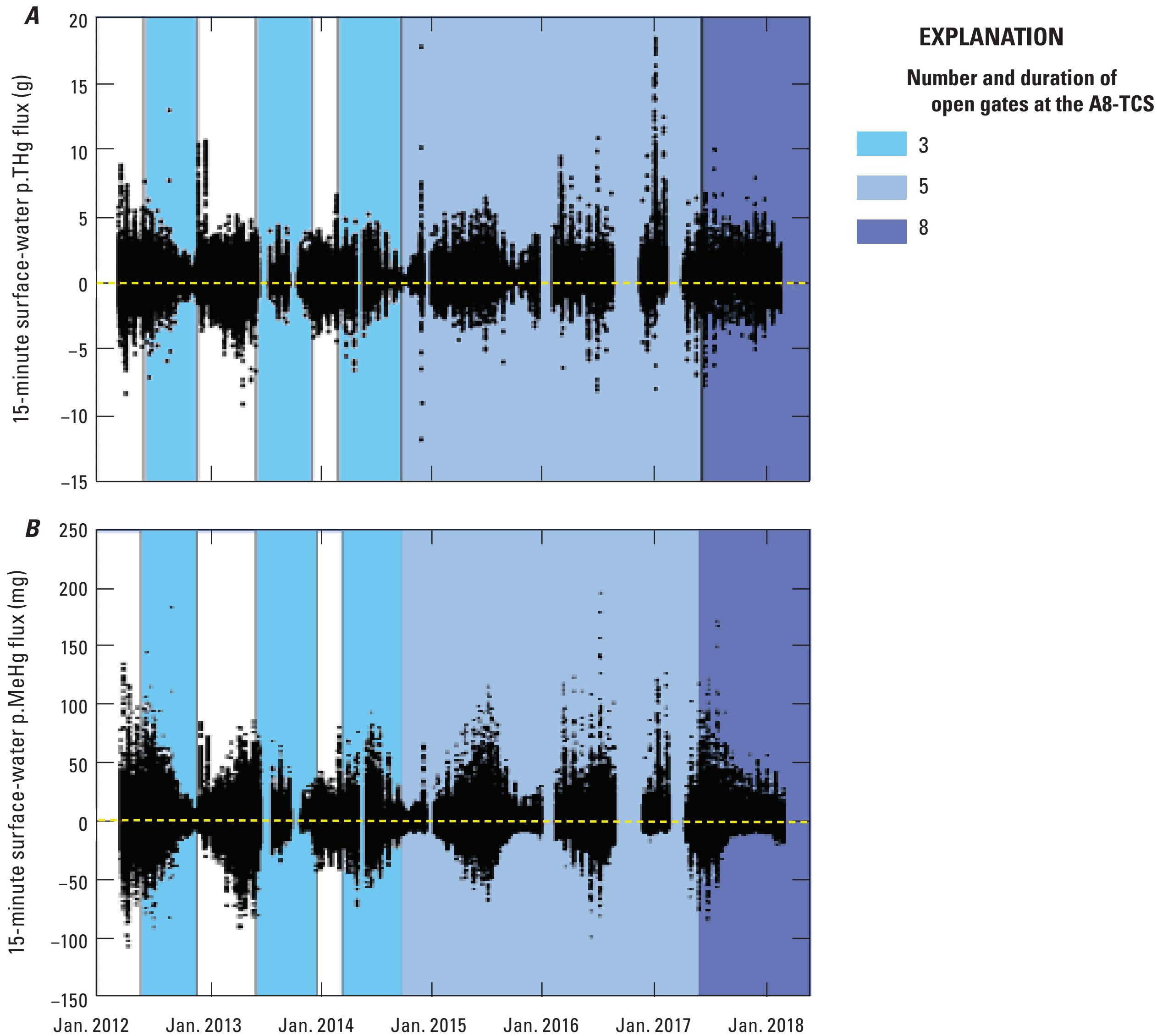

Figure 48. High-resolution (15-minute) time series graphs showing model-predicted surface-water particulate total mercury (p.THg) (*A*) and particulate methylmercury (p.MeHg) (*B*) flux at U.S. Geological Survey station 11169750 (site ALSL-3). Positive values indicate flux in the bayward direction, and negative values indicate flux in the landward direction. The yellow dashed line indicates zero flux. Nonshaded background represents duration when all gates are closed. Values of p.THg and p.MeHg are given in grams (g) and milligrams (mg), respectively.

cumulative flux was calculated (fig. 49). From the perspective of site ALSL-3, net flux for both p.THg and p.MeHg was demonstrably in the bayward direction (positive slope) throughout the full period of study (fig. 49). The sharp rise in cumulative p.THg flux during the January–February 2017 extreme water event was more apparent compared to the cumulative p.MeHg flux. Each 15-minute model-predicted p.THg and p.MeHg mass flux value (fig. 48) was converted to a daily flux rate. An ANOVA was then conducted on p.THg and p.MeHg daily flux rates grouped by A8-TCS gate condition (the number of gates open). The results of a post-hoc Tukey's pairwise comparison indicate that the daily mean flux rates for both mercury species significantly increased as the number of open A8-TCS gates increased, but that the 5-gate condition had the highest flux in both cases (fig. 50). Because the January–February 2017 high-flow event was associated with a notable short-term increase in cumulative p.THg and p.MeHg flux (indicated on fig. 49) during the 5-gate condition, the ANOVA comparing daily mean flux rates was rerun with the 2017 storm event data excluded (fig. 50). The results indicate that even with the effect of the January–February 2017 storm removed, the 5-gate condition still exhibited the highest rate, and that there was still more than a two-fold increase for both mercury species associated

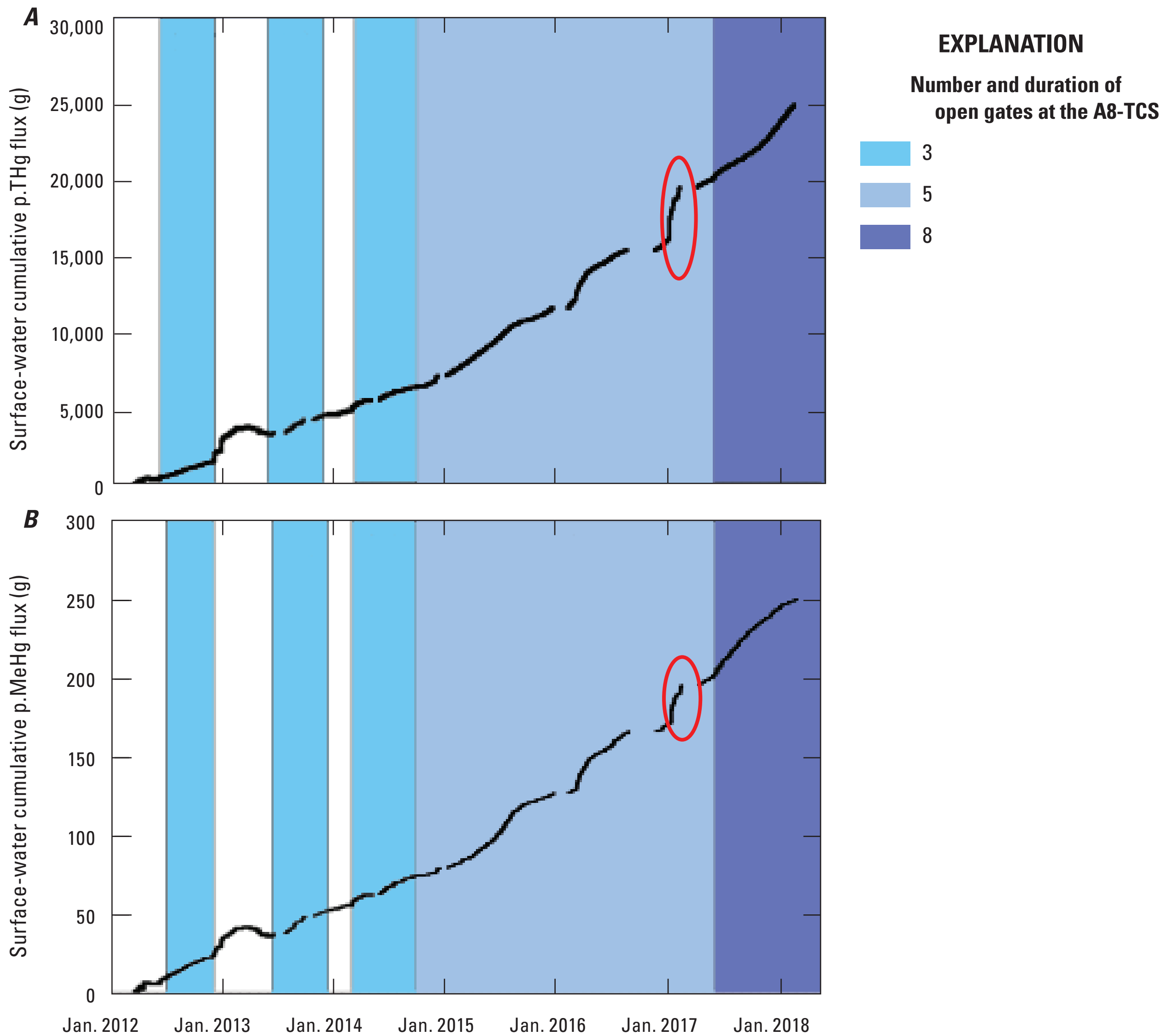

Figure 49. High-resolution time series graphs showing model-predicted surface-water cumulative particulate total mercury (p.THg) (*A*) and particulate methylmercury (p.MeHg) (*B*) flux at U.S. Geological Survey station 11169750 (site ALSL-3). Positive values indicate flux in the bayward direction, and negative values indicate flux in the landward direction. The red ovals in parts *A* and *B* highlight the January 2017 high-flow event, and nonshaded background represents duration when all gates are closed. Values of p.THg and p.MeHg are given in grams (g).

with the transition from the 3-gate to the 5-gate condition. This indicates that A8-TCS gate operations were primarily responsible for this substantial increase in the daily mean bayward flux of both p.THg and p.MeHg, and that this transition to the 5-gate condition represents a significant shift in the mercury flux and bed sediment erosion dynamics within Alviso Slough.

By converting the ALSL-3 bayward daily mean flux rates for p.THg depicted in figure 50 (“all data” in the ANOVA results) to annual rates, we are able to calculate annual flux rates of 3.1 kilograms per year (kg/yr), 4.4 kg/yr, 11.8 kg/ yr and 8.2 kg/yr for the 0-, 3-, 5- and 8-gate conditions, respectively. This range of values is much lower than the 139 kg/yr climatically adjusted mean wet season THg load estimated by McKee and others (2017) for the streamgage station 11169025 in the Guadalupe River. This Guadalupe River THg load estimate (99% as p.THg) is approximately six-fold greater than the arithmetic mean load estimate of 24 kg/yr for the same site on the basis of 8 years of available data collected between 2003 and 2016 (McKee and others, 2017). The use of the climatically adjusted loads approach is more accurate because it better accounts for rarely sampled extreme flow events that transport a disproportionate amount of the load.

A few factors may account for the large difference between our estimated loads at ALSL-3 and those cited for the Guadalupe River. First, apart from the high flow event during January 2017, the majority of the Phase 1 study was conducted under moderate to severe drought conditions, whereas the data used to estimate the Guadalupe River loads spanned a much longer time frame with more high-flow events. Second, the field data used to model p.THg concentrations (appendix 2) did not include any data collected during extreme flow events, such as the January–February 2017 event, and therefore may underestimate the disproportional importance of these less common but important short-term high flux events. Third, although a majority of the annual THg load is transported past the Guadalupe River monitoring site during high flow events, it is unclear how much sediment and associated THg makes it as far as ALSL-3 or out to the greater San Francisco Bay once the unidirectional river joins with the tidally influenced Alviso Slough. Some unknown proportion of the sediment and THg load undoubtedly gets deposited in the upper reaches of Alviso Slough or is diverted into the A8-complex and above site ALSL-3 where our modeled estimates of p.THg flux were made. However, considering the model-predicted cumulative bayward flux of p.THg past site ALSL-3 was approximately 25,000 g (25 kg) for the entire period of record (March 2012–February 2018, fig. 49*A*), and that a conservative estimate of THg load associated with the January 2017 event alone was 70 kg as measured at the Guadalupe River site (McKee and others, 2018), it is most likely that the current model underpredicts p.THg flux at site ALSL-3, particularly fluxes associated with extreme high-flow events.

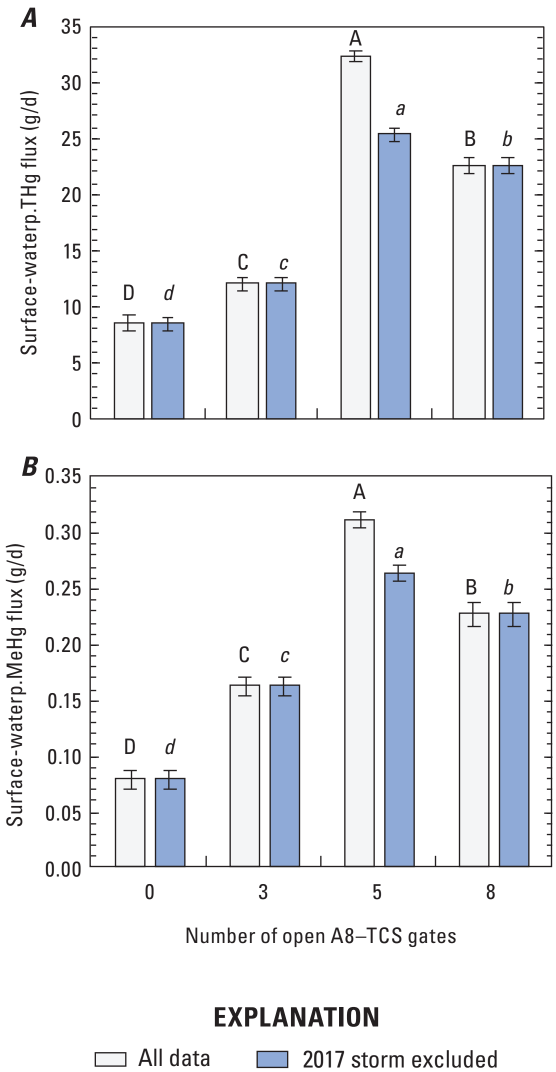

Figure 50. Bar graphs showing surface-water particulate total mercury (p.THg) (*A*) and particulate methylmercury (p.MeHg) (*B*) daily mean flux at U.S. Geological Survey station 11169750 (site ALSL-3) as a function of the number of open A8-TCS gates. Flux is in the bayward direction for both p.THg and p.MeHg, given in units of grams per day (g/d). Error bars represent standard errors. To examine the effect of the 2017 high-flow event, an analysis of variance was done using all data (grey bars) and with the 2017 storm data excluded (blue bars). In both instances, a post-hoc Tukey's pair-wise ranking analysis was done with the results depicted above each bar, and with capital letters being associated with the 'all data' analysis and lowercase italicized letters associated with the "2017 storm data excluded" analysis. Letters 'A' and 'a' reflect the highest Tukey's ranking, and bars sharing the same letter of the same style are not significantly different.

The Effect of A8-TCS Gate Operations on Surface-Water Particulate Mercury Concentration at Middle Alviso Slough

The high-resolution (15-minute) model-predicted time-series graphs of p.THg and p.MeHg flux (on a mass basis) at site ALSL-3 showed substantial season periodicity (fig. 48). Model SW.5 (equation 10) was developed to get a more quantitative assessment of both seasonal and inter-annual differences in particulate mercury species concentration, as modeled at site ALSL-3. All four mercury parameters (p.THg and p.MeHg, both volumetric and gravimetric) had significant [SEASON x YEAR] interaction terms with respect to Model SW.5 (results not shown). Interannual trends were subsequently assessed by each season individually, and with linear regression to quantify apparent interannual trends at ALSL-3 for the period of record for the high-resolution mercury modeling (March 2012–February 2018). These results are shown graphically (fig. 51, with linear regression lines depicted through annual mean concentrations, by season) and in table 8, where the linear regression slope results are given, as calculated from the complete high-resolution dataset. These regression slopes reflect the annual rate of change (increasing or decreasing) for concentrations of each particulate mercury parameter, by season. The results indicate that both volumetric p.THg (fig. 51*A*) and volumetric p.MeHg (fig. 51*C*) concentrations decreased (negative slopes) during every season between spring 2012 and winter 2017, with annual decreases in p.THg ranging from −7.53 nanograms per liter per year (ng/L/yr) during spring to −2.26 ng/L/yr

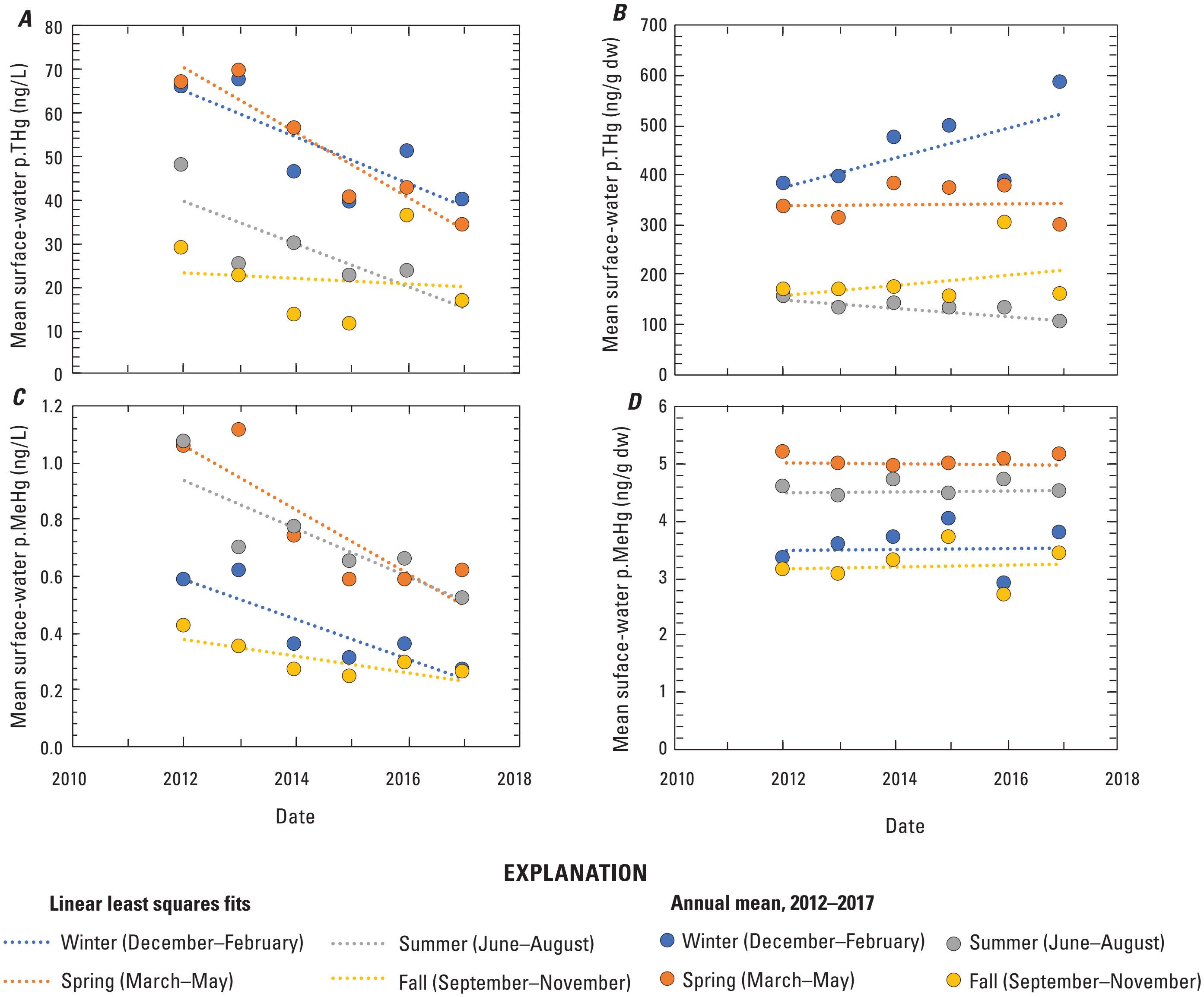

Figure 51. Line graphs showing annual mean high-resolution model-predicted surface-water volumetric particulate total mercury (p.THg) (*A*); gravimetric p.THg (*B*); volumetric particulate methylmercury (p.MeHg) (*C*); and gravimetric p.MeHg (*D*) concentration at USGS station 11169750 (site ALSL-3), by season and as a function of year. The four seasonal groupings represent winter (December–February), spring (March–May), summer (June–August) and fall (September–November). The year associated with winter reflects the year in which the previous December falls (for example, the point that plots on the winter of 2017 represents the duration of December 2017–February 2018). Values of volumetric p.THg and p.MeHg are given in nanograms per liter (ng/L). Values of gravimetric p.THg and p.MeHg are given in nanograms per gram dry weight (ng/g dw). Seasonal regression lines are plotted on the basis of the N=6 mean annual values shown and differ slightly from the slopes given in table 8, which are based on the complete 15-minute modeled mercury species concentration data record in each instance.

during fall, and annual decreases for p.MeHg ranging from −0.123 ng/L/yr during spring to −0.031 ng/L/yr during fall (table 8). This interannual trend was likely due at least in part to the increase in tidal prism and associated suspended-particulate dilution as the A8-TCS gates opened increased from the 0-gate or 3-gate condition (intermittently from March 2012 to September 2014) to the 5-gate condition (September 2014–June 2017) to finally the 8-gate condition (June 2017–February 2018) (table 2). However, changes in gravimetric concentrations were more varied in nature. Annual mean gravimetric p.THg concentrations (fig. 51*B*) actually increased substantially during winter (39.6 ng/g dw/yr) and more modestly during spring (4.67 ng/g dw/yr), but decreased during summer (−8.85 ng/g dw/yr) and fall (−1.69 ng/g dw/ yr)

Table 8. Annual rate of change in particulate mercury species concentration at U.S. Geological Survey station 11169750 (site ALSL-3), by season, between spring 2012 and winter 2017.

[Data for both particulate total mercury (p.THg) and particulate methylmercury (p.MeHg) are presented as the annual rate of change on volumetric (nanograms per liter per year [ng/L/yr]) and gravimetric (nanograms per gram dry weight per year [ng/g dw/yr]) bases. Linear regressions and associated slopes are calculated from the complete 15-minute modeled data record for each season and mercury species concentration. Seasons are defined by months given in parentheses. The probability (p) associated with the slope estimate of committing a Type II error is presented. AUG, August; DEC, December; FEB, February; JUN, June; MAR, March; NOV, November; SEP, September]

SEASON	Volumetric Rate Slope Estimate (ng/L/yr)	P	Gravimetric Rate Slope Estimate (ng/g dw/yr)	P
p.THg				
Spring (MAR–MAY)	−7.53 (0.15)[1]	< 0.0001	4.67 (0.60)[2]	< 0.0001
Summer (JUN–AUG)	−5.30 (0.12)[1]	< 0.0001	−8.85 (0.38)[1]	< 0.0001
Fall (SEP–NOV)	−2.26 (0.09)[1]	< 0.0001	−1.69 (0.62)[1]	0.0062
Winter (DEC–FEB)	−4.42 (0.11)[1]	< 0.0001	39.60 (0.6)[2]	< 0.0001
p.Me.Hg				
Spring (MAR–MAY)	−0.123 (0.002)[1]	< 0.0001	−0.014 (0.004)[1]	0.0005
Summer (JUN–AUG)	−0.093 (0.002)[1]	< 0.0001	−0.004 (0.004)	0.3528
Fall (SEP–NOV)	−0.031 (0.001)[1]	< 0.0001	0.071 (0.005)[2]	< 0.0001
Winter (DEC–FEB)	−0.058 (0.001)[1]	< 0.0001	0.082 (0.003)[2]	< 0.0001

[1]Number represents a significant negative slope.

[2]Number represents a significant positive slope.

(table 8). The trend of increasing p.THg concentration, by weight, is likely due to bed sediment erosion (including zones of previously buried legacy THg) that occurred during this period of A8-TCS gate manipulation, which was most pronounced during the winter period (see "Deep Cores and the Modeling of Bed Sediment and Total Mercury Mobilization in Alviso Slough" section).

Interannual increases in gravimetric p.MeHg (fig. 51*D*) during fall (0.071 ng/g dw/yr) and winter (0.082 ng/g dw/ yr) were also measurable, as were decreasing concentrations during spring (−0.014 ng/g dw/yr). However, although statistically significant, these changes were minor given the range in mean p.MeHg concentrations observed (2.7–5.2 ng/g dw, fig. 51*D*). There was no significant change in gravimetric p.MeHg during summer over the period of analysis (table 8).

The Effect of A8-TCS Gate Operations on Mercury Flux into and out of the A8-Complex

Our ability to model the flux of different mercury species into and out of the A8-complex, as assessed at the A8-TCS, was less precise than our ability to model mercury flux at the middle Alviso Slough (site ALSL-3). There were three reasons for this. The first reason was related to a lower data density available to build predictive mercury species concentration models associated with the A8-TCS fixed monitoring station (USGS station 372525121584701) compared to the ALSL-3 monitoring station (USGS station 11169750), because the former only included data associated with the 19 monthly sampling events (1 observation per site and per event) done between February 2014 and February 2018, whereas the latter also included the 5 diel studies (between May 2012 and February 2013) that represented hourly data over 2 tidal cycles (an additional 125 observations). The second reason was that the surface-water mercury data used to develop the predictive models at the A8-TCS were not co-located with the A8-TCS fixed monitoring site, as was the case with ALSL-3. Instead, flood and ebb tide predictive models needed to be developed separately, for which site ALSL-2b data were used to derive predictive equations for flood tide mercury flux and data collected from within the A8-complex were used to derived predictive equations for ebb tide mercury flux (fig. 4, appendix 2). Finally, the high-resolution record of observation available for modeling mercury flux at the two fixed monitoring sites was much longer for ALSL-3 (5.9 years; March 2012–February 2018) than for the A8-TCS (2.0 years; February 2016–February 2018).

The model-predicted filter-passing and particulate mercury mass flux, calculated at the 15-minute time step, is depicted in the following figures: f.THg (fig. 52*A*), f.MeHg, (fig. 52*B*), p.THg (fig. 53*A*), and p.MeHg, (fig. 53*B*), in which negative values reflect flux into the A8-complex. The greatest mass flux for all mercury species into the A8-complex was associated with the high flow event of January–February 2017. A substantial export of both dissolved species (f.THg and f.MeHg) on ebb tides was also associated with this high-flow event (fig. 52).

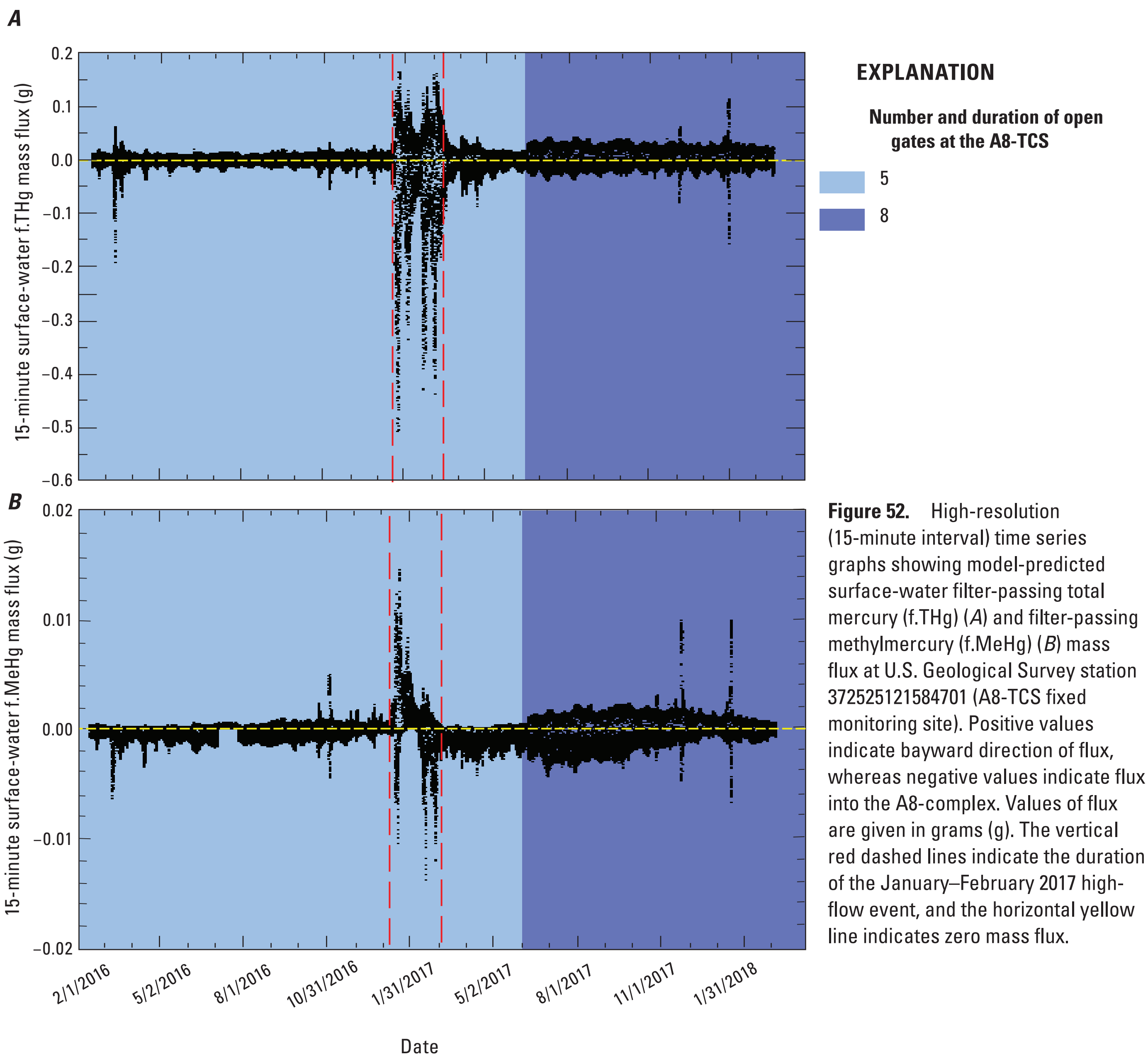

Figure 52. High-resolution (15-minute interval) time series graphs showing model-predicted surface-water filter-passing total mercury (f.THg) (*A*) and filter-passing methylmercury (f.MeHg) (*B*) mass flux at U.S. Geological Survey station 372525121584701 (A8-TCS fixed monitoring site). Positive values indicate bayward direction of flux, whereas negative values indicate flux into the A8-complex. Values of flux are given in grams (g). The vertical red dashed lines indicate the duration of the January–February 2017 high-flow event, and the horizontal yellow line indicates zero mass flux.

To more directly quantify the flux of the different mercury species into or out of the A8-complex, an approach similar to that used for assessing suspended-sediment and water flux (fig. 44, table 7) was taken, in which the cumulative mass flux was first calculated from the model-predicted 15-minute data for f.THg (fig. 54*A*), f.MeHg, (fig. 54B), p.THg (fig. 55*A*), and p.MeHg, (fig. 55*B*). Next, meaningful time periods were identified on the basis of substantial observable changes in the slope of the cumulative time-series data and the transition from the 5-gate to the 8-gate condition. Finally, the mean (± standard error) of all 15-minute interval mass flux data (converted to daily rates) was calculated for each time period to provide a directional daily mean flux rate for each time period and mercury species (table 9). The relevant time periods considered were as follows: the low-flow and 5-gate condition prior to the January-February 2017 high-flow event (period A, fig. 54); the 2017 high-flow event (fig. 40; period B, fig. 54); the relatively brief three-month window (March–May 2017) after the high flow event but preceding the 8-gate condition (period C, fig. 54); and the 8-gate condition through the end of the period of record (period D, fig. 54).

The A8-complex was a sink for f.THg, p.THg, and p.MeHg under the 5-gate condition, with the largest daily mean flux rates into the A8-complex being associated with the January–February 2017 high-flow event (period B, table 9).

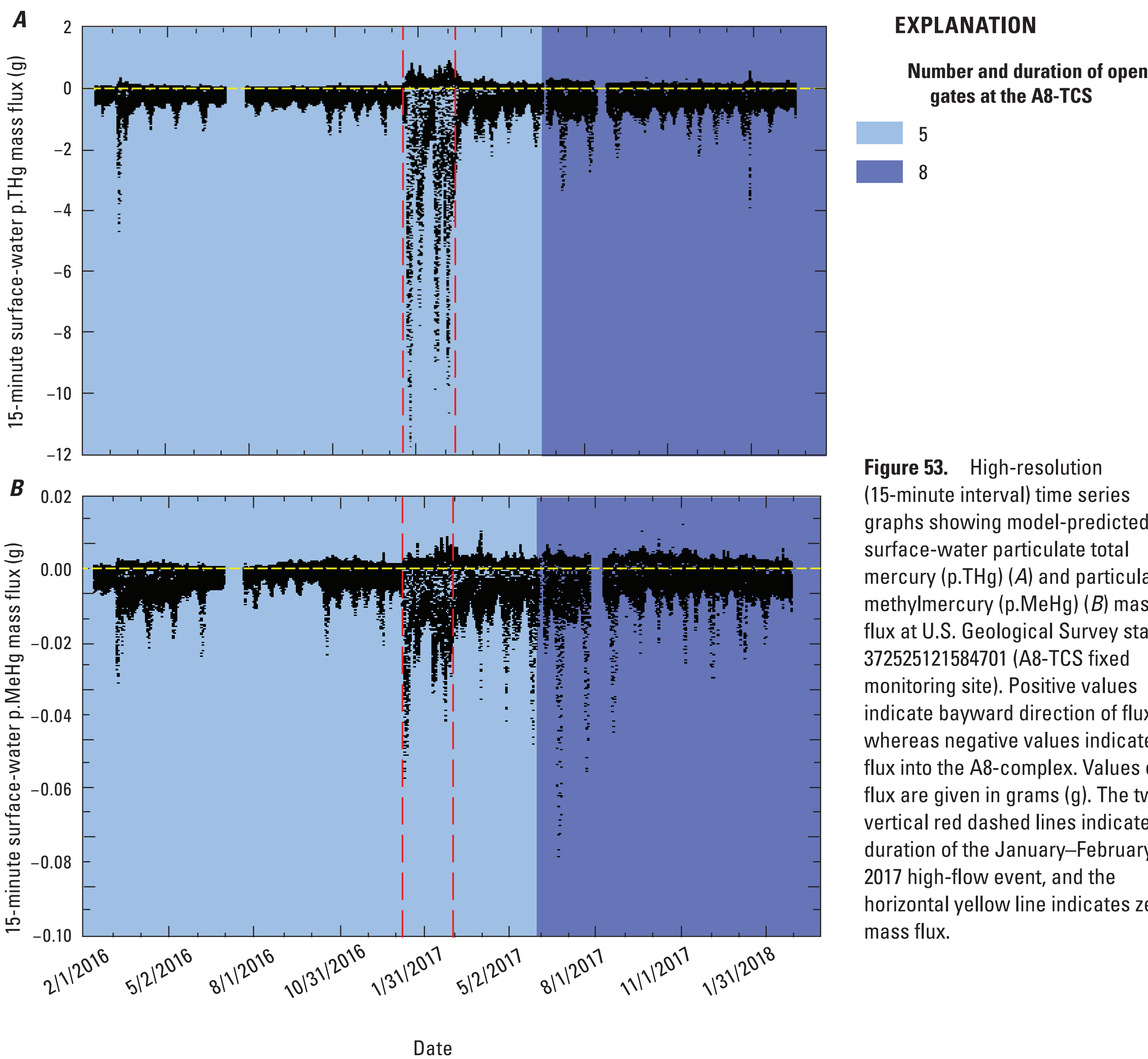

Figure 53. High-resolution (15-minute interval) time series graphs showing model-predicted surface-water particulate total mercury (p.THg) (*A*) and particulate methylmercury (p.MeHg) (*B*) mass flux at U.S. Geological Survey station 372525121584701 (A8-TCS fixed monitoring site). Positive values indicate bayward direction of flux, whereas negative values indicate flux into the A8-complex. Values of flux are given in grams (g). The two vertical red dashed lines indicate the duration of the January–February 2017 high-flow event, and the horizontal yellow line indicates zero mass flux.

However, the predictive model indicates that the 2017 high-flow event resulted in the A8-complex becoming a source of f.MeHg to Alviso Slough for a one month period (January 7 through February 8, 2017, period B, fig. 54*B*), before returning to being a sink for f.MeHg (period C, fig. 54*B*).

McKee and others (2018) estimated a THg flux of 70 kg past streamgage station 1169025 in the Guadalupe River associated with the high flow event between January 7 and 13, 2017 (6 days). On the basis of this prior estimate and our modeled daily p.THg flux estimate of 135±3 grams per day (g/d) into the A8-complex between January 7 and February 28, 2017 (period B, table 9), we calculate that a total of 0.81±0.02 kg of p.THg was diverted into the A8-complex during this same 6-day period that Mckee and others (2018) considered. This mass of p.THg amounts to 1.15±0.03 percent of the 6-day storm flux of THg delivered from the Guadalupe River being diverted into the A8-complex. This is a maximum estimate, because this calculation assumes that all of the

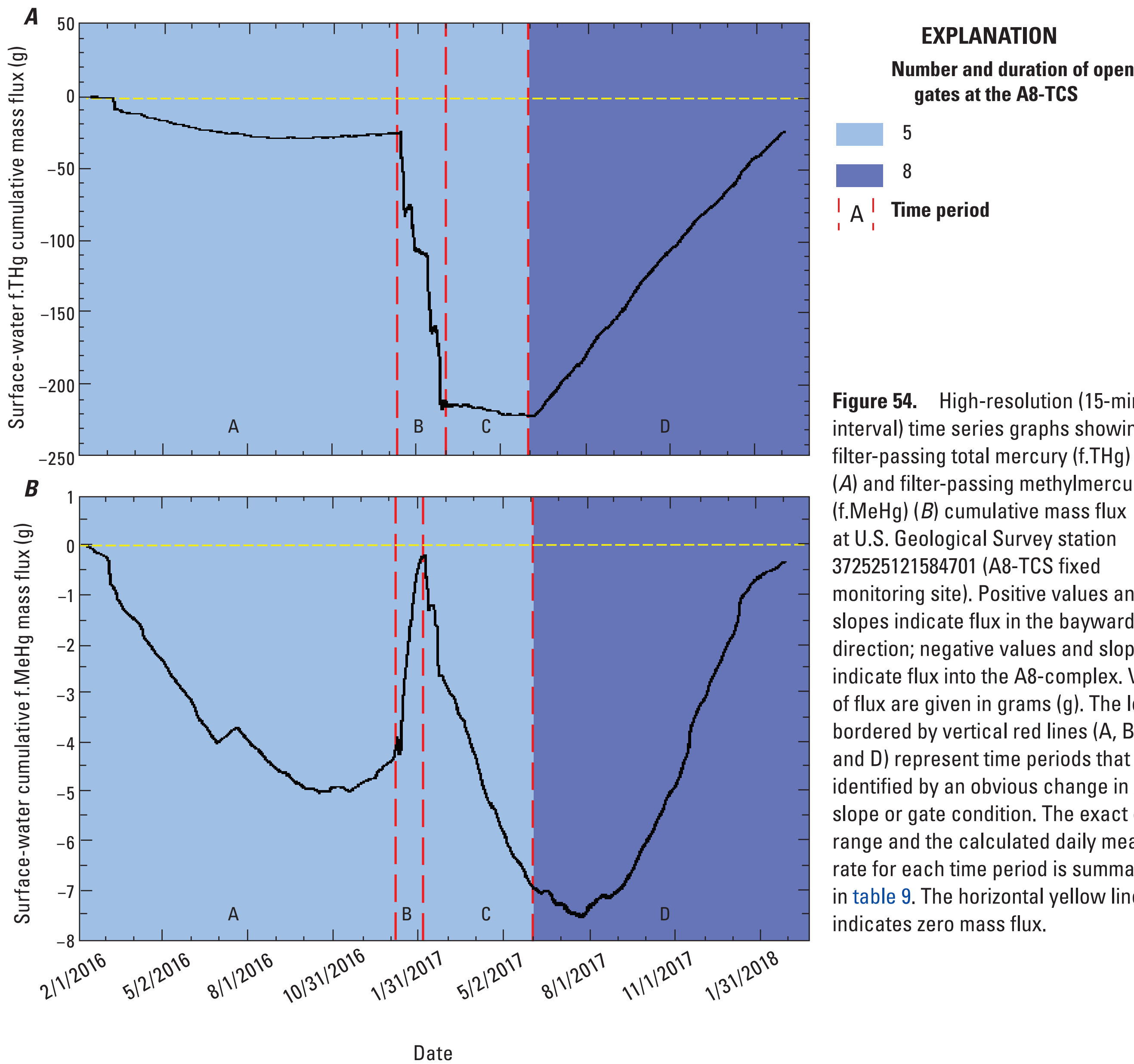

Figure 54. High-resolution (15-minute interval) time series graphs showing filter-passing total mercury (f.THg) (*A*) and filter-passing methylmercury (f.MeHg) (*B*) cumulative mass flux at U.S. Geological Survey station 372525121584701 (A8-TCS fixed monitoring site). Positive values and slopes indicate flux in the bayward direction; negative values and slopes indicate flux into the A8-complex. Values of flux are given in grams (g). The letters bordered by vertical red lines (A, B, C, and D) represent time periods that are identified by an obvious change in X-Y slope or gate condition. The exact date range and the calculated daily mean flux rate for each time period is summarized in table 9. The horizontal yellow line indicates zero mass flux.

sediment entering the A8-complex during this 6-day period is from the watershed and none is derived from bed sediment scour within Alviso Slough.

Once all eight gates at the A8-TCS were opened (period D, fig. 54) our model indicates that the A8-complex became a source of both f.THg (fig. 54*A*) and f.MeHg (fig. 54*B*) but remained a sink for p.THg (fig. 55*A*) and p.MeHg (fig. 55*B*). These trends for f.THg and f.MeHg make sense in the context of the A8-complex being a sink for water overall under the 5-gate condition, and then much less so under the 8-gate condition (fig. 44, table 7), coupled with the fact that f.THg and f.MeHg concentrations within the A8-complex were generally higher than in upper Alviso Slough (appendix 5). Thus, because water flux into and out of the A8-complex is more in balance under the 8-gate condition, the mercury species concentration gradient between the A8-complex and upper Alviso Slough influences the flux of both f.THg and f.MeHg towards the A8-complex becoming a source as opposed to a sink. It is unknown if these trends continued beyond the period of record, and if so, for how long. It should also be reiterated that our ability to model this mercury species fluxes at the A8-TCS was more limited than our ability to do so at the ALSL-3 fixed monitoring site, for the reasons previously discussed at the beginning of this section.

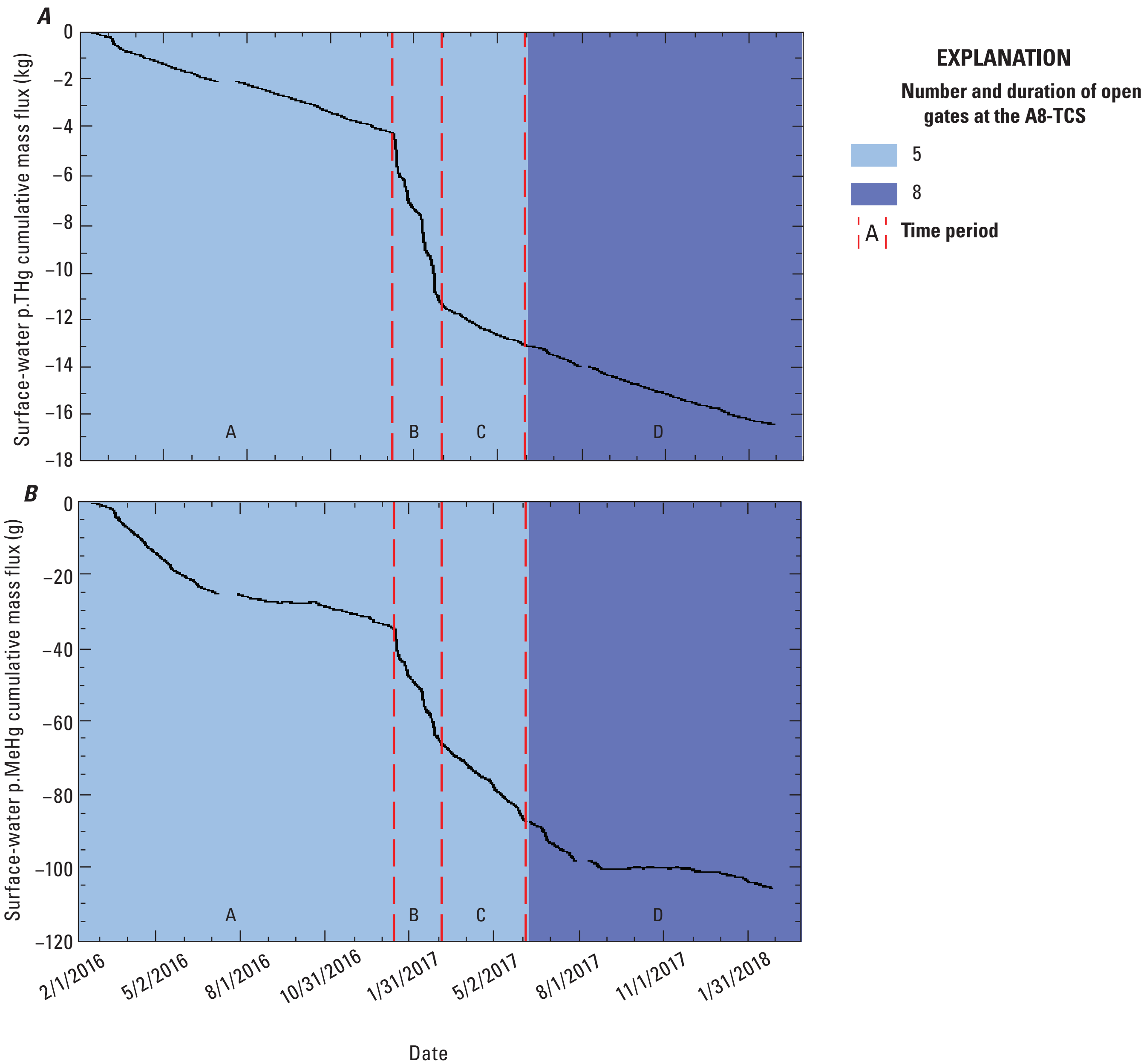

Figure 55. High-resolution (15-minute interval) time series graphs showing surface-water particulate total mercury (p.THg) (*A*) and particulate methylmercury (p.MeHg) (*B*) cumulative mass flux at U.S. Geological Survey station 372525121584701 (A8-TCS fixed monitoring site). Positive values and slopes indicate flux in the bayward direction; negative values and slopes indicate flux into the A8-complex. Values of flux for p.THg and p.MeHg are given in kilograms (kg) and grams (g), respectively. The letters bordered by vertical red lines (A, B, C, and D) represent time periods that are identified by an obvious change in X-Y slope or gate condition. The exact date range and the calculated daily mean flux rate for each time period is summarized in table 9.

Table 9. Daily mean flux rates of mercury species at U.S. Geological Survey station 372525121584701 (A8-TCS fixed monitoring site), as a function of time period.

[Daily mean flux rates for each time period (A, B, C, and D) represent those identified in figures 54 and 55. The date ranges are in month, day, year (mm/dd/yyyy) format. Means are calculated from all individual 15-minute time-integrated and model-predicted concentration data (figs. 52, 53) converted to daily rates. The value in parenthesis represents the standard error of the mean. Negative values represent flux into the A8-complex. Whether the A8-complex represents a source or sink for a given time period and mercury species is indicated. The defined time periods represent: A, 5-gate condition at the A8 tidal control structure (A8-TCS) and low flow of the Guadalupe River prior to the January–February 2017 high streamflow event; B, 5-gate condition at the A8-TCS during the 2017 high-flow event; C, 5-gate condition at the A8-TCS and low flow of the Guadalupe River after the 2017 high flow event; and D, 8-gate condition at the A8-TCS. f.MeHg, filter-passing methylmercury; f.THg, filter-passing total mercury; g/d, gram per day; mg/d, milligram per day; p.MeHg, particulate methylmercury; p. THg, particulate total mercury]

Time period	Start date	End date	Total days	Daily flux rate	Units	Source or sink
			f.THg (fig. 54*A*)			
A	02/10/2016	01/07/2017	332	−77.0 (6.0)	mg/d	Sink
B	010/7/2017	02/28/2017	52	−3,571.0 (156.0)	mg/d	Sink
C	03/01/2017	06/01/2017	92	−85.0 (22.0)	mg/d	Sink
D	06/01/2017	02/27/2018	271	727.0 (12.0)	mg/d	Source
			f.MeHg (fig. 54*B*)			
A	02/10/2016	01/07/2017	332	−12.7.0 (0.4)	mg/d	Sink
B	01/07/2017	02/08/2017	32	127.1 (5.1)	mg/d	Source
C	02/08/2017	06/01/2017	113	−59.8 (1.3)	mg/d	Sink
D	06/01/2017	02/27/2018	271	24.5 (0.9)	mg/d	Source
			p.THg (fig. 55*A*)			
A	02/10/2016	01/07/2017	332	−13.8 (0.2)	g/d	Sink
B	010/7/2017	02/28/2017	52	−134.5 (3.2)	g/d	Sink
C	03/01/2017	06/01/2017	92	−18.9 (0.5)	g/d	Sink
D	06/01/2017	02/27/2018	271	−13.1 (0.2)	g/d	Sink
			p.MeHg (fig. 55*B*)			
A	02/10/2016	01/07/2017	332	−111.0 (2.0)	mg/d	Sink
B	01/07/2017	02/28/2017	52	−601.0 (15.0)	mg/d	Sink
C	03/01/2017	06/01/2017	92	−233.0 (6.0)	mg/d	Sink
D	06/01/2017	02/27/2018	271	−74.0 (3.0)	mg/d	Sink

Bed Sediment

The results associated with bed sediment data collected during Phase 1 from the study area ponds and sloughs can be grouped into three subject areas: (1) ponds and sloughs: shallow sediment routine sampling, 2010–11; (2) pond A6: intensive sampling of shallow sediment, 2010–12; and (3) Alviso Slough deep cores, 2012 and 2016. The deep core results are then used in the calculations associated with the sediment remobilization study. The results of these topical areas are briefly presented below and in the context of addressing the four central synthesis questions (Q.1–4) posed in the "Mercury Synthesis—Organizing Questions" section. All of the primary mercury and nonmercury data associated with both the shallow bed sediment sampling and deep core sampling have been previously published and are available online in machine readable format (Marvin-DiPasquale and others, 2018; Marvin-DiPasquale and others, 2019).

Ponds and Sloughs: Shallow Sediment Routine Sampling, 2010–11

The focus of the 2010–11 shallow sediment sampling efforts was to determine if there were any demonstrable changes in shallow bed sediment mercury concentrations in Alviso Slough or in the A8-complex that were directly attributable to the breaching of pond A6 and during the months immediately afterwards (Q.1) or the initial and gradual opening of the A8-TCS (Q.2 and Q.3). Surface-sediment Model SED.1 was developed to provide an initial qualitative assessment of statistically significant differences that existed between years (2010 versus 2011), between habitat type (ponds versus sloughs), and among the six sampling regions (3 pond regions: A8-complex, A3N, and A16; 3 slough regions: upper Alviso Slough, lower Alviso Slough, Mallard Slough [at site MALSL]). The results of this model are qualitatively presented in appendix 10. Although all mercury parameters (except for percent RHg) and several nonmercury whole sediment and pore-water parameters showed significant differences among the six sampling regions, and many nonmercury parameters showed significant differences between habitat types (ponds versus sloughs), the most salient results with respect to addressing Q.1 are associated with parameters that had a significant interaction effect for the model term [REGION x YEAR]. There were only two mercury parameters (percent MeHg and mercury methylation rate constant [K_{meth}]) in this category. Sediment Model SED.2 (qualitative results in appendix 11) was subsequently employed to more precisely resolve instances where an interaction effect in Model SED.1 was observed. The results of Model SED.2 indicate that, (1) in the lower Alviso Slough region, percent MeHg was higher in 2010 compared to 2011, and (2) in the MALSL reference site, K_{meth} was higher in 2010 compared to 2011. No other regions showed significant differences between 2010 and 2011 for any of the mercury specific parameters. Because MALSL was a reference site, the significant result for K_{meth} was very likely not associated with either of the two management actions under study but was instead due to interannual differences unique to Mallard Slough. This leaves the significant result observed for percent MeHg, which was unique to the lower Alviso Slough model region, as the one demonstrable effect on sediment mercury that may have been directly linked to the breaching of pond A6. Although the exact mechanism underlying the higher percent MeHg during 2010 compared to 2011 is not clear, one likely explanation is that once pond A6 was breached in December 2010, rapid and extensive sediment scour ensued in the lower reaches of Alviso Slough (see "Bed Sediment Mobilization" section). The newly exposed surface-sediment layers (0–2 cm sampled during 2011), which were previously buried at a deeper depth, had a lower percent MeHg concentration compared to the original surface-sediment layers (0–2 cm interval sampled during 2010) that existed prior to the pond A6 breach action.

Although Models SED.1 and SED.2 are appropriate for assessing changes in sediment mercury parameters relative to the breaching of pond A6 (and associated Q.1), they are less appropriate for examining temporal difference that may have occurred among regions as a result of A8-TCS manipulations, because sediment sampling during 2011 included one event prior to (May) and two events after (June and August) the initial opening of the A8-TCS in June 2011. Thus, the temporal categorical model term YEAR (with factors 2010 and 2011), as used in Models SED.1 and SED.2, does not reflect the most appropriate time step. Sediment Model SED.3 was thus developed to provide a more appropriate examination of the temporal trends and included the model terms REGION, sampling EVENT (with factors defined by month and year), and an interaction term [REGION x EVENT]. The results are qualitatively presented in appendix 12. The most salient results for addressing Q.2 and Q.3 are those where the interaction term was statistically significant for specific mercury parameters. For the three pond regions, there were no mercury parameters that had a significant interaction term. For the slough regions, four mercury parameters had a significant interaction term: MeHg concentration, percent MeHg, K_{meth}, and methylmercury production potential (MPP) rate. However, resolving these temporal and spatial interactions further, using an approach that is akin to that taken for sediment models SED.1 and SED.2, is problematic owing to the fact that there is not the necessary replication at site MALSL and ponds A3N and A16, where only one sample was collected per sampling event. Although there is enough replication associated with the A8-complex (multiple sites per sampling event) and the upper and lower Alviso Slough (two sites per region) to assess potential differences among events, we cannot compare any observed difference to the respective reference sites to assess if these differences were specific to the treatment area or more regional in nature.

An alternative statistical assessment was attempted to directly assess Q.2 and Q.3, by which May 2010 and May 2011 data were excluded, June and August data were pooled (within each year), and a variation of sediment model SED.1 was constructed with the main terms of REGION and YEAR as well as the interaction term [REGION x YEAR]. This assessment allowed for the minimal necessary replication (n=2) at the reference sites and a more appropriate year-to-year comparison (through the inclusion of the June and August data only). However, the exclusion of the May 2010 and 2011 data only further limited the number of observations and thereby weakened our ability to detect differences. The results of this analysis (not shown) were, (1) significant interaction terms were not observed for any of the mercury parameters associated with the three pond regions; (2) two mercury parameters (K_{meth} and MPP) associated with the slough regions had a significant interaction effect; (3) when K_{meth} and MPP were subsequently assessed on the basis of individual slough region, only the reference site (MALSL) showed significant differences between years, with both parameters being higher in 2010 than in 2011. Since the only significant YEAR effect observed was for the reference site, we conclude that this was specific to conditions in Mallard Slough generally and likely not associated with either of the two pond beach management actions under consideration.

The conclusions from the overall analysis of the 2010–11 surface-sediment data at the suite of pond and slough sites is that apart from the observed 2010 to 2011 decrease in percent MeHg observed in the lower Alviso Slough, which was most likely attributable to the pond A6 breach, there is little statistical evidence that the initial 1-gate condition of the A8-TCS on June 1, 2011, had any substantial effect on surface-sediment mercury conditions inside of the A8-complex, or in either the upper or lower Alviso Slough. Although there may well have been some effect on benthic mercury cycling in these study regions, our ability to statistically detect differences was limited by the existing data density.

Pond A6: Intensive Sampling of Shallow Sediment, 2010–12

In addition to the pond A6 sediment flux study conducted by University of San Francisco researchers (Callaway and others, 2013), the USGS examined sediment associated THg flux and mercury speciation in 0–2 cm interval sediment samples co-collected for this purpose. Of the 10 sites repeatedly sampled within pond A6 between the December 2010 breach event and March 2013, 9 sites were depositional, and one was erosional. Pond A6 had a mean annual sediment accumulation rate of 20.5±1.2 cm/yr during the December 2010 through March 2013 period of study, as calculated from the mean sediment cumulative accretion and erosion data presented in table 1 of Callaway and others (2013). Given the size of pond A6 (133.6 hectares), this annual mean sediment accumulation rate is equal to approximately 526,000 m^3 of sediment deposited into pond A6 between December 2010 and October 2012, which is fifty-five-fold greater than the approximately 9,500 m^3 of net sediment eroded from the lower one-third of Alviso Slough during the same 23 month period (Foxgrover and others, 2019). This large comparative difference indicates that much of the sediment that was deposited into pond A6 during the first two years after the breach event came from outside of Alviso Slough (that is, sediment likely came from Guadalupe Slough and [or] the southern San Francisco Bay).

The accumulation of THg in pond A6, between the December 2010 breach and November 2012, was subsequently calculated on the basis of the aforementioned sediment accumulation rate, the mean sediment bulk density (0.86 g dw/cm^3) reported by Callaway and others (2013) for the top 5.7 cm sediment interval, and the THg concentration data measured in the 0–2 cm sediment interval at all 10 sites over 5 sampling events. During the 1.9 year period of study since the breach event, areal THg accumulation reached 90.6±17.1 mg/m^2 (fig. 56), which is equivalent to 132±25 kg THg for pond A6 overall and an annualized accumulation rate of 70.2 kg/yr. Between December 2010 and October 2012, approximately 8.5 kg of bed sediment-associated THg was mobilized in the lower one-third of Alviso Slough (Foxgrover and others, 2019), which is fifteenfold lower than the 132 kg THg that was transported into pond A6 during roughly the same time period. However, this ratio is much lower than the above noted fifty-five-fold difference between sediment accumulated in pond A6 and that eroded from the lower one-third of Alviso Slough. These results indicate that the A6 breach had effects beyond the immediate proximity of Alviso Slough, which included more sediment imported into A6 than was eroded from lower Alviso (that is, additional inputs sourced from Guadalupe Slough and the southern San Francisco Bay). This additional sediment had an overall lower THg concentration than bed sediment eroded from lower Alviso Slough itself. These results directly address Q.1 and indicate that the management action associated with the ponds A6 breach resulted in a measurable transfer of previously buried THg from both the lower portion of Alviso Slough and additional nearby regions into the subsided pond during the two-year period following the breach.

In addition to THg, MeHg and RHg concentrations were measured in the samples collected within pond A6. Since these MeHg and RHg are transient and their concentrations can change seasonally, an assessment of accumulation was not done. However, because of the periodicity of the sample collection dates post-pond A6 breach, two during summer (June 2011, July 2012) and two in late fall to winter (December 2011, November 2012), there was a unique opportunity to contrast and compare how their concentrations changed seasonally in 0–2 cm surface-sediment samples. A statistical analysis was conducted on the data grouped by season (summer, winter), for both MeHg and RHg concentrations, as well as their percentages of THg. The

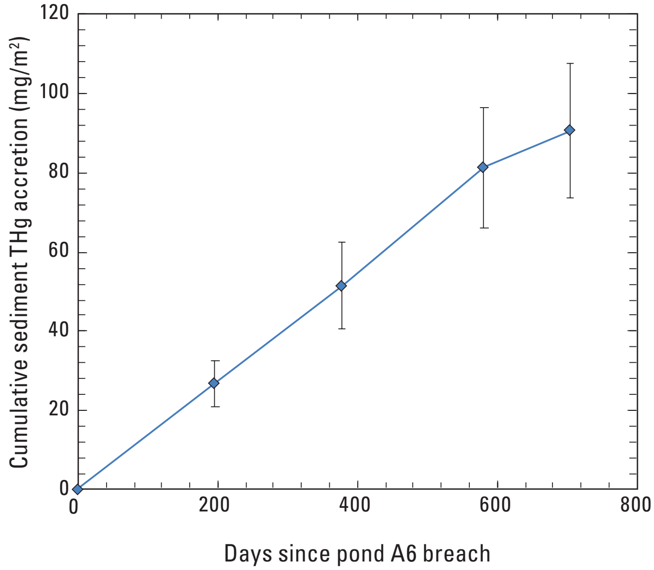

Figure 56. Graph showing cumulative sediment total mercury (THg) areal mass accretion in pond A6. The x-axis denotes the number of days since the pond A6 breach (December 6, 2010; Day = 0). The final date of measurement was November 9, 2012 (Day 704). Values of cumulative sediment THg areal mass accretion are given in milligrams per square meter (mg/m^2) Error bars represent the standard error associated with mean of n=10 sampling locations within pond A6.

LSM model used had fixed model terms of "SEASON" (with factors: summer, winter) and sampling "EVENT" (nested under SEASON), and sampling "SITE" as a random variable. All seasonal comparisons were statistically significant ($p < 0.05$, $n = 40$) with the following results (LSM±standard error): (1) MeHg concentration was greater in summer (4.90±1.61 ng/g) than in winter (2.90±1.61 ng/g); (2) percent MeHg was greater in summer (1.56±0.36 % of THg) than in winter (1.04±0.36 % of THg); (3) RHg concentration was lower in summer (1.23±0.50 ng/g) than in winter (4.91±0.50 ng/g); and (4) percent RHg was lower in summer (0.50±0.25 % of THg) than in winter (1.97±0.25 % of THg). Only THg showed no significant difference between summer (268±22 ng/g) and winter (270±22 ng/g). Although the results do not directly address any of the four central questions (Q.1– 4) defined in the "Mercury Synthesis—Organizing Questions" section, they do demonstrate the seasonally cyclic and counter-posing nature between MeHg and RHg in estuarine wetland surface sediment.

Deep Cores and the Modeling of Bed Sediment and Total Mercury Mobilization in Alviso Slough

The data associated with the Alviso Slough deep cores collected during 2006, 2012, and 2016, and how they were used in combination with biannual bathymetric surveys to model bed sediment THg mobilization as a function of Phase 1 management actions, have been previously published (Marvin-DiPasquale and Cox, 2007; Marvin-DiPasquale and others, 2018; Foxgrover and others, 2019). Here we briefly summarize the key findings associated with this earlier work.

Bed Sediment Mobilization

There was a net erosion of sediment during December 2010–March 2017, but patterns of morphologic change varied both through time and along the length of Alviso Slough (figs. 57, 58). The net erosional portions of the slough deepened by an average of 42 cm from December 2010 to

March 2017 and scour greater than 2 m was confined to localized hotspots immediately adjacent to breaches, culverts, or A8-TCS. In terms of total survey area, 22 percent of the slough eroded more than 0.5 m, 6 percent eroded more than 1 m, and 1 percent eroded more than 1.5 m. To help assess the effect of the A6 breaches versus the A8-TCS on bed sediment and associated THg mobilization, Alviso Slough was divided into three reaches of comparable length (fig. 57): lower (0.2 to 2.7 km from the mouth), mid- (2.7 to 5.0 km from the mouth), and upper Alviso Slough (5.0 to 7.1 km from the mouth). When considering results of sediment erosion and deposition by slough reach, it is informative to do so on two different scales, volumetrically (for example, units of cubic meters per month [m^3/mo]) as well as vertically (for example, units of centimeters per month [cm/mo]), because the size of each reach differs and slough width narrows with distance upstream (about 100 m near pond A6 to 30 m or less near the A8-TCS). To convert from the volumetric scale to the vertical scale, one divides by the surface area of each slough reach (area normalization). Thus, although the greatest volumetric change of sediment mobilization often occurred within the lower slough, closest to pond A6, when normalized by area, the middle and upper slough can exceed the area-normalized vertical change of the lower slough (figs. 59*A*, 60*A*).

Bathymetric change analyses revealed a general pattern of increased sediment erosion during the fall and winter (October–March) and decreased erosion or a net sediment deposition during the spring and summer (April–September) (fig. 59*A*). To investigate potential factors influencing this seasonal variability, measurements of net change were compared to the timing of A8-TCS gate conditions and upstream discharge as measured from streamgage station 11169025 in the Guadalupe River. Much of the study period, fall 2011–spring 2015, happened to coincide with a severe drought in California, which was followed by record precipitation during January–February 2017 (fig. 59*B*). The three periods with highest net erosion rates (fig. 59*A*) spanned a variety of hydrologic conditions and A8-TCS gate conditions. The first of these three periods of peak erosion (October 2011–February 2012) occurred during the onset of the drought when there was very little freshwater discharge, approximately one year after pond A6 was breached, and when a single A8-TCS gate had been opened for 6 months. The second period of erosion (October 2014–April 2015) encompassed a single large discharge event (December 2014 peak of 150 m^3/s), during the period when the A8-TCS opening was expanded from three gates to five gates (late September 2014) and when, for the first time, the A8-TCS remained open throughout the winter. During the third period of erosion (October 2016–March 2017) the A8-TCS had remained open in the 5-gate condition for over 2 years and the Guadalupe River experienced record-high discharges (fig. 59*B*).

The temporal and spatial variability in net sedimentation patterns, as well as erosional peaks of similar magnitude, despite varying watershed discharge conditions, indicate that a combination of factors influence erosion within Alviso Slough. Although restoration actions have undoubtedly influenced sedimentation trends, large-scale natural sedimentation patterns in the southern San Francisco Bay area (for example, those driven by precipitation, river discharge, and tides) and pre-restoration trends confirm that erosion is not driven solely by restoration actions. A comparison between a 2005 survey (Jaffe and Foxgrover, 2006) and the 2010 baseline indicates that Alviso Slough also experienced an average net erosion in the 5.7 years preceding the restoration project. Over the entire slough, the average area-normalized net erosion rate was 1.8 cm/yr during April 2005–December 2010 (prior to the pond A6 breaches and A8-TCS operations but spanning the time period when the Island ponds were breached along Coyote Creek). This pre-restoration rate of 1.8 cm/yr is comparable to the net erosion rate of 2.4 cm/yr measured during the Phase 1 restoration from December 2010 to October 2016. However, it is important to emphasize that net sedimentation rates can vary greatly from year to year. Thus, it is most valuable to consider sediment mobilization patterns across multiple timespans to assess the significance of differences between time periods.

Cumulative net sediment erosion in lower Alviso Slough began to slow after 3–5 years, and parts downstream of the pond A6 breaches deposited sediment (fig. 58), a possible indication that this reach was beginning to approach a new equilibrium. In contrast, cumulative net change for the middle and upper Alviso Slough followed a more stable-to-erosional trend (Foxgrover and others, 2019). An analysis of daily mean sediment erosion, by slough reach, was done for the periods before (PRE) and after (POST) the opening to five gates at the A8-TCS (5-gate condition, table 10). Although the PRE versus POST periods were not statistically different, chiefly because of the limited number of observations (n=6–7 bathymetric change survey periods per regression analysis), the resulting spatial trend (by slough reach) indicated a 57 percent increase in erosion in the upper reach, a 22 percent increase in the middle reach, and a 18 percent decrease in the lower reach, in the period following the opening of the A8-TCS to the 5-gate condition (table 10). These results lend further credence to the suggestion that transition from the 3-gate to 5-gate condition represented a significant tipping point in the balance between hydrology (increased tidal prism) and response in sediment erosion, particularly in the upper reach of Alviso Slough, as was suggested above with respect to the Q-Ratio analysis (fig. 45; section "The Effect of A8-TCS Gate Operations on Alviso Slough Discharge—The Q Ratio").

The maximum depth of scour throughout much of the middle and upper Alviso Slough reaches was coincident with the last survey period (October 2016–March 2017, see Foxgrover and others, 2019), which indicates that the morphology was still evolving, potentially in direct and continued response to both upstream discharge and management actions associated with A8-TCS manipulations that preceded this period.

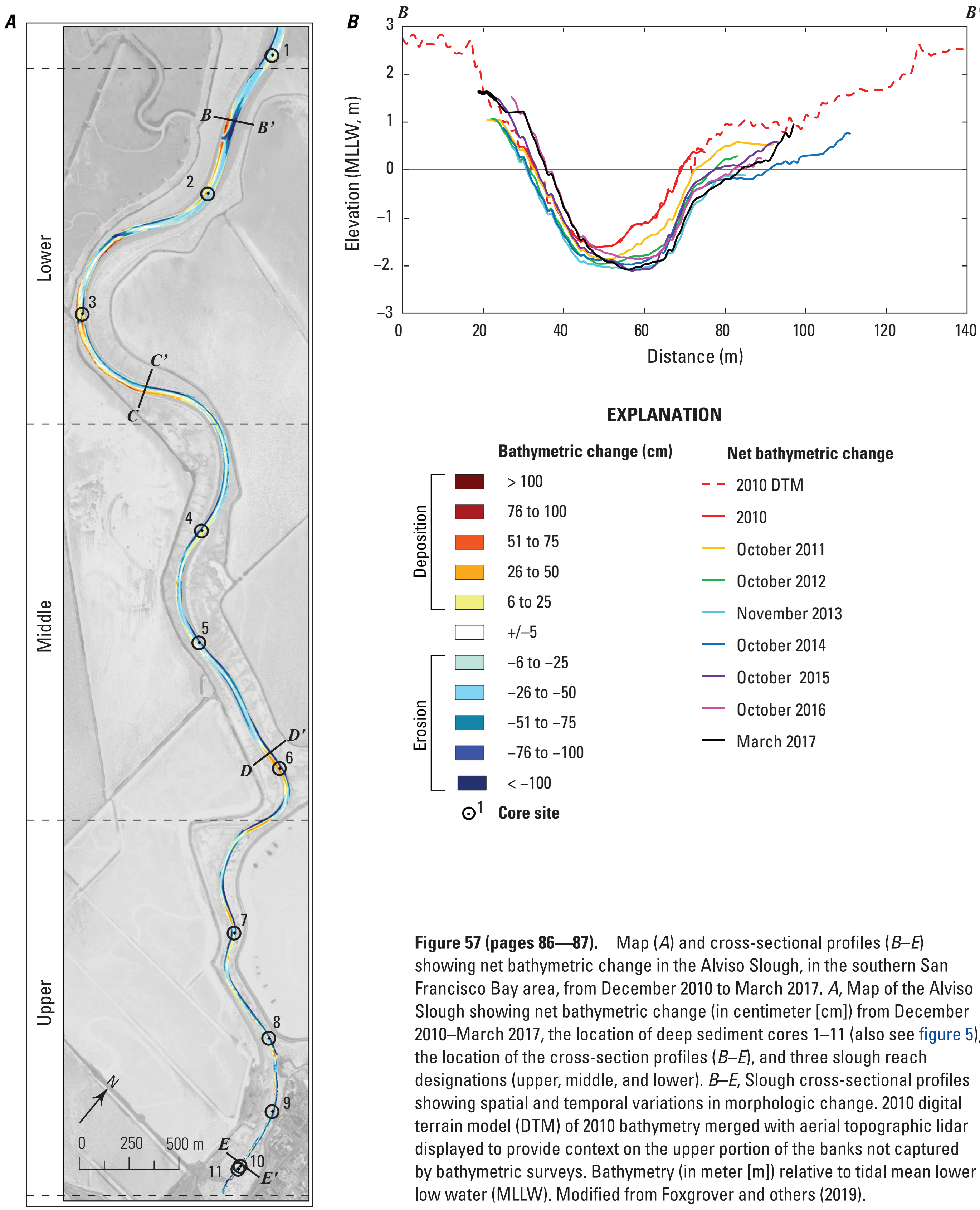

Figure 57 (pages 86—87). Map (*A*) and cross-sectional profiles (*B–E*) showing net bathymetric change in the Alviso Slough, in the southern San Francisco Bay area, from December 2010 to March 2017. *A*, Map of the Alviso Slough showing net bathymetric change (in centimeter [cm]) from December 2010–March 2017, the location of deep sediment cores 1–11 (also see figure 5), the location of the cross-section profiles (*B–E*), and three slough reach designations (upper, middle, and lower). *B–E*, Slough cross-sectional profiles showing spatial and temporal variations in morphologic change. 2010 digital terrain model (DTM) of 2010 bathymetry merged with aerial topographic lidar displayed to provide context on the upper portion of the banks not captured by bathymetric surveys. Bathymetry (in meter [m]) relative to tidal mean lower low water (MLLW). Modified from Foxgrover and others (2019).

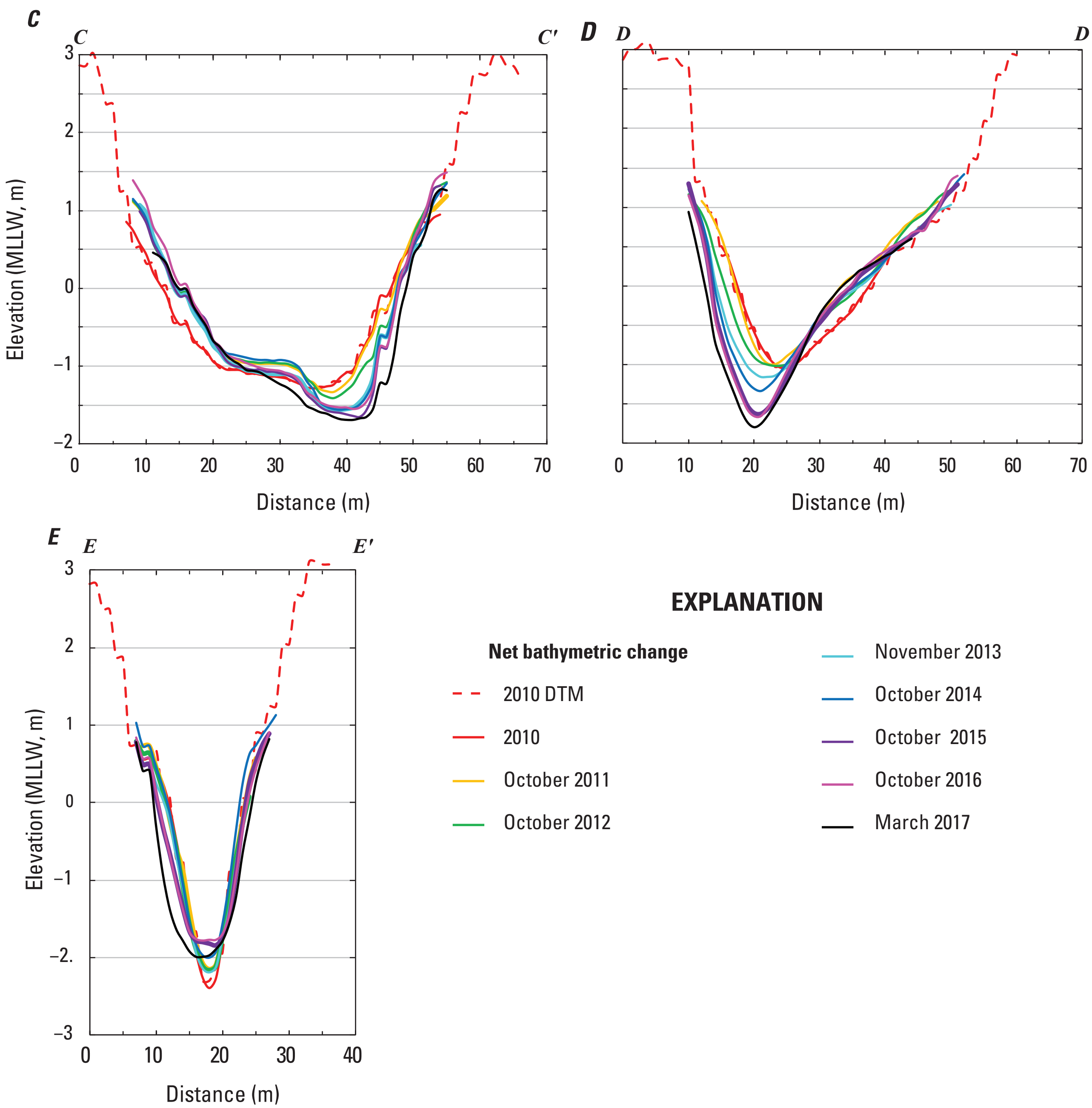
C
C
C′
Elevation (MLLW, m)
3
2
1
0
–1
–2
0
10
20
30
40
50
60
70
Distance (m)
D
D
D′
0
10
20
30
40
50
60
70
Distance (m)
E
E
E′
3
2
1
0
–1
–2.
–3
Elevation (MLLW, m)
0
10
20
30
40
Distance (m)
EXPLANATION
Net bathymetric change
2010 DTM
2010
October 2011
October 2012
November 2013
October 2014
October 2015
October 2016
March 2017

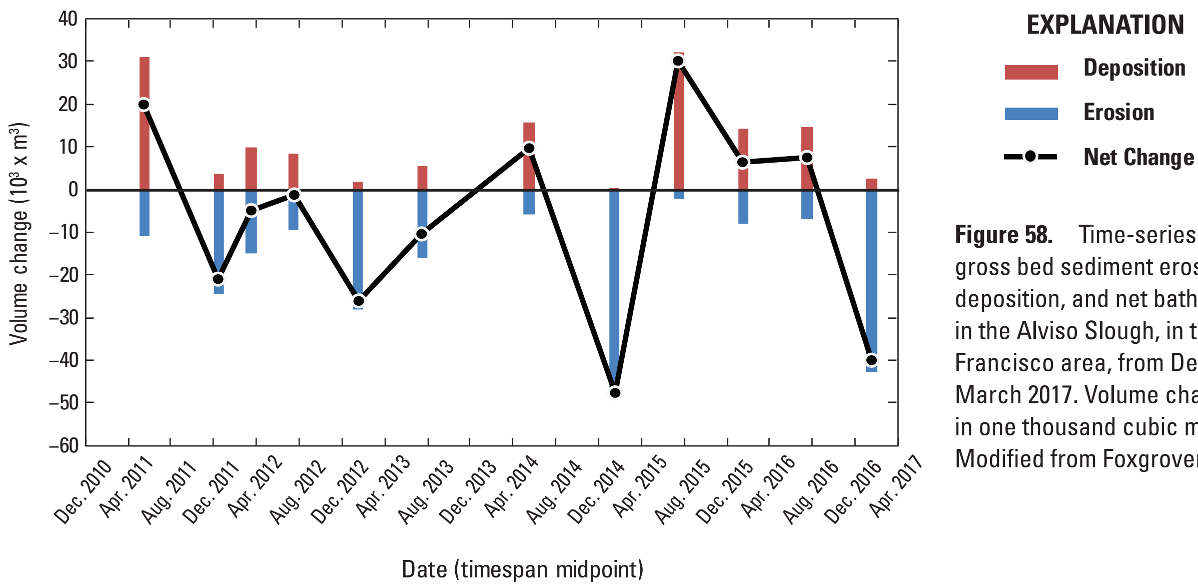

Figure 58. Time-series graph showing gross bed sediment erosion, gross deposition, and net bathymetric change in the Alviso Slough, in the southern San Francisco area, from December 2010 to March 2017. Volume change measured in one thousand cubic meters (m^3 x 10^3). Modified from Foxgrover and others (2019).

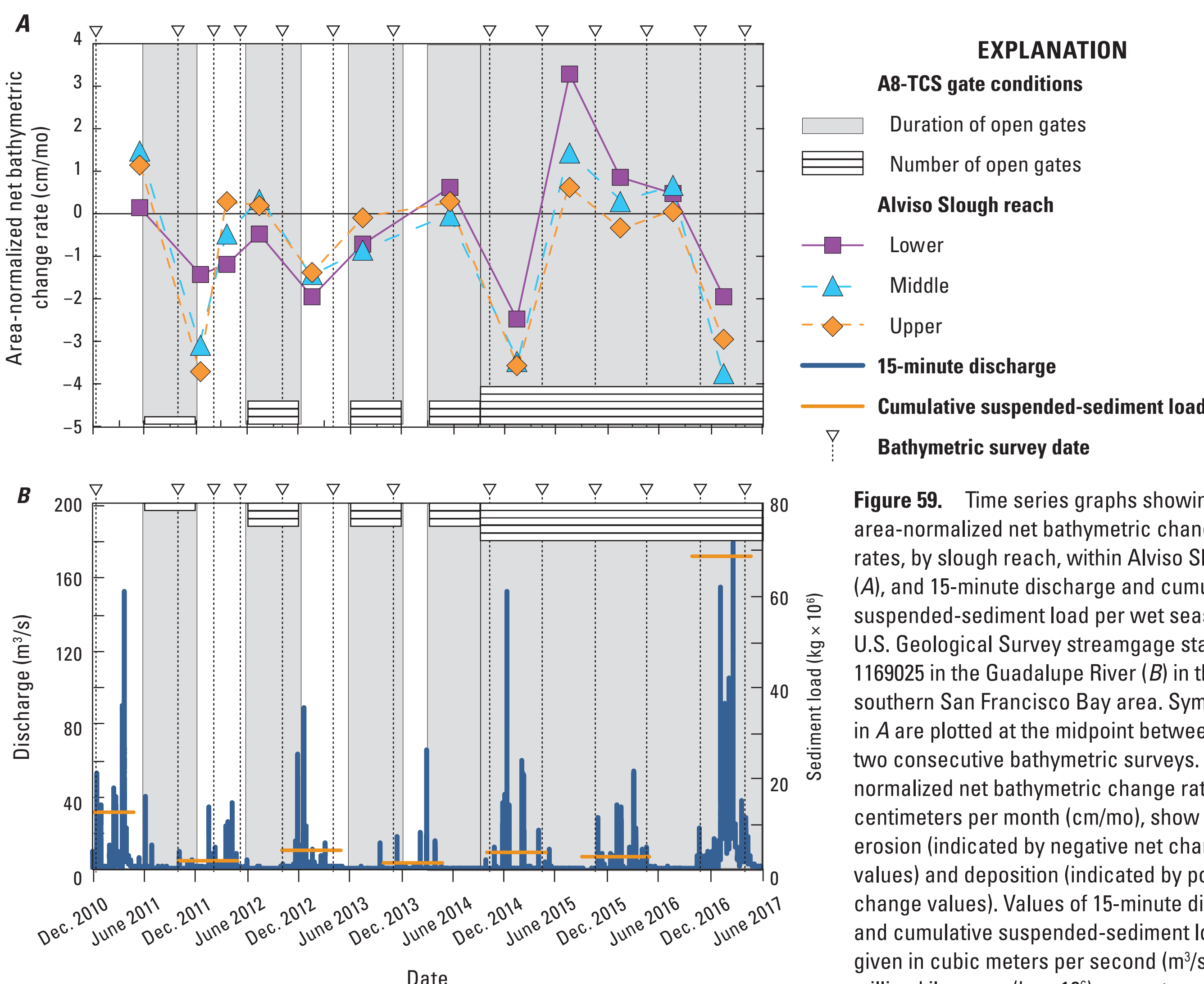

Figure 59. Time series graphs showing area-normalized net bathymetric change rates, by slough reach, within Alviso Slough (*A*), and 15-minute discharge and cumulative suspended-sediment load per wet season at U.S. Geological Survey streamgage station 1169025 in the Guadalupe River (*B*) in the southern San Francisco Bay area. Symbols in *A* are plotted at the midpoint between two consecutive bathymetric surveys. Area-normalized net bathymetric change rates, in centimeters per month (cm/mo), show sediment erosion (indicated by negative net change values) and deposition (indicated by positive net change values). Values of 15-minute discharge and cumulative suspended-sediment load are given in cubic meters per second (m^3/s) and million kilograms (kg x 10^6) per wet season, respectively. Graphs modified from Foxgrover and others (2019).

Bed Sediment Associated Total Mercury Mobilization

The Alviso Slough sediment deep cores revealed a general pattern of higher THg concentrations in deeper sediments in the middle and upper reaches of the slough. The trend in THg concentrations did not show a clear increase of THg with core depth or with distance upstream, but instead show an increase of THg concentrations at depths > 30 cm, in which the cores from the middle and upper reaches of the Alviso Slough had the highest overall concentrations, and the three highest peak measurements (all > 4,000 ng/cm^3) were from the upper reach of the Alviso Slough (see Marvin-DiPasquale and Cox (2007) and Foxgrover and others (2019) for core profile plots). The THg concentration data were used in combination with the above measurements of sediment scour to estimate the amount of deep-bed sediment-associated THg remobilized within the slough. During the first 3 years of the restoration project, THg remobilization increased modestly during the winter and was coincident with increased rates of sediment erosion (fig. 60). From the perspective of total sediment volume, the greatest amount of erosion and associated THg remobilization occurred in the lower slough (fig. 61), where mercury concentration is lowest. However, when normalized on the basis of area, peak periods of mean vertical erosion and THg remobilization were typically higher in the middle and upper reaches of Alviso Slough (fig. 60). During the first 4 years of study (through September 2014), when A8-TCS management varied between the 0-gate, 1-gate, and 3-gate conditions, THg remobilization rates were similar among the three defined slough reaches and varied between 0.6–6.5 milligram of THg per month per square meter (mg/mo/m^2) (fig. 60). However, after the 5-gate condition was initiated, peak THg remobilization rates were substantially higher in the middle and upper reaches of Alviso Slough (9.6–15.7 mg/mo/m^2), as compared with the lower reach of Alviso Slough (1.6–5.4 mg/mo/m^2). As analyzed by regression analysis, along with sediment erosion for each slough reach

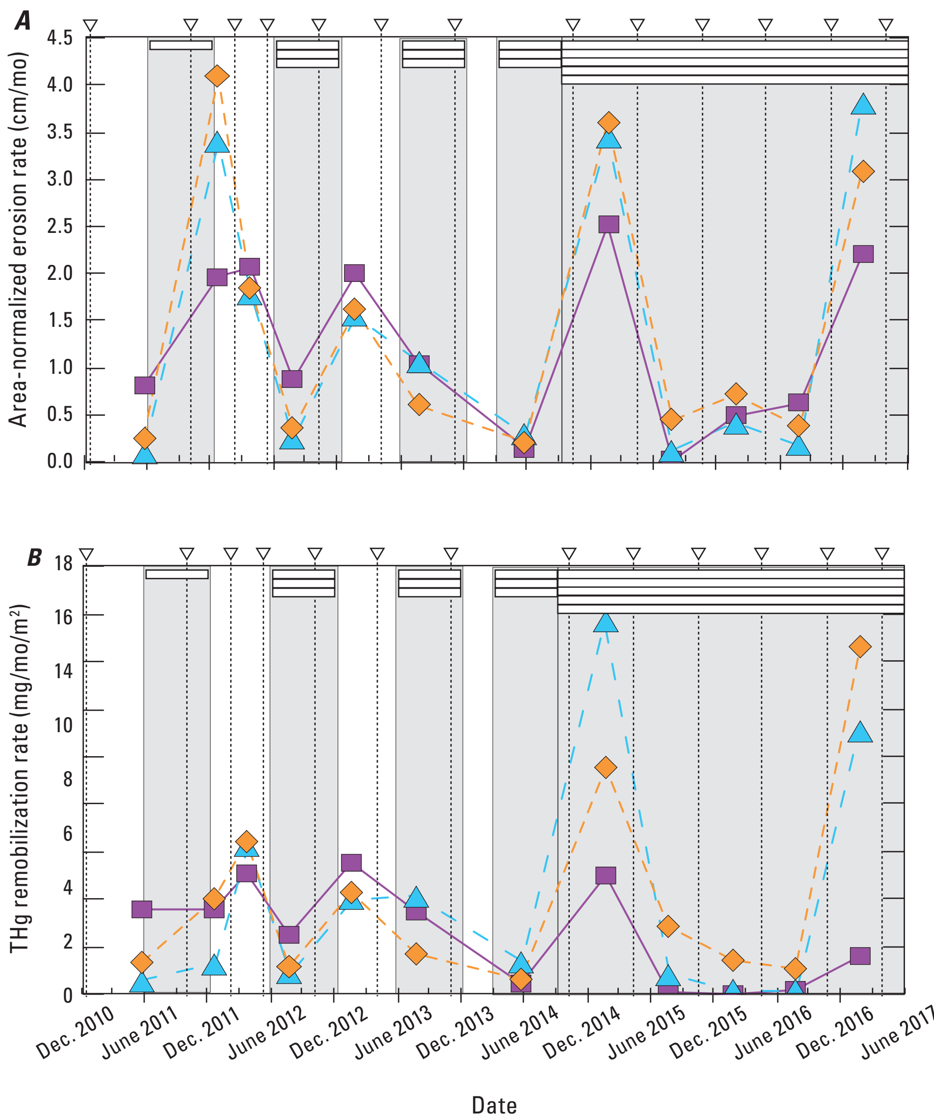

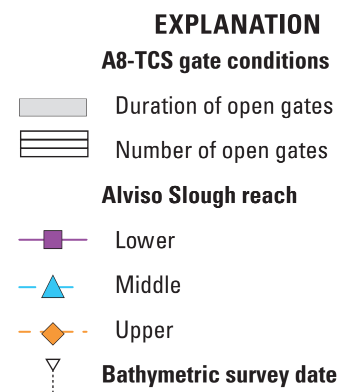

Figure 60. Time series graphs showing the area-normalized sediment gross erosion rate (*A*), in centimeters per month (cm/mo), and rate of total mercury (THg) remobilization (*B*), in milligrams per month per square meters (mg/mo/m^2), by reach in the Alviso Slough of the southern San Francisco Bay area. Symbols in *A* and *B* are plotted at the midpoint between two consecutive bathymetric surveys. Values for sediment gross erosion rate and THg remobilization rate are given in centimeters per month (cm/mo) and milligrams per month per square meters (mg/mo/m^2), respectively. Modified from Foxgrover and others (2019).

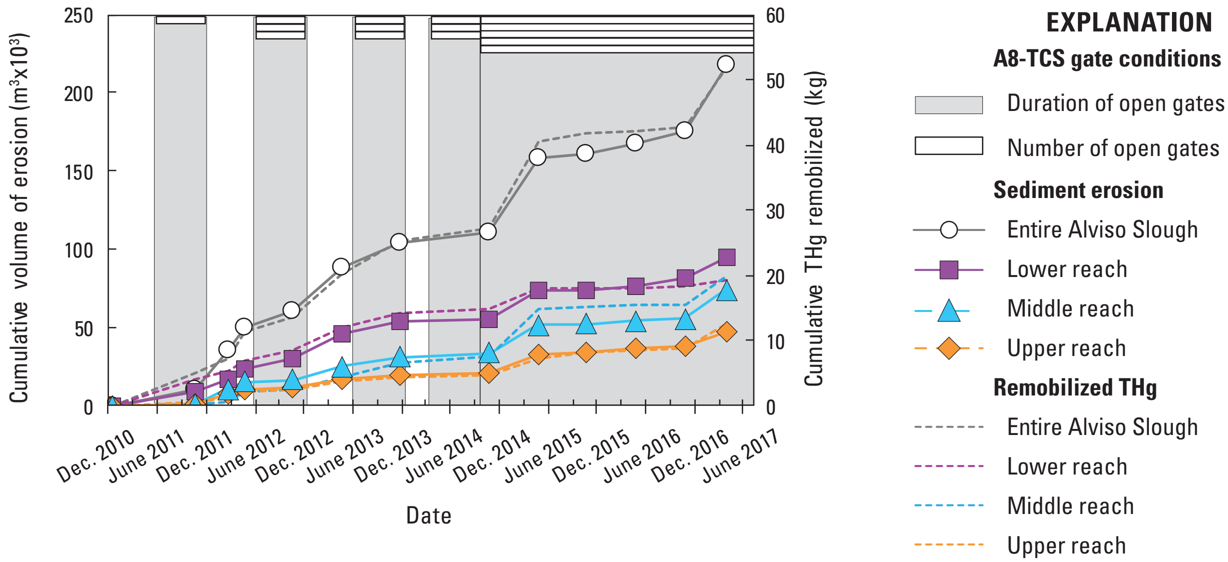

Figure 61. Time series graph showing the cumulative volume of sediment eroded by reach in the Alviso Slough of the southern San Francisco Bay area. Values of cumulative volume eroded and cumulative mass of total mercury (THg) remobilized are given in one thousand cubic meters ($m^3 \times 10^3$) and in kilograms (kg), respectively. Modified from Foxgrover and others (2019).

section, we find that the remobilization of THg nearly doubled (94 percent increase) after establishment of the 5-gate condition, and that this increase was statistically significant (table 10). Likewise, THg remobilization in the middle slough reach increased 44 percent after the transition from a 3-gate to 5-gate condition, although the PRE and POST periods were not significantly different. In contrast, there was a 67 percent decrease in THg remobilization in the lower reach in the period following the transition from a 3-gate to 5-gate condition, and this decrease was statistically significant (table 10).

The two large peaks in erosion and associated THg mobilization observed during the winters of 2014–2015 and 2016–2017 were coincident with increased maximum depths of scour, exposing previously buried layers of sediment with particularly elevated THg concentrations in the middle and upper slough (Foxgrover and others, 2019). For the entire slough, an estimated 52±3 kg of THg was remobilized during the 6.2 years bathymetry changes were measured since restoration began (fig. 61). This equates to a mean annual THg flux of 8.2 kg/yr associated with bed sediment remobilization, during the period of study.

The estimated 52 kg of THg remobilized is nearly 80 percent of the 66 kg initially projected by Marvin- DiPasquale and Cox (2007) under the 4-gate condition (20 ft) A8-TCS opening scenario and approximately 40 percent of the 125 kg projected under the 8-gate condition (40 ft) A8-TCS opening scenario. These earlier projections used a simple estimate of changes in cross-sectional area and average THg concentration values on the basis of five deep sediment cores collected during 2006 only. Furthermore, these earlier estimates were for the full 50-year planning horizon of the project and considered A8-TCS gate operations only and did not consider the breaching of pond A6. Likewise, there are several uncertainties associated with the updated THg remobilization calculation provided here and several reasons why the current estimate of 52 kg of THg mobilized between December 2010 and March 2017 may be considered a minimum estimate (see Foxgrover and others, 2019). Overall, the morphology of the middle and upper reaches of Alviso Slough is still likely evolving and will continue to serve as a source of THg remobilization in the future. This may be particularly true if and when more breach points are added along Alviso Slough, like the one being considered at the north-western corner of pond A8.

Another important component to consider is the amount of THg being delivered from the upstream watershed. McKee and others (2017) emphasized the importance of rare, large flow events transporting the bulk of suspended sediments and associated contaminants from the upstream watershed. These authors proposed using a climatically adjusted mean to account for such variability and on the basis of data spanning water years 2003–2016, derived a THg flux estimate of 139 kg/yr for USGS streamgage station 11169025 in the Guadalupe River. This estimate is sixteen-fold higher than the 8.2 kg/yr mean annual THg flux associated with bed sediment remobilization calculated in this study. Furthermore, through a targeted, storm-focused sampling regime, McKee and others (2018) estimated a flux of 70 kg of THg at the same gaging station over a single series of storms during January 7–13, 2017. Additional storms occurred during the following months that were not sampled,

Table 10. Daily mean bed sediment erosion rate and total mercury mobilization, by Alviso Slough reach, before and after the A8-TCS 5-gate condition.

[Bed sediment erosion rates are provided on both a volumetric, in cubic meters per day (m^3/d), and vertical (area normalized in millimeters per day [mm/d]) basis. Daily rates are calculated as the linear slope associated with the regression of cumulative bed sediment erosion or total mercury remobilization versus the number of days since December 6, 2010 (date of pond A6 Breach). The standard error of the slope value is given in parenthesis (#). For each Alviso Slough reach and the entire Alviso Slough (total), regressions were conducted on bathymetric survey data collected before (PRE, n=7) and after (POST, n=6) the opening the A8-TCS to the 5-gate condition (shown as PRE [5 gates] and POST [5gates] respectively). Data associated with time interval bounded by the November 1, 2013, and October 23, 2014, bathymetric surveys were included in both the PRE and POST slope calculations. The latter survey occurred 24 days after the A8-TCS was opened to the 5-gate condition and 356 days after the previous survey. Thus, for the bathymetric change interval bounding these two surveys, 93 percent of it was during the PRE [5-gate condition] period and 7 percent was in the POST period. The percent (%) of change for the POST condition, relative to the PRE condition, is given as change (%). An analysis of covariance was conducted to compare if PRE versus POST slopes values were significantly different in each case. Slopes that were not significantly (N.S.) different are indicated with a probability (p) value of > 0.05. The F-statistic and p value are given in cases for which a significant difference was found, with the numbers in parenthesis representing the numerator and denominator degrees of freedom (ndf, ddf), respectively]

Slough reach	PRE [5 gates]		POST [5 gates]		Change (%)	F-stat	p
			Sediment cumulative volumetric erosion (m^3/d)				
Upper	16.00	(3.30)	25.10	(4.80)	57	N.S.	> 0.050
Middle	28.30	(4.50)	34.50	(8.60)	22	N.S.	> 0.050
Lower	44.60	(6.60)	36.50	(6.90)	−18	N.S.	> 0.050
Total	88.90	(13.90)	96.10	(20.10)	8	N.S.	> 0.050
			Sediment vertical (area normalized) erosion (mm/d)				
Upper	0.33	(0.07)	0.52	(0.10)	57	N.S.	> 0.050
Middle	0.37	(0.06)	0.46	(0.11)	22	N.S.	> 0.050
Lower	0.43	(0.06)	0.35	(0.07)	−18	N.S.	> 0.050
Total	0.39	(0.06)	0.42	(0.09)	8	N.S.	> 0.050
			Total mercury remobilized (g/d)				
Upper	3.70	(0.60)	7.20	(1.50)	94	5.97 (1, 9)	0.037
Middle	7.00	(0.60)	10.10	(3.10)	44	N.S.	> 0.050
Lower	10.80	(1.40)	3.50	(1.30)	−67	12.89 (1, 9)	0.006
Total	21.50	(2.40)	20.80	(5.60)	−3	N.S.	> 0.050

which McKee and others (2018) suggest that 100s or even 1,000 kg of THg could have been transported over that single, albeit large, wet season of water year 2017. Thus, THg flux from the upper watershed may be substantially larger THg flux associated with episodes of Alviso Slough bed sediment scour, which are the focus of our study.

Hydrodynamic and Geomorphic Models

The hydrodynamic and geomorphic models were successful in demonstrating the effect of restoration on sediment scour in Alviso Slough and the associated mercury remobilization and transport (Rey, 2015; Achete, 2016; van der Wegen and others, 2018). Model simulations included runs with the existing levee breaches, culverts, and control structures (for example, the A8-TCS); current configuration with sea level rise; and changed configurations with additional levee breaches. Model results included, (1) breaching of pond A6 levees induced scour, especially in the vicinity of the breaches and in the bayward part of Alviso Slough, by increasing the tidal prism and thereby flow velocities; (2) particle tracking showed that scoured mercury-contaminated sediment was deposited throughout the slough, in ponds, and in the San Francisco Bay; (3) modeled sediment deposition in pond A6 was several times the amount eroded from Alviso Slough, indicating that the San Francisco Bay is a significant source of sediment for pond A6; (4) residual flows in Alviso Slough are subject to both tidal and nontidal components, trend landward during periods of low Guadalupe River discharge (and conversely, trend bayward during periods of high discharge), and exhibit spatially variable exchange with both pond A6 and the A8-complex (fig. 62); (5) residual sediment transport in Alviso Slough is landward only along pond A6 and bayward elsewhere along Alviso Slough during low Guadalupe River discharge and bayward throughout Alviso Slough during high Guadalupe River discharge (fig. 63); (6) residual sediment transport is into pond A6 and the A8-complex and is dominated by transport during high river discharge events

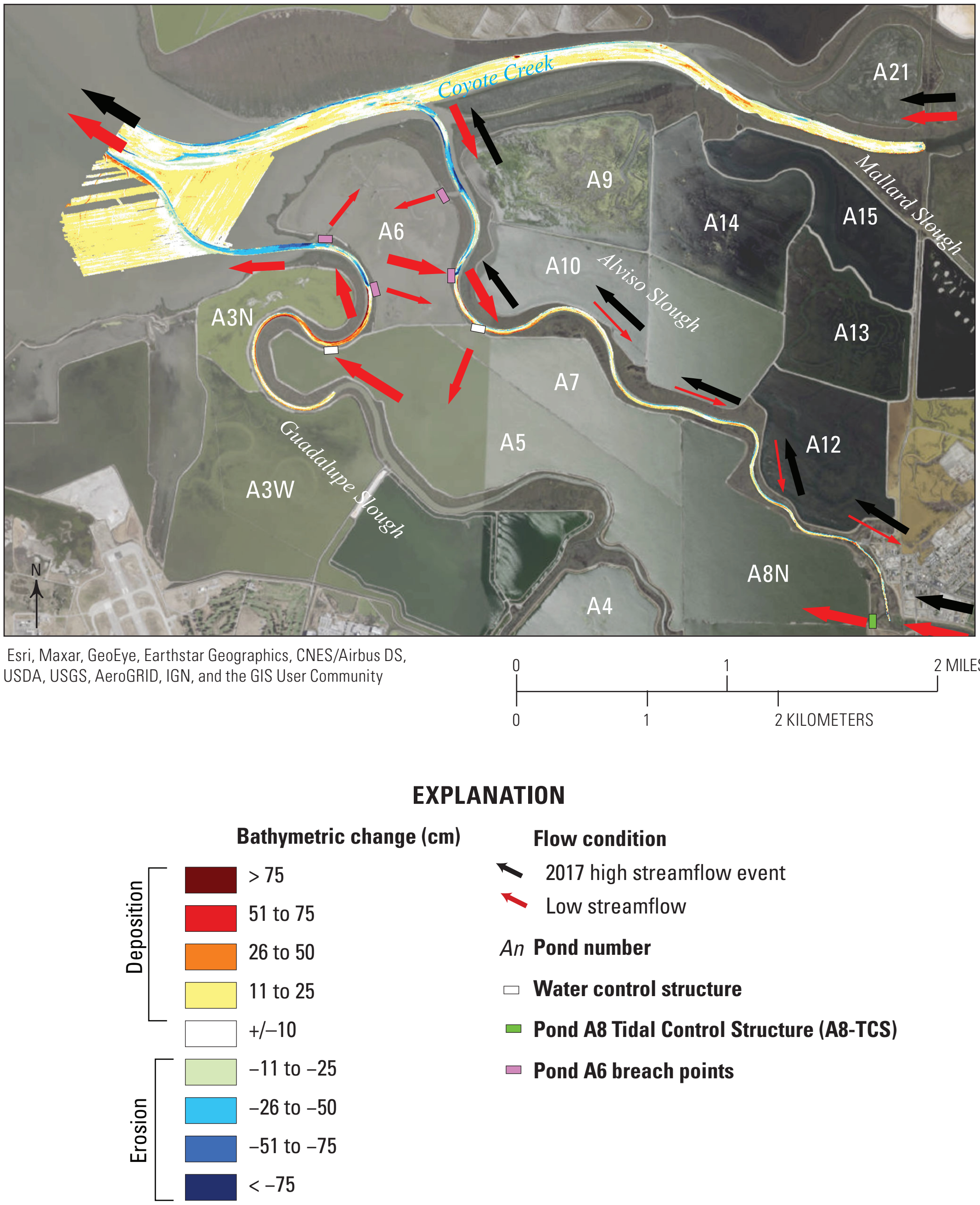

Figure 62. Satellite image of southern San Francisco Bay area showing residual streamflow and bathymetric change of the Coyote Creek and Alviso and Guadalupe Sloughs during 2012–16 low streamflow conditions (red arrows) and during the January–February 2017 high streamflow event (black arrows). Arrow size approximates transport volumes. Values of bathymetric change are given in centimeters (cm). Figure modified from van der Wegen and others (2018).

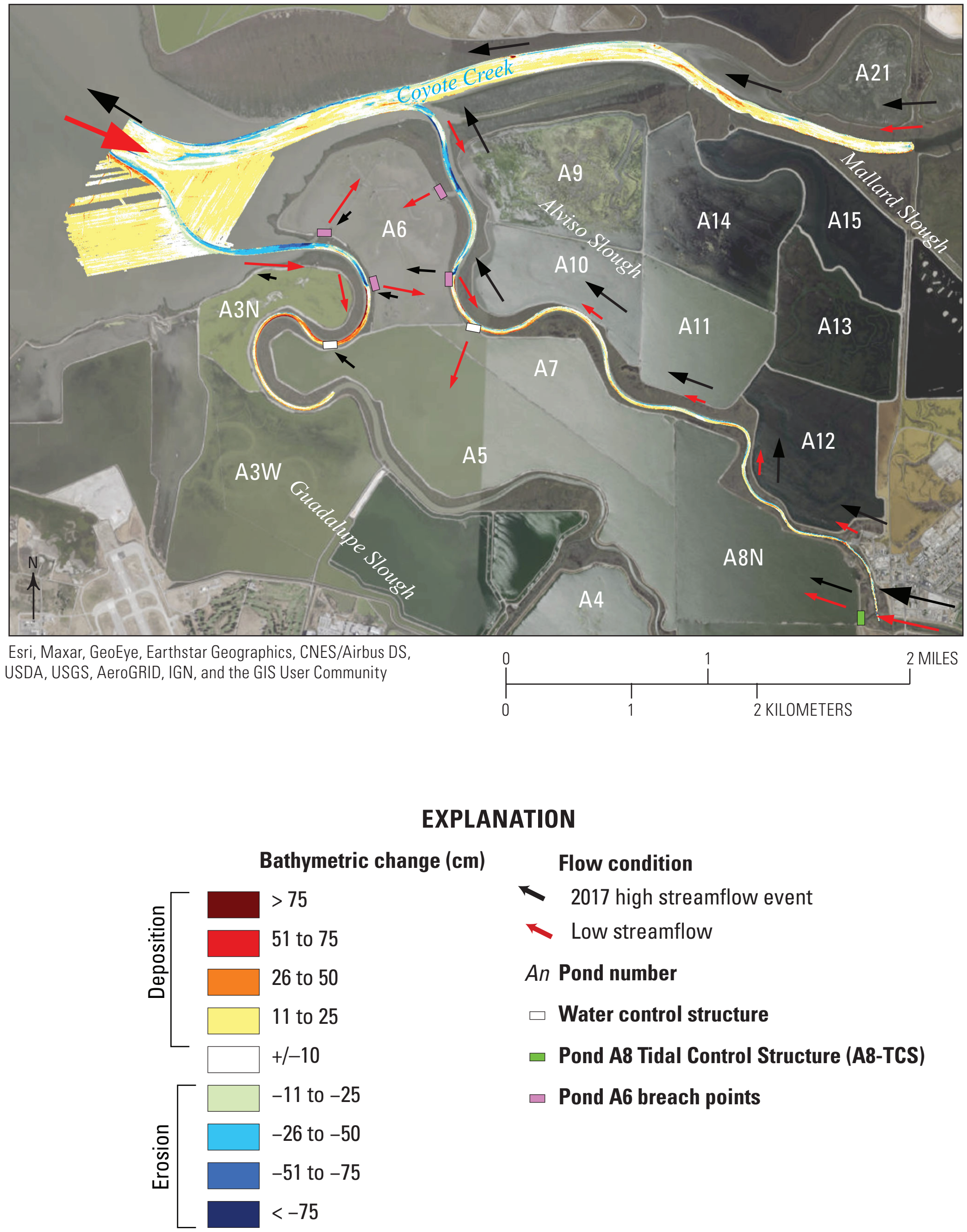

Figure 63. Satellite image of southern San Francisco Bay area showing residual sediment transport during 2012–16 low streamflow conditions (red arrows) and during the January–February 2017 high streamflow event (black arrows). Arrow size approximates transport volumes. Values of bathymetric change are given in centimeters (cm). Modified from van der Wegen and others (2018).

(fig. 63); (7) compared to the current configuration of existing breaches and the A8-TCS (the reference condition, fig. 64*A*), additional levee-breaching simulated scenarios increased scour in the Alviso Slough and sediment deposition into pond A6 and the A8-complex (fig. 64*B*); and (8) sea-level rise increases sediment scour in Alviso Slough and deposition into pond A6 and the A8-complex (fig. 64*C*).

Although this modeling effort was extensive, the model can be improved. For example, the fully geomorphic model was able to reproduce geomorphic change but was not able to accurately reproduce the observed SSC. This is a known challenge for geomorphic modeling. We conclude that SSC model results can be improved with more sensitivity analysis with respect to the floc layer model and by increasing the settling velocity for particles. Also, a 3D hydrologic flow model may improve the fully geomorphic model results. However, even in the current state of development the model is useful for understanding how water and mercury-contaminated sediment moves through Alviso Slough and the adjacent ponds. It is especially useful for evaluating restoration scenarios such as additional levee breaching and to prepare for changes in the system that will accompany sea-level rise.

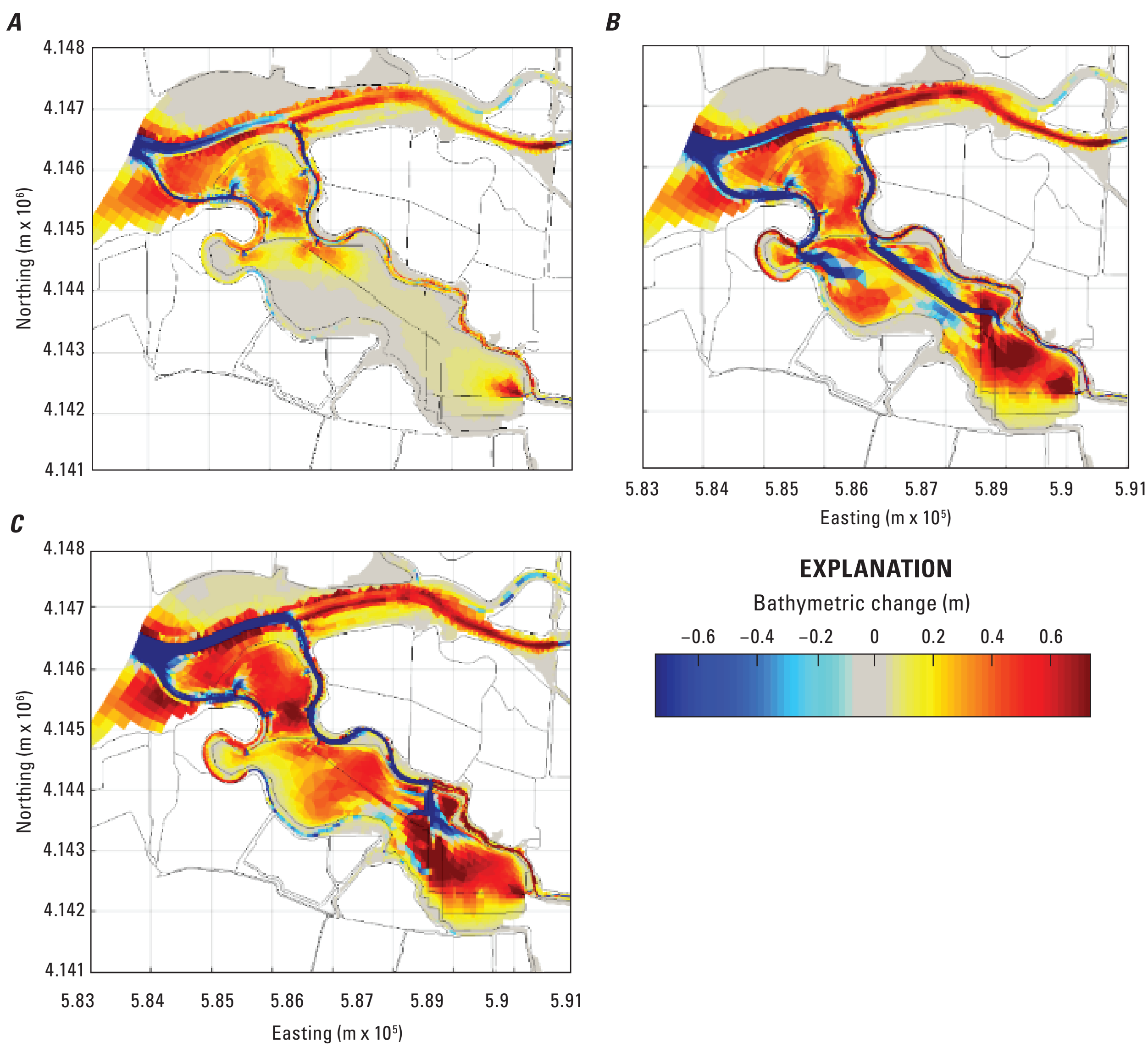

Figure 64. Model maps of southern San Francisco Bay area showing erosion and sedimentation patterns between 2010 and 2017 for the current reference condition (*A*), the reference condition with a 0.5-meter rise in mean sea level (*B*), and adding additional breaches (*C*). The reference condition refers to the current configuration of breaches and the existence of the A8-TCS along the Alviso Slough. Bathymetric change is given in meters (m). Modified from van der Wegen and others (2018).

Mercury Specific Modeling Results

The primary hydrodynamic modeling results that relate specifically to mercury are associated with the research described in Achete (2016), where 3-month simulations were conducted for a range of pond breach scenarios. Each scenario considered the simultaneous remobilization of three distinct pools of Alviso Slough bed sediment, representing comparatively low (lower Alviso Slough), moderate (upper Alviso Slough) and high (middle Alviso Slough) THg concentrations (model fractions fr05 (168 ng/ cm^3), fr03 (370 ng/ cm^3), and fr04 (757 ng/ cm^3), respectively). Although these three reach areas are similar to those defined in Foxgrover and others (2019), in this instance the three reach areas were defined by the location of discrete deep cores previously collected, as described in Achete (2016). Although the original modeling effort included five scenarios, we focus here on the results of the two extremes, which are referred to as the base-case scenario (no ponds breached) and the open-case scenario (existing pond A6 breaches along Alviso Slough and A8-TCS at full opening [8-gate condition] plus a theoretical full breach in the northwest corner of pond A8). This modeling effort did not include the two existing breaches in pond A6 along the Guadalupe Slough, nor the existing pond A5 intake. Results from this 3-month model simulation of sediment and mercury transport (fig. 65) are summarized as follows:

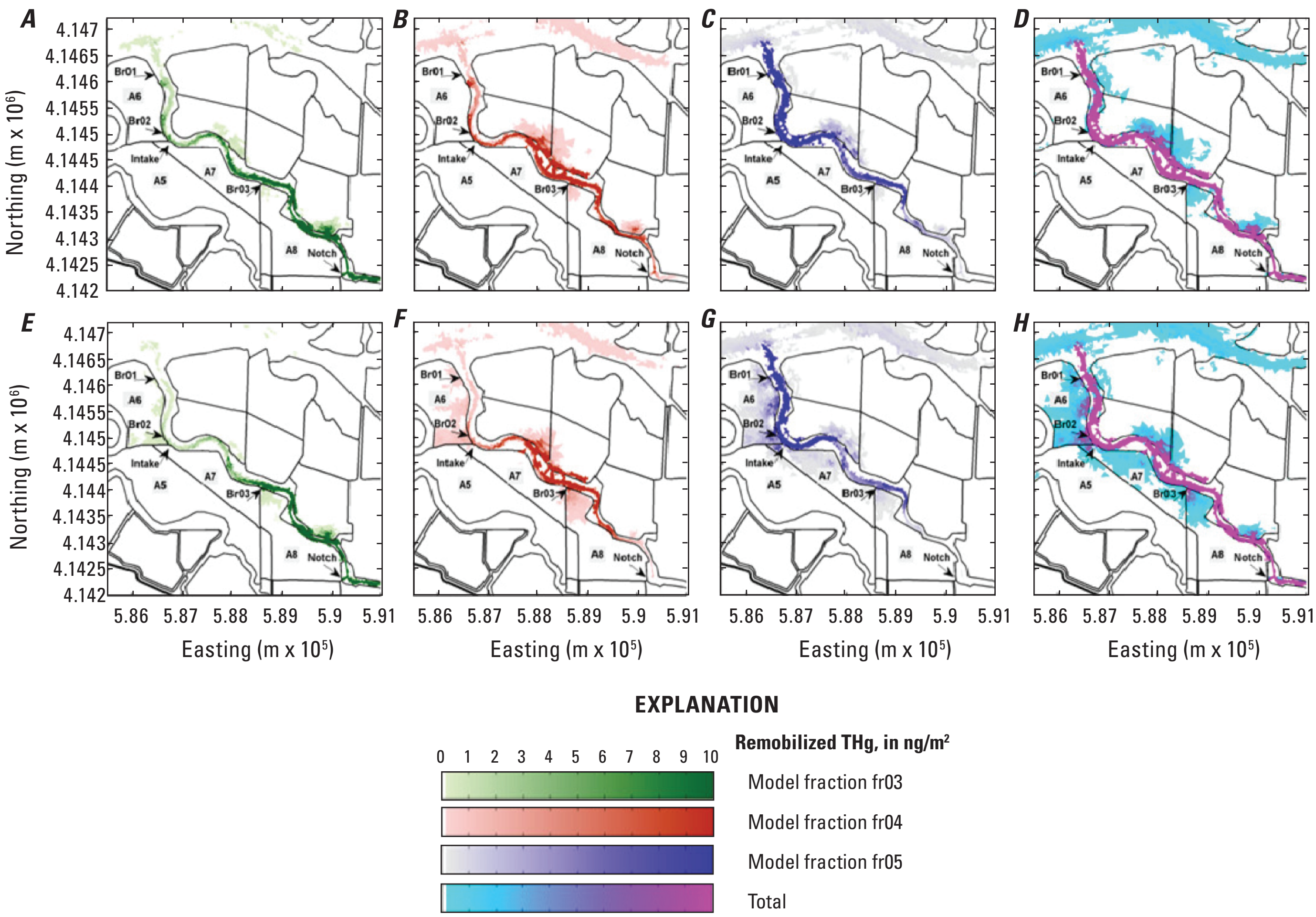

Figure 65. Maps of mercury-contaminated bed sediment remobilized from upper, middle, and lower Alviso Slough, based on 3-month model simulations, for both the base-case and open-case scenarios. The base-case scenario (*A*–*D*) assumes no ponds are breached. The open-case scenario (*E*–*H*) assumes multiple breaches (black arrows) along the Alviso Slough only, including the two breaches in pond A6 (Br01 and Br02), the intake point in pond A7 (Intake), a theoretical breach in the northwest corner of pond A8 (Br03), and the A8-TCS open to eight gates. Bed sediment originating from the three defined reaches of Alviso Slough (see fig. 57*A*) is identified with fraction numbers (fr##) and with differing levels of total mercury (THg) concentration (in brackets and given in nanograms per cubic centimeters [ng/cm^3]): *A* and *E*, upper Alviso Slough reach (fr03 [370 ng/cm^3], moderate THg, green); *B* and *F*, middle Alviso Slough reach (fr04 [757 ng/cm^3], high THg, red); *C* and *G* lower Alviso Slough reach (fr05 [168 ng/cm^3], low THg, blue). The maps shown for the individual fractions and the combination of all three fractions (*D* and *H*) represent the sediment distribution at the last time step (after 3 months) of the base-case and open-case scenarios. The color scale represents areal THg concentration in nanograms per square meters (ng/m^2). Figure modified from Achete 2016.

- The sediment load associated with Guadalupe River is very low compared to the amount of sediment in the water column from bed sediment remobilization in Alviso Slough, and the majority of this riverine load deposits upstream from the A8-TCS.

- San Francisco Bay derived sediment is primarily transported into Coyote Creek or into pond A6 under the open-case scenario.

- Under the base-case scenario, 1,300 tons of remobilized bed sediment and 0.35 kg of associated THg (fr03) from upper Alviso Slough are transported towards the San Francisco Bay all the way to the mouth of Alviso Slough. Under the open-case scenario, the majority of fr03 sediment remains in place (is not remobilized) or is transported upstream and transported into pond A8 (about 1,000 tons of sediment and 0.26 kg THg), and a smaller amount is transported into pond A6 and < 0.1 percent exported to the San Francisco Bay.

- Under the base-case scenario, 900 tons of remobilized bed sediment and 0.52 kg of associated THg (fr04) from middle Alviso Slough are transported out to the bay, whereas the majority of sediment and THg remains mostly within the slough (similar to fr03). Under the open-case scenario, 2,200 tons of sediment and 1.28 kg of THg is transported into pond A6, partly owing to the change in the transport convergence point, relative to the base-case scenario. Further, the hypothetical breach (Br03 of fig. 65) located in front of a previously depositional area in the middle Alviso Slough, transports 3,500 tons of sediment (2.03 kg of THg) into pond A6 and 4,700 tons of sediment (2.73 kg of THg) into ponds A7 and A8.

- Sediment and associated THg originating from lower Alviso Slough (fr05) is closest to the slough mouth and most influenced by the tides. For both base-case and open-case scenario, this material is deposited upstream in Alviso Slough, into the ponds and downstream to Coyote Creek. For the open-case scenario, the larger tidal velocities associated with the larger tidal prism transports sediment and associated THg even farther bayward and upriver into Coyote Creek, compared with the base case.

- Almost 60 percent of the sedimentation into ponds A6 and A8 consists of material originating from the middle Alviso Slough (fr04); approximately 4,000 tons of sediment (2.32 kg of THg) for each pond.

- Approximately 80 percent of the sediment and associated THg transported out to the San Francisco Bay comprises bed sediment from lower Alviso Slough (fr05) and Guadalupe River suspended-sediment inputs into Alviso Slough.

Synthesis of the Independent Studies

The primary goal of this synthesis product was to summarize the findings of the individual Phase 1 studies and to forge these results into a more comprehensive understanding of how Phase 1 management actions affected mercury speciation, transport and bioaccumulation. Towards this end, four overarching questions were developed (see "Mercury Synthesis—Organizing Questions" section) that the authors felt the totality of the communal data was best able to address. This synthesis section aims to directly address each question by drawing from the most relevant aspects of the previously presented individual and combined study results, organized by the three primary matrices; biota, surface water, and bed sediment. In each case we attempt to provide a qualitative assessment of how precisely the existing data was able to answer each question and point to potential future studies that would help to better quantify and predict how wetland restoration management actions, within the study area and elsewhere, will affect mercury speciation, transport and bioaccumulation. A bulleted summary of the key findings presented below, for each question and by matrix type, is provided in appendix 13.

Question 1

Q.1—To what extent did the pond A6 levee breach result in directly measurable changes in mercury concentrations in Alviso Slough biota, surface water, and (or) bed sediment?

Biota

The evidence in support of the hypothesis that the pond A6 breach management action resulted in a measurable effect on biota mercury concentrations is limited, although there are a few observations that do indicate a short-term response. The strongest evidence was associated with the Mississippi silverside data, which showed a spike of THg concentration in both upper and lower Alviso Slough after this management action but prior to the initial opening of the A8-TCS (fig. 15). This response for Mississippi silverside was statistically significant only within Alviso Slough and not in the reference slough (Mallard Slough at site MALSL) during the April–July 2011 period (fig. 19). A similar statistically significant result was not observed for the three-spine stickleback also collected within Alviso Slough during the same period.

The small fish data collected during 2010–11 from within the A8-complex is less convincing. Our primary conclusion is that the higher April and May year-over-year difference (2011 minus 2010) in THg concentrations of fish within the A8-complex (fig. 14) was due to construction activities within the A8-complex (that is, internal levee breaches and A8-TCS construction; see discussion in the "Question 2" section). However, we cannot rule out the possibility that the hydrologic connection between lower Alviso Slough and the northwestern end of pond A7 (via the A7 water control structure, fig. 2), coupled with the pond A6 breach induced sediment mobilization event in lower Alviso Slough during the December 2010–May 2011 period (fig. 57), played a contributing role.

No bird eggs were sampled within pond A6 to directly examine the effect of the A6 breach on birds within that pond. However, a spike in THg concentration of Forster's tern eggs was observed both for the greater southern San Francisco Bay Forster's tern population (fig. 11) and more locally within ponds A7 and A8 (relative to reference ponds) during 2011 (fig. 9), the period immediately after the pond A6 breach and initiation of extensive sediment erosion and mercury mobilization in lower Alviso Slough. Our primary conclusion for the A7 and A8 Forster's tern population is that this 2011 spike in THg concentration was related to construction activities within the A8-complex, prior to the opening of the A8-TCS (see discussion in the "Question 2" section below). However, we cannot rule out the possibility that because of the close proximity of the sampled bird nests in pond A7 (fig. 2) to both pond A6 and the zone of intense sediment scour in lower Alviso Slough (fig. 57) caused by pond A6 breach, as well as the direct hydrologic connection between lower Alviso Slough and the northern tip of pond A7 (via the A7 water control structure, fig. 2), that the pond A6 breach played some role in the observed spike in the THg concentration of Forster's tern eggs in ponds A7 and A8.

Thus, the totality of the data linking the pond A6 breach to measurable effects on biota mercury levels is limited to the aforementioned April–July 2011 spike in THg concentration of Mississippi silverside in lower Alviso Slough. Any other lines of evidence, such as co-occurring spikes in THg concentrations in fish or bird egg mercury concentrations collected from within the A8-complex, or the spike in THg concentration of Forster's tern eggs collected in the greater southern San Francisco Bay during 2011, is indicative at best, and not conclusive. The extent that post-breach sediment scour and associated mercury mobilization in the lower Alviso Slough had any effect on A8-complex biota mercury concentrations is unquantifiable and cannot be readily separated from the effect of construction activities within the A8-complex during the same period. One certainty is that all quantified or indicated effects on biota mercury levels were short lived and virtually limited to 2011, which is an important observation and conclusion with respect to what might be expected regarding the duration of mercury spikes in biota from further pond breaches or wetland restorations management actions elsewhere.

Surface Water

Direct evidence that the pond A6 breach event caused a measurable change in surface-water mercury species concentration is primarily supported by volumetric p.THg and uf.THg concentration data, where surface-water Model SW.1 (equation 6) indicated that concentrations of both species were significantly higher in lower Alviso Slough during the post-breach (2011) period than during the pre-breach (2010) period (appendix 6, figs. 30*A*, 32*A*). In contrast, the MALSL reference site exhibited no such year-to-year difference. These statistical results parallel those seen for Mississippi silverside in lower Alviso Slough, as previously discussed. The likely explanation for these observations is that the substantial sediment scour in Alviso Slough, adjacent to the two breach locations (figs. 57, 62–64), which began just after the December 2010 pond A6 breach event, began to expose and remobilize long buried sediment layers containing THg concentrations that were more elevated than those in the active (routinely mobilized) layer. In addition, volumetric p.MeHg was significantly higher in lower Alviso Slough compared to the Mallard Slough reference site (MALSL), during 2011, even though the two sampling areas were not significantly different from each other during 2010 (appendix 6, fig. 30*B*). The single highest peak in both the volumetric p.MeHg and p.THg 2010–2011 time series, also occurred soon after the June 2011 opening of the A8-TCS. However, because of the closer proximity of the lower Alviso Slough sampling sites relative to the pond A6 breach points versus the proximity to the A8-TCS, and because of the relative physical size of these two management actions (four 20–30 m breaches in pond A6 versus one 1.5 m gate opening for the A8-TCS), it seems most likely that these spikes in p.THg and p.MeHg concentration were driven by the pond A6 breach event and not the comparatively minor A8-TCS opening. On the basis of the statistical significance, timing, and physical location of these observed surface-water spikes in particulate mercury species concentration, we place a medium-to-high level of confidence on the conclusion that the spikes in particulate mercury species concentration were directly related to the pond A6 management action.

Bed Sediment

The primary Alviso Slough bed sediment mercury species data available (for 2010–2011 only) had only a single mercury parameter (MeHg as a percentage of THg) that exhibited a clear statistical result that can reasonably be linked to the breaching of pond A6. Sediment MeHg (as a percentage of THg) was significantly lower in the lower Alviso Slough model region during 2011, compared to 2010, as assessed by sediment Model SED.2 (appendix 11, equation 12). No parallel annual trend was observed at the MALSL reference site. We conclude that this difference between years in the lower Alviso Slough model region is very likely reflective of the extensive sediment erosion during 2011, associated with the pond A6 breach event. Typically, benthic MeHg concentrations tend to be highest in the uppermost sediment layers (for example, see Alviso Slough deep core MeHg profiles in figure 5 of Marvin-DiPasquale and Cox, [2007]). Thus, in a rapid and sudden scour event, like the one associated with the pond A6 breach, we would expect that as sediment scour deepened and exposed sediment horizons deeper than the typical active layer, the newly exposed surface horizon (for example, the 0–2 cm interval sampled) would likely have lower MeHg (as both absolute concentration and as a percent of THg) compared to the previous surface horizon sampled prior to the erosion event. This proposed scenario and the conclusion that the pond A6 breach resulted in the observed decrease in percent MeHg in the 0–2 cm interval sampled in 2011, compared with 2010, is consistent with the conclusions noted above for yearly differences in surface-water p.THg and p.MeHg concentrations in the lower Alviso Slough model region, noted above.

Apart from the above observation regarding Alviso Slough surface-sediment mercury speciation, a direct effect of the pond A6 breach was the transport and deposition of both sediment (Callaway and others, 2013) and sediment bound THg (fig. 56) to the interior of pond A6. Our estimated THg annual deposition rate of 70 kg/yr into pond A6, calculated for the period between December 2010 and November 2012, represents about half of the 139 kg/yr mean annual load for streamgage station 11169025 in the Guadalupe River estimated by McKee and others (2017), and is equivalent to the minimum THg load estimate (70 kg) at the same streamgage station (11169025) associated with the January–February 2017 storms (McKee and others, 2018). Independent hydrodynamic and geomorphic modeling efforts confirm both sediment (fig. 64*A*) and sediment associated THg (fig. 65) deposition into pond A6, with extensive swaths of Alviso Slough and Guadalupe Slough bed sediment erosion associated with the breach points (figs. 62, 63, 64*A*). Although THg transported into pond A6 from mobilized bed sediment within Alviso Slough was primarily from the lower and middle slough reaches (fig. 65), calculations by Foxgrover and others (2019) suggest that a majority of the sediment and associated THg transported into pond A6 originated outside of Alviso Slough; presumably from the nearby shallows, Guadalupe Slough, and the southern San Francisco Bay (fig. 64*A*). There was also a notable and statistically significant 67 percent reduction in the daily rate of THg remobilization in the lower reach of Alviso Slough, from 10.8±1.4 g/d in the 3.8 year period bounded by December 2010 through October 2014 to 3.5±1.3 g/d in the 3.4 year period from October 2014 through February 2017 (table 10). This slowing of THg remobilization in lower Alviso Slough, and the related 18 percent decrease in sediment erosion (table 10, not statistically significant), indicates that pond A6 may be coming into dynamic equilibrium with respect to sediment and mercury transport to and from the bordering sloughs, and that this timeframe is on the order of 3–5 years. This is important information with respect to what timeframes might be expected for future breach scenarios with respect to periods of extensive sediment erosion and transport and reaching new states of dynamic equilibrium in sediment-rich environments.

Question 2

Q.2—To what extent did the construction and gradual increased opening of the A8-TCS result in measurable changes in mercury concentrations in biota, surface water, and (or) bed sediment within the pond A8-complex?

Biota

Biosentinel data collected from within the A8-complex indicate that Phase 1 restoration activities, particularly those associated with construction activities within the A8-complex, resulted in a large spike in THg bioaccumulation as measured in both piscivorous bird (Forster's tern) eggs (fig. 9) and pond fish (fig. 14). The spike as measured in pond fish was short-lived, because the 3-month period immediately following the establishment of the A8-TCS 1-gate condition coincided with a significant decline in fish THg levels relative to reference ponds (fig. 14). Pond fish were not collected after 2011, so it is unknown how these populations responded to subsequent gate opening and closing events beyond the initial 2010–11 study period. The observed spike in THg concentrations of Forster's tern eggs during 2011 was similarly short-lived; two years post-construction activities (2013) THg concentrations of Forster's tern eggs were comparable to those found in the reference ponds (see figure 9 explanation for full list of reference ponds). Owing to the flooding out of nests, no Forster's tern egg data past 2013 was collected. American avocet eggs collected in the A8-complex did not show an equivalent spike in THg during 2011, and the interannual temporal pattern for this nonpiscivorous avian species paralleled that for the reference ponds through 2015, although with higher absolute concentrations associated with the A8-complex (fig. 10). We conclude on the basis of the timing of the spike in THg of A8-complex fish (early 2011 prior to the 1-gate condition being initiated in June 2011) and the overall 2011 spike in THg of Forster's tern eggs, that these observed THg spikes were chiefly due to construction activities within the A8-complex. However, as noted in the "Question 1" section above, we cannot rule out the possibility that the intense sediment scour in lower Alviso Slough (fig. 57) caused by the December 2010 pond A6 breach, coupled with the direct hydrologic connection between lower Alviso Slough and the northern tip of pond A7 (via the A7 water control structure, fig. 64*A*), played an unquantified contributing role to these observed biotic THg spikes. Regardless of the proximate cause and relative contributions of construction internal to the A8-complex or nearby sediment and THg mobilization in lower Alviso Slough, the key conclusion is that these observed spikes in THg were short-lived, which contrasts with other studies such as those associated with newly created reservoirs, where elevated mercury levels in biota persisted for at least 6 to 9 consecutive years after the reservoir was created (Kelly and others, 1997; Gerrard and St. Louis, 2001; St. Louis and others, 2004). This is important information for any future planned restoration activities associated with the SBSPRP study area and elsewhere.

Surface Water

All MeHg associated surface-water mercury parameters within the A8-complex were directly affected by returning tidal flushing to the A8-complex through the opening of the A8-TCS, as assessed by surface-water model SW.2 (equation 7, appendix 7). Specifically, as the number of open A8-TCS gates increased, there was a statistically significant decrease in f.MeHg (concentration and as percentage of THg), p.MeHg (volumetric and gravimetric concentration and as a percentage of THg), and uf.MeHg (concentration and as percentage of THg) (appendix 7, figs. 22*B*, 23*B*, 24*B*, 25*B*, 27). Although there were also statistically significant differences in p.THg with the number of A8-TCS open gates, a clear decrease in concentration with an increasing number of open gates was less obvious (appendix 7). This was largely due to the large spike in THg into the A8-complex associated with the January–February 2017 high-flow event that took place under the 5-gate condition (figs. 22*A*, 24*A*, 25*A*), which confounded the analysis of gate condition only.

A clear indicator of an event associated with a disproportionate amount of sediment- bound mercury transport is an obvious spike in the distribution coefficient (Kd), as we see in the A8-complex for both Kd(THg) and Kd(MeHg) coincident with the January–February 2017 high-flow event, (fig. 28). The second highest spike in Kd(THg) (April 2015) occurred soon after the transition from a 3-gate to 5-gate condition at the A8-TCS (fig. 28*A*). A comparable spike is not observed for Kd(MeHg) during April 2015 (fig. 28*B*). This April 2015 spike in Kd(THg) is coincident with a period of maximum erosion of Alviso Slough bed sediment (fig. 59*A*, 60*A*) and THg remobilization (fig. 60*B*), particularly in the upper and middle slough reaches. This spike in Kd(THg) also occurs near the onset of a very high range in Q ratios observed during the 1.5 gt6years (September 2014 through April 2016) after initiation of the 5-gate condition (fig. 45), which we interpret as a prolonged period of energetic instability with respect to the water budget and the tidal prism relative to the slough geometry. We conclude that this spike in surface water Kd(THg) is additional evidence that the opening of five gates represented a critical tipping point that facilitated a period of increased bed sediment erosion and the remobilization of previously buried legacy THg in the upper and middle Alviso Slough reaches. Our confidence in this conclusion regarding the significance of the transition from the 3-gate to 5-gate condition is moderate-to-high, based on the multiple lines of evidence.

Bed Sediment

Bed sediment within the A8-complex was not sampled after the initial 2010–2011 study, which focused on the period just before and after the first A8-TCS 1-gate condition. Owing in part to the limited number of sampling events and the unbalanced data distribution relative to the June 2011 initial 1-gate condition (4 sampling events before and 2 after the gate opening, appendix 1), the statistical analysis of the data yielded no compelling evidence that the initial opening of the A8-TCS resulted in any significant change in bed sediment mercury species concentration within the A8-complex. However, the hydrodynamic and geomorphic modeling clearly predict the transport and deposition of sediment (fig. 64*A*) and associated mercury (fig. 65) into ponds A7 and A8 through breach points along Alviso Slough. This modeling indicates that the majority of the THg currently being transported into the A8-complex via the A8-TCS originates from bed sediment scour in upper Alviso Slough, with a smaller amount being contributed from sediment scour in the middle Alviso Slough reach, and little to none is contributed from the lower Alviso Slough reach (fig. 65, see also Achete, 2016). Deposition into the A8-complex would be expected to increase in the event additional breach points are added along the levees adjacent to Alviso Slough, and much of the sediment would come from enhanced erosion in the middle and lower Alviso Slough reaches (fig. 64*B*). Although the precise distribution of buried legacy mercury along middle and lower Alviso Slough reaches is not known, it is clear that multiple horizons of elevated mercury concentrations exist (Marvin-DiPasquale and Cox, 2007; Foxgrover and others, 2019). Thus, it is reasonable to assume that additional levee breaches along Alviso Slough will lead to some additional amount of transfer of mercury containing bed sediment from Alviso Slough into the A8-complex, on the basis of the aforementioned modeling and the results from both the pond A6 breach (fig. 56) and the opening of the A8-TCS (fig. 55). This additional transfer of both sediment and mercury into the A8-complex would be expected to continue until the A8-complex and resulting eroded zones within Alviso Slough reach a new state of quasi-equilibrium. After which, we might expect that the rapidly created new surface horizon within the A8-complex will begin to be slowly buried with new sediment primarily sourced from the San Francisco Bay and the upstream watershed. An abrupt remobilization of both bed sediment and legacy mercury, resulting from new breaches between the A8-complex and Alviso Slough, will also likely lead to yet another short-term spike in mercury in biota, as has been suggested in this report for both birds (figs. 9, 11) and fish (figs. 14, 15, 19).

Question 3

Q.3—To what extent did the construction and gradually increased opening of the A8-TCS result in measurable changes in mercury concentrations in Alviso Slough biota, surface water, and (or) bed sediment?

Biota

In addressing Q.3 we focus explicitly on the Mississippi silverside and three-spine stickleback data collected from Alviso Slough and the two reference sloughs (Mallard Slough and Guadalupe Slough), because there exists no relevant bird egg data that can be leveraged in this regard. Of these two fish species, we rely most heavily on the Mississippi silverside data (fig. 15*A*), because the three-spine stickleback data were more temporally limited (fig. 15*B*) and do not exhibit a clear length versus THg concentration relationship among or within sampling regions (fig. 16*B*). The more consistent length versus THg relationship seen in the Mississippi silverside data (fig. 16*A*) allowed for the development of more predictive size-standardized fish THg concentration data, which in turn helped to minimize unexplained statistical error in subsequent models focused on resolving temporal and spatial differences of interest. The difference in these two species, with respect to the observed length versus THg relationship, is thought to be related to the stronger site fidelity of the Mississippi silverside, compared to the three-spine stickleback.

There are primarily two major spikes of THg concentration in Mississippi silverside that were investigated regarding the likelihood of A8-TCS management as the ultimate cause. The first spike in THg occurred during 2011, about the time of A8-TCS construction and the initial opening of one gate. The second and larger spike was during October 2016 (fig. 15).

The conclusion that the peak in THg concentration in Mississippi silverside during 2011 was caused by A8-TCS management actions, and particularly on A8-TCS construction activities, is based upon multiple lines of evidence. First and foremost, the 2011 spike in Mississippi silverside THg (> 1 µg/g dw) occurred during April and May 2011, before the initial gate opening and during the 2010–11 construction period (fig. 15). Seasonally pooled data indicate that size-standardized fish THg concentrations of Mississippi silverside in 2011were significantly greater during the early season (April–July), than for any other year, and that this effect was not observed at the MALSL reference site (fig. 19). Second, the highest THg concentrations seen for three-spine stickleback (about 1 µg/g dw) was during October 2010 (fig. 15), during the construction period. Third, this conclusion is consistent with that reached for Q.2, in that construction activities resulted in the observed THg spikes seen in the 2010–11 study of both small fish and bird eggs sampled within the A8-complex. The fact that the April–May 2011 spike in Mississippi silverside THg concentrations was seen in both upper and lower Alviso Slough indicates that the December 2010 pond A6 breach, and the significant sediment disturbance and erosion associated with it, may have also been a factor contributing to the timing and intensity of the THg spike in Mississippi silverside, particularly in the lower Alviso Slough.

Although the above conclusions regarding the circumstances and cause of the observed spike in THg concentration of Mississippi silverside during 2011 seem well founded on the basis of the available evidence, the circumstances and cause associated with the subsequent larger spike observed during October 2016 are less obvious. This spike, evident in both upper and lower Alviso Slough (fig. 15) occurred 2 years after the most recent management action (the opening of the A8-TCS to five gates), after two comparatively mild wet seasons with low sediment loads from the watershed, and prior to the high-flow and high-sediment-load event of January–February 2017 (fig. 59*B*). Although peak THg concentrations of Mississippi silverside were seen in October 2016, the data indicate that concentrations were declining but still elevated by February 2017 (fig. 21). Seasonally pooled data confirm that size-standardized fish THg concentrations of Mississippi silverside in 2016 were significantly greater during the late season (August–February), than for any other year, and that this effect was not observed at either the MALSL or GUASL reference sites (fig. 20). With no obvious cause immediately preceding this spike in Mississippi silverside THg levels, we considered the sequence of events and observations that unfolded over the 2-year period leading up to it.

Multiple lines of evidence indicate the A8-TCS management transition from a 3-gate to 5-gate condition in September 2014 represented a critical tipping point in the energetics of study area that led to a bed sediment high erosion event, which included the remobilization of deeply buried legacy THg in Alviso Slough. The evidence for this is discussed in various places throughout this report, including as part of the discussion of Q.2 (“Surface Water” section) and Q.3 (“Bed Sediment” section). This evidence includes (1) an immediate and abrupt reversal in the direction of suspended-sediment flux as measured at the ALSL-3 site, from landward to bayward, immediately after the transition from the 3-gate to 5-gate condition, which persisted for 1.6 years (periods E–F, fig. 42, table 6); (2) the abrupt and prolonged shift in the Q ratio to a high range of values immediately after the establishment of the 5-gate condition, which persisted for 1.6 years and explicitly coincides with aforementioned bayward suspended-sediment flux (periods E–F, figs. 42, 46) ; (3) a large sediment erosion event for the full length of Alviso Slough and the highest rate of bed sediment THg mobilization occurring immediately after the establishment of the 5-gate condition (the period bounded by bathymetric surveys in October 2014 and April 2015; fig. 60); (4) a two-fold increase in the bayward daily mean flux of p.THg during the 5-gate condition, relative to the 3-gate condition, even after controlling for the January–February 2017 high-flow event (fig. 50A) and (5) the spike in Kd(THg) within the A8-complex observed in April 2015 soon after the establishment of the 5-gate condition (fig. 28*A*).

Early March 2016 marked the end of the prolonged steady period of high Q ratios and the co-occurring period of bayward suspended-sediment flux at ALSL-3 (period E, figs. 42, 45). This preceded period F (March through mid-May 2016), which was characterized by a sharp but short-lived increase in both water flux and bayward suspended-sediment flux. During this period we also observed a substantial spike in surface-water p.MeHg in upper Alviso Slough during April 2016 (fig. 30*B* and 31*B*). Although the underlying processes that precipitated this p.MeHg spike are unclear, the timing of these observations indicate a linkage. One possibility is that this spike in p.MeHg represents MeHg production within the upper Alviso or the A8-complex that was linked to the rapidly changing conditions associated with period F. It is also possible that this spike in p.MeHg originated in the upper watershed and was transported to the upper Alviso Slough sampling region during the early stages of period F (March–early April). However, although period F did represent a time of high watershed flow, particularly compared with the period E, daily mean water flux at monitoring site ALSL-3 (597,400±28,800 m^3/d) was 2.7-fold higher than for the Guadalupe River (216,100±43,300 m^3/d measured streamgage station 1169025) and suspended-sediment flux at ALSL-3 (60.8±5.2 t/d) was three-fold higher than Guadalupe River (19.7±8.6 t/d calculated for streamgage station 1169025) for the same period (table 6). This indicates that excess water, presumably stored in the A8-complex, was responsible for approximately two-thirds of this flux and that period F represented a time frame associated with enhanced sediment remobilization. It is thus most likely that the observed p.MeHg spike originated in the study area, either in upper Alviso Slough itself or exported from the A8-complex. Although the modeling results indicate that the flux of p.MeHg is generally from the upper Alviso Slough reach into the A8-complex (fig. 55*B*), this result does not preclude the possibility that elevated levels of p.MeHg also can be exported from the A8-complex on ebb tide cycles.

The October 2016 spike in THg concentrations in Mississippi silverside (fig. 15) occurred 6 months after the April 2016 spike in water column p.MeHg in the upper Alviso Slough (fig. 30*B*, 31*B*). Six months represents a temporal offset that is reasonable for propagating the bioaccumulation of MeHg from the base of the food web (that is, bioaccumulation of MeHg in phytoplankton) through primary consumers (for example, zooplankton) and into secondary consumers, such as small prey fish (for example, Mississippi silverside). Owing to the low temporal resolution associated with the field sampling of both surface water and slough fish (every 1–3 months during the field season), it is unclear if the observed peaks in either of these matrices (biota and surface water) represented the actual peak concentrations in the environment. Owing to the limitations in sampling frequency, it is unlikely that the observed peak in Mississippi silverside THg concentration and the observed peak in water column p.MeHg concentration represented the maximum peak values that may have existed in either instance. Thus, the actual temporal offset between peak surface-water p.MeHg concentrations and peak THg concentrations in Mississippi silverside may have been even narrower (or wider) than those measured as part of our routine sampling schedule.

In an earlier study done in reference pond A16 and in the adjacent salt marsh, Eagles-Smith and Ackerman (2009) showed comparatively rapid changes in THg concentrations in biosentinel fish (longjaw mudsucker and three-spine stickleback). Depending on fish species and site, biosentinel THg concentrations increased 33–79 percent over a 3-month period (May–July) and subsequently decreased 37–53 percent over the next two months (July–August). Although these results were not tied to any changes in surface-water mercury concentrations, they do show how rapidly THg concentrations in small fish can change. These reported short periods of quantifiable change are one-third to one-half of the window of time between the April 2016 spike in surface-water p.MeHg (figs. 30*B*, 31*B*) and the October 2016 spike of THg concentration in Mississippi silverside (fig. 15). However, the magnitude of the measured changes in the pond A16 study (Eagles-Smith and Ackerman, 2009) were smaller (approximate range 30–80 percent) than the 276–348 percent (about 3.8-fold to 4.5-fold) increase observed for Mississippi silverside in upper Alviso Slough during October 2016 compared to the three prior sampling events (April, May, and July 2016). Any uncertainty in the implied linkage between the spike in surface-water p.MeHg in April 2016 and the spike in Mississippi silverside THg concentration in October 2016 stems partially from the fact that no process-level data are available to quantify and track the transfer of MeHg from the abiotic compartments (surface-water and sediment) to the base of the food web (phytoplankton and zooplankton) and subsequently into Mississippi silverside. Investigations of mercury accumulation into biological trophic levels below those of the biosentinel species used were not part of Phase 1 studies.

Based on the totality of the data, here we summarize what we conclude to be the most likely sequence of events that led to the pronounced October 2016 spike in THg concentrations in Mississippi silverside in Alviso Slough, when no obvious driver (management action or watershed flux event) immediately preceded this spike. First, the transition from the 3-gate to the 5-gate condition at the A8-TCS (September 2014) was a tipping point in the energetics of the system that resulted in extensive slough scour and (or) mobilization in upper and middle Alviso Slough reaches, and a reversal in the direction of suspended-sediment flux (from landward to bayward) at site ALSL-3, which persisted for 1.6 years (until May 2016). Before the culmination of this period, and during a phase of high flow (much of which was presumably coming from the A8-complex) and enhanced suspended-sediment flux (March–May 2016), a related spike in surface-water p.MeHg occurred (April 2016), which ultimately resulted in the THg concentration spike observed in Alviso Slough Mississippi silverside six months later (October 2016). Although we can only claim moderate confidence in this conclusion, owing to the number of linkages involved and in lieu of any contradictory evidence, the sequence of events based on the data available seems reasonable. This proposed sequence of events speaks to the value of this synthesis effort, in that it brings together the results from the individual studies in a manner that allows for a more comprehensive understanding of the linkage between management actions and systems response to a degree that would not be achievable based on the results of any one of the individual studies alone.

Surface Water

A8-TCS gate operations had measurable effects on Alviso Slough water quality overall. When all A8-TCS gates were closed, the ALSL-3 site exhibited lower salinity during ebb tides, owing to the higher proportion of watershed derived freshwater outflow, compared to when gates were open (fig. 41). Further, when three or more gates were open, salinity was generally higher than during the 1-gate condition, which reflects an increased tidal prism and more saline bay water moving farther up Alviso Slough as more A8-TCS gates were opened. Dissolved oxygen was also higher during ebb tides when three or more gates were open, compared to the 0-gate or 1-gate conditions (fig. 41), an observation likely linked to enhanced primary production (which produces DO) in the A8-complex and the release of a higher proportion of A8-complex water to Alviso Slough with more gates open.

Substantial evidence indicates that A8-TCS operations had direct and measurable effects on a range of surface-water mercury parameters within Alviso Slough. First, during the period of A8-TCS construction, concentrations of gravimetric p.THg and p.MeHg (fig. 31), as well as Kd(THg) and Kd(MeHg) (fig. 35) peaked in upper Alviso Slough (only). On the basis of timing, we conclude that these short-term spikes in particulate associated mercury species were a direct result of construction activities.

Second, a clear decrease in ebb tide surface-water SSC at ALSL-3 was observed (fig. 46) as more A8-TCS gates were opened, and a similar consistent annual decrease in volumetric p.THg and p.MeHg was observed during all seasons (figs. 51*A*, 51*C*; table 8). These decreasing trends in SSC, p.THg, and p.MeHg concentrations during ebb tides with the increasing number of open A8-TCS gates are indicative of particulate dilution with increased tidal prism (more bay water moving upstream during flood tide). However, there was also an increase in p.THg and p.MeHg daily mass flux (fig. 50) in the bayward direction as more gates opened, as well as a notable annual increase in gravimetric p.THg concentration during winter (fig. 51*B*, table 8), which is the season associated with the highest sediment and THg watershed flux (McKee and others, 2017) and with the highest net sediment erosion and THg remobilization rates in Alviso Slough (fig. 60). Although wintertime discharge from the watershed was variable during the period of study (fig. 40), the annual increase in gravimetric p.THg concentration was at a generally steady rate of 40 ng/g dw per year during the winter (fig. 51*B*, table 8). This temporal trend of increasing gravimetric p.THg concentration is most likely associated with Alviso Slough bed sediment scour eroding and mobilizing progressively deeper layers of previously buried THg with increasing concentration (Foxgrover and others, 2019). This progressive increase in scour depth is likely a direct result of the gradual gate opening associated with the A8-TCS. It is unknown if this temporal trend in increasing gravimetric p.THg concentration continued beyond 2017 once all eight A8-TCS gates were open (full width).

Third, statistical analysis of mercury species concentrations (primary, low-temporal resolution data) in both up.ALSL and low.ALSL model regions as a function of A8-TCS gate operations (surface-water Model SW.4) indicates that there was an initial increase in f.MeHg (concentration and as percentage of THg) in upper Alviso Slough under the 1-gate condition. However as more gates were opened, and the tidal prism and flushing of the A8-complex increased, f.MeHg decreased in model region up.ALSL (appendix 9, figs. 29*B*, 34*A*). This initial increase in f.MeHg concentration under the 1-gate condition likely represents the initial release of A8-complex water with a comparatively high f.MeHg concentration into upper Alviso Slough. A similar temporal trend was found for f.MeHg (concentration and as percentage of THg) in the low.ALSL model region, where concentrations under the 5-gate and 8-gate conditions were lower than under the earlier 0-gate and 1-gate conditions (appendix 9, figs. 29*B*, 34*A*), which indicates that increased tidal prism and the introduction of bay water with lower f.MeHg concentration led to a dilution of f.MeHg in Alviso Slough overall.

On the basis of the propensity of observations and statistically significant results summarized above, we have a high degree of certainty in the conclusion that A8-TCS operations resulted in measurable changes in surface-water mercury species concentration within Alviso Slough.

Bed Sediment

Evidence that A8-TCS operations directly affected mercury concentrations in Alviso Slough is lacking for the surface-sediment (0–2 cm interval) data collected during 2010–11. In fact, statistically significant results did not show a clear linkage between A8-TCS gate operations and changes in Alviso Slough surface-sediment mercury species. This lack of evidence may have been partially due to the low number of observations in this early dataset overall and to the unbalanced number of surface sediment sampling events prior to (n=4) and after (n=2) June 2011, when one gate was initially opened on the A8-TCS (appendix 1).

However, substantial evidence indicates that A8-TCS gate operations did affect bed sediment and associated THg mobilization overall, as demonstrated by the combined deep core and bathymetric change survey datasets (Foxgrover and others, 2019). Three major bed sediment erosional peaks relevant to Q.3, all three occurred during the winter period and are of similar magnitude (between −2.4 and −3.0 cm/month as area normalized net change [fig. 59*A*] and between

2.9 and 3.1 cm/month erosion [fig. 60*A*], averaged for the entire slough). The first peak was during the 3.3-month window between the October 2011 and February 2012 survey, which followed the initial opening of the A8-TCS (June 2011), and where the greatest extent of area normalized erosion was in upper and middle Alviso Slough reaches (figs. 59*A*, 60*A*). The second was not until 3 years later, during the 6-month window between the October 2014 and April 2015 bathymetric surveys, which was the period immediately after the transition from a 3-gate to 5-gate condition transition (September 2014). This erosion event affected all three defined reaches of Alviso Slough. The third major net erosional event occurred during the 5-month window between the October 2016 and March 2017 bathymetric surveys, which encompassed the January–February 2017 high-flow event. As a comparative measure, Guadalupe River sediment loads (measured at streamgage station 1169025) for the same three periods were low for the first two (0.7 x 10^6 and 3.6 x 10^6 kilograms per day, respectively) and very high (67 x 10^6 kilograms per day) for the third (fig. 59*B*). This variation in Guadalupe River sediment loads associated with the natural variability in winter flow intensity was not proportional to the extent of bed sediment erosion observed within Alviso Slough, which were similar in magnitude for all three observed wintertime peak events. On the basis of these observations, we conclude that the first two Alviso Slough bed sediment erosion events were linked to A8-TCS management, specifically the initial opening of the A8-TCS and the transition from a 3-gate to 5-gate condition that represented a tipping point in the balance between increased tidal prism and its effect on sediment erosion. This conclusion is further supported by the observed extreme and immediate jump in Q-ratio range observed immediately after the transition from a 3-gate to 5-gate condition (fig. 45), and that this period was associated with the single largest increase in cumulative bed sediment erosion for the entire Alviso Slough during the period of record (fig. 61). In contrast, we conclude that the third major erosional event during the October 2016 and March 2017 period was a direct result of the extreme high-flow event of January–February 2017, because no change in A8-TCS gate condition preceded this event for more than 2 years.

Foxgrover and others (2019) concluded that annual erosion rates in lower Alviso Slough began to slow approximately three years after the breach of pond A6. A subsequent analysis of daily mean bed sediment erosion, before and after the opening of five gates at the A8-TCS, supports this earlier conclusion with respect to lower Alviso Sough (table 10). This same analysis also indicates that daily mean bed sediment erosion rates in middle and upper Alviso Slough increased after five gates were open (table 10). Although these differences in erosion rates, before and after the 5-gate condition, were not statistically significant (chiefly owing to limited data), the general trends are consistent with the conclusion of this synthesis that posits that the initiation of the A8-TCS 5-gate condition represented a significant transition point in the erosional response of Alviso Slough to the increase in tidal prism. In addition to these trends in bed sediment erosion, there was a statistically significant 94 percent increase in the associated THg remobilized rate in upper Alviso Slough after the initiation of the 5-gate condition (table 10). We conclude that this result is a critical link in the sequence of events to led to the spike in THg concentrations of Mississippi silverside in Alviso Slough observed during October 2016 (fig. 15), as discussed above ("Question 3, Biota" section).

Question 4

Q.4—To what extent is the pond A8-complex a source or sink for THg and (or) MeHg?

There are no specific biota or bed sediment data that directly address Q.4. Thus, the following comments are limited to the modeling of surface-water mercury species concentrations into and out of the A8-complex.

Surface Water

The flux of both water and suspended sediment was into the A8-complex for all periods monitored between February 2016 and February 2018 (table 7, fig. 44). There was a substantial (3.4-fold) increase in sediment flux and a comparatively smaller (35 percent) increase in water flux into the A8-complex during the high-flow event of January–February 2017 (period B), compared to the preceding low-flow period (period A). Upon transitioning from the 5-gate to 8-gate condition, there was a substantial (4-fold) decrease in water flux into the A8-complex, but no significant change in suspended-sediment flux when compared to the low-flow 5-gate condition.

Our ability to model filter-passing and particulate mercury species into and out of the A8-complex was limited by both data density and the fact that surface-water mercury data were not collected right at the location of the A8-TCS high-resolution water quality fixed monitoring station. Instead, we had to model flood and ebb tide mercury concentrations separately and needed to rely on data collected down-stream of the fixed-station (site ALSL-2b) and from within the A8-complex, respectively (appendix 2). We also did not have the benefit of mercury data collected over a full tidal range, as was done at the ALSL-3 site. Thus, the results associated with modeling of mercury species concentrations at the A8-TCS (figs. 52–55) are likely less precise than the flux modeling of mercury species conducted for the ALSL-3 site.

During low-flow periods, under the 5-gate condition, the A8-complex was a sink for all four mercury species modeled (f.THg, f.MeHg, p.THg and p.MeHg; table 9, figs. 52–55). The effect of the high-flow event of January–February 2017 was that the flux of f.THg, p.THg, and p.MeHg into the A8-complex increased substantially. However, the model predicted that the A8-complex became a source of f.MeHg to Alviso Slough during this high-flow period. The biggest observed effect of the transition from a 5-gate to 8-gates condition was the reversal in the direction of flux for f.THg and f.MeHg, in which the A8-complex went from being a sink to a source (fig. 54, table 9). This appears to be a combined result of the A8-complex being less of a sink for water overall under the 8-gate condition (fig. 44) and the generally higher concentration of both species in the A8-complex compared to the adjacent upper Alviso Slough (appendix 5). We again emphasize that this assessment of the A8-complex as a source or sink for the various mercury species is only relative to the measurements made at the A8-TCS. We have not conducted a complete water or sediment budget for the whole A8-complex, which would also need to include fluxes measured at the two northern water control structures associated with ponds A5 and A7 (located approximately 5 km and 4 km to the northwest of the A8-TCS, respectively). Owing to the aforementioned reasons, our confidence in the precision of these modeling results is best described as moderate, although our confidence in the overall direction of flux is moderate to high.

Unanswered Questions and Future Directions

Although this synthesis report goes a long way towards constructing a more comprehensive narrative regarding how specific SBSPRP management actions affected mercury speciation, mobilization, and bioaccumulation in the study area, several unanswered questions remain, which were not able to be addressed by the individual studies or this synthesis effort. In this section, key outstanding questions that could not be addressed adequately (or at all) with the existing data are identified and some potential future efforts to address these information gaps are discussed.

Future Levee Breaches

One of the biggest tools wetland restoration managers have at their disposal is the reintroduction of tidal flushing to historical wetland habitat by creating breaches in existing levees that were previously built to drain or hydrologically isolate large swaths of bay habitat. During Phase 1, the effects of both a levee breach (pond A6) and the construction and management of the A8-TCS were studied with respect to how they each affected mercury speciation, transport, and bioaccumulation. The integration of the findings from the individual studies presented in this report indicate several observations regarding these two hydrologic manipulations that can serve to inform future similar management options. First, both the pond A6 breach and the gradual opening of the A8-TCS resulted in demonstrable but short-lived mercury concentration spikes in biota. However, mercury concentrations in Forster's tern eggs are still above toxicity benchmarks and remain relatively elevated within the SBSPRP area, which indicates that cumulative restoration actions may be elevating biotic mercury concentrations over historical levels. Second, the creation of both levee types led to the transfer and deposition of sediment and sediment-bound mercury into the breached ponds, but at a certain point and breach width (for example, under the A8-TCS 8-gate condition) the A8-complex became a source of f.THg and f.MeHg to Alviso Slough (fig. 54). Although some of these conclusions may be generally transferable to what might be expected from future levee breaches, the data available are still fairly limited with respect to providing detailed estimates or answers to specific questions. Outstanding questions remain:

- Will continued restoration actions keep mercury concentrations in bird eggs above toxicity benchmarks?
- How much additional bed sediment erosion and legacy THg remobilization will occur if a new levee breach is placed in the northwest corner of pond A8 or along the southern levee separating pond A8 from Guadalupe Slough (San Francisco Estuary Institute-Aquatic Science Center, 2018)?
- How accurate is the model prediction that the A8-complex became a source of f.THg and f.MeHg upon the opening of eight gates at the A8-TCS, given the limited data availability for predicting mercury species concentrations?
- If accurate, what is the seasonality of this trend, the long-term trajectory, and magnitude of this flux once the interior of the A8-complex begins to reach a new state of equilibrium with respect to its bordering sloughs, or as various areas within it begin to develop emergent marsh structure?

To answer the above questions and similar ones with respect to planned breaches in other areas within the larger SBSPRP area and elsewhere, there are several actions that could be taken. First, although it was beyond the scope of the current synthesis effort, the hydrodynamic and geomorphic modeling platform recently developed for the study area (figs. 62–64) (Röbke and van der Wegen, 2018; van der Wegen and others, 2018) can take advantage of the surface-water and sediment mercury data collected as part of the Phase 1 effort (Marvin-DiPasquale and others, 2018; Marvin-DiPasquale and others, 2019) to further advance the modeling of mercury dynamics in the study region without collecting additional field data.

Second, although the deep cores collected along Alviso Slough (Marvin-DiPasquale and Cox, 2007; Marvin-DiPasquale and others, 2018) were an essential part of modeling legacy mercury remobilization as a function of bed sediment erosion (figs. 60*B*, 61) (Foxgrover and others, 2019), the majority of these core collections were focused in the upper reach of Alviso Slough, closest to the A8-TCS, which was a primary focus area of the Phase 1 studies. If additional breaches are being considered for the northwest corner of pond A8 along Alviso Slough and (or) along the southern border of pond A8 adjacent to Guadalupe Slough, the collection of additional deep cores in these adjacent slough reaches would greatly inform estimates of how much legacy mercury is likely to be remobilized and largely transferred into the A8-complex. Currently, sediment data do not exist from Guadalupe Slough and only two deep cores within 0.5 km of the proposed A8 breach currently collected from within the main channel of Alviso Slough (cores T2B and T3B, in Marvin-DiPasquale and Cox, 2007). Because Guadalupe River historically drained into Guadalupe Slough prior to being diverted to Alviso Slough in the late 1800's, we anticipate that there is a substantial amount of buried legacy mercury in Guadalupe Slough. Isotopic dating (^{210}Pb, ^{137}Cs) of any future cores collected, or existing archived material from previously collected cores, would provide additional information on contemporary and historical sedimentation rates within these sloughs, as well as dates associated with peak mercury concentration horizons, which can be useful from a historical perspective.

Third, one of the challenges with modeling the flux of water, sediment and mercury into and out of the A8-complex, as presented in this report (figs. 44, 52–55) was that the A8-complex is not a closed system. Although valuable high-resolution water quality data were collected at the A8-TCS, there exist two additional water control structures associated with ponds A7 and A5 that were not being similarly monitored. Thus, complete water, sediment and mercury budgets were not able to be constructed for the A8-complex. However, through this synthesis effort an approach was developed for coupling low temporal resolution surface-water mercury data with high-temporal resolution fixed-station water quality monitoring (for example, tidal stage, SSC, temperature, and salinity) to derive high-resolution mercury time series for several important mercury species. This approach was particularly successful at the ALSL-3 site (USGS station 11169750) where surface-water mercury sampling was co-located with the fixed monitoring station, and where mercury samples were collected through a number of full tidal cycles over multiple seasons (figs. 36–39).

To the extent that monitoring mercury flux remains an important issue for the SBSPRP, particularly as associated with new levee breaches, this approach of combining high-resolution fixed-monitoring sites for basic water quality metrics with a routine lower resolution surface water monitoring program for mercury species may prove particularly useful for more accurately modeling mercury flux into and out of the ponds. An expanded network of high-resolution water quality fixed sites located at all major pond and (or) slough exchange points, and operated for an appropriate length of time before and after new breaches are implemented, would be optimal for such a monitoring program. In addition, the Q-ratio metric (Q_{ALSL}/Q_{GR}) developed as part of this synthesis effort to identify periods of ecosystem transition in response to rapid shifts in tidal prism and hydrology (fig. 45), is another tool that can be leveraged in future studies when high-resolution water quality monitoring is used.

Fourth, conducting bathymetric change survey mapping within ponds, before and after any additional breach events, would add yet another valuable level of information. This information can be used in conjunction with geomorphic models to provide a much more accurate assessment of sediment and mercury dynamics associated with restoration activities that would not only inform the SBSPRP but wetland restoration efforts globally.

Finally, because present egg MeHg concentrations are elevated above those concentrations measured prior to the SBSPRP, the continued long-term monitoring of mercury concentrations in bird eggs within the SBSPRP would help determine the trajectory of their elevated MeHg levels. Such a monitoring program would consist of measuring mercury concentrations in bird eggs at a number of colonies throughout the SBSPRP area.

High-Resolution Monitoring

Given the sheer size of the SBSPRP restoration area and the human resource associated with traditional field sampling approaches necessary to study the effect of management actions in enough detail to be informative, the use of platforms and technologies that allow for the collection of high-resolution temporal and spatial data is obvious. However, not every parameter of interest can be readily monitored at high-resolution. Mercury in surface water is a good example. In the current synthesis, one example is provided to show how high-temporal resolution water quality data can be coupled with the mercury data obtained with traditional field collection approaches (low temporal resolution) and successfully modeled to provide a high-resolution time series of mercury species flux that is informative for assessing how management actions affected mercury remobilization and transport. By deploying a network of water quality sondes, this approach can be replicated at strategic sites throughout the restoration area, including within ponds that are being newly opened to tidal exchange through breaching. Such a network could be coupled with telemetry, which would allow restoration managers to view field data in real time and make more informed decisions on shorter time scales.

Similarly, studies are currently underway in the San Francisco Bay Delta to develop relationships between key mercury parameters and optical water properties in surface water that can be gathered at high spatial resolution via remote sensing platforms (that is, satellite, manned aircraft, drones). As these relationships are further refined, such approaches will greatly expand our ability to observe and monitor water quality and contaminants of concern in much greater spatial detail than has been the case to date. Further, the collection of high-resolution temporal and spatial data that are useful in predicting mercury species concentrations can be coupled with the hydrologic and geomorphic modeling approaches currently being developed for the SBSPRP area and subsequently improve our ability to run prediction simulations associated with proposed restoration activities.

Biota Studies

Concern regarding mercury effects on wildlife is a primary driver of most mercury research, including for the SBSPRP. The use of biosentinel small fish, bird eggs, and other biotic proxies for mercury bioaccumulation are powerful tools for monitoring and assessing the effects of both management actions associated with restoration projects and ecosystem changes through long timeframes. Long-term (figs. 11, 12) and regional (figs 7, 8) datasets are a critical element in this regard, in that they allow us to contextualize biota mercury concentration data collected as part of individual studies that may be more narrowly focused with regards to study areas and timeframe. Owing to the 50-year program-level time horizon for the high-visibility SBSPRP, the many restoration actions yet to come, and larger regional changes that will continue to occur (for example climate change and sea level rise, fig. 64*C*), the continued use of biosentinels and the continuation of long-term datasets will undoubtedly prove to be an invaluable tool for understanding the effects of specific restoration actions, isolating these effects from the backdrop of larger regional changes that may be co-occurring, and informing the progression of restoration management decisions for the SBSPRP and elsewhere.

One of the biggest initial mysteries tackled as part of this synthesis effort was understanding what caused the October 2016 THg concentration spike in slough Mississippi silverside (fig.15) that seemed to have occurred without a proximate precipitating event. Through the process of developing this report and lining up the existing data from the individual studies we eventually pieced together what we believe is the most likely sequence of events that led to this spike. As detailed in the "Synthesis" section, this sequence began more than a year prior, with the opening of the fifth gate at the A8-TCS, which started a period of enhanced sediment and mercury mobilization that abruptly ended with a large spike in surface-water MeHg, followed 6 months later by the observed spike in THg concentrations in slough fish. In lieu of additional evidence to the contrary, our confidence in the implied cause and effect linkages of this sequence is best characterized as moderate.

One of the key presumptions in the above sequence is the linkage between the spike in surface-water MeHg during April 2016 (figs. 30*B*, 31*B*) and the subsequent spike in THg of fish during October 2016 (fig. 15). What are missing in this linkage are data that similarly track, over time, the transfer of mercury from the abiotic compartment (that is, the surface-water) into the base of the food web (that is, phytoplankton and zooplankton) and ultimately into the small fish sampled. Phase 1 studies did not include a component that examined temporal and spatial mercury trends in that important base of food web compartment. Indeed, most studies that focus on mercury in biota (for example, biosentinels), and which often do have an abiotic (water and sediment) component, rarely include the phytoplankton and zooplankton compartments linking the two. This is not uncommon, because base-of-food-web type studies are complicated and resource intensive owing to the diversity of species that make up the primary producer, primary consumer, and detritivore community, which support small prey fish. This fact alone makes the use of biosentinel proxies very appealing, practical, and comparatively cost effective, because the complexity that exists in the food web below the biosentinel proxy is assumed but not quantified. Detailed food web studies may be beyond the scope of the current and future SBSPRP. However, this "Unanswered Questions and Future Directions" section is intended to highlight known information gaps in our process level understanding regarding observed temporal and (or) spatial changes in mercury species concentrations in the abiotic compartments (water and sediment) and observed changes in biosentinel species. Base-of-food-web processes in the study region represent one such information gap.

The Marsh Environment

Phase 1 studies highlighted in this synthesis were all focused on open-water areas associated with the primary sloughs and ponds studied. However, part of the restoration habitat includes the fringing emergent marsh, and the ultimate trajectory of the SBSPRP will be a mosaic of emergent marsh existing along slough channels and within restored pond, as well as open water areas in slough channels and managed ponds. Thus, as far as understanding the effects of Phase 1 actions on the study area at large, emergent marsh areas were not represented, although vegetated salt marsh habitats have been shown to be particularly important zones for MeHg production (Marvin-DiPasquale and others, 2003). Limited research has been done in the fringing marsh zones along Alviso Slough during the Initial Stewardship Plan period of the restoration that preceded Phase 1, including the collection of deep sediment cores (Marvin-DiPasquale and Cox, 2007). One study examined benthic MeHg production in the rhizosphere (plant root) zone and demonstrated with devegetation plots that the very presence of the emergent marsh plants enhanced MeHg production in the salt marsh environment (Windham-Myers and others, 2009). In another early study that preceded Phase 1 activities, Grenier and others (2010) found a positive correlation between MeHg (as percentage of THg) in marsh surface sediment and mercury in song sparrow blood throughout the greater southern San Francisco Bay (including the fringing marsh of Alviso Slough). The processes that underlie this observed relationship remain unstudied.

Although we were able to model the flux of various mercury species at two locations (site ALSL-3 and the A8-TCS), as well as into pond A6 (figs. 48, 49, 52–56), the Phase 1 studies were not designed to fully account for where all of the remobilized mercury was eventually redeposited, and specifically how much was deposited in the emergent marsh environment during high-tide events. The lack of accounting for redeposited mercury in the fringing and emergent marsh environment represents an information gap with respect to potential mercury accumulation in biota that reside in this critical transition zone (for example the endangered *Reithrodontomys raviventris* [salt marsh harvest mouse]). A related information gap is a clear understanding of how the development of emergent marsh habitat over time will affect the net balance of MeHg production in the restoration area overall. Thus, as the SBSPRP proceeds, and as emergent marsh habitat becomes an ever-larger component of the restored area, studies that examine mercury biogeochemistry, transport processes, and bioaccumulation in this important zone may need to take on a new level of importance.

The Effect of Nutrients

Relative to other areas of San Francisco Bay, the lower southern San Francisco Bay, which encompasses all wetland restoration areas of the SBSPRP, is enriched in nutrients, owing chiefly to effluent discharge from three waste water treatment plants that service the densely populated southern San Francisco Bay region and supply the majority of freshwater input to the lower southern San Francisco Bay during the annual dry season (Crauder and others, 2016). There are several interrelated processes that indicate the biogeochemical cycling of nutrients can play an important role in the biogeochemical cycling of mercury and its subsequent bioaccumulation.

First, nutrients fuel phytoplankton growth. Senescent (dying, decaying, and sinking) phytoplankton is a very labile (easily degraded) form of organic matter that is deposited to the sediment zone and fuels benthic anaerobic bacteria that are involved in producing MeHg. Areas that receive a higher flux of senescent phytoplankton to the sediment zone tend to have more organic-rich sediment and higher rates of MeHg production.

Second, as phytoplankton cells die and lyse (break down), they release dissolved organic carbon (DOC) to the water column, and phytoplankton blooms are typically associated with high levels of water column DOC. The partitioning of THg and MeHg in the water column and sediment zone is primarily controlled by DOC concentrations. As DOC concentrations increase the proportion of mercury in the aqueous and (or) dissolved (filter-passing) phase increases. The partitioning of mercury between the particulate and aqueous phases has a direct effect on the uptake of mercury into the base of the food web, as uptake of MeHg by living phytoplankton is increased as DOC increases (Pickhardt and Fisher, 2007)

Third, phytoplankton are the entry point for mercury into the base of the food web. When phytoplankton concentrations are high, a decrease in the amount of MeHg taken up per phytoplankton cell can occur (biodilution) and thus decrease the amount of MeHg transferred to higher trophic levels in the food web (for example, into zooplankton) (Pickhardt and others, 2002; Luengen and Flegal, 2009). Thus, spatial and temporal variations in phytoplankton biomass, as mediated by both nutrients and light availability, have a direct effect on the mass transfer of MeHg into the base of the food web and subsequently the bioaccumulation of MeHg to upper trophic level species (fish and birds).

These relationships between nutrients, phytoplankton production and biomass and mercury dynamics (that is, microbial MeHg production, mercury species partitioning and the transfer of MeHg into the base of the food web) are complicated and poorly understood in most systems. Although some critical research examining these interactions has been done in the greater southern San Francisco Bay area (Luengen and Flegal, 2009), little is known about how they play out in the complex mosaic of habitats that make up the SBSPRP study area. Unraveling these interactions was beyond the scope of this synthesis product, which focused almost exclusively on mercury chemistry, transport, and bioaccumulation. However, as part of the Phase 1 data collection efforts there exists a significant amount of nonmercury ancillary data for surface water and sediment (tables 2 and 3; Marvin-DiPasquale and others[2019]) that were not discussed in this report, but were statistically analyzed (appendices 5–12) and provide an invaluable starting point for better understanding how nutrients and phytoplankton dynamics impact the mercury cycle in the SBSPRP study area. While much work remains to be done, we provide below a few brief observations based on the data collected thus far that may help to focus future research efforts.

Both reference sloughs (Mallard and Guadalupe Sloughs at sample sites MALSL and GUASL, respectively) sampled during Phase 1 are associated with wastewater treatment plants, with site MALSL having the highest mean dissolved inorganic nitrogen (DIN) levels (as $NO_3^- + NO_2^-$) of all sites sampled; 2.7-fold higher than site GUASL, 5.5 to 7.0-fold higher than Alviso Slough sites, and 6-fold to 130-fold higher levels than any of the pond sites (appendix 5). In contrast, mean ortho-phosphate (PO_4^{3-}) concentrations were highest at site GUASL; 2.3-fold higher than site MALSL, 3.1 to 4.8-fold higher than Alviso Slough sites, and 3.1 to 3.6-fold higher than any of the ponds (appendix 5). Mean Chl.a concentration was highest at site MALSL followed by site GUASL, and both were higher than Alviso Slough sites (appendix 5). Mean DOC in surface water was also elevated in both MALSL and GUASL, relative to Alviso Slough sites (appendix 5).

Although the two reference sloughs exhibited differences in nutrient status and Chl.a concentrations (as previously described), they are similar in that neither receives significant contemporary mercury inputs from the watershed. However, surface water p.MeHg (volumetric) concentration was 2-fold higher in site GUASL compared to site MALSL (appendix 5) and THg levels in Mississippi silverside were also generally higher in site GUASL compared to site MASL (fig. 15). One possible explanation that could account for the higher observed THg levels in Mississippi silverside at site GUASL, compared to site MALSL, is excess dissolved inorganic nitrogen loading in Mallard Slough, leading to more plankton biomass and the biodilution of MeHg into the base of the food web. We also note statistically higher MeHg concentrations, MeHg as a percentage of THg, and values of k_{meth} in the surface sediment of site MALSL, compared to model term low.ASLS (appendix 10; as assessed in MODEL SED.1 by Tukey's post-hoc pair-wise comparison). These observations related to sediment mercury metrics are consistent with the enhanced labile organic loading in the form of phytoplankton to the sediment compartment within Mallard Slough and to subsequent enhanced benthic MeHg production, owing to dissolved inorganic nitrogen eutrophication. An alternate explanation could be that sediment scour in Alviso Slough resulted in lower MeHg concentrations in surface sediment than would otherwise be the case. Finally, we note that as more A8-TCS gates were opened (from 0 or 1 gate to 3, 5, or 8 gates) we observed higher Chl.a concentrations within the A8-complex, along with an increasing $[NO_3^- + NO_2^-]/PO_3^{4-}$ ratio, and a decrease in p.MeHg (appendix 7), again indicating a potential linkage between nutrients, phytoplankton production, and the biodilution of MeHg at the base of the food web.

Future research focused on the direct and indirect effects of nutrients on MeHg formation, transport and bioaccumulation would greatly inform the current process-level understanding of how these relations are themselves affected by SBSPRP management actions and wetland restoration more generally. With the current emphasis on the monitoring and reduction of nutrients in San Francisco Bay, particular southern San Francisco Bay (https://sfbaynutrients.sfei.org/), there is a potential opportunity to coordinate activities of this ongoing nutrient monitoring program with focused studies designed to address some of the above outstanding questions related to nutrient-mercury interaction in support of SBSPRP management.

Conclusion

The purpose of this report was to bring together the findings from several loosely coordinated and separately funded studies that took place as part of Phase 1 of the South Bay Salt Pond Restoration Project (SBSPRP) effort (between 2010 and 2018), and to synthesize those findings into a more unified and holistic narrative regarding how restoration activities affected mercury mobilization and bioaccumulation in and around the restoration area. The development of this more comprehensive narrative was accomplished by considering the key results of the individual studies side-by-side and in some instances combining data from separate studies to derive new insights.

As the SBSPRP moves forward with additional planned or proposed restoration actions, there is a potential benefit in the creation of larger and more tightly coordinated research working groups, made up of scientists with unique expertise in contaminants and estuarine biogeochemistry, biota studies, geomorphology, field-based high-resolution water quality monitoring, remote sensing technology, and modeling (hydrologic, geomorphic, and contaminants). In an optimal scenario, such a working group would develop an overarching study plan that is well integrated and coordinated from the onset, and the study plan would consist of a framework that allows for routine and timely data sharing and a common vision for products that are more comprehensive and holistic than the sum of the individually contributed parts, which is akin to and in the spirit of the current synthesis document. Towards this vision is the idea of coordinating studies intensively in a single or in a limited number of restoration areas; a common study area for the team of collaborators to conduct highly integrated research activities, with the idea that this spatially focused multidiscipline approach can maximize what can be learned regarding specific types of restoration activities and how or to what extent they affect mercury cycling and bioaccumulation.

References Cited

Achete, F.M., 2016, Multiple scales of suspended sediment dynamics in a complex geometry estuary: Delft, The Netherlands, Delft University of Technology, Department of Coastal Engineering and Port Development, Doctoral thesis 593, 138 p.

Achete, F.M., van der Wegen, M., Roelvink, D., and Jaffe, B., 2015, A 2-D process-based model for suspended sediment dynamics—A first step towards ecological modeling: Hydrology and Earth System Science, v. 19, p. 2837–2857.

Ackerman, J., Herzog, M.P., Evers, D.C., Cristol, D.A., Kenow, K.P., Heinz, G.H., Lavoie, R.A., Brasso, R.L., Mallory, M.L., Provencher, J.F., Braune, B.M., Matz, A., Schmutz, J.A., Eagles-Smith, C.A., Savoy, L.I., Meyer, M.W., and Hartman, C., 2020, Synthesis of maternal transfer of mercury in birds—Implications for altered toxicity risk: Environmental Science and Technology, v. 54, p. 2878–2891.

Ackerman, J.T., and Eagles-Smith, C.A., 2009, Selenium bioaccumulation and body condition in shorebirds and terns breeding in San Francisco Bay, California, USA: Environmental Toxicology and Chemistry, v. 28, no. 10, p. 2134–2141.

Ackerman, J.T., Eagles-Smith, C.A., Heinz, G., De La Cruz, S.E., Takekawa, J.Y., Miles, A.K., Adelsbach, T.L., Herzog, M.P., Bluso-Demers, J.D., Demers, S.A., Herring, G., Hoffman, D.J., Hartman, C.A., Willacker, J.J., Suchanek, T.H., Schwarzbach, S.E., and Maurer, T.C., 2014a, Mercury in birds of San Francisco Bay-Delta, California—Trophic pathways, bioaccumulation, and ecotoxicological risk to avian reproduction: U.S. Geological Survey, Open-File Report 2014–1251, 222 p., https://doi.org/10.3133/ofr20141251.

Ackerman, J.T., Eagles-Smith, C.A., Herzog, M.P., and Hartman, C.A., 2016a, Maternal transfer of contaminants in birds—Mercury and selenium concentrations in parents and their eggs: Environmental Pollution, v. 210, p. 145–154.

Ackerman, J.T., Eagles-Smith, C.A., Herzog, M.P., Hartman, C.A., Peterson, S.H., Evers, D.C., Jackson, A.K., Elliott, J.E., Vander Pol, S.S., and Bryan, C.E., 2016b, Avian mercury exposure and toxicological risk across western North America—A synthesis: Science of The Total Environment, v. 568, p. 749–769.

Ackerman, J.T., Eagles-Smith, C.A., Herzog, M.P., Herring, G., Strong, C., and Mruz, E., 2010, Response of waterbird breeding effort, nest success, and mercury concentrations in eggs and fish to altered salt pond water management; Data summary: South Bay Salt Pond Restoration Project and Resources Legacy Fund, prepared by U.S. Geological Survey, 28 p.

Ackerman, J.T., Eagles-Smith, C.A., Herzog, M.P., Yee, J.L., and Hartman, C.A., 2016c, Egg laying sequence influences egg mercury concentrations and egg size in three bird species—Implications for contaminant monitoring programs: Environmental Toxicology and Chemistry, v. 35, p. 1458–1469.

Ackerman, J.T., Eagles-Smith, C.A., Takekawa, J.Y., Bluso, J.D., and Adelsbach, T.L., 2008a, Mercury concentration in blood and feathers of prebreeding Forster's terns in relation to space use of San Francisco Bay, California, USA, habitats: Environmental Toxicology and Chemistry, v. 27, no. 4, p. 897–908.

Ackerman, J.T., Eagles-Smith, C.A., Takekawa, J.Y., Demers, S.A., Adelsbach, T.L., Bluso, J.D., Miles, A.K., Warnock, N., Suchanek, T.H., and Schwarzbach, S.E., 2007, Mercury concentrations and space use of prebreeding American avocets and black-necked stilts in San Francisco Bay: Science of The Total Environment, v. 384, p. 452–466.

Ackerman, J.T., Eagles-Smith, C.A., Takekawa, J.Y., and Iverson, S.A., 2008b, Survival of postfledging Forster's terns in relation to mercury exposure in San Francisco Bay: Ecotoxicology, v. 17, p. 789–801.

Ackerman, J.T., Hartman, C.A., Herzog, M.P., Takekawa, J.Y., Robinson, J.A., Oring, L.W., Skorupa, J.P., and Boettcher, R., 2020b, American avocet (*Recurvirostra americana*) in Poole, A., ed., Birds of World: Ithaca, New York, Cornell Lab of Ornithology, accessed March 9, 2022, at https://birdsoftheworld.org/bow/species/ameavo/1.0/introduction.

Ackerman, J.T., Herzog, M.P., and Hartman, C.A., 2014b, Waterbird egg mercury concentrations in South San Francisco Bay; 2010–2014: South Bay Salt Pond Restoration Project and Resources Legacy Fund, prepared by U.S. Geological Survey,13 p.

Ackerman, J.T., Herzog, M.P., and Hartman, C.A., 2015, Waterbird Egg Mercury Concentrations in South San Francisco Bay; 2010–2015: South Bay Salt Pond Restoration Project and Resources Legacy Fund, prepared by U.S. Geological Survey, 12 p.

Ackerman, J.T., Herzog, M.P., and Hartman, C.A., 2016d, Waterbird Egg Mercury Concentrations in South San Francisco Bay; 2010–2016: South Bay Salt Pond Restoration Project and Resources Legacy Fund, prepared by U.S. Geological Survey, 12 p.

Ackerman, J.T., Herzog, M.P., and Hartman, C.A., 2017, Waterbird Egg Mercury Concentrations in South San Francisco Bay; 2010–2017: South Bay Salt Pond Restoration Project and Resources Legacy Fund, prepared by U.S. Geological Survey, 15 p.

Ackerman, J.T., Herzog, M.P., Hartman, C.A., Watts, T., and Barr, J., 2014c, Waterbird egg mercury concentrations in response to wetland restoration in south San Francisco Bay, California: U.S. Geological Survey, Open-File Report 2014–1189, 22 p.

Ackerman, J.T., Herzog, M.P., and Hobbs, J., 2014d, Data summary of fish mercury concentrations in 2014 for the South Bay Salt Pond Restoration Project: South Bay Salt Pond Restoration Project and Resources Legacy Fund, prepared by U.S. Geological Survey, 5 p.

Ackerman, J.T., Herzog, M.P., and Schwarzbach, S.E., 2013a, Methylmercury is the predominant form of mercury in bird eggs—A synthesis: Environmental Science & Technology, v. 47, p. 2052–2060.

Ackerman, J.T., Marvin-DiPasquale, M., Slotton, D., Eagles-Smith, C.A., Herzog, M.P., Hartman, C.A., Agee, J.L., and Ayers, S., 2013b, The South Bay Mercury Project—Using biosentinels to monitor effects of wetland restoration for the South Bay Salt Pond Restoration Project: South Bay Salt Pond Restoration Project and Resources Legacy Fund, prepared by U.S. Geological Survey and University of California at Davis, 227 p., accessed June 2, 2020, at https://www.southbayrestoration.org/document/south-bay-mercury-project-using-biosentinels-monitor-effects-wetland-restoration-south-0.

Ackerman, J.T., Overton, C.T., Casazza, M.L., Takekawa, J.Y., Eagles-Smith, C.A., Keister, R.A., and Herzog, M.P., 2012, Does mercury contamination reduce body condition of endangered California clapper rails?: Environmental Pollution, v. 162, p. 439–448.

Ackerman, J.T., Takekawa, J.Y., Eagles-Smith, C.A., and Iverson, S.A., 2008c, Mercury contamination and effects on survival of American avocet and black-necked stilt chicks in San Francisco Bay: Ecotoxicology, v. 17, p. 103–116.

Athearn, N.D., Takekawa, J.Y., Jaffe, B., Hattenbach, B.J., and Foxgrover, A.C., 2010, Mapping elevations of tidal wetland restoration sites in San Francisco Bay: comparing accuracy of aerial lidar with a singlebeam echosounder: Journal of Coastal Research, v. 26, no. 2, p. 312–319.

Austin, C.M., 2006, Guadalupe River Watershed—Mercury Total Maximum Daily Load Project Report: California Regional Water Quality Control Board, San Francisco Bay Region, 150 p., accessed June 10, 2020, at https://www.waterboards.ca.gov/rwqcb2/water_issues/programs/TMDLs/guadalupe_river_mercury/guadalupemercuryprojectreport012406.pdf.

Bailey, E.H., and Everhart, D.L., 1964, Geology and quicksilver deposits of the New Almaden district, Santa Clara County, California: U.S. Geological Survey Professional Paper 360, 214 p., https://doi.org/10.3133/pp360.

Bluso-Demers, J.D., Colwell, M.A., Takekawa, J.Y., and Ackerman, J.T., 2008, Space use by Forster's terns breeding in South San Francisco Bay: Waterbirds, v. 31, p. 357–364.

Booker, M., DeGroot, M., and Harris, K., 2010, From salt ponds to refuge in San Francisco Bay: Stanford University—Spatial History Lab, accessed June 10, 2020, at https://web.stanford.edu/group/spatialhistory/cgi-bin/site/pub.php?id=49&project_id=.

California Water Boards, 2019, Water quality objectives, chap. 3 *of* Water Quality Control Plan (Basin Plan) for the San Francisco Bay Basin: State of California Water Boards, Region 2—San Francisco, accessed November 21, 2019, at www.waterboards.ca.gov/sanfranciscobay/basin_planning.html.

Callaway, J.C., Schile, L.M., Borgnis, E.L., Busnardo, M., Archbald, G., and Duke, R., 2013, Sediment dynamics and vegetation recruitment in newly restored salt ponds—Final report for pond A6 sediment study: Resources Legacy Fund and South San Francisco Bay Salt pond Restoration Project, 29 p., accessed December 3, 2019, at https://www.southbayrestoration.org/document/sediment-dynamics-and-vegetation-recruitment-newly-restored-salt-ponds-final-report-pond.

Chételat, J., Ackerman, J.T., Eagles-Smith, C.A., and Hebert, C.E., 2020, Methylmercury exposure in wildlife—A review of the ecological and physiological processes affecting contaminant concentrations and their interpretation: Science of the Total Environment, v. 711, no. 135117, 18 p.

Conaway, C.H., Watson, E.B., Flanders, J.R., and Flegal, A.R., 2004, Mercury deposition in a tidal marsh of south San Francisco Bay downstream of the historic New Almaden mining district, California: Marine Chemistry, v. 90, p. 175–184.

Crauder, J., Downing-Kunz, M.A., Hobbs, J.A., Manning, A.J., Novick, E., Parchaseo, F., Wu, J., Schoellhamer, D.H., Senn, D.B., Shellenbarger, G.G., Thompson, J., and Yee, D., 2016, Lower south bay nutrient synthesis: San Francisco Estuary Institute & Aquatic Science Center, Contribution 732, 237 p.

Deltare, 2014, D-Flow Flexible Mesh, technical reference manual: Deltares Systems, 170 p. accessed December 10, 2019, at https://content.oss.deltares.nl/delft3d/manuals/D-Flow_FM_Technical_Reference_Manual.pdf.

Demers, S.A., Colwell, M.A., Takekawa, J.Y., and Ackerman, J.T., 2008, Breeding stage influences space use of female American avocets in San Francisco Bay, California: Waterbirds, v. 31, p. 365–371.

Downing-Kunz, M.A., and Schoellhamer, D.H., 2015, Suspended-sediment trapping in the tidal reach of an estuarine tributary channel: Estuaries and Coasts, v. 38, no. 6, p. 2198–2212.

Eagles-Smith, C.A., and Ackerman, J.T., 2009, Rapid changes in small fish mercury concentrations in estuarine wetlands—Implications for wildlife risk and monitoring programs: Environmental Science and Technology, v. 43, p. 8658–8664.

Eagles-Smith, C.A., and Ackerman, J.T., 2014, Mercury bioaccumulation in estuarine wetland fishes—Evaluating habitats and risk to coastal wildlife: Environmental Pollution, v. 193, p. 147–155.

Eagles-Smith, C.A., Ackerman, J.T., Yee, J., and Adelsbach, T.L., 2009, Mercury demethylation in waterbird livers—Dose-response thresholds and differences among species: Environmental Toxicology and Chemistry, v. 28, p. 568–577.

EDAW, Philip Williams and Associates, L., H.T. Harvey and Associates, Brown and Caldwell, and Geomatrix, 2007, South bay salt pond restoration project environmental impact statement/report—Volumes 1 and 2: U.S. Fish and Wildlife Service, California Department of Fish Game, and U.S. Army Corps of Engineers, prepared by EDAW, Philip Williams and Associates, L., H.T. Harvey and Associates, Brown and Caldwell, and Geomatrix, accessed April 10, 2020, at https://www.southbayrestoration.org/document/final-eisr-downloads-december-2007.

Edwards, T.K., and Glysson, G.D., 1999, Field methods for measurement of fluvial sediment: US. Geological Survey Techniques of Water-Resources Investigations, book 3, chap. 2, 89 p.

Foxgrover, A.C., Finlayson, D.P., Jaffe, B.E., and Fregoso, T.A., 2018, Bathymetry and digital elevation models of Coyote Creek and Alviso Slough, South San Francisco Bay, California (ver. 4.0, March 2018): U.S. Geological Survey Open-File Report 2011–1315, 24 p., https://doi.org/10.3133/ofr20111315.

Foxgrover, A.C., Marvin-DiPasquale, M., Jaffe, B.E., and Fregoso, T.A., 2019, Slough evolution and legacy mercury remobilization induced by wetland restoration in South San Francisco Bay: Estuarine, Coastal and Shelf Science, v. 202, p. 1–12.

Gerrard, P., and St. Louis, V., 2001, The effects of experimental reservoir creation on the bioaccumulation of methylmercury and reproductive success of tree swallows (*Tachycineta bicolor*): Environmental Science & Technology, v. 35, p. 1329–1338.

Gray, J.R., Glysson, G.D., Turcios, L.M., and Schwarz, G.E., 2000, Comparability of suspended-sediment concentration and total suspended solids data: U.S. Geological Survey Water-Resources Investigations Report 2000-4191, 20 p.

Greenfield, B.K., and Jahn, A., 2010, Mercury in San Francisco Bay forage fish: Environmental Pollution, v. 158, no. 8, p. 2716–2724.

Greenfield, B.K., Slotton, D.G., and Harrold, K.H., 2013, Predictors of mercury spatial patterns in San Francisco Bay forage fish: Environmental Toxicology & Chemistry, v. 32, no. 12, p. 2728–2737.

Grenier, L., Marvin-DiPasquale, M., Drury, D., Hunt, J., Robinson, A., Bezalel, S., Melwani, A., Agee, J., Kakouros, E., Kieu, L., Windham-Myers, L., and Collins, J., 2010, South Baylands Mercury Project: California State Coastal Conservancy, prepared by San Francisco Estuary Institute, U.S. Geological Survey, and Santa Clara Valley Water District, 97 p., accessed October 29, 2019, at https://www.southbayrestoration.org/sites/default/files/documents/SBMP_Final%20Report%2010FEB2010.pdf.

Grieb, T.M., Bowie, G.L., Driscoll, C.T., Gloss, S.P., Schofield, C.L., and Porcella, D.B., 1990, Factors affecting mercury accumulation in fish in the upper Michigan peninsula: Environmental Toxicology and Chemistry, v. 9, no. 7, p. 919–930.

Hartman, A.C., Ackerman, J.T., Schacter, C., Herzog, M.P., Tarjan, M., Wang, Y., Strong, C., Tertes, R., and Warnock, N., 2021, Breeding waterbird populations have declined in San Francisco Bay—An assessment over two decades: San Francisco Estuary and Watershed Science, v. 19, no. 3, p. 1–28.

Hartman, C.A., Ackerman, J.T., Herzog, M.P., Strong, C.M., Trachtenbarg, D., and Shore, C.A., 2017, Evaluation of Caspian Tern (*Hydroprogne caspia*) and Snowy Plover (*Charadrius alexandrinus nivosus*) Nesting on Modified Islands at the Don Edwards San Francisco Bay National Wildlife Refuge, California—2016 Annual Report: U.S. Geological Survey Open-file Report 2017–1055, 37 p., https://doi.org/10.3133/ofr20171055.

Heinz, G.H., Hoffman, D.J., Klimstra, J.D., and Stebbins, K.R., 2009, Rapid increases in mercury concentrations in the eggs of mallards fed methylmercury: Environmental Toxicology and Chemistry, v. 28, p. 1979–1981.

Herring, G., Ackerman, J.T., and Eagles-Smith, C.A., 2010, Embryo malposition as a potential mechanism for mercury-induced hatching failure in bird eggs: Environmental Toxicology and Chemistry, v. 29, p. 1788–1794.

Herzog, M.P., Ackerman, J.T., Eagles-Smith, C.A., and Hartman, C.A., 2016, It's what's inside that counts—Egg contaminant concentrations are influenced by estimates of egg density, egg volume, and fresh egg mass: Ecotoxicology, v. 25, p. 770–776.

Hobbs, J., 2018, Aquatic species response to restoring tidal flows to the pond A8 complex, Alviso Marsh, South San Francisco Bay, Final Report, Survey Years 2014-2018: Santa Clara Valley Water District and South Bay Salt Pond Restoration Project, 27 p., accessed March 9, 2022, at https://www.southbayrestoration.org/sites/default/files/documents/hobbs_nekton_comparison_sloughs.pdf.

Hoffman, D.J., Eagles-Smith, C.A., Ackerman, J.T., Adelsbach, T.L., and Stebbins, K.R., 2011, Oxidative stress response of Forster's terns (*Sterna forsteri*) and Caspian terns (*Hydroprogne caspia*) to mercury and selenium bioaccumulation in liver, kidney, and brain: Environmental Toxicology and Chemistry, v. 30, p. 920–929.

Jaffe, B., and Foxgrover, A.C., 2006, Sediment deposition and erosion in south San Francisco Bay, California, from 1956 to 2005: U.S. Geological Survey Open-File Report 2006-1287, 24 p., https://doi.org/10.3133/ofr20061287.

Kelly, C.A., Rudd, J.W.M., Bodaly, R.A., Roulet, N.P., St.Louis, V.L., Heyes, A., Moore, T.R., Schiff, S., Aravena, R., Scott, K.J., Dyck, B., Harris, R., Warner, B., and Edwards, G., 1997, Increases in fluxes of greenhouse gases and methyl mercury following flooding of an experimental reservoir: Environmental Science and Technology, v. 31, p. 1334–1344.

Kendall, C., Silva, S.R., and Kelly, V.J., 2001, Carbon and nitrogen isotopic compositions of particulate organic matter in four large river systems across the United States: Hydrological Processes, no. 15, p. 1301–1346.

Levesque, V.A., and Oberg, K.A., 2012, Computing discharge using the index velocity method: U.S. Geological Survey Techniques and Methods 3–A23, 148 p., https://pubs.usgs.gov/tm/3a23/.

Life Science!, Inc., 2004, South Bay Salt Ponds Initial Stewardship Plan - Final environmental impact report/environmental impact statement: California Department of Fish and Game, and U.S. Fish and Wildlife Service, prepared by Life Science!, Inc., 618 p., accessed October 10, 2019, at https://www.southbayrestoration.org/document/initial-stewardship-plan.

Luengen, A.C., and Flegal, A.R., 2009, Role of phytoplankton in mercury cycling in the San Francisco Bay estuary: Limnology and Oceanography, v. 54, p. 23–40.

Lutz, M.A., Brigham, M.E., and Marvin-DiPasquale, M., 2008, Procedures for collecting and processing streambed sediment and pore water for analysis of mercury as part of the National Water-Quality Assessment Program: U.S. Geological Survey Open-File Report 2008–1279, 68 p., https://pubs.usgs.gov/of/2008/1279/.

Marvin-DiPasquale, M., Agee, J., Bouse, R., and Jaffe, B., 2003, Microbial cycling of mercury in contaminated pelagic and wetland sediments of San Pablo Bay, California: Environmental Geology, v. 43, no. 3, p. 260–267.

Marvin-DiPasquale, M., and Cox, M.H., 2007, Legacy mercury in Alviso Slough, south San Francisco Bay, California—Concentration, speciation and mobility: U.S. Geological Survey Open-File Report number 2007-1240, 98 p., https://pubs.usgs.gov/of/2007/1240/.

Marvin-DiPasquale, M.C., Agee, J.L., Arias, M.R., Kakouros, E., and Kieu, L.H., 2019, Mercury speciation and other constituent data for surface sediment and water associated with the South San Francisco Bay Salt Pond Restoration, 2010–18: U.S. Geological Survey Data Release, https://doi.org/10.5066/P9MERSKP.

Marvin-DiPasquale, M.C., Arias, M.R., Agee, J.L., Kieu, L.H., Kakouros, E., Jaffe, B.E., and Wahl, D.B., 2018, Mercury speciation and other constituent data from deep sediment cores in Alviso Slough, South San Francisco Bay, California, 2012–16: U.S. Geological Survey, Data Release, https://doi.org/10.5066/F7HQ3Z3K.

McKee, L.J., Bonnema, A., David, N., Davis, J.A., Franz, A., Grace, R., Greenfield, B.K., Gilbreath, A.N., Grosso, C., Heim, W.A., Hunt, J.A., Leatherbarrow, J.E., Lowe, S., Pearce, S.A., Ross, J.R.M., and Yee, D., 2017, Long-term variation in concentrations and mass loads in a semi-arid watershed influenced by historic mercury mining and urban pollutant sources: Science of the Total Environment, v. 605–606, p. 482–497.

McKee, L.J., Gilbreath, A., Pearce, S., and Shimabuku, I., 2018, Guadalupe River mercury concentrations and loads during the large rare January 2017 storm: San Francisco Estuary Institute, Contribution No. 837, 41 p., accessed December 20, 2019, at https://www.sfei.org/documents/guadalupe-river-mercury-concentrations-and-loads-during-large-rare-january-2017-storm.

McNicholl, M.K., Lowther, P.E., and Hall, J.A., 2020, Forster's Tern (*Sterna forsteri*), (ver. 1.0), *in* Poole, A., ed., Birds of the World: Ithaca, New York, Cornell Lab of Ornithology, accessed March 9, 2022, at https://doi.org/10.2173/bow.forter.01.

Miles, A.K., and Ricca, M.A., 2010, Temporal and spatial distributions of sediment mercury at salt pond wetland restoration sites, San Francisco Bay, CA, USA: Science of The Total Environment, v. 408, no. 5, p. 1154–1165.

Oakland Museum of CA, [undated], Guide to San Francisco Bay area creeks—Guadalupe Slough Watershed: An Oakland Museum of CA website, accessed on June 26, 2020, at http://explore.museumca.org/creeks/1410-RescGuadSl.html.

Ohlendorf, H.M., Custer, T.W., R.W., L., Rigney, M., and Cromartie, E., 1988, Organochlorines and mercury in eggs of coastal terns and herons in California, USA: Colonial Waterbirds, v. 11, p. 85–94.

Pickhardt, P.C., and Fisher, N.S., 2007, Accumulation of inorganic and methylmercury by freshwater phytoplankton in two contrasting water bodies: Environmental Science and Technology, v. 41, p. 125–131.

Pickhardt, P.C., Folt, C.L., Chen, Y.C., Klaue, B., and Blum, J.D., 2002, Algal blooms reduce the uptake of toxic methylmercury in freshwater food webs, v. 99, no. 7, p. 4419–4423.

Rasmussen, P.P., Gray, J.R., Glysson, G.D., and Ziegler, A.C., 2009, Guidelines and procedures for computing time-series suspended-sediment concentrations and loads from in-stream turbidity-sensor and streamflow data: U.S. Geological Survey Techniques and Methods, book 3, chap. C4, 52 p., https://doi.org/10.3133/tm3C4.

Rey, C., 2015, Mud dynamics in a tidal channel—The impact of opening salt ponds on channel deepening: Delft, the Netherlands, UNESCO-IHE Institute for Water Education, master's thesis, 93 p.

Röbke, B.R., and van der Wegen, M., 2018, Calabazas-San Tomas Aquino pond A8 reconnection—Preliminary scenario simulations: Santa Clara Valley Water District, prepared by Deltares, document 11200020-002, 15 p., accessed January 23, 2020, at https://www.southbayrestoration.org/sites/default/files/documents/creek_realignment_-_deltares.pdf.

Ruhl, C.A., and Simpson, M.R., 2005, Computation of discharge using the Index-Velocity Method in tidally affected areas: U.S. Geological Survey Scientific Investigations Report 2005–5004, 31 p., https://doi.org/10.3133/sir20055004.

Rytuba, J.J., 2003, Mercury from mineral deposits and potential environmental impact: Environmental Geology, v. 43, p. 326–338.

San Francisco Bay Conservation and Development Commission, 2005, Salt ponds: San Francisco Bay Conservation and Development Commission Staff Report, 78 p., accessed October 5, 2019, at https://bcdc.ca.gov/planning/reports/SaltPonds_Jun2005.pdf.

San Francisco Estuary Institute-Aquatic Science Center, 2018, Resilient landscape vision for the Calabazas Creek, San Tomas Aquino Creek, and pond A8 area—Bayland-creek reconnection opportunities: San Francisco Estuary Institute-Aquatic Science Center, Healthy Watersheds, Resilient Baylands Design Advisory Team, Santa Clara Valley Water District, and South Bay Salt Ponds Restoration Project, Publication #870, 40p., accessed December 12, 2020, at https://www.sfei.org/sites/default/files/biblio_files/CalabazasVision_SFEI_061118_lowres_v2.pdf.

Scheuhammer, A.M., Meyer, M.W., Sandheinrich, M.B., and Murray, M.W., 2007, Effects of environmental methylmercury on the health of wild birds, mammals, and fish: Ambio, v. 36, p. 12–18.

Schwarzbach, S., and Adelsbach, T., 2003, Field assessment of avian mercury exposure in the bay-delta ecosystem. CALFED Bay-Delta Mercury Project, subtask 3B *of* Aassessment of ecological and human health impacts of mercury in the bay-delta watershed: CALFED Bay-Delta Program, prepared by U.S. Geological Survey and U.S. Fish and Wildlife Service, 30 p., 30 p.

Schwarzbach, S.E., Albertson, J.D., and Thomas, C.M., 2006, Effects of predation, flooding, and contamination on reproductive success of California clapper rails (*Rallus longirostris obsoletus*) in San Francisco Bay: Auk, v. 123, no. 1, p. 45–60.

Seelos, M., 2017, Guadalupe River Watershed mercury TMDL [total maximum daily load]—2016–2017 progress report on methylmercury production and control measures: Environmental Planning Unit, Watershed Stewardship and Planning Division, and Santa Clara Valley Water District, 130 p., accessed March 9, 2020, at https://californiarevealed.org/islandora/object/cavpp%3A172541.

Slotton, D.G., Ayers, S.M., Suchanek, T.H., Weyand, R.D., and Liston, A.M., 2004, Mercury bioaccumulation and trophic transfer in the Cache Creek watershed of California, in relation to diverse aqueous mercury exposure conditions—Subtask 5B *of* Assessment of ecological and human health impacts of mercury in the San Francisco Bay-Delta Watershed: CALFED Bay-Delta Program, prepared by University of California at Davis and U.S. Fish and Wildlife Service, 74 p., accessed September 5, 2019, at https://loer.tamug.edu/calfed/Report/Final/UCDavis_Cache_Bio_Final.pdf.

Slotton, D.G., Ayers, S.M., Suchanek, T.H., Weyand, R.D., Liston, A.M., Asher, C., Nelson, D.C., and Johnson, B., 2002, The effects of wetlands restoration on the production and bioaccumulation of methylmercury in the Sacramento-San Joaquin Delta, California: CALFED Bay-Delta Program, prepared by University of California at Davis and U.S. Fish and Wildlife Service, 76 p., accessed March 10, 2022, at https://loer.tamug.edu/calfed/Report/DraftFinal/UCD_Delta_Report.pdf.

St. Louis, V.L., Rudd, J.W.M., Kelly, C.A., Bodaly, R.A.D., Paterson, M.J., Beaty, K.G., Hesslein, R.H., Heyes, A., and Majewski, A.R., 2004, The rise and fall of mercury methylation in an experimental reservoir: Environmental Science and Technology, v. 38, no. 5, p. 1348–1358.

Stickel, L., Wiemeyer, S., and Blus, L.J., 1973, Pesticide residues in eggs of wild birds—Adjustment for loss of moisture and lipid: Bulletin of Environmental Contamination and Toxicology, v. 9, p. 193–196.

Trulio, L.D., Clark, D., Ritchie, S., Hutzel, A., Callaway, J., Collins, J., Gross, E., Herbold, B., Josselyn, M., Nichols, F., O’Doherty, G., Schoellhamer, D., Strong, C., LeFer, D., Takahashi, L., Takekawa, J., Trivedi, D., and Warnock, N., 2007, Appendix D (Adaptive management plan) *of* Final environmental impact statement/report: South Bay Salt Pond Restoration Project, 143 p., accessed March 10, 2022, at https://www.southbayrestoration.org/sites/default/files/documents/appendix_d_final_amp.pdf.

U.S. Environmental Protection Agency, 1991, Determination of mercury in tissues by cold vapor atomic absorption spectrophotometry: U.S. Environmental Protection Agency Method 245.6, 13 p.

U.S. Environmental Protection Agency, 2000, Mercury in solids and solutions by thermal decomposition, amalgamation, and atomic absorption spectrophotometry: U.S. Environmental Protection Agency Method 7473 (SW 846, update IVA), 17 p.

van der Wegen, M., Reyns, J., Jaffe, B., and Foxgrover, A., 2018, Modeling morphodynamic development in the Alviso Slough system, South San Francisco Bay, California: South San Francisco Bay Salt Pond Restoration Project, prepared by IHE Delft and U.S. Geological Survey, 30 p., accessed March 30, 2020, at https://www.southbayrestoration.org/document/modeling-morphodynamic-development-alviso-slough-system-south-san-francisco-bay-california.

Wagner, R.J., Boulger, R.W., Jr., Oblinger, C.J., and Smith, B.A., 2006, Guidelines and standard procedures for continuous water-quality monitors—Station operation, record computation, and data reporting: U.S. Geological Survey Techniques and Methods 1–D3, 51 p.

Willacker, J.J., Eagles-Smith, C.A., Lutz, M.A., Tate, M.T., Lepak, J.M., and Ackerman, J.T., 2016, Reservoirs and water management influence fish mercury concentrations in the western United States and Canada: Science of The Total Environment, v. 568, p. 739–748.

Williams, B.K., Nichols, J.D., and Conroy, M.J., 2002, Analysis and management of animal populations—Modeling, estimation, and decision making: San Diego, California, Academic Press, 817 p.

Windham-Myers, L., Marvin-DiPasquale, M., Krabbenhoft, D.P., Agee, J.L., Cox, M.H., Heredia-Middleton, P., Coates, C., and Kakouros, E., 2009, Experimental removal of wetland emergent vegetation leads to decreased methylmercury production in surface sediment: Journal of Geophysical Research—Biogeosciences, 14 p., https://doi.org/10.1029/2008JG000815.

Wood, J., Hayden, M., Veloz, S., Nur, N., Snyder, R., and Elrod, M., 2019, South bay salt pond restoration project—Phase 2 science synthesis report: South Bay Salt Pond Restoration Project and the California Wildlife Foundation, prepared by Point Blue Conservation Science (Contribution No. 2265), accessed June 1, 2020, at https://www.southbayrestoration.org/document/phase-2-science-synthesis.

Appendixes

Appendix 1. South Bay Salt Ponds: Coordinated Studies and Field Sampling Timeline [2010–2018]

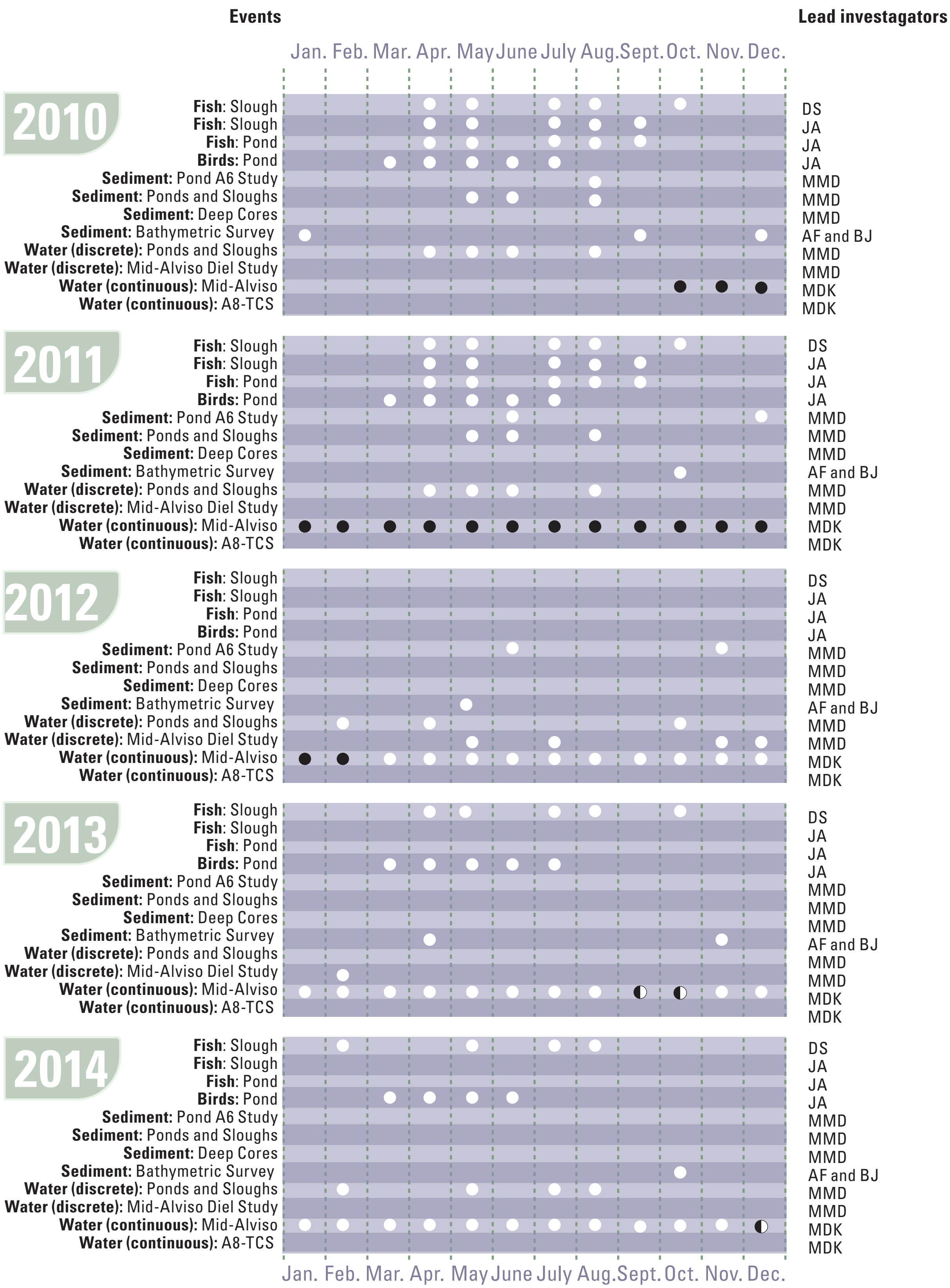

South Bay Salt Ponds—Coordinated Studies and Field Sampling Timeline (2010–2018)

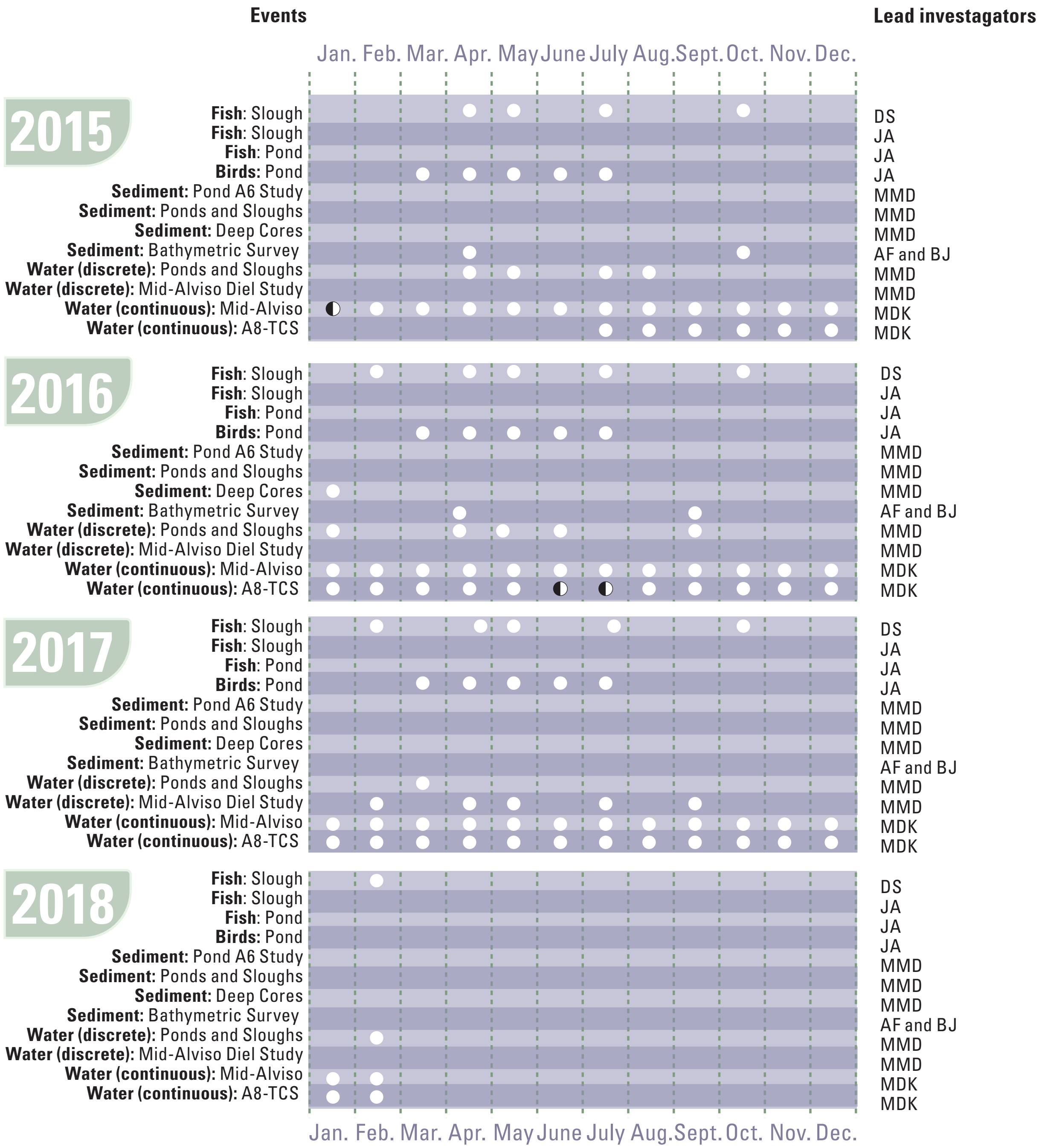

Figure 1.1 (pages 116 and 117). Diagram showing the timing (year and month) of the various field sampling efforts conducted during the 2010–18 study period, as part of the multiple South Bay Salt Pond Restoration Project (SBSPRP) activities detailed in this report. Fields with circles indicate when field activities were done and who the lead investigator was for each activity. Black circles indicate periods (October 2010 through February 2012) where data collected from the middle Alviso Slough were limited to temperature, conductivity, and (or) turbidity, and did not include water velocity, which was added beginning in March 2012). Half black and white circles indicate periods when all fixed-station continuous monitoring was interrupted for more than a few days. The lead investigator(s) overseeing each listed field activity are identified by initials: AF, Amy Foxgrover; BJ, Bruce Jaffe; DS, Darell Slotton; JA, Josh Ackerman; MMD, Mark Marvin-DiPasquale; MDK, Maureen Downing-Kunz. TCS, tidal control structure.

Appendix 2. Predictive Models for Mercury Species Concentrations

Table 2.1. Model equations derived for estimating mercury species concentrations at sample locations used to calculate mercury flux at fixed monitoring site ALSL-3 (USGS station 11169750, March 2012 through February 2018) and at fixed monitoring site A8-TCS (USGS station 372525121584701, February 2016 through February 2018), within the Alviso Slough study area of the Southern San Francisco Bay region.

[Specific linear models developed to predict mercury species concentrations for the purpose of calculating mercury flux at high-resolution fixed-monitoring sites ALSL-3 and A8-TCS. A8-complex refers to interconnected ponds A5, A7, and A8(S). ALSL-2(b) refers to models in which data from sites ALSL-2 and ALSL-2b were combined. Mercury species notations are defined in table 2. All mercury species are modeled on a volumetric basis (nanograms per liter). In addition to the model derived equations used to calculate the site-specific mercury concentrations, the following model specific information is provided: tidal direction modeled, coefficient of determination (R^2), and the number of observations (N) in each model. Dates given in the Cos [JD] minimum date column are in month and day format. Definitions of model variables: p.THg, particulate total mercury; TSS, total suspended sediment (as measured on a 0.7 micrometer glass fiber filter, in milligrams per liter); COS[JD], Julian day as a cosine function adjusted so that the function minimum value falls on the date noted; ST, water column stage (depth in feet); p.MeHg, particulate methylmercury; f.THg, filter-passing total mercury; NA, not applicable; Q_{GR}, Guadalupe River discharge (in cubic meters per second); f.MeHg, filter-passing methylmercury; TEMP, temperature (in degrees Celsius); SpC, specific conductance (in millisiemens per centimeter)]

Location	Tidal direction modeled	Mercury species	Model R2	N	Cos[JD] minimum date	Model Equation
ALSL-3	flood and ebb	p.THg	0.80	146	October 17	(0.290*TSS)+(26.62*COS[JD])+(−30.61*ST)+((TSS-203.9)*(ST−2.13)*(−0.0679)+32.62
ALSL-3	flood and ebb	p.MeHg	0.92	146	May 18	(0.00307*TSS)+(−0.298*COS[JD])+(−0.341*ST)+(TSS−203.9)*(ST−2.13)*(−0.00222)+(COS[JD]−1.11)*(TSS-203.9)*(−0.00159)+1.13
ALSL-2(b)	flood only	f.THg	0.96	12	NA	(0.143 * Q_{GR})+(0.245*ST)−0.113
ALSL-2(b)	flood only	f.MeHg	0.60	19	NA	(0.00704*TEMP)+(0.0180*Q_{GR})+((TEMP−20.23)*(Q_{GR}−2.34)*0.00209)−0.0992
ALSL-2(b)	flood only	p.THg	0.88	19	NA	(0.0774*TSS)+(3.18*Q_{GR})+16.11
ALSL-2(b)	flood only	p.MeHg	0.37	19	NA	(−0.0165*SpC)+(0.00264*TSS)+0.387
Pond A8	ebb only	f.THg	0.89	42	NA	(0.181*Q_{GR})+1.58
Pond A8	ebb only	f.MeHg	0.41	42	October 1	(0.0167*Q_{GR})+(−0.0668*COS[JD])+(Q_{GR}−2.115)*(COS[JD]−1.226)*(−0.0297)+0.138
Pond A8	ebb only	p.THg	0.64	40	NA	(−0.406*SpC)+(0.0621*TSS)+(0.721*Q_{GR})+15.8
A8-complex	ebb only	p.MeHg	0.36	75	May 1	(−0.00755*SpC)+(0.00224*TSS)+(0.109*COS[JD])+((SpC−24.14)*(COS[JD]−0.608)*0.0108)+0.160

Appendix 3. Year-Over-Year Change in Total Mercury of Three-Spine Stickleback

Table 3.1. Year-over-year change between 2010 and 2011 in three-spine stickleback total mercury, by site and month, in the Alviso Slough of the southern San Francisco Bay region.

[Same-site inter-annual trends at three Alviso Slough sites (ALSL-2, ALSL-3 and ALSL-4) and the Mallard Slough reference site (MALSL). The number of individual fish (N) is indicated for each month and year grouping. For each month and site, the year-over-year change (2011 minus 2010) in mean THg is given as percent change (relative to 2010 values). The statistical significance associated with this % change calculation was assessed based on a one-way analysis of variance (ANOVA) conducted for each month and site specific 2010 and 2011 data pair. THg, total mercury; µg/g, microgram per gram; dw, dry weight; Std error, standard error; Min, minimum; Max, maximum; P-value, probability value; –, no available data; NS, not significant]

Month	Year	N	Mean THg (µg/g dw)	Std error (µg/g dw)	Min (µg/g dw)	Max (µg/g dw)	Percent change	P value
				ALSL-2				
April	2010	–	–	–	–	–		
	2011	12	0.26	0.02	0.14	0.41	–	–
May	2010	10	0.30	0.02	0.17	0.46		
	2011	12	0.27	0.02	0.16	0.43	−12	NS
July	2010	12	0.36	0.03	0.20	0.57		
	[1]2011	12	0.47	0.05	0.23	0.75	31	0.034
August	2010	12	0.41	0.04	0.28	0.70		
	[1]2011	12	0.74	0.03	0.62	0.93	79	< 0.001
October	2010	12	1.00	0.12	0.38	1.61		
	[2]2011	12	0.62	0.05	0.38	0.97	−38	0.003
				ALSL-3				
April	2010	3	0.51	0.10	0.32	0.65		
	[2]2011	12	0.33	0.03	0.22	0.63	−35	0.019
May	2010	10	0.38	0.03	0.22	0.47		
	[2]2011	12	0.29	0.03	0.17	0.45	−24	0.015
July	2010	12	0.46	0.04	0.28	0.63		
	2011	12	0.50	0.09	0.15	1.28	9	NS
August	2010	12	0.38	0.02	0.31	0.56		
	[1]2011	12	0.59	0.04	0.28	0.76	54	< 0.001
October	2010	12	0.55	0.03	0.41	0.77		
	2011	12	0.59	0.04	0.35	0.76	7	NS

Table 3.1. Year-over-year change between 2010 and 2011 in three-spine stickleback total mercury, by site and month, in the Alviso Slough of the southern San Francisco Bay region.—Continued

Month	Year	N	Mean THg (µg/g dw)	Std error (µg/g dw)	Min (µg/g dw)	Max (µg/g dw)	Percent change	P value
				ALSL-4				
April	2010	–	–	–	–	–		
	2011	12	0.29	0.02	0.18	0.41	–	–
May	2010	10	0.34	0.03	0.18	0.44		
	[2]2011	12	0.25	0.02	0.12	0.33	−29	0.005
July	2010	12	0.50	0.06	0.14	0.90		
	2011	12	0.48	0.05	0.23	0.87	−4	NS
August	2010	12	0.41	0.04	0.20	0.67		
	[1]2011	12	0.62	0.06	0.33	0.83	52	0.003
October	2010	12	0.48	0.04	0.22	0.70		
	2011	12	0.45	0.04	0.20	0.68	−7	NS
				MALSL				
April	2010	10	0.24	0.01	0.19	0.30		
	2011	12	0.28	0.02	0.13	0.42	18	NS
May	2010	10	0.33	0.03	0.19	0.52		
	[2]2011	12	0.22	0.02	0.14	0.35	−34	0.003
July	2010	12	0.43	0.03	0.22	0.58		
	[2]2011	12	0.26	0.07	0.09	0.91	−41	0.010
August	2010	12	0.37	0.03	0.20	0.50		
	[2]2011	12	0.30	0.01	0.21	0.35	−20	0.010
October	2010	12	0.33	0.04	0.14	0.58		
	[1]2011	12	0.49	0.04	0.29	0.86	51	0.004

[1]Row of values represents significant increases at a probability level of $p < 0.05$

[2]Row of values represents significant decreases at a probability level of $p < 0.05$

Appendix 4. Year-Over-Year Change in Total Mercury of Mississippi Silverside

Table 4.1. Year-over-Year change between 2010 and 2011 in Mississippi silverside total mercury concentration, by site and month, in the Alviso Slough of the southern San Francisco Bay region.

[Same-site inter-annual trends at three Alviso Slough sites (ALSL-2, ALSL-3 and ALSL-4) and the Mallard Slough reference site (MALSL). The number of composites (N) and individual fish (total inds.) are indicated for each month and year grouping. For each month and site, the year-over-year change (2011 minus 2010) in mean THg is given as percent change (relative to 2010 values). The statistical significance associated with this percent change calculation was assessed on the basis of a one-way one-way analysis of variance (ANOVA) done for each month and site specific 2010 and 2011 data pair. THg, total mercury; µg/g, microgram per gram; dw, dry weight; Std error, standard error; Min, minimum; Max, maximum; P value, probability; –, no available data; NS, not significant]

Month	Year	N	n (total inds.)	Mean THg (µg/g dw)	Std error (µg/g dw)	Min (µg/g dw)	Max (µg/g dw)	Percent change	P value (if significant)
				ALSL-2					
April	2010	–	–	–	–	–	–		
	2011	6	41	1.46	0.14	0.99	1.93	–	–
May	2010	6	32	0.78	0.08	0.48	0.94		
	2011	6	38	0.81	0.15	0.41	1.45	4	NS
July	2010	6	37	0.64	0.14	0.23	1.08		
	[1]2011	6	16	1.26	0.17	0.74	1.80	97	0.008
August	2010	6	44	1.02	0.09	0.81	1.27		
	[2]2011	6	40	0.67	0.06	0.50	0.84	−35	0.003
October	2010	6	48	0.75	0.07	0.54	0.96		
	2011	6	48	0.72	0.05	0.61	0.89	−4	NS
				ALSL-3					
April	2010	–	–	–	–	–	–		
	2011	6	48	1.30	0.08	1.09	1.62	–	–
May	2010	6	34	0.95	0.09	0.62	1.18		
	[1]2011	6	31	1.26	0.11	0.96	1.72	33	0.026
July	2010	6	28	0.73	0.14	0.48	1.40		
	2011	6	24	0.93	0.17	0.43	1.45	26	NS
August	2010	6	47	0.97	0.08	0.71	1.26		
	[2]2011	6	46	0.67	0.07	0.51	1.00	−30	0.010
October	2010	6	48	0.93	0.05	0.77	1.08		
	[2]2011	6	48	0.67	0.02	0.61	0.71	−28	< 0.001

Table 4.1. Year-over-Year change between 2010 and 2011 in Mississippi silverside total mercury concentration, by site and month, in the Alviso Slough of the southern San Francisco Bay region.—Continued

Month	Year	N	n (total inds.)	Mean THg (µg/g dw)	Std error (µg/g dw)	Min (µg/g dw)	Max (µg/g dw)	Percent change	P value (if significant)
				ALSL-4					
April	2010	–	–	–	–	–	–		
	2011	4	4	2.18	0.40	1.25	2.85	–	–
May	2010	12	12	0.68	0.11	0.13	1.74		
	[1]2011	6	9	1.3	0.09	0.95	1.54	92	0.001
July	2010	8	8	0.62	0.19	0.22	1.94		
	2011	–	–	–	–	–	–	–	–
August	2010	6	22	0.97	0.17	0.55	1.42		
	2011	6	48	0.82	0.09	0.65	1.26	−16	NS
October	2010	6	30	0.71	0.11	0.32	1.04		
	2011	6	48	0.63	0.05	0.46	0.78	−11	NS
				MALSL					
April	2010	5	10	0.39	0.06	0.23	0.57		
	[1]2011	6	39	0.69	0.10	0.5	1.00	79	0.015
May	2010	6	40	0.57	0.07	0.31	0.76		
	2011	6	19	0.62	0.06	0.48	0.83	8	NS
July	2010	6	48	0.42	0.10	0.25	0.91		
	[2]2011	6	48	0.22	0.03	0.16	0.35	−49	0.041
August	2010	6	45	0.36	0.02	0.31	0.45		
	[2]2011	6	48	0.21	0.01	0.17	0.26	−42	< 0.001
October	2010	6	48	0.37	0.03	0.25	0.47		
	2011	6	48	0.38	0.02	0.28	0.45	2	NS

[1]Row of values represents significant increases at a probability level of $p < 0.05$

[2]Row of values represents significant decreases at a probability level of $p < 0.05$

Appendix 5. Surface-Water Statistics for 2010–18

Table 5.1. Surface-water summary statistics by sample location (site or area) in the southern San Francisco Bay study area for years 2010–18.

[The summary statistics given for each surface-water parameter include the number of observations (N); mean, standard error (Std Err) of the mean, geometric (mean, minimum (Min), 25th percent quartile (25%Q), median, 75th percent quartile (75%Q) and maximum (Max). The locations listed reflect either individual sampling sites (pond A3N [site A3N], pond A16 [site A16], Mallard Slough [site MALSL], Guadalupe Slough [site GUASL]) or two or more sites in a sampling area (A8-complex [multiple sites as shown on fig. 4], upper Alviso Slough [up.ALSL [sites ALSL-1 and ALSL-2], lower Alviso Slough (low.ALSLS [sites ALSL-3 and ALSL-4]). Nc, not calculated (geometric mean is not able to be calculated on negative numbers). See table 2 in the report for parameter and unit definitions]

Type	Location	N	Mean	Mean std err	Geometric mean	Min	25%Q	Median	75%Q	Max
f.THg, in ng/L										
Pond	A8-complex	115	2.08	0.09	1.94	1.12	1.57	1.80	2.15	6.61
Pond	A3N	32	1.50	0.09	1.42	0.58	1.09	1.49	1.82	2.60
Pond	A16	29	1.92	0.12	1.82	1.04	1.44	1.67	2.33	3.36
Slough	up.ALSL	35	1.56	0.18	1.35	0.63	0.92	1.26	1.76	5.49
Slough	low.ALSL	43	1.82	0.13	1.70	0.96	1.41	1.55	1.98	5.81
Slough	MALSL	27	1.52	0.12	1.42	0.58	1.11	1.39	1.81	3.43
Slough	GUASL	21	1.54	0.10	1.46	0.63	1.12	1.59	1.87	2.43
f.MeHg, in ng/L										
Pond	A8-complex	115	0.30	0.05	0.13	0.02	0.05	0.10	0.24	3.31
Pond	A3N	33	0.30	0.03	0.23	0.02	0.19	0.27	0.46	0.69
Pond	A16	29	0.18	0.05	0.10	0.02	0.05	0.09	0.21	1.43
Slough	up.ALSL	35	0.07	0.00	0.07	0.03	0.04	0.07	0.09	0.16
Slough	low.ALSL	33	0.08	0.01	0.07	0.01	0.04	0.07	0.11	0.25
Slough	MALSL	27	0.10	0.01	0.09	0.02	0.07	0.10	0.13	0.19
Slough	GUASL	21	0.13	0.01	0.11	0.03	0.07	0.12	0.17	0.27
f.MeHg, as a % of f.THg										
Pond	Complex	115	12.60	1.80	6.50	1.10	3.00	5.60	11.80	93.60
Pond	A3N	32	20.10	2.40	15.90	1.60	15.20	18.10	23.60	72.80
Pond	A16	29	10.70	3.20	5.70	1.00	2.40	5.10	12.60	91.10
Slough	up.ALSL	35	5.80	0.60	5.00	1.80	3.20	4.70	8.20	14.00
Slough	low.ALSL	33	5.20	0.80	4.00	1.20	2.20	3.30	8.00	17.30
Slough	MALSL	27	6.90	0.60	6.30	3.20	4.40	6.30	9.70	12.60
Slough	GUASL	21	8.30	1.10	7.30	3.40	4.90	6.90	9.60	24.90
p.THg, in ng/g, dw										
Pond	A8-complex	114	168.00	18.00	115.00	11.00	74.00	102.00	170.00	1,089.00
Pond	A3N	33	27.00	3.00	24.00	8.00	18.00	23.00	32.00	96.00
Pond	A16	29	89.00	13.00	71.00	14.00	44.00	75.00	104.00	369.00
Slough	up.ALSL	35	602.00	84.00	440.00	87.00	205.00	388.00	884.00	2,016.00
Slough	low.ALSL	43	241.00	39.00	183.00	61.00	111.00	144.00	273.00	1,613.00
Slough	MALSL	27	186.00	21.00	163.00	77.00	100.00	166.00	250.00	556.00
Slough	GUASL	21	134.00	9.00	129.00	84.00	97.00	137.00	159.00	253.00

Table 5.1. Surface-water summary statistics by sample location (site or area) in the southern San Francisco Bay study area for years 2010–18.—Continued

Type	Location	N	Mean	Mean std err	Geometric mean	Min	25%Q	Median	75%Q	Max
p.THg, in ng/L										
Pond	A8-complex	114	13.3	0.8	11.0	1.3	7.6	11.6	16.9	58.0
Pond	A3N	33	37.6	3.0	34.4	15.5	25.0	38.0	42.6	104.3
Pond	A16	29	6.6	0.7	5.7	0.7	4.6	6.0	7.5	20.9
Slough	up.ALSL	35	28.5	2.8	25.6	9.4	20.3	24.8	33.0	106.7
Slough	low.ALSL	43	29.1	4.3	22.3	7.6	14.2	20.1	32.6	163.0
Slough	MALSL	27	12.0	2.6	8.1	1.4	4.5	8.7	13.2	67.7
Slough	GUASL	21	18.3	2.0	16.4	8.8	10.6	14.0	25.3	39.6
p.MeHg, in ng/g dw										
Pond	A8-complex	115	5.59	0.48	3.98	0.53	2.41	3.59	8.46	38.02
Pond	A3N	33	2.11	0.27	1.46	0.06	1.34	1.79	2.34	7.71
Pond	A16	29	7.46	1.90	4.78	0.54	2.95	5.25	9.85	57.54
Slough	up.ALSL	35	7.10	0.81	5.21	0.92	2.73	7.29	10.42	17.39
Slough	low.ALSL	43	2.75	0.30	2.16	0.49	1.33	2.23	3.73	9.16
Slough	MALSL	27	3.51	0.33	3.05	0.77	2.14	3.55	4.58	8.29
Slough	GUASL	21	3.44	0.52	2.82	1.31	1.64	2.34	5.24	8.88
p.MeHg, in ng/L										
Pond	A8-complex	115	0.67	0.09	0.38	0.06	0.18	0.41	0.59	6.38
Pond	A3N	33	2.93	0.31	2.18	0.19	1.76	2.51	4.69	5.89
Pond	A16	29	0.60	0.14	0.38	0.06	0.24	0.47	0.63	3.99
Slough	up.ALSL	35	0.34	0.03	0.30	0.11	0.23	0.30	0.43	0.80
Slough	low.ALSL	43	0.33	0.04	0.26	0.10	0.16	0.24	0.40	1.04
Slough	MALSL	27	0.24	0.05	0.15	0.03	0.08	0.15	0.30	1.29
Slough	GUASL	21	0.48	0.09	0.36	0.12	0.18	0.31	0.76	1.69
p.MeHg, as a % of p.THg										
Pond	A8-complex	114	5.74	0.62	3.48	0.72	1.64	2.92	7.66	32.84
Pond	A3N	33	7.98	0.85	6.17	0.58	5.58	7.25	10.44	22.15
Pond	A16	29	8.68	1.34	6.69	1.55	3.93	8.45	10.46	39.43
Slough	up.ALSL	35	1.38	0.13	1.19	0.45	0.76	1.21	1.85	3.81
Slough	low.ALSL	43	1.36	0.12	1.19	0.39	0.82	1.23	1.66	4.26
Slough	MALSL	27	2.34	0.38	1.88	0.65	1.22	2.01	2.79	10.34
Slough	GUASL	21	2.67	0.41	2.19	0.98	1.28	1.83	3.65	7.00
p.RHg, in ng/g dw										
Pond	A8-complex	77	4.33	0.38	3.49	0.88	2.14	3.31	5.27	19.82
Pond	A3N	24	0.80	0.10	0.68	0.20	0.47	0.70	1.02	2.34
Pond	A16	20	2.21	0.35	1.73	0.34	1.07	1.61	2.91	5.72
Slough	up.ALSL	19	4.69	0.76	3.34	0.06	2.10	4.05	6.01	13.86
Slough	low.ALSL	27	4.14	0.36	3.82	1.90	2.80	3.89	5.28	10.16
Slough	MALSL	19	4.11	0.44	3.42	0.50	3.09	4.13	5.68	7.24
Slough	GUASL	21	3.19	0.24	2.94	0.54	2.49	3.18	3.69	5.90

Table 5.1. Surface-water summary statistics by sample location (site or area) in the southern San Francisco Bay study area for years 2010–18.—Continued

Type	Location	N	Mean	Mean std err	Geometric mean	Min	25%Q	Median	75%Q	Max
p.RHg, in ng/L										
Pond	A8-complex	77	0.32	0.03	0.27	0.04	0.20	0.29	0.39	1.95
Pond	A3N	24	1.40	0.18	1.13	0.23	0.66	1.15	2.09	3.39
Pond	A16	20	0.19	0.03	0.16	0.06	0.12	0.14	0.24	0.46
Slough	up.ALSL	19	0.47	0.06	0.42	0.21	0.30	0.39	0.58	1.12
Slough	low.ALSL	27	0.54	0.04	0.50	0.27	0.34	0.52	0.77	0.98
Slough	MALSL	19	0.28	0.05	0.21	0.03	0.12	0.23	0.40	0.87
Slough	GUASL	21	0.45	0.06	0.38	0.07	0.24	0.39	0.62	1.26
p.RHg, as a % of p.THg										
Pond	A8-complex	76	2.92	0.18	2.55	0.84	1.66	2.50	3.95	8.67
Pond	A3N	24	4.05	0.38	3.58	0.58	2.98	3.24	5.63	8.91
Pond	A16	20	3.56	0.60	2.76	0.59	1.72	2.83	4.24	10.66
Slough	up.ALSL	19	1.53	0.19	1.16	0.02	0.95	1.21	2.33	3.09
Slough	low.ALSL	27	2.49	0.19	2.28	0.51	1.81	2.39	3.08	4.96
Slough	MALSL	19	2.81	0.33	2.41	0.62	1.70	2.48	4.22	5.11
Slough	GUASL	21	2.43	0.17	2.28	0.56	1.97	2.26	2.99	3.88
Kd(THg), in L/kg										
Pond	A8-complex	114	78,758	6,493	58,819	7,298	39,821	53,974	93,026	364,750
Pond	A3N	32	17,671	1,451	16,033	5,566	12,480	16,686	20,346	44,955
Pond	A16	29	46,303	5,045	39,169	8,832	25,408	38,740	59,777	118,326
Slough	up.ALSL	35	523,010	102,071	324,959	65,643	125,911	269,994	790,113	3,202,524
Slough	low.ALSL	43	137,198	16,067	107,149	35,195	65,230	88,896	214,404	480,806
Slough	MALSL	27	132,530	14,131	114,832	39,363	75,791	117,983	160,707	307,078
Slough	GUASL	21	98,868	15,541	87,895	46,310	74,161	89,807	99,452	399,452
Kd(MeHg), in L/kg										
Pond	A8-complex	115	46,308	4,158	31,637	1,797	20,179	33,217	56,589	286,872
Pond	A3N	33	6,960	564	6,294	2,400	4,573	6,397	8,479	15,128
Pond	A16	29	83,052	15,440	45,844	3,672	15,955	77,682	124,761	341,058
Slough	up.ALSL	35	105,610	15,234	77,415	11,028	43,515	86,563	123,603	382,977
Slough	low.ALSL	33	39,394	5,181	31,013	11,269	16,878	27,241	55,874	131,078
Slough	MALSL	27	50,616	14,972	34,032	10,168	20,495	31,539	55,140	427,183
Slough	GUASL	21	33,774	5,767	26,279	6,406	16,277	27,754	39,913	113,260
POC, in % dw										
Pond	A8-complex	113	5.49	0.34	4.01	0.10	3.21	5.37	7.46	25.35
Pond	A3N	33	4.62	0.45	3.58	0.21	3.07	4.61	6.34	11.70
Pond	A16	29	7.94	0.94	6.33	1.55	3.37	7.03	11.29	19.45
Slough	up.ALSL	35	5.10	0.96	3.85	1.08	2.44	3.47	5.56	34.36
Slough	low.ALSL	43	2.64	0.24	2.29	0.95	1.50	2.04	3.52	8.34
Slough	MALSL	27	6.87	0.83	5.73	1.18	4.17	5.76	9.25	18.15
Slough	GUASL	21	3.38	0.43	2.83	0.84	1.87	2.90	5.19	7.50

Table 5.1. Surface-water summary statistics by sample location (site or area) in the southern San Francisco Bay study area for years 2010–18.—Continued

Type	Location	N	Mean	Mean std err	Geometric mean	Min	25%Q	Median	75%Q	Max
PN, in % dw										
Pond	A8-complex	113	0.80	0.04	0.60	0.02	0.51	0.75	1.08	2.56
Pond	A3N	32	0.49	0.04	0.42	0.09	0.32	0.48	0.65	1.17
Pond	A16	29	1.20	0.14	0.97	0.22	0.51	1.13	1.81	2.55
Slough	up.ALSL	35	0.72	0.17	0.50	0.13	0.33	0.47	0.72	5.99
Slough	low.ALSL	43	0.39	0.04	0.32	0.08	0.20	0.28	0.54	1.28
Slough	MALSL	27	0.96	0.14	0.76	0.14	0.52	0.72	1.13	3.10
Slough	GUASL	21	0.53	0.07	0.43	0.11	0.27	0.43	0.81	1.37
POC/PN, in molar ratio										
Pond	A8-complex	113	7.95	0.14	7.83	5.31	6.89	7.78	8.75	15.29
Pond	A3N	33	10.98	0.53	10.35	2.52	9.25	11.54	13.18	15.54
Pond	A16	29	7.77	0.27	7.65	5.83	6.40	7.88	8.51	11.80
Slough	up.ALSL	35	9.23	0.42	8.94	5.89	7.68	8.50	10.14	15.06
Slough	low.ALSL	43	8.90	0.45	8.53	4.63	7.29	8.55	9.44	23.08
Slough	MALSL	27	9.08	0.56	8.76	6.67	7.44	8.15	10.14	20.92
Slough	GUASL	21	7.72	0.22	7.66	5.96	7.08	7.61	8.22	9.85
δ13C-POC, in per mil										
Pond	A8-complex	114	−27.344	0.354	Nc	−36.237	−30.072	−28.235	−26.165	−15.467
Pond	A3N	33	−24.300	1.016	Nc	−44.404	−24.307	−22.615	−21.563	−18.144
Pond	A16	29	−24.204	0.612	Nc	−30.653	−27.095	−23.908	−21.626	−18.527
Slough	up.ALSL	35	−28.899	0.512	Nc	−36.009	−30.711	−28.695	−27.266	−21.354
Slough	low.ALSL	43	−28.046	0.480	Nc	−36.459	−28.936	−27.375	−26.195	−23.588
Slough	MALSL	27	−26.528	0.453	Nc	−32.533	−27.771	−26.243	−25.030	−22.460
Slough	GUASL	21	−25.287	0.374	Nc	−27.899	−26.546	−25.712	−23.916	−21.753
δ15N-PN, in per mil										
Pond	A8-complex	113	12.015	0.340	11.363	3.938	9.282	12.246	15.478	17.576
Pond	A3N	31	5.430	0.392	5.124	2.682	4.293	4.875	5.835	13.306
Pond	A16	29	15.980	0.913	14.920	3.759	13.103	16.065	20.071	24.069
Slough	up.ALSL	31	10.721	0.803	9.534	1.988	7.914	11.038	13.501	19.179
Slough	low.ALSL	42	9.602	0.775	8.523	1.466	7.169	8.978	10.987	30.789
Slough	MALSL	27	10.341	0.867	9.454	1.924	8.553	10.027	11.245	27.635
Slough	GUASL	21	9.881	0.922	8.652	1.018	6.865	9.678	13.614	18.065
E_h, in mv										
Pond	A8-complex	115	328	7	318	114	268	345	386	470
Pond	A3N	31	305	14	295	166	248	301	375	428
Pond	A16	29	293	14	284	186	226	284	353	414
Slough	up.ALSL	35	325	8	322	236	297	312	361	427
Slough	low.ALSL	41	324	10	317	231	268	300	388	443
Slough	MALSL	27	328	11	323	220	283	335	376	427
Slough	GUASL	21	351	15	344	205	306	360	397	472

Table 5.1. Surface-water summary statistics by sample location (site or area) in the southern San Francisco Bay study area for years 2010–18.—Continued

Type	Location	N	Mean	Mean std err	Geometric mean	Min	25%Q	Median	75%Q	Max
pH, in pH units										
Pond	A8-complex	115	8.52	0.04	8.51	7.53	8.22	8.51	8.78	9.63
Pond	A3N	31	8.81	0.07	8.80	7.98	8.45	8.92	9.10	9.48
Pond	A16	29	8.86	0.11	8.84	7.23	8.56	8.99	9.33	9.81
Slough	up.ALSL	35	7.96	0.07	7.95	7.24	7.64	7.92	8.25	9.13
Slough	low.ALSL	43	7.87	0.07	7.86	6.78	7.68	7.90	8.14	9.13
Slough	MALSL	27	7.98	0.10	7.96	6.62	7.69	8.02	8.30	9.08
Slough	GUASL	21	8.15	0.07	8.14	7.69	7.94	8.10	8.33	8.79
DO, in mg/L										
Pond	A8-complex	104	8.50	0.33	7.85	2.70	5.93	7.80	10.57	20.00
Pond	A3N	27	7.98	0.97	6.71	2.40	4.65	6.52	10.69	21.10
Pond	A16	27	11.56	0.84	10.68	4.50	7.90	11.91	14.60	18.30
Slough	up.ALSL	34	6.87	0.26	6.71	3.50	5.85	6.78	7.81	10.50
Slough	low.ALSL	41	6.69	0.26	6.49	3.80	5.73	6.40	7.71	12.52
Slough	MALSL	26	6.90	0.31	6.72	3.70	5.73	7.10	7.98	10.83
Slough	GUASL	18	6.16	0.40	5.96	4.00	4.90	5.63	7.38	10.00
DO, as % saturation										
Pond	A8-complex	100	94.3	3.8	86.9	28.0	64.3	89.4	114.0	206.0
Pond	A3N	26	107.1	12.3	88.9	26.0	53.8	102.2	149.9	271.0
Pond	A16	26	130.6	10.0	119.8	47.0	86.5	135.7	173.8	217.7
Slough	up.ALSL	33	76.0	2.9	74.2	42.0	64.2	71.5	87.1	110.1
Slough	low.ALSL	40	73.1	2.5	71.4	42.0	64.2	72.6	82.2	128.4
Slough	MALSL	25	79.2	3.9	76.8	40.0	69.0	80.1	89.2	134.3
Slough	GUASL	17	70.3	3.4	69.0	48.0	58.9	70.0	78.1	95.7
SpC, in mS/cm										
Pond	A8-complex	113	39.9	4.0	26.5	1.9	18.5	28.2	37.7	191.7
Pond	A3N	29	76.4	4.3	71.0	7.5	61.8	72.1	89.1	134.2
Pond	A16	29	21.9	2.3	17.5	4.4	7.6	23.6	32.9	41.9
Slough	up.ALSL	35	12.4	2.2	5.3	0.5	1.1	8.1	21.2	45.0
Slough	low.ALSL	42	20.8	1.9	15.9	0.9	10.1	19.9	31.5	43.4
Slough	MALSL	27	11.6	1.6	8.7	2.0	4.2	9.9	17.4	31.3
Slough	GUSL	20	22.0	2.3	17.6	0.7	15.1	21.6	28.2	38.7
DOC, in mg/L										
Pond	A8-complex	115	12.30	1.53	8.25	2.82	5.84	7.22	8.93	76.14
Pond	A3N	33	25.24	1.47	24.15	15.35	19.45	23.70	28.30	56.15
Pond	A16	29	7.58	0.25	7.45	4.49	6.76	7.67	8.70	9.78
Slough	up.ALSL	35	4.32	0.42	3.73	1.33	2.38	3.78	6.31	13.31
Slough	low.ALSL	32	5.01	0.22	4.84	2.52	4.12	5.10	6.18	7.65
Slough	MALSL	27	7.57	0.18	7.52	5.79	6.96	7.50	8.13	10.69
Slough	GUASL	21	8.05	0.36	7.87	4.68	6.79	8.22	9.18	10.55

Table 5.1. Surface-water summary statistics by sample location (site or area) in the southern San Francisco Bay study area for years 2010–18.—Continued

Type	Location	N	Mean	Mean std err	Geometric mean	Min	25%Q	Median	75%Q	Max
					$SUVA_{254}$, in L/mg C*m					
Pond	A8-complex	115	2.12	0.06	1.91	0.11	1.91	2.21	2.44	4.04
Pond	A3N	33	1.65	0.10	1.49	0.30	1.46	1.76	1.94	2.79
Pond	A16	29	2.47	0.19	2.22	0.17	1.96	2.16	2.53	5.15
Slough	up.ALSL	35	2.67	0.11	2.46	0.11	2.32	2.53	3.00	3.93
Slough	low.ALSL	32	2.35	0.09	2.18	0.10	2.21	2.34	2.54	3.19
Slough	MALSL	27	2.07	0.09	1.94	0.15	1.94	2.14	2.27	2.68
Slough	GUASL	21	2.12	0.12	1.86	0.06	2.01	2.12	2.35	2.93
					$NO_2^- + NO_3^-$, in mg/L as N					
Pond	A8-complex	115	0.17	0.02	0.10	0.03	0.03	0.07	0.30	1.15
Pond	A3N	33	0.06	0.01	0.05	0.03	0.03	0.03	0.07	0.20
Pond	A16	29	1.37	0.33	0.49	0.03	0.15	0.64	1.69	7.68
Slough	up.ALSL	35	1.20	0.13	0.89	0.03	0.55	1.00	1.76	2.73
Slough	low.ALSL	33	1.51	0.13	1.30	0.21	1.02	1.51	1.88	3.58
Slough	MALSL	27	8.38	0.75	7.53	3.55	4.73	8.24	11.24	17.88
Slough	GUASL	21	3.08	0.41	2.61	0.92	1.67	3.14	3.89	8.92
					PO_4^{3-}, in mg/L as P					
Pond	A8-complex	115	0.47	0.04	0.30	0.01	0.15	0.34	0.64	2.39
Pond	A3N	33	0.40	0.08	0.25	0.07	0.13	0.20	0.46	2.03
Pond	A16	29	0.45	0.05	0.33	0.03	0.22	0.37	0.68	1.05
Slough	up.ALSL	35	0.29	0.04	0.22	0.07	0.12	0.18	0.49	0.72
Slough	low.ALSL	33	0.45	0.05	0.35	0.02	0.24	0.42	0.63	1.46
Slough	MALSL	27	0.61	0.10	0.45	0.05	0.28	0.57	0.78	2.54
Slough	GUASL	21	1.43	0.17	1.16	0.12	0.93	1.44	1.87	3.27
					$(NO_2^-+NO_3^-)/PO_4^{3-}$, as molar ratio					
Pond	A8-complex	113	1.60	0.27	0.69	0.10	0.25	0.57	1.50	19.24
Pond	A3N	31	0.70	0.19	0.44	0.06	0.27	0.52	0.74	5.98
Pond	A16	29	11.43	2.86	3.26	0.08	0.77	2.97	19.68	46.15
Slough	up.ALSL	35	16.65	2.59	8.80	0.10	3.83	11.00	27.75	51.73
Slough	low.ALSL	33	16.33	7.16	8.29	0.32	5.13	7.82	13.09	243.73
Slough	MALSL	27	61.45	16.29	37.26	9.95	18.48	36.35	49.03	410.74
Slough	GUASL	21	6.14	0.92	4.98	1.76	2.91	4.46	9.71	17.08
					Chl.a, in mg/m^3					
Pond	A8-complex	115	29.9	3.4	18.5	0.4	12.6	23.1	38.3	343.2
Pond	A3N	33	72.8	8.1	59.1	12.1	35.5	59.7	103.6	231.9
Pond	A16	29	103.5	18.6	54.5	3.7	19.3	70.5	168.9	376.8
Slough	up.ALSL	35	14.8	2.9	6.5	0.2	1.9	8.4	21.0	72.7
Slough	low.ALSL	43	14.3	2.1	9.3	1.2	3.9	8.8	19.7	53.9
Slough	MALSL	27	33.2	11.4	11.5	1.2	3.2	10.3	24.6	254.6
Slough	GUASL	21	23.6	7.1	11.6	1.6	3.5	10.1	31.1	148.0

Table 5.1. Surface-water summary statistics by sample location (site or area) in the southern San Francisco Bay study area for years 2010–18.—Continued

Type	Location	N	Mean	Mean std err	Geometric mean	Min	25%Q	Median	75%Q	Max
TSS, in mg/L										
Pond	A8-complex	115	135	13	97	20	55	94	148	695
Pond	A3N	33	1,639	137	1,474	614	1,020	1,512	1,934	3,570
Pond	A16	29	94	12	79	26	53	78	110	350
Slough	up.ALSL	35	81	11	58	12	29	60	131	267
Slough	low.ALSL	43	142	12	123	39	85	122	174	426
Slough	MALSL	27	74	14	50	8	25	57	94	259
Slough	GUASL	21	145	17	128	41	100	123	176	397
Chl/TSS ratio, in mg/g, dw										
Pond	A8-complex	115	0.37	0.03	0.19	0.00	0.13	0.24	0.48	1.62
Pond	A3N	33	0.05	0.01	0.04	0.01	0.02	0.04	0.07	0.13
Pond	A16	29	1.19	0.20	0.69	0.07	0.26	0.90	1.96	3.38
Slough	up.ALSL	35	0.18	0.03	0.11	0.01	0.05	0.11	0.30	0.53
Slough	low.ALSL	43	0.12	0.02	0.08	0.01	0.03	0.07	0.18	0.54
Slough	MALSL	27	0.41	0.09	0.23	0.01	0.11	0.23	0.54	2.19
Slough	GUASL	21	0.18	0.06	0.09	0.02	0.04	0.07	0.25	1.18
SO_4^{2-}, in mmol/L										
Pond	A8-complex	77	12.2	0.7	9.5	0.9	8.5	12.6	16.3	24.9
Pond	A3N	24	54.8	2.7	53.3	36.1	45.4	49.8	65.9	94.2
Pond	A16	20	12.4	1.3	10.6	1.9	9.3	12.3	17.1	21.3
Slough	up.ALSL	19	10.6	1.4	7.8	0.7	7.8	10.2	13.7	23.2
Slough	low.ALSL	17	13.2	1.6	10.0	0.6	8.8	14.5	19.1	22.3
Slough	MALSL	19	6.7	0.9	5.5	1.5	3.5	5.8	9.2	15.1
Slough	GUASL	21	10.7	1.1	8.9	0.6	5.9	10.7	13.9	19.9
Cl^-, in mmol/L										
Pond	A8-complex	77	233	15	174	13	149	242	323	496
Pond	A3N	24	971	60	929	447	776	924	1,206	1,750
Pond	A16	20	237	25	197	27	175	236	310	434
Slough	up.ALSL	19	195	27	123	4	128	184	282	417
Slough	low.ALSL	17	251	32	173	4	153	306	352	408
Slough	MALSL	19	119	18	90	11	60	101	172	294
Slough	GUASL	21	204	23	155	2	124	199	262	410
SO_4^{2-}/Cl^-, as molar ratio										
Pond	A8-complex	77	0.055	0.001	0.055	0.046	0.050	0.053	0.056	0.093
Pond	A3N	24	0.060	0.004	0.057	0.048	0.050	0.054	0.059	0.150
Pond	A16	20	0.054	0.001	0.054	0.046	0.049	0.054	0.056	0.070
Slough	up.ALSL	19	0.071	0.010	0.064	0.046	0.052	0.056	0.062	0.233
Slough	low.ALSL	17	0.060	0.005	0.058	0.042	0.049	0.055	0.062	0.141
Slough	MALSL	19	0.064	0.005	0.061	0.045	0.052	0.058	0.066	0.136
Slough	GUASL	21	0.065	0.011	0.057	0.045	0.050	0.055	0.058	0.292

Table 5.1. Surface-water summary statistics by sample location (site or area) in the southern San Francisco Bay study area for years 2010–18.—Continued

Type	Location	N	Mean	Mean std err	Geometric mean	Min	25%Q	Median	75%Q	Max
EXO temp, in °C										
Pond	A8-complex	62	19.6	0.5	19.2	13.8	16.2	18.4	23.5	25.2
Pond	A3N	16	20.1	1.1	19.6	13.0	16.0	19.0	23.8	28.5
Pond	A16	16	19.8	0.9	19.5	14.7	16.4	19.6	23.5	25.8
Slough	up.ALSL	16	19.9	1.1	19.4	12.8	16.9	19.8	23.8	26.1
Slough	low.ALSL	15	19.4	1.0	19.0	12.7	17.0	19.6	22.7	25.0
Slough	MALSL	15	21.4	0.8	21.2	17.6	18.7	21.5	23.5	26.5
Slough	GUASL	15	19.0	1.0	18.6	13.3	15.7	18.2	22.6	24.5
EXO SpC, in µS/cm										
Pond	A8-complex	62	22,051	1,587	16,919	1,947	14,131	22,998	30,184	47,655
Pond	A3N	16	82,276	5,928	78,842	34,274	68,101	76,899	100,763	134,196
Pond	A16	16	23,675	2,793	20,083	4,362	16,200	23,860	32,259	41,038
Slough	up.ALSL	16	20,413	3,301	13,323	990	13,039	20,186	30,081	45,008
Slough	low.ALSL	15	24,256	3,571	17,051	847	14,611	26,953	36,103	43,371
Slough	MALSL	15	11,156	1,893	8,635	2,036	3,424	9,804	15,948	24,788
Slough	GUASL	15	17,471	2,239	13,747	649	9,878	18,892	21,487	34,093
EXO TDS, in mg/L										
Pond	A8-complex	62	14,333	1,032	10,997	1,266	9,185	14,948	19,620	30,976
Pond	A3N	16	53,479	3,854	51,247	22,278	44,266	49,985	65,496	87,228
Pond	A16	16	15,389	1,815	13,054	2,835	10,530	15,509	20,969	26,675
Slough	up.ALSL	16	13,268	2,145	8,660	644	8,475	13,121	19,552	29,255
Slough	low.ALSL	15	15,766	2,321	11,082	550	9,498	17,520	23,467	28,191
Slough	MALSL	15	7,251	1,231	5,613	1,323	2,225	6,373	10,367	16,112
Slough	GUASL	15	11,356	1,455	8,935	422	6,420	12,281	13,967	22,161
EXO salinity, in psu										
Pond	A8-complex	62	13.6	1.0	10.0	1.0	8.2	13.9	18.8	31.0
Pond	A3N	16	58.6	4.9	55.5	23.3	46.5	53.4	73.4	104.0
Pond	A16	16	14.6	1.8	12.1	2.3	9.5	14.5	20.2	26.3
Slough	up.ALSL	16	12.5	2.1	7.8	0.5	7.5	12.1	18.7	29.1
Slough	low.ALSL	15	15.1	2.3	10.2	0.4	8.5	16.6	22.8	27.9
Slough	MALSL	15	6.5	1.2	4.8	1.0	1.8	5.5	9.3	15.1
Slough	GUASL	15	10.5	1.4	8.1	0.3	5.6	11.2	12.9	21.4
EXO ODO, as % saturation										
Pond	A8-complex	62	114	4	110	53	96	112	135	189
Pond	A3N	16	119	10	112	48	85	117	156	189
Pond	A16	16	142	12	134	65	101	146	176	218
Slough	up.ALSL	16	84	5	82	55	66	82	104	110
Slough	low.ALSL	15	81	5	79	55	73	82	86	128
Slough	MALSL	15	87	4	86	64	78	88	92	134
Slough	GUASL	15	70	3	69	54	59	70	77	96

Table 5.1. Surface-water summary statistics by sample location (site or area) in the southern San Francisco Bay study area for years 2010–18.—Continued

Type	Location	N	Mean	Mean std err	Geometric mean	Min	25%Q	Median	75%Q	Max
EXO ODO, in mg/L										
Pond	A8-complex	62	9.78	0.37	9.32	3.88	7.59	9.82	11.60	16.57
Pond	A3N	16	7.72	0.69	7.21	3.50	5.36	7.75	10.56	11.47
Pond	A16	16	11.99	0.99	11.24	5.35	9.25	12.49	14.58	18.09
Slough	up.ALSL	16	7.14	0.44	6.94	4.66	5.61	6.92	8.62	10.50
Slough	low.ALSL	15	6.93	0.55	6.67	4.08	5.81	6.30	7.85	12.52
Slough	MALSL	15	7.47	0.34	7.36	5.30	6.84	7.18	8.26	10.83
Slough	GUASL	15	6.20	0.41	6.03	4.51	4.93	5.74	7.37	10.00
EXO pH, in pH units										
Pond	A8-complex	58	8.46	0.05	8.46	7.85	8.17	8.39	8.77	9.54
Pond	A3N	15	8.84	0.13	8.83	7.50	8.53	8.91	9.18	9.45
Pond	A16	15	8.86	0.18	8.84	7.52	8.74	9.05	9.32	9.90
Slough	up.ALSL	15	8.05	0.10	8.04	7.11	7.96	8.06	8.31	8.72
Slough	low.ALSL	14	7.87	0.11	7.86	7.06	7.72	7.85	8.14	8.57
Slough	MALSL	14	8.10	0.10	8.09	7.55	7.82	8.12	8.41	8.80
Slough	GUASL	14	8.03	0.09	8.03	7.30	7.73	8.09	8.32	8.51
EXO turbidity, in FNU										
Pond	A8-complex	62	15.5	1.0	12.8	1.5	9.6	14.8	20.2	36.2
Pond	A3N	16	75.1	7.8	67.9	20.7	46.8	75.7	100.6	129.5
Pond	A16	16	14.9	2.7	11.4	1.5	7.1	14.1	18.0	44.7
Slough	up.ALSL	16	31.9	4.2	28.7	16.6	19.7	25.0	39.4	73.0
Slough	low.ALSL	15	43.1	6.2	37.8	17.7	24.0	34.7	59.9	94.6
Slough	MALSL	15	23.2	4.7	18.3	5.3	13.5	18.3	28.6	76.3
Slough	GUASL	15	38.4	3.9	35.9	21.2	26.7	33.1	50.0	67.5
EXO Chlorophyll, in µg/L										
Pond	A8-complex	62	46.8	5.0	31.6	3.0	14.5	35.2	65.0	177.1
Pond	A3N	16	535.0	42.2	500.9	216.8	416.3	616.6	651.5	698.4
Pond	A16	16	86.5	19.7	45.1	3.6	12.5	48.7	172.2	216.7
Slough	up.ALSL	16	31.8	8.2	19.3	2.6	9.2	24.8	41.7	120.6
Slough	low.ALSL	15	15.9	4.0	10.7	2.1	5.5	9.8	21.0	60.8
Slough	MALSL	15	24.3	5.4	16.6	4.2	7.6	14.9	48.8	67.5
Slough	GUASL	15	24.3	7.3	11.2	1.3	4.1	7.1	53.9	81.0
EXO BGA-PC, in µg/L										
Pond	A8-complex	62	3.26	0.29	2.26	0.09	1.46	2.81	5.03	9.93
Pond	A3N	16	54.96	7.94	45.54	12.80	31.12	46.01	74.34	118.09
Pond	A16	16	9.31	3.60	3.44	0.04	0.88	6.00	12.02	60.02
Slough	up.ALSL	16	2.41	0.60	1.57	0.27	0.79	1.43	3.32	9.08
Slough	low.ALSL	15	1.47	0.36	0.96	0.05	0.53	1.01	1.59	5.22
Slough	MALSL	15	6.21	3.44	1.95	0.50	0.68	1.06	3.58	50.84
Slough	GUASL	15	1.97	0.47	1.05	0.06	0.29	1.57	4.07	5.37

Table 5.1. Surface-water summary statistics by sample location (site or area) in the southern San Francisco Bay study area for years 2010–18.—Continued

Type	Location	N	Mean	Mean std err	Geometric mean	Min	25%Q	Median	75%Q	Max
EXO fDOM, in QSU										
Pond	A8-complex	62	47.0	1.2	46.2	30.9	38.9	45.9	52.6	78.8
Pond	A3N	16	55.6	4.8	52.7	24.1	43.9	46.9	67.6	97.4
Pond	A16	16	63.0	2.5	62.3	43.8	54.9	61.9	71.2	78.1
Slough	up.ALSL	16	53.0	8.1	47.8	27.8	36.0	49.3	53.3	168.2
Slough	low.ALSL	15	44.9	2.6	43.7	28.7	35.0	47.2	52.6	62.0
Slough	MALSL	15	117.7	11.7	111.3	75.2	86.9	97.8	139.2	245.5
Slough	GUASL	15	59.1	5.0	55.5	22.3	50.7	55.6	70.3	91.0

Appendix 6. Surface-Water Model SW.1 Summary Statistics

Table 6.1. Summary statistics associated with surface-water Model SW.1.

[Surface-water Model SW.1 is a multivariable least squares mean model with two main terms, YEAR (2010, 2011) and REGION (low.ALSL, MALSL), and an interaction term (YEAR x REGION). Model regions low.ALSL refers to the lower Alviso Slough, whereas MALSL refers to Mallard Slough. The table below summarizes the results of this model as individually applied to the suite of water column parameters as the dependent (Y) variable. For each model term the resulting F statistic and probability (P) is given. For the F statistic, the value in parentheses (n.df, d.df) represent the numerator degrees of freedom (n.df) and denominator degrees of freedom (d.df), respectively. A post-hoc Student t-test (for the main terms) or Tukey's pairwise analysis (for the interaction term) was done for significant model main terms, The resulting ranking is indicated with "A" being the highest ranking and with factors sharing the same letter not being significant model main terms. Nonsignificant model terms are represented as "ns." See table 2 in the report for full definitions of each parameter and units]

Parameter	Units	Year (with student T-test rankings)			Region (with student T-test rankings)		
		F statistic	2010	2011	F statistic	low.ALSL	MALSL
f.THg	ng/L	F = (1, 20) 1.96; P > 0.18	ns	ns	F = (1, 20) 0.38; P > 0.54	ns	ns
f.MeHg	ng/L	F = (1, 20) 1.82; P > 0.19	ns	ns	F = (1, 20) 0.87; P > 0.36	ns	ns
f.MeHg	% of f.THg	F = (1, 20) 0.64; P > 0.43	ns	ns	F = (1, 20) 0.92; P > 0.35	ns	ns
p.THg	ng/g, dw	F = (1, 20) 5.56; P > 0.029	B	A	F = (1, 20) 0.02; P > 0.9	ns	ns
p.THg	ng/L	F = (1, 20) 3.47; P > 0.077	ns	ns	F = (1, 20) 5.81; P > 0.026	A	B
p.MeHg	ng/g, dw	F = (1, 20) 0.22; P > 0.65	ns	ns	F = (1, 20) 1.72; P > 0.2	ns	ns
p.MeHg	ng/L	F = (1, 20) 0.96; P > 0.34	ns	ns	F = (1, 20) 4.16; P > 0.05	ns	ns
p.MeHg	% of p.THg	F = (1, 20) 7.06; P > 0.015	A	B	F = (1, 20) 4.3; P > 0.051	ns	ns
uf.THg	ng/L	F = (1, 20) 3.32; P > 0.083	ns	ns	F = (1, 20) 5.85; P > 0.025	A	B
uf.MeHg	ng/L	F = (1, 20) 0.3; P > 0.59	ns	ns	F = (1, 20) 2.7; P > 0.12	ns	ns
uf.MeHg	% of uf.THg	F = (1, 20) 5.97; P > 0.024	A	B	F = (1, 20) 10.44; P > 0.004	B	A
Kd(THg)	L/kg	F = (1, 20) 7.54; P > 0.013	B	A	F = (1, 20) 0.002; P > 0.97	ns	ns
Kd(MeHg)	L/kg	F = (1, 20) 2.51; P > 0.13	ns	ns	F = (1, 20) 0.03; P > 0.86	ns	ns
Eh	mv	F = (1, 20) 16.93; P > 0.001	A	B	F = (1, 20) 0.81; P > 0.38	ns	ns
pH	standard units	F = (1, 20) 0.03; P > 0.87	ns	ns	F = (1, 20) 5.18; P > 0.034	A	B
DO	mg/L	F = (1, 20) 0.72; P > 0.41	ns	ns	F = (1, 20) 2.96; P > 0.1	ns	v
DO	% saturation	F = (1, 20) 1.22; P > 0.28	ns	ns	F = (1, 20) 1.7; P > 0.21	ns	ns
SpC	mS/cm	F = (1, 20) 1.5; P > 0.24	ns	ns	F = (1, 20) 4; P > 0.06	ns	ns
DOC	mg/L	F = (1, 20) 1.02; P > 0.32	ns	ns	F = (1, 20) 40.77; P > 0.0001	B	A
$SUVA_{254}$	L/mg C*m	F = (1, 20) 0.21; P > 0.65	ns	ns	F = (1, 20) 6.47; P > 0.019	A	B
NO_{2-}+NO_{3-}	(mg/L as N)	F = (1, 20) 11.52; P > 0.003	B	A	F = (1, 20) 119.94; P > 0.0001	B	A
PO_4^{3-}	(mg/L as P)	F = (1, 20) 0.04; P > 0.85	ns	ns	F = (1, 20) 2.03; P > 0.17	ns	ns
[NO_{2-}+NO_{3-}]/PO_4^{3-}	molar ratio	F = (1, 20) 2.59; P > 0.12	ns	ns	F = (1, 20) 1.86; P > 0.19	ns	ns
Chl.a	mg/m^3	F = (1, 20) 1.76; P > 0.2	ns	ns	F = (1, 20) 0.95; P > 0.34	ns	ns
TSS	mg/L	F = (1, 20) 0.32; P > 0.58	ns	ns	F = (1, 20) 5.11; P > 0.035	A	B
Chl/TSS	mg/g, dw	F = (1, 20) 9.76; P > 0.005	B	A	F = (1, 20) 8.2; P > 0.01	B	A
POC	% dw	F = (1, 20) 12.95; P > 0.002	B	A	F = (1, 20) 11.33; P > 0.003	B	A
PN	% dw	F = (1, 20) 8.38; P > 0.009	B	A	F = (1, 20) 11.62; P > 0.003	B	A
POC/PN	molar ratio	F = (1, 20) 3.7; P > 0.07	ns	ns	F = (1, 20) 0.15; P > 0.71	ns	ns
δ13C-POC	‰ (per mil)	F = (1, 20) 7.74; P > 0.012	A	B	F = (1, 20) 5.24; P > 0.033	B	A
δ15N-PN	‰ (per mil)	F = (1, 19) 1.15; P > 0.3	ns	ns	F = (1, 19) 0.1; P > 0.76	ns	ns

Table 6.1 Summary statistics associated with surface-water Model SW.1.—Continued

Interaction (YEAR x REGION)				
F statistic	low.ALSL 2010	low.ALSL 2011	MALSL 2010	MALSL 2011
F = (1, 20) 0.31; P > 0.58	ns	ns	ns	ns
F = (1, 20) 0.01; P > 0.92	ns	ns	ns	ns
F = (1, 20) 0.004; P > 0.95	ns	ns	ns	ns
F = (1, 20) 0.02; P > 0.88	ns	ns	ns	ns
F = (1, 20) 5.59; P > 0.028	B	A	B	B
F = (1, 20) 0.29; P > 0.6	ns	ns	ns	ns
F = (1, 20) 4.94; P > 0.038	AB	A	AB	B
F = (1, 20) 0.42; P > 0.53	ns	ns	ns	ns
F = (1, 20) 5.49; P > 0.03	B	A	B	B
F = (1, 20) 4.15; P > 0.06	ns	ns	ns	ns
F = (1, 20) 0.004; P > 0.95	ns	ns	ns	ns
F = (1, 20) 0.1; P > 0.76	ns	ns	ns	ns
F = (1, 20) 0.1; P > 0.76	ns	ns	ns	ns
F = (1, 20) 0.05; P > 0.82	ns	ns	ns	ns
F = (1, 20) 0.1; P > 0.75	ns	ns	ns	ns
F = (1, 20) 0.06; P > 0.81	ns	ns	ns	ns
F = (1, 20) 0.31; P > 0.59	ns	ns	ns	ns
F = (1, 20) 0.03; P > 0.88	ns	ns	ns	ns
F = (1, 20) 0.38; P > 0.54	ns	ns	ns	ns
F = (1, 20) 0.49; P > 0.49	ns	ns	ns	ns
F = (1, 20) 15.28; P > 0.001	C	C	B	A
F = (1, 20) 0.73; P > 0.4	ns	ns	ns	ns
F = (1, 20) 0.69; P > 0.42	ns	ns	ns	ns
F = (1, 20) 0.16; P > 0.69	ns	ns	ns	ns
F = (1, 20) 4.2; P > 0.05	ns	ns	ns	ns
F = (1, 20) 5.7; P > 0.027	B	B	B	A
F = (1, 20) 4.27; P > 0.05	ns	ns	ns	ns
F = (1, 20) 4.39; P > 0.049	B	B	B	A
F = (1, 20) 1.01; P > 0.33	ns	ns	ns	ns
F = (1, 20) 0.26; P > 0.61	ns	ns	ns	ns
F = (1, 19) 0.18; P > 0.68	ns	ns	ns	ns

Appendix 7. Surface-Water Model SW.2 Summary Statistics

Table 7.1. Summary statistics associated with surface-water Model SW.2.

[Surface-water Model SW.2 focused on surface water within the A8-complex (ponds A5, A7, and A8) and included only one independent (X) variable (GATE; also referred to as the gate condition, which is the number of gates open at the pond A8 tidal control structure). The April 2010—May 2011 time period, before the initial gate opening event in June 2011, is defined as the 'Pre' condition. The table below summarizes the results of this model as individually applied to the suite of water-column parameters as the dependent (Y) variable. For each model term the resulting model F statistic (F stat) and probability (P) is given. For the F-statistic, the value in parentheses (n.df, d.df) represent the numerator degrees of freedom (n.df) and denominator degrees of freedom (d.df), respectively. For each gate condition, the LSM result is given, as well as the standard error in parentheses. A post-hoc Tukey's pairwise analysis was conducted on gate condition for each Y variable and the resulting ranking is indicated with "A" being the highest ranking, and factors that share the same letter are not significantly different. See table 2 and the report front matter for full definitions of each parameter and units. NA, not applicable]

Parameter	Units	F stat	P > F	Pre		
f.THg	ng/L	(4, 107) 1.0	0.3865	2.21	(0.06)	A
f.MeHg	ng/L	(4, 107) 13.0	< 0.0001	0.86	(0.06)	A
f.MeHg	% of f.THg	(4, 107) 20.5	< 0.0001	33.60	(2.80)	A
p.THg	ng/g, dw	(4, 107) 20.5	< 0.0001	97.90	(36.20)	B
p.THg	ng/L	(4, 106) 3.3	0.0143	17.10	(1.60)	A
p.MeHg	ng/g, dw	(4, 107) 8.2	< 0.0001	7.44	(0.06)	AB
p.MeHg	ng/L	(4, 107) 15.0	< 0.0001	1.68	(0.06)	A
p.MeHg	% of p.THg	(4, 106) 17.8	< 0.0001	11.50	(1.00)	A
uf.THg	ng/L	(4, 106) 3.0	0.0218	19.30	(1.60)	A
uf.MeHg	ng/L	(4, 107) 17.0	< 0.0001	2.54	(0.06)	A
uf.MeHg	% of uf.THg	(4, 106) 23.7	< 0.0001	14.80	(1.10)	A
p.RHg	ng/g, dw	(2, 71) 1.1	0.3489	NA	NA	NA
p.RHg	ng/L	(2, 71) 18.7	< 0.0001	NA	NA	NA
p.RHg	% of p.THg	(2, 70) 11.3	< 0.0001	NA	NA	NA
Kd(MeHg)	L/kg	(4, 107) 4.7	0.0016	20,707.00	(8,017.00)	B
Kd(THg)	L/kg	(4, 106) 3.6	0.0090	52,103.00	(12,679.00)	B
E_h	mv	(4, 107) 16.7	< 0.0001	276.00	(10.90)	B
pH	standard units	(4, 107) 2.0	0.104	8.37	(0.06)	A
DO	mg/L	(4, 97) 16.2	< 0.0001	5.71	(0.06)	B
DO	% saturation	(4, 93) 25.2	< 0.0001	58.80	(4.80)	B
SpC	mS/cm	(4, 105) 20.0	< 0.0001	88.00	(6.20)	A
DOC	mg/L	(4, 107) 18.4	< 0.0001	30.70	(2.50)	A
$SUVA_{254}$	L/mg C*m	(4, 107) 7.7	< 0.0001	1.65	(0.06)	B
NO_2^-+NO_3^-	(mg/L as N)	(4, 107) 3.6	0.0088	0.23	(0.06)	AB
PO43−	(mg/L as P)	(4, 107) 19.6	< 0.0001	0.97	(0.06)	A
[NO_2^-+NO_3^-]/PO_4^{3-}	molar ratio	(4, 105) 3.2	0.0171	0.74	(0.06)	B
CHL.a	mg/m³	(4, 107) 7.4	< 0.0001	11.60	(3.60)	B
TSS	mg/L	(4, 107) 14	< 0.0001	267.00	(22.00)	A
Chl/TSS	mg/g, dw	(4, 107) 9.8	< 0.0001	0.09	(0.06)	B
POC	% dw	(4, 105) 2.6	0.0430	3.80	(0.06)	A
PN	% dw	(4, 105) 4.3	0.0030	0.51	(0.06)	B
POC/PN	molar ratio	(4, 105) 4.0	0.0044	8.23	(0.06)	AB
δ13C-POC	‰ (per mil)	(4, 106) 21.2	< 0.0001	−23.10	(0.50)	A
δ15N-PN	‰ (per mil)	(4, 105) 8.9	< 0.0001	9.70	(0.60)	C
SO_4^{2-}	mmol/L	(2, 71) 4.8	0.0108	NA	NA	NA
Cl−	mmol/L	(2, 71) 5.5	0.0062	NA	NA	NA
SO_4^{2-}/Cl−	molar ratio	(2, 71) 6.8	0.0020	NA	NA	NA

Table 7.1. Summary statistics associated with surface-water Model SW.2.—Continued

	Gate condition											
Parameter	1 gate			3 gates			5 gates			8 gates		
f.THg (ng/L)	2.19	(0.31)	A	1.64	(0.32)	A	2.18	(0.13)	A	1.79	(0.27)	A
f.MeHg (ng/L)	0.41	(0.15)	AB	0.07	(0.16)	B	0.07	(0.07)	B	0.11	(0.14)	B
f.MeHg (% of f.THg)	17.70	(4.70)	B	4.70	(4.90)	B	3.60	(2.10)	B	5.60	(4.10)	B
p.THg (ng/g, dw)	102.60	(60.60)	AB	81.30	(67.80)	AB	234.10	(26.60)	A	175.60	(53.20)	AB
p.THg (ng/L)	6.70	(2.60)	B	14.60	(2.90)	AB	12.40	(1.10)	AB	13.70	(2.30)	AB
p.MeHg (ng/g, dw)	12.04	(1.45)	A	3.04	(1.53)	BC	4.32	(0.64)	C	3.90	(1.28)	BC
p.MeHg (ng/L)	0.79	(0.26)	B	0.51	(0.27)	B	0.24	(0.11)	B	0.28	(0.23)	B
p.MeHg (% of p.THg)	11.70	(1.70)	A	3.80	(1.90)	B	2.60	(0.70)	B	2.50	(1.50)	B
uf.THg (ng/L)	8.90	(2.70)	B	16.30	(3.00)	AB	14.60	(1.20)	AB	15.50	(2.40)	AB
uf.MeHg (ng/L)	1.20	(0.38)	B	0.58	(0.40)	B	0.31	(0.17)	B	0.39	(0.33)	B
uf.MeHg (% of uf.THg)	13.40	(1.90)	A	3.80	(2.10)	B	2.70	(0.80)	B	3.00	(1.60)	B
p.RHg (ng/g, dw)	NA	NA	NA	3.78	(1.12)	A	4.79	(0.47)	A	3.40	(0.93)	A
p.RHg (ng/L)	NA	NA	NA	0.69	(0.06)	A	0.28	(0.03)	B	0.25	(0.05)	B
p.RHg (% of p.THg)	NA	NA	NA	4.88	(0.49)	A	2.87	(0.19)	B	1.97	(0.38)	B
Kd(MeHg) (L/kg)	33,353.00	(13,415.00)	AB	43,427.00	(14,140.00)	AB	62,385.00	(5,883.00)	A	51,133.00	(11,765.00)	AB
Kd(THg) (L/kg)	48,576.00	(21,216.00)	AB	48,919.00	(23,721.00)	AB	98,823.00	(9,304.00)	A	102,357.00	(18,608.00)	AB
E_h (mv)	283.00	(18.20)	B	285.00	(19.20)	B	372.00	(8.00)	A	356.00	(16.00)	A
pH (standard units)	8.42	(0.13)	A	8.53	(0.13)	A	8.56	(0.06)	A	8.71	(0.11)	A
DO (mg/L)	6.15	(0.80)	B	11.90	(1.26)	A	9.67	(0.36)	A	10.01	(0.73)	A
DO (% saturation)	69.50	(8.10)	B	141.50	(12.80)	A	112.10	(3.70)	A	103.30	(9.00)	A
SpC (mS/cm)	23.30	(10.40)	B	32.40	(11.00)	B	22.60	(4.60)	B	21.40	(9.50)	B
DOC (mg/L)	8.80	(4.10)	B	7.60	(4.30)	B	5.90	(1.80)	B	5.90	(3.60)	B
$SUVA_{254}$ (L/mg C*m)	1.84	(0.19)	AB	2.22	(0.20)	AB	2.40	(0.08)	A	2.19	(0.17)	AB
NO_2^-+NO_3^- (mg/L as N)	0.03	(0.06)	B	0.04	(0.07)	AB	0.18	(0.03)	AB	0.26	(0.05)	A
PO43− (mg/L as P)	0.11	(0.11)	B	0.43	(0.12)	B	0.35	(0.05)	B	0.24	(0.10)	B
[NO_2^-+NO_3^-]/PO_4^{3-} (molar ratio)	0.96	(0.94)	AB	0.22	(0.94)	B	1.81	(0.39)	AB	3.70	(0.78)	A
CHL.a (mg/m³)	21.90	(6.10)	AB	39.50	(6.40)	A	33.40	(2.70)	A	32.80	(5.30)	A
TSS (mg/L)	69.00	(36.00)	AB	174.00	(38.00)	B	84.00	(16.00)	B	74.00	(32.00)	B
Chl/TSS (mg/g, dw)	0.34	(0.09)	AB	0.25	(0.10)	AB	0.51	(0.04)	A	0.42	(0.08)	A
POC (% dw)	5.53	(1.13)	A	7.53	(1.19)	A	5.94	(0.50)	A	5.87	(0.99)	A
PN (% dw)	0.81	(0.14)	AB	0.94	(0.15)	AB	0.90	(0.06)	A	0.93	(0.12)	A
POC/PN (molar ratio)	8.12	(0.44)	AB	9.37	(0.46)	A	7.64	(0.20)	B	7.29	(0.39)	B
δ13C-POC (‰ (per mil))	−28.90	(0.90)	B	−28.10	(1.00)	B	−29.20	(0.40)	B	−27.60	(0.80)	B
δ15N-PN (‰ (per mil))	11.00	(1.00)	BC	15.80	(1.10)	A	13.00	(0.50)	AB	10.70	(0.90)	BC
SO_4^{2-} (mmol/L)	NA	NA	NA	17.80	(2.10)	A	11.30	(0.90)	B	10.10	(1.70)	B
Cl− (mmol/L)	NA	NA	NA	352.00	(40.00)	A	211.00	(17.00)	B	205.00	(33.00)	B
SO_4^{2-}/Cl− (molar ratio)	NA	NA	NA	0.051	(0.003)	AB	0.057	(0.001)	A	0.05	(0.002)	B

Appendix 8. Surface-Water Model SW.3 Summary Statistics

Table 8.1. Tabulated results of surface-water Model SW.3 for the main model term GATE.

[Surface-water Model SW.3 focused on surface water within Alviso Slough and included two main model terms: GATE (the number of gates open at the pond A8 tidal control structure, with factors: 0, 1, 3, 5, and 8 in parentheses) and REGION (with factors: up.ALSL and low.ALSL), in addition to an interaction term (GATE x REGION). Table 8.1 summarizes the results of Model SW.3 for the model term GATE and includes only the subset of surface-water parameters (as the dependent (Y) variable) for which the model term GATE was statistically significant ($p < 0.05$). The resulting model F statistic (F stat) and probability (P) are given for the model term GATE. For the F statistic, the value in parentheses (n.df, d.df) represent the numerator degrees of freedom (n.df) and denominator degrees of freedom (d.df), respectively. The following are given for each surface-water parameter and factors associated with the model term GATE: the Least Squares Mean (LSM), the standard error (Std error) in parentheses, and the post-hoc Tukey's pairwise analysis ranking (Rank). The Tukey's ranking is indicated with 'A' being the highest ranking and with factors sharing the same letter not being significantly different. In instances where the interaction term was significant (not shown), the parameter was reanalyzed with MODEL SW.4 (see appendix 9). See table 2 and the report front matter for full definitions of each surface-water parameter and associated units. nd, no data]

				GATE (0)			GATE (1)			GATE (3)			GATE (5)			wGATE (8)		
Parameter	Units	F stat	P	LSM	Std error	Rank	LSM	Std error	Rank	LSM	Std error	Rank	LSM	Std error	Rank	LSM	Std error	Rank
p.MeHg	(ng/g) dw	(4, 52) 2.9	0.032	6.24	(0.75)	A	4.88	(1.57)	A	2.57	(1.20)	A	3.96	(0.63)	A	2.50	(1.20)	A
p.MeHg	(% of THg)	(4, 52) 5.6	0.001	1.80	(0.18)	A	1.40	(0.37)	AB	2.26	(0.29)	A	0.99	(0.15)	B	1.15	(0.29)	AB
p.RHg	(% of THg)	(3, 38) 2.9	0.046	2.75	(0.47)	A	nd	nd	nd	2.70	(0.33)	A	1.79	(0.17)	A	1.85	(0.33)	A
Kd(THg)	(L/Kg)	(4, 52) 4.1	0.005	366,919.00	(42,400.00)	A	273,378.00	(89,151.00)	AB	104,187.00	(68,090.00)	B	193,599.00	(35,689.00)	B	146,575.00	(68,090.00)	AB
E_h	(mv)	(4, 50) 10.1	<0.0001	307.00	(12.00)	A	252.00	(24.00)	A	276.00	(19.00)	A	363.00	(10.00)	B	377.00	(19.00)	B
pH	(pH units)	(4, 52) 3.0	0.028	7.72	(0.10)	B	7.99	(0.21)	AB	7.86	(0.16)	AB	8.10	(0.08)	A	8.23	(0.16)	AB
DO	(% saturation)	(4, 47) 3.4	0.016	73.30	(3.80)	A	61.30	(8.00)	A	62.00	(6.90)	A	81.60	(3.30)	A	89.00	(8.00)	A
SpC	(mS/cm)	(4, 51) 6.0	0.001	8.70	(2.70)	B	9.90	(5.70)	AB	27.40	(4.30)	A	21.80	(2.30)	A	25.00	(4.60)	A
TSS	(mg/L)	(4, 52) 5.9	0.001	72.00	(14.00)	B	99.00	(30.00)	AB	201.00	(23.00)	A	119.00	(12.00)	B	137.00	(23.00)	AB
δ13C-POC	(per mil)	(4, 52) 2.6	0.045	−29.90	(0.70)	A	−28.70	(1.40)	A	−28.00	(1.10)	A	−27.70	(0.60)	A	−26.40	(1.10)	A

Table 8.1. Tabulated results of surface-water Model SW.3 for the main model term GATE —Continued

Table 8.2. Tabulated results for surface-water Model SW.3 for the main model term REGION.

[Table 8.2 summarizes the results of Model SW.3 for the model term REGION (with factors: up.ALSL and low.ALSL) and includes only the subset of surface-water parameters (as the dependent [Y] variable) for which the model term REGION was statistically significant ($p < 0.05$). The resulting model F statistic (F stat) and probability (P) are given for the model term REGION. For the F statistic, the value in parentheses (n.df, d.df) represent the numerator degrees of freedom (n.df) and denominator degrees of freedom (d.df), respectively. The following are given for each surface-water parameter and factors associated with main model term REGION: the Least Squares Mean (LSM), the standard error (Std error) in parentheses, and the post-hoc Tukey's pairwise analysis ranking (Rank). The Tukey's ranking is indicated with 'A' being the highest ranking and with factors sharing the same letter not being significantly different. In instances where the interaction term was significant (not shown), the parameter was reanalyzed with MODEL SW.4 (see appendix 9). See table 2 and report front matter for full definitions of each surface-water parameter and associated units.]

Parameter	Units	F stat	P	up.ALSL			low.ALSL		
				LSM	Std error	Rank	LSM	Std error	Rank
p.MeHg	(ng/g) dw	(1, 52) 5.4	0.025	5.19	(0.74)	A	2.86	(0.68)	B
p.RHg	(% of THg)	(1, 38) 4.2	0.048	1.92	(0.29)	B	2.62	(0.19)	A
Kd(THg)	(L/Kg)	(1, 52) 6.4	0.014	289,230.00	(42,086.00)	A	144,633.00	(38,412.00)	B
POC	(%) dw	(1, 52) 5.4	0.024	4.22	(0.42)	A	2.89	(0.38)	B

Appendix 9. Surface-Water Model SW.4 Summary Statistics

Table 9.1. Tabulated results for surface-water Model SW.4 when model factor for REGION is up.ALSL.

[Surface-water Model SW.4 focused on surface water within the Alviso Slough and included one explanatory (X variable) term: GATE (the number of A8-TCS gates open, with model factors 0, 1, 3, 5, and 8 given in parentheses). This model focused on surface-water parameters (Y variable) that were initially assessed using Model SW.3, but either resulted in an interaction effect or the model did not converge. Thus, Model SW.4 was run independently for data grouped by REGION factor: up.ALSL (table 9.1) or low.ALSL (table 9.2). Results are provided for parameters with statistically significant models only. For each model term the resulting model F statistic and probability (P) is given. For the F statistic, the value in parentheses (n.df, d.df) represent the numerator degrees of freedom (n.df) and denominator degrees of freedom (d.df), respectively. The following are given for each surface-water parameter and GATE condition: the Least Squares Mean (LSM), the standard error (Std error) in parentheses, and the post-hoc Tukey's pairwise analysis ranking (Rank). In the Tukey's ranking "A" indicates the highest ranking and factors that share the same letter are not significantly different. See table 2 and the report front matter for full definitions of each surface-water parameter and associated units.]

Parameter	Units	F stat	P	GATE (0)			GATE (1)		
				LSM	Std error	Rank	LSM	Std error	Rank
f.MeHg	(ng/L)	(4, 22) 5.5	0.0033	0.079	(0.008)	B	0.133	(0.016)	A
f.MeHg	(% of f.THg)	(4, 22) 10.0	<.0001	7.750	(0.730)	AB	10.820	(1.370)	A
DOC	(mg/L)	(4, 22) 3.2	0.0319	2.470	(0.830)	B	4.120	(1.550)	AB
NO_3+NO_2	(mg/L as N)	(4, 22) 6.3	0.0015	1.550	(0.190)	A	1.440	(0.360)	AB
CHL.a	(µg/L)	(4, 22) 3.1	0.0383	7.480	(5.880)	B	11.280	(11.000)	AB
POC/PN	(molar ratio)	(4, 22) 6.3	0.0016	11.610	(0.640)	A	8.770	(1.200)	AB
δ15N-PN	(per mil)	(4, 20) 3.8	0.0195	6.750	(1.600)	B	15.350	(2.530)	AB

Table 9.2. Tabulated results for surface-water Model SW.4 when model factor for REGION is low.ALSL.

[Surface-water Model SW.4 focused on surface water within the Alviso Slough and included one explanatory (X variable) term: GATE (the number of A8-TCS gates open, with factors 0, 1, 3, 5, and 8 given in parentheses). This model focused on surface-water parameters (Y variable) that were initially assessed using Model SW.3, but either resulted in an interaction effect or the model did not converge. Thus, Model SW.4 was run independently for data grouped by REGION: up.ALSL (table 9.1) or low.ALSL (table 9.2). Results are provided for parameters with statistically significant models only. For each model term the resulting model F statistic and probability (P) is given. For the F statistic, the value in parentheses (n.df, d.df) represent the numerator degrees of freedom (n.df) and denominator degrees of freedom (d.df), respectively. The following are given for each surface-water parameter and GATE condition: the Least Squares Mean (LSM), the standard error (Std error) in parentheses, and the post-hoc Tukey's pairwise analysis ranking (Rank). In the Tukey's ranking, "A" indicates the highest ranking and factors that share the same letter are not significantly different. See table 2 and the report front matter for full definitions of each surface-water parameter and associated units. nd, no data]

Parameter	Units	F stat	P	Gates (0)			Gates (1)		
				LSM	Std error	Rank	LSM	Std error	Rank
f.MeHg	(ng/L)	(3, 21) 9.5	0.0004	0.14	(0.02)	A	0.15	(0.03)	AB
f.MeHg	(% of f.THg)	(3, 21) 13.7	<0.0001	9.43	(1.05)	A	10.80	(1.81)	A
uf.MeHg	(% of uf.THg)	(3, 21) 6.9	0.0021	2.39	(0.25)	A	1.74	(0.44)	AB

Table 9.1. Tabulated results for surface-water Model SW.4 when model factor for REGION is up.ALSL. —Continued

GATE (3)			GATE (5)			GATE (8)		
LSM	Std error	Rank	LSM	Std error	Rank	LSM	Std error	Rank
0.045	(0.013)	B	0.064	(0.006)	B	0.072	(0.013)	B
4.120	(1.120)	BC	3.440	(0.560)	C	4.620	(1.120)	BC
6.530	(1.260)	AB	5.840	(0.630)	A	5.260	(1.260)	AB
0.580	(0.300)	AB	0.590	(0.150)	B	1.740	(0.300)	A
44.010	(8.980)	A	18.420	(4.490)	AB	22.610	(8.980)	AB
7.480	(0.980)	B	7.980	(0.490)	B	7.610	(0.980)	B
15.500	(2.060)	A	10.760	(1.030)	AB	10.020	(2.060)	AB

Table 9.2. Tabulated results for surface-water Model SW.4 when model factor for REGION is low.ALSL.—Continued

Gates (3)			Gates (5)			Gates (8)		
LSM	Std error	Rank	LSM	Std error	Rank	LSM	Std error	Rank
nd	nd	nd	0.05	(0.01)	C	0.06	(0.02)	BC
nd	nd	nd	2.53	(0.71)	B	3.67	(1.28)	B
nd	nd	nd	1.02	(0.17)	AB	1.43	(0.31)	B

Appendix 10. Qualitative Results for Surface-Sediment Model SED.1

Table 10.1. Tabulated qualitive results of surface-sediment Model SED.1 for model terms YEAR, TYPE, and REGION, as well as an interaction term [REGION x YEAR].

[Groups of parameters are separated into three categories: mercury parameters (whole sediment), nonmercury parameters (whole sediment), and nonmercury parameters (porewater). For each sediment parameter, the least squares mean fixed model terms associated with Model SED.1 are qualitatively represented as either significant (SIG) or nonsignificant (ns). For significant model main terms (YEAR and TYPE), a post-hoc Student t-test ranking of the specific factors for that term is shown in capital letters, where letter “A” is the highest ranking. For significant REGION factors, a pairwise Tukey’s post-hoc analysis was conducted. Factor rankings sharing the same letter are not significantly different. For the interaction term [REGION x YEAR], the differences among the various factors are not shown, although this interaction is more fully explored by Model SED.2 (see appendix 11). Instances where the resulting model residuals were more normally distributed using a natural logarithm (ln) transformation of the Y variable are indicated in the “Trans” column with “ln”. Otherwise “NONE” indicates that no data transformations were used. The overall model coefficient of determination (R^2 value) is also provided. See table 3 for parameter definitions. A8-complex, Alviso ponds A5, A7, and A8; up.ALSL, model factor used for upper Alviso Slough; low.ALSL, model factor used for lower Alviso Slough; MALSL, model factor used for Mallard Slough]

Parameter	Trans	R^2	Year		Type		Region						Interaction
							Ponds			Sloughs			[Region x Year]
			2010	2011	Pond	Slough	A8-complex	A3N	A16	Up.ALSL	Low.ALSL	MALSL	
Mercury parameters (whole sediment)													
THg	ln	0.47	ns	ns	ns	ns	A	C	BC	AB	C	BC	ns
RHg	ln	0.30	ns	ns	ns	ns	A	B	B	AB	AB	B	ns
RHg (%)	ln	0.17	ns	ns	ns	ns	ns	ns	ns	ns	ns	ns	ns
MeHg	ln	0.58	A	B	ns	ns	A	BC	BC	BC	C	AB	ns
MeHg (%)	ln	0.62	A	B	ns	ns	A	AB	BC	C	BC	A	SIG
K_{meth}	ln	0.47	ns	ns	ns	ns	A	AB	AB	B	B	A	SIG
MPP	ln	0.41	ns	ns	ns	ns	A	AB	AB	B	B	AB	ns
Nonmercury parameters (whole sediment)													
pH	NONE	0.39	ns	ns	A	B	ns	ns	ns	ns	ns	ns	SIG
E_h	NONE	0.72	ns	ns	B	A	C	C	C	A	AB	B	ns
LOI	ln	0.79	ns	ns	A	B	ns	ns	ns	ns	ns	ns	ns
GS	NONE	0.39	ns	ns	B	A	ns	ns	ns	ns	ns	ns	SIG
$Fe(II)_{AE}$	ln	0.36	ns	ns	ns	ns	A	AB	B	AB	B	AB	ns
$Fe(III)_c$	ln	0.28	ns	ns	B	A	ns	ns	ns	ns	ns	ns	ns
$Fe(III)_a$	ln	0.58	ns	ns	B	A	ns	ns	ns	ns	ns	ns	ns
$Fe(II)_{AE}$ (%)	ln	0.44	ns	ns	A	B	ns	ns	ns	ns	ns	ns	ns
TRS	ln	0.63	ns	ns	A	B	AB	AB	A	C	C	BC	ns
SRR	ln	0.55	A	B	A	B	A	A	A	C	BC	AB	ns
Nonmercury parameters (porewater)													
SO_4^{2-}	ln	0.77	A	B	A	B	A	A	BC	C	B	C	SIG
Cl^-	ln	0.78	ns	ns	A	B	A	A	B	C	B	B	ns
SO_4^{2-}/Cl^- ratio	ln	0.46	ns	ns	B	A	B	B	B	A	B	B	ns
Fe(II)	ln	0.19	ns	ns	B	A	ns	ns	ns	ns	ns	ns	ns
DOC	ln	0.64	ns	ns	A	B	A	AB	C	C	C	BC	ns
H_2S	ln	0.61	ns	ns	A	B	B	A	A	C	C	BC	ns

Appendix 11. Qualitative Results for Surface-Sediment Model SED.2

Table 11.1. Tabulated qualitive results of surface-sediment Model SED.2 for interaction term [REGION x YEAR].

[Model SED.2 is focused on the subset of surface-sediment parameters that showed a significant [REGION x YEAR] interaction term in Model SED.1. Model SED.2 assesses the difference between years (2010 and 2011) for each of the six individual REGION spatial groupings, which include three pond (A8-complex [A5, A7, and A8 ponds], pond A3N, and pond A16) and three slough groupings (upper Alviso Slough [model term up.ALSL]; lower Alviso Slough [model term low. ALSL]; and Mallard Slough [model term MALSL]). Results are qualitatively represented as either significant or nonsignificant (ns). For significant differences between years, the Student t-test ranking is given as capital letters, where letter "A" is the highest ranking. Instances where the resulting model residuals were more normally distributed using a natural logarithm (ln) transformation of the Y variable are indicated in the "Trans" column with "ln". Otherwise "NONE" indicates that no data transformations were used. See tables 2 and 3 for parameter definitions.]

Parameter	Trans	Ponds						Sloughs					
		A8-complex		A3N		A16		up.ALSL		low.ALSL		MALSL	
		2010	2011	2010	2011	2010	2011	2010	2011	2010	2011	2010	2011
MeHg (% of THg)	ln	ns	ns	ns	ns	ns	ns	ns	ns	A	B	ns	ns
K_{meth}	ln	ns	ns	ns	ns	ns	ns	ns	ns	ns	ns	A	B
pH	NONE	B	A	ns	ns	ns	ns	ns	ns	ns	ns	ns	ns
GS	NONE	ns	ns	ns	ns	ns	ns	A	B	ns	ns	ns	ns
SO_4^{2-} (porewater)	ln	A	B	ns	ns	ns	ns	ns	ns	ns	ns	ns	ns

Appendix 12. Statistical Results for Surface-Sediment Model SED.3

Table 12.1. Tabulated statistical results for surface-sediment Model SED.3 for which the model term TYPE is pond.

[For each sediment parameter, multivariate Model SED.3 significance results are provided for each model term, including main effects of the REGION spatial group and sampling EVENT, and the interaction term between them [REGION x EVENT]. TYPE data groupings (ponds and sloughs) were analyzed independently, with the results of the pond data grouping being provided in this table (table 12.1) and the results of the slough data grouping being provided in table 12.2. The resulting model F statistic is reported for each term, along with (n.df, d.df), where n.df is the numerator degrees of freedom associated with the individual model term, and the d.df is the denominator degrees of freedom associated with the overall unattributed (residual) model variance. The resulting probability (P) for each significant model term is given with significance set at the 5 percent probability level ($p<0.05$). For non-significant model terms, the P value is indicated as "—". For significant model main terms (REGION and (or) EVENT), a post-hoc Tukey's pairwise analysis was done. The resulting ranking is indicated by letters, where "A" is the highest ranking and factors that share the same letter are not significantly different. In the case of the interaction term [REGION x EVENT] the differences among the various factors are not shown. See tables 2 and 3 for parameter definitions.]

Parameter	Main effect: Region					Main effect: Event								Interaction	
	(n.df, d.df), F statistic	P	A8-complex	A3N	A16	F Statistic	P	MAY 2010	JUN 2010	AUG 2010	MAY 2011	JUN 2011	AUG 2011	F Statistic	P
THg	(2, 24) 4.87	0.0168	A	B	AB	(5, 24) 0.09	—							(10, 24) 0.31	—
K_{meth}	(2, 24) 1.85	—				(5, 24) 4.17	0.0072	B	A	B	AB	AB	B	(10, 24) 1.87	—
TRS	(2, 24) 4.41	0.0234	B	B	A	(5, 24) 0.99	—							(10, 24) 0.69	—
$Fe(III)_a$	(2, 24) 7.37	0.0032	B	A	AB	(5, 24) 3.22	0.0230	A	A	A	A	A	A	(10, 24) 1.47	—
H_2S (porewater)	(2, 24) 84.16	0.0001	B	A	B	(5, 24) 20.03	0.0001	BC	C	C	B	B	A	(10, 24) 13.14	0.0001

Table 12.2. Tabulated statistical results for surface-sediment Model SED.3 for which the model term TYPE is slough.

[For each sediment parameter, multivariate Model SED.3 significance results are provided for each model term, including main effects of the REGION spatial group and sampling EVENT, and the interaction term between them [REGION x EVENT]. TYPE data groupings (ponds and sloughs) were analyzed independently, with the results of the pond data grouping being provided in table 12.1 and the results of the slough data grouping being provided in this table (table 12.2). The resulting model F statistic is reported for each term, along with (n.df, d.df), where n.df is the numerator degrees of freedom associated with the individual model term, and the d.df is the denominator degrees of freedom associated with the overall unattributed (residual) model variance. The resulting probability (P) for each significant model term is given with significance set at the 5 percent probability level ($p<0.05$). For non-significant model terms, the P value is indicated as "—". For significant model main terms (REGION and (or) EVENT), a post-hoc Tukey's pairwise analysis was done. The resulting ranking is indicated by letters, where "A" is the highest ranking and factors that share the same letter are not significantly different. In the case of the interaction term [REGION x EVENT] the differences among the various factors are not shown. See table 3 for parameter definitions.]

Parameter	Main effect: Region					Main effect: Event								Interaction	
	n.df, d.df), F statistic	P	up.ALSL	low. ALSL	MALSL	F-Statistic	P	MAY 2010	JUN 2010	AUG 2010	MAY 2011	JUN 2011	AUG 2011	F-Statistic	P
THg	(2, 12) 6.65	0.0114	A	B	B	(5, 12) 0.46	—							(10, 12) 0.60	—
MeHg	(2, 12) 77.94	0.0001	B	B	A	(5, 12) 17.99	0.0001	A	B	B	C	BC	BC	(10, 12) 8.46	0.0005
MeHg (% of THg)	(2, 12) 93.11	0.0001	B	B	A	(5, 12) 37.31	0.0001	A	BC	B	C	BC	BC	(10, 12) 25.04	0.0001
K_{meth}	(2, 12) 160.40	0.0001	B	B	A	(5, 12) 36.93	0.0001	A	A	A	B	B	B	(10, 12) 24.88	0.0001
MPP	(2, 12) 97.48	0.0001	B	B	A	(5, 12) 29.20	0.0001	A	AB	BC	D	D	CD	(10, 12) 20.90	0.0001
SRR	(2, 12) 49.29	0.0001	B	B	A	(5, 12) 14.83	0.0001	A	A	A	B	B	B	(10, 12) 7.48	0.0009
TRS	(2, 12) 15.47	0.0005	B	B	A	(5, 12) 8.06	0.0015	AB	A	ABC	C	BC	BC	(10, 12) 2.41	—
$Fe(II)_{AE}$	(2, 12) 5.65	0.0186	A	B	AB	(5, 12) 0.52	—							(10, 12) 0.99	—
E_h	(2, 12) 5.57	0.0195	A	AB	B	(5, 12) 2.97	—							(10, 12) 1.02	—
LOI	(2, 12) 9.72	0.0031	AB	B	A	(5, 12) 1.35	—							(10, 12) 2.02	—
GS	(2, 12) 4.83	0.0289	B	A	AB	(5, 12) 2.07	—							(10, 12) 0.94	—
SO_4^{2-} (porewater)	(2, 12) 24.21	0.0001	B	A	B	(5, 12) 0.78	—							(10, 12) 0.51	—
Cl^- (porewater)	(2, 12) 25.60	0.0001	B	A	B	(5, 12) 0.94	—							(10, 12) 0.31	—
DOC (porewater)	(2, 12) 10.64	0.0022	B	B	A	(5, 12) 1.44	—							(10, 12) 1.04	—

Appendix 13. Summary of Key Findings

1. To what extent did the pond A6 levee breach result in directly measurable changes in mercury concentrations in Alviso Slough biota, surface water, and (or) bed sediment?

	BIOTA[1]	WATER	SEDIMENT
MODERATE	Possible effect in northern portion of pond A7 (short term spike in fish and Forsters' tern eggs THg) associated with pond A6 breach and adjacent scour of Alviso Slough bed sediment via close proximity and the hydrologic connection lower Alviso Slough and pond A7 through the A7-WCS.	Short-lived spike in volumetric p.MeHg in lower Alviso Slough 6 months after breach.	Decrease in percent MeHg in surface sediment (2011 compared to 2010) in lower Alviso Slough, presumed to be associated with rapid bed sediment scour in this region.
HIGH	Short term spike in Alviso Slough Mississippi silverside mercury after pond A6 breach (but before A8-TCS initial opening.	Short-lived spike in volumetric p.THg in lower Alviso Slough just after breach.	Quantifiable THg mobilized into pond A6 (70 kg/yr between December 2010 and November 2012), with some (but not all) coming from bed sediment scour in lower Alviso Slough.

[1]No bird egg or fish data for Pond A6 itself

2. To what extent did the construction and gradual increased opening of the A8-TCS result in measurable changes in mercury concentrations in biota, surface water, and (or) bed sediment within the pond A8-complex?

	BIOTA	WATER	SEDIMENT
MODERATE	Initial short-term spike in pond fish THg during construction period prior to initial A8-TCS opening, followed by a dramatic decrease in pond fish THg after gate opening.	Significant spike in the partitioning of THg between the particulate and dissolved phase (increased Kd[THg]), within the A8-complex, associated with the transition from 3 gates to 5 gates open, signaling the initiation of an enhanced period of Alviso Slough bed-sediment scour linked to gate operations at the A8-TCS.	Hydrodynamic and geomorphic modeling predicts the transport and deposition of sediment and associated mercury into the A8-complex through the A8-TCS, as well as through the A5 and A7 WCSs.
HIGH	Short-term spike in Forster's tern egg THg associated with construction phase and initial opening of the A8-TCS.		

Figure 13.1 (pages 146 and 147). Diagram summarizing the key findings and their confidence associated with the four questions that this synthesis was designed to address. The bulleted findings are organized by the three primary matrices sampled: biota, water, and (bed) sediment. Our confidence for each stated conclusion is qualitatively assessed as either MODERATE or HIGH, which are based on the totality of the statistical, quantitative, and (or) qualitative evidence presented in the main text. Abbreviations: cm, centimeter; f.MeHg, filter-passing methylmercury; f.THg, filter-passing total mercury; Kd[MeHg], distribution coefficient for methylmercury; Kd[THg], distribution coefficient for total mercury; kg/yr, kilogram per year; MeHg, methylmercury; p.MeHg, particulate methylmercury; p.THg, particulate methylmercury; SSC, suspended-sediment concentration TCS, tidal control structure; THg, total mercury; WCS, water control structure.

3. To what extent did the construction and gradual increased opening of the A8-TCS result in measurable changes in mercury concentrations in Alviso Slough biota, surface water, and (or) bed sediment?

BIOTA[1]

MODERATE

Short-term significant spike in Alviso Slough Mississippi silverside THg following spike in Alviso Slough water MeHg (prior to 2017 high flow event), ultimately associated with the transition from 3 to 5 open A8-TCS gates (September 2014) and the subsequent prolonged period of system instability, culminating in a spike in Alviso Slough surface water MeHg (April 2016) and finally a spike in Alviso Slough Mississippi silverside THg (October 2016).

HIGH

	BIOTA	WATER	SEDIMENT[2]
HIGH	Short-term spike in ALSL silverside THg during the 2010-11 construction period and the initial opening of the A8-TCS.	Increased salinity at site ALSL-3 with A8-TCS gates opened, indicative of increasing tidal prism. Decrease in SSC on ebb tide at site ALSL-3 as more gates opened, suggesting SSC deposition into the A8-complex during flood tide. Spike in gravimetric p.THg and p.MeHg, Kd[THg], and Kd[MeHg] in upper Alviso Slough (only) during the A8-TCS construction period. Immediate increase in the range of Q-ratio values upon the transition from 3 to 5 gates open, which represented an abrupt change in the energetics of the system and was coincident with an abrupt reversal in the direction of site ALSL-3 suspended sediment flux (from landward to bayward) that persisted for 1.6 years and culminated in a spike in Alviso Slough water column p.MeHg. Increase in volumetric mass flux of p.THg and p.MeHg in the bayward direction as more gates opened, indicative of buried Hg sediment erosion as tidal prism increased.	Bathymetric survey and deep core data: Peaks in bed sediment erosion (and THg remobilized) in upper and middle Alivos Slough after the initial 1-gate opening of the A8-TCS. Bathymetric survey and deep core data: Peaks in bed sediment erosion (and THg remobilized) in upper, middle, and lower Alviso Slough after the A8-TCS transition from 3 gates to 5 gates open.

[1]No relevant bird egg data to directly address this question

[2]No statistically significant results that showed a clear linkage between A8-TCS gate operations and changes in Alviso Slough surface sediment (top 0-2 cm) Hg species during 2010–11 (limited data)

4. To what extent is the pond A8-complex a source or sink for THg and (or) MeHg?

WATER[1]

MODERATE

The cumulative mass flux of f.THg (dissolved) past the A8-TCS was INTO the Complex during the 5-gate condition and OUT of the complex during the 8-gate condition

The cumulative mass flux of f.MeHg (dissolved) past the A8-TCS was INTO the Complex during the 5-gate condition (with the exception of the January–February 2017 high flow period) and OUT of the complex during the 8-gate condition

HIGH

The cumulative mass flux of p.THg and p.MeHg (particulate) past the A8-TCS was INTO the Complex during both the 5-gate and 8-gate conditions

[1]Question is not applicable to biota data and bed sediment

Moffett Field Service Center, California
Manuscript approved for publication October 26, 2022
Edited by Phil A. Frederick
Layout and design by Kimber Petersen

Marvin-DiPasquale and others—**South San Francisco Bay Salt Pond Restoration Project—A Synthesis of Phase-1 Mercury Studies**—Scientific Investigations Report 2022–5113

ISSN 2328-0328 (online)
https://doi.org/10.3133/sir20225113